A STUDY OF AIR-WATER, TWO-PHASE FLOW USING THE NEUTRON ATTENUATION TECHNIQUE

By

MOHAMED HOSNY YOUNIS, B.Sc., M.Eng.

A Thesis

Submitted to the Faculty of Graduate Studies

in Partial Fulfilment of the Requirements

for the Degree

Doctor of Philosophy

McMaster University

October, 1979

A STUDY OF AIR-WATER, TWO-PHASE FLOW USING THE NEUTRON ATTENUATION TECHNIQUE

DOCTOR OF PHILOSOPHY (1979)
(Chemical Engineering)

McMASTER UNIVERSITY
Hamilton, Ontario

TITLE: A Study of Air-Water, Two-Phase Flow Using the Neutron Attenuation Technique

AUTHOR: Mohamed Hosny Younis, B.Sc. (Alexandria University),
M. Eng. (McMaster University)

SUPERVISORS: Dr. T. W. Hoffman, Department of Chemical Engineering

Dr. A. A. Harms, Department of Engineering Physics

NUMBER OF PAGES: 374, xxvii

ABSTRACT

The purpose of this research program was to investigate the void behaviour in a vertical conduit containing a flowing mixture of air and water.

The local void fraction was measured by a neutron attenuation technique which was developed for this study. A neutron beam extracted from McMaster's 2MW Swimming Pool Nuclear Reactor was conditioned to provide a collimated beam of thermal neutrons with low gamma and fast neutron background. An atmospheric vertical upward cocurrent air-water loop was constructed in front of the beam port.

A series of experiments was performed to obtain information on the steady-state radial void profile in the bubbly and annular flow regimes for a 3/4 in. I.D. test section with gas and liquid volumetric fluxes up to about 32 m/sec and 80 cm/sec, respectively. The dynamic behaviour of the system to a perturbation in gas flowrate was measured and compared to that predicted by the void propagation equation.

The adequacy of the neutron attenuation method for radial void profile measurements in two-phase flow was ascertained. This was achieved by integrating the measured radial void profile and comparing the resulting cross-sectional average void fraction with that obtained by a trapping method. The

neutron attenuation method was also shown to be an excellent tool for flow regime recognition and for testing the flow development. The effect of the statistical fluctuations of the neutron source on its capability for void fraction measurement was examined and a counting strategy was recommended to reduce the resulting bias.

From the steady-state measurements of the radial void profiles and the gas and liquid flowrates, estimates of important flow parameters were obtained for the fully-developed bubbly and annular flow regimes. These estimates indicated that the flow parameters remain essentially constant for a specific flow regime.

To reduce the experimental effort considerably, an alternative method was presented which enables the designer to evaluate these parameters by performing a single experiment where the radial void profile is measured. Based on the momentum equation and Prandtl's turbulent mixing length hypothesis, a general form of the shear stress radial distribution was derived and integrated to yield the radial profile of the mixture velocity. By combining the radial profiles of the mixture velocity and void fraction, the values of the flow parameters were predicted. The proposed method indicated systematic variations of the flow parameters with the gas and liquid flowrates which were not consistent with observations. The estimated flow parameters, however, were shown to be adequate to predict

the average void fraction without introducing appreciable errors.

The results of the current experimental observations and analysis were compared with selected models and correlations which have been used by many designers to describe two-phase flow behaviour. This was done to evaluate the validity of the assumptions made in deriving these models and correlations. In general, this comparison indicated that the present experimental results and model predictions were consistent with expectations and previous observations and predictions. However, many of the published models and correlations were found to yield misleading results and conclusions which were attributed to the simplifying assumptions included in their derivation.

The void propagation equation was applied to predict the transient response of void fraction to perturbations in the gas flowrate in the adiabatic gas-liquid flow system employed. To solve this equation, values of the distribution parameter are required under changing flow conditions. It is usually assumed that the parameter values obtained for steady-state, fully-developed flow are valid under transient developing-flow situations. That is to say that the steady-state distribution parameter pertaining to the local average voidage condition applies in the transient system. Since this parameter cannot be obtained from steady-state experiments under all voidage conditions experienced during the transient, a continuous

functional relationship was assumed in order to interpolate over those regions where the parameter cannot be obtained.

An analysis was performed to examine the sensitivity of the predicted void transient response to errors in the distribution parameter. This analysis showed that a comparison between predicted and observed void transient responses should permit the evaluation of the validity of the assumptions made concerning the distribution parameter and its interpolating relationship. A satisfactory agreement between these responses was obtained in bubbly flow. This indicated that the steady-state values of the distribution parameter for fully-developed flow and the assumed interpolating relationship can be used to predict the void transient response in the considered experimental apparatus over the flow conditions studied herein.

ACKNOWLEDGEMENTS

The author wishes to express his sincere and deep thanks to his research supervisors, Dr. T. W. Hoffman and Dr. A. A. Harms, for their continued guidance, support and understanding throughout the course of this work. In addition, thanks are due to the other members of his thesis committee, Dr. J. Vlachopoulos and Dr. J. E. Robinson, for their encouragement and suggestions.

The author is also indebted to McMaster University and to the National Research Council of Canada for financial support.

Special thanks are due to Mr. R. Dunn and Mr. A. Singh for their assistance in constructing the experimental facility and to Mrs. H. Kennelly for her patience in typing this thesis.

Finally, the author is grateful to his wife for her encouragement and understanding which have been a continuing source of comfort.

TABLE OF CONTENTS

LIST OF TABLES

LIST OF FIGURES

CHAPTER (1)

INTRODUCTION

(1.1) Outlines of the Subject Area

The simultaneous flow of liquid and gas (or vapour) through pipes is a commonly observed industrial phenomenon. This is because of its occurrence in boilers [1,2], condensers [3], chemical reactor equipment, nuclear reactor cores [4-9] and pipelines carrying both oil and natural gas [10], etc.

The general problem of two-phase flow has received an increasing attention by a number of research workers from the early days of the invention of the gas-lift pump to the present time. The application of gas-lift principles to oil well production in the late 1920's stimulated further interest in two-phase vertical flow and resulted in a number of mathematical and experimental studies [11].

The design, cost, efficiency and reliability of high-power systems which are characterized by the presence of two-phase flow depend, to a great extent, upon the understanding of two-phase flow and boiling processes. For nuclear reactors in which the coolant and/or the liquid moderator are allowed to boil or in which vapour voids are formed under accident conditions, precise knowledge of the volumetric concentration is essential to study the reactor stability and controllability.

This is due to the important effect which the volumetric concentration has on the core reactivity, the fuel burnup rate and the critical heat flux [12]. In fact, the importance of the design and safety analysis of nuclear power systems has been responsible for the numerous publications dealing with the subject of two-phase flow [13,14].

(1.2) Problem Definition

Because of the important effect which the vapour volumetric concentration in a nuclear reactor has on its performance and reliability, it is of considerable interest to predict its response to perturbations in power input and/or inlet flowrate. Steady-state oscillations of flow and/or vapour content have been observed in two-phase flow systems. Under some conditions, the amplitude of such oscillations may increase with time and lead to unstable operation. An understanding of the conditions leading to these instabilities is essential to ensure safe and reliable operation of nuclear reactors characterized by the existence of two-phase flow. The ability to predict these conditions depends on the correct formulation of the transient response of the volumetric concentration to pertur bations in power and/or flowrate. These perturbations are of considerable interest because they are realistic and simulate possible conditions in nuclear reactors during normal operation as well as during some types of reactor accidents. Under normal operation, these perturbations may occur due to reactor refuelling, poison buildup, control rod manipulation and reactor

shutdown or startup. On the other hand, possible failure of a heat transfer unit and a reduction in coolant flow to the reactor core, due to flow blockage or pump failure, cause perturbations of these types.

In extreme situations, a loss-of-coolant accident, as caused by a main pipe failure in a pressurized system, can lead to fast transients where compressibility effects may become important. The analysis presented in this study applies only to slow transients, as caused by a flow blockage or a pump failure, where compressibility effects can be ignored. Hence, this analysis needs to be modified to account for the compressibility effects which could occur during severe accidents.

Under the incompressible flow conditions postulated, the transient response of two-phase flow can be analyzed in terms of the integrated form of the vapour continuity equation [15,16] which is given by

$$\frac{\partial \langle\alpha\rangle}{\partial t} + U \frac{\partial \langle\alpha\rangle}{\partial z} = \Omega \ , \tag{1.1}$$

where

$$U = \langle\alpha\rangle[\langle j_m\rangle \frac{\partial C_o}{\partial \langle\alpha\rangle} + \frac{\partial \bar{V}_{gj}}{\partial \langle\alpha\rangle}] + C_o\langle j_m\rangle + \bar{V}_{gj} \ , \tag{1.2}$$

and

$$\Omega = \frac{\langle\Gamma_g\rangle}{\rho_g} [1-\langle\alpha\rangle C_o(1 - \frac{\rho_g}{\rho_\ell})] \ . \tag{1.3}$$

Here α and j_m are the local values of void fraction and mixture volumetric flux density and the angle bracket, $< >$, indicates a quantity averaged over the entire tube cross-sectional area, A, which for the variable ψ is

$$<\psi> = \frac{1}{A} \int_A \psi \, dA \, . \qquad (1.4)$$

In equation (1.3), ρ_g and ρ_ℓ are the vapour and liquid densities and $<\Gamma_g>$ represents the vapour source term which is defined as the rate of mass formation of the vapour phase per unit mixture volume.

Equation (1.1) is usually referred to as the void propagation equation and was first derived and applied to transient experiments by Zuber and Staub [15]. The distribution parameter, C_o, and the mean drift velocity, $\bar{V}_{gj}$, are introduced to account for the non-uniformity of the mixture velocity and void fraction distributions across the tube and the fact that the local phase velocities are not equal. These flow parameters are defined by

$$C_o = \frac{<\alpha j_m>}{<\alpha><j_m>} \, , \qquad (1.5\text{-a})$$

and

$$\bar{V}_{gj} = \frac{<\alpha \, V_{gj}>}{<\alpha>} \, , \qquad (1.5\text{-b})$$

where V_{gj} is the relative velocity of the vapour phase, v_g, with respect to the volumetric flux density of the mixture; that is,

$$V_{gj} = v_g - j_m \quad . \tag{1.6}$$

It is clear from equations (1.1), (1.2) and (1.3) that the values of the flow parameters, C_o and $\bar{V}_{gj}$, are required when using the propagation equation to predict the void transient response to perturbations in inlet flow and/or power input.

The dependence of these parameters on flow regime can be explained as follows: A change in flow regime implies a change of the mixture velocity and/or concentration radial profiles as well as the geometry of the interface between the phases. It can be seen from equation (1.5) that both $\bar{V}_{gj}$ and C_o are affected by any change in void fraction and velocity radial profiles. Furthermore, the drift velocity depends on the momentum transfer between the phases which, in turn, depends on the interface geometry. For the same reason, the values of these flow parameters are expected to change along a tube containing a developing two-phase flow where the velocity and void radial profiles keep changing till the flow is completely developed. It is important to indicate that the fully-developed condition which has been used to describe the single-phase liquid flow does not, in general, exist in gas-liquid flow systems. This is because of the effect of the continuous gas volume change, due to pressure change along the flow conduit, on the radial profiles of the velocity and void fraction. Moreover, these profiles are affected by upstream conditions, that is, the design of the air-water mixer. How-

ever, in the experimental apparatus employed in this study, the pressure change along the flow conduit was very small. Hence, an approximate equilibrium state, with essentially unchanged void and velocity radial profiles, developed downstream of the air-water mixer. Thus, the flow may be described as fully developed where it is actually in an approximate equilibrium state.

Zuber and Findlay [17] and Shiralkar et al. [18] assumed that for vertical upward flow, the flow parameters depend only on the type of flow regime, that is, they remain essentially constant for a given flow regime. Garland [19] found that in boiling systems, where large changes in void fraction occur along the flow tube, the void response models are sensitive to the distribution parameter, C_o, and even a small error in C_o may lead to a significant error in the predicted void response. This shows the important role played by the flow parameters in the analysis of two-phase flow systems and emphasizes the requirement of accurate determination of their values a priori.

As will be shown later, one can evaluate these parameters by using the experimental measurements of the average void fraction and the gas and liquid flowrates to plot the relation between the gas weighted mean velocity and total mixture velocity. An alternative method can be realized from the definition of these parameters (equation (1.5)) which indicates

that the mixture velocity and void fraction radial profiles should be independently determined. The determination of these profiles were also recommended by several research workers in the field [17,20-22] in order to have a better understanding of the two-phase flow and boiling phenomena.

The overall program which has been planned to study two-phase flow and boiling phenomena can be summarized as follows:

(i) Evaluate the feasibility of using neutron radiation as a diagnostic tool for void fraction measurement, flow regime recognition and flow development testing.

(ii) Present and evaluate the possible methods which can be used to estimate the flow parameters for a steady-state air-water flow system.

(iii) Investigate the applicability of these flow parameters, as determined under steady-state flow conditions, in predicting the transient response of the air-water flow system to different types of perturbations.

(iv) Modify the adiabatic experimental facility to simulate a boiling two-phase flow system where the gas phase is added through the channel wall to an air-water flow mixture. Then apply the developed experimental technique and mathematical model to estimate the steady-state values of the flow parameters under conditions where the flow is developing. This would require developing a model for each flow parameter as a function of the system operating conditions.

(v) Test the applicability of the steady-state values of the flow parameters, as determined for a flow developing situation, under dynamic conditions where a perturbation occurs to the injected gas flow. This test requires the solution of the void propagation equation using the models developed for the flow parameters.

(vi) Construct a boiling two-phase flow system which accommodates different working fluids and measure the void transient response to perturbations in the inlet flow and/or input power. The previously developed models for the flow parameters will be tested along with the assumptions concerning thermodynamic equilibrium, the thermal capacity of the heating system, etc.

It is important to realize that the present research has been limited to studying the adiabatic flow of air-water mixtures in a vertical tube at atmospheric pressure. Obviously, this is a restricted class of two-phase flow and does not represent, in general, the flow of a boiling coolant in a nuclear reactor. However, the present work is only the first part of the overall program outlined above.

Thus, the main objective of this work was to examine the possibility of applying the neutron diagnostic technique to measure the radial void profiles, to characterize the flow regime and to test the flow development. Moreover, the possible methods which can be used to estimate the fundamental flow parameters at steady-state, fully-developed flow will be presented

and evaluated. As a further objective of this program, it was desired to evaluate the applicability of the flow parameters, as determined under steady-state conditions, in predicting the transient response of the two-phase flow system to perturbations in the inlet gas flowrate.

(1.3) Synopsis of Research Program

To achieve these goals, an atmospheric vertical upward cocurrent water-air adiabatic two-phase flow loop was constructed in front of a beam port of McMaster's 2 MW Swimming Pool Nuclear Reactor. The extracted neutron beam was used as a diagnostic tool to determine the void fraction radial profiles under a variety of experimental conditions [23]. Experimental data were determined for a 3/4 in. I.D. test section with gas volumetric fluxes up to about 32 m/sec and liquid volumetric fluxes up to about 80 cm/sec. Additionally, a general form of the shear stress radial distribution was derived and then integrated to yield the mixture velocity radial profile. The derivation of the shear stress distribution was based on the momentum conservation equation together with the Prandtl's turbulent mixing length hypothesis.

The results obtained in the present study were compared with selected models and correlations which have been used by many designers to describe two-phase flow behaviour.

This was done to evaluate the validity of the assumptions made in deriving these models and correlations.

After the flow parameters were determined under steady-state flow conditions, the applicability of these parameters to unsteady-state flow was evaluated. This involved the use of the void propagation model first introduced by Zuber and Staub [15] and then used by Hancox and Nicoll [24] and Shiralkar et al. [18]. It was adapted to predict the transient response of void fraction to perturbations in gas flowrate for the adiabatic two-phase flow system under consideration. The void propagation equation, derived from the mass conservation equations for the two phases using Zuber's cross-sectional average approach, was solved using the method of characteristics. The predicted cross-sectionally averaged void variations with time were then compared with those measured experimentally by means of the neutron attenuation method.

CHAPTER (2)

LITERATURE REVIEW

(2.1) Void Fraction Measuring Techniques

The recognition of the importance of the precise knowledge of void fraction distribution has been responsible for the increasing interest in developing measuring techniques for void fraction in two-phase flow systems. Jones and Delhaye [25] presented a detailed review of measurement techniques for two-phase flow in general. A summary of the techniques used in void fraction measurement is given below.

(2.1.1) Conductivity Probe

The conductivity probe, as applied to void fraction measurement in two-phase flow, consists of two electrodes inserted into the two-phase mixture. The different designs of conductivity probes usually differ only in the relative position, shape and size of the electrodes. If an electric potential is applied between the electrodes, an electric current is observed; this current is a direct measure of the conductivity of the two-phase mixture between the electrodes. This, in turn, represents the relative volumetric concentration of conducting and non-conducting fluids, that is liquid and gas, in the path of the electric current. Obviously, the conduc-

tivity probe cannot be used for high-resistivity liquid systems or for systems where there is no substantial difference between the conductivity of the two phases.

The conductivity probe has been used by several investigators: Solomon [26] constructed a needle-type conductivity probe to obtain qualitative information on the flow regime transition in an air-water flow system. His probe consisted of a grounded electrode imbedded in the tube wall and an isolated needle, with an exposed tip, which was inserted into the two-phase flow tube such that it was aligned parallel to and opposing the flow.

Neal and Bankoff [27] developed and used a similar conductivity probe to measure void fraction radial profiles in mercury-nitrogen flow. This was achieved by summing up the time during which the needle came in contact with the gas and dividing by the total observation time. The results were reported to be satisfactory although no calibration was performed. Nassos and Bankoff [28] tested the adequacy of this probe for radial void profile measurement in an air-water system in the quality range of $(0.125 \text{ to } 1.045)\times10^{-3}$. This was done by integrating the radial void profiles obtained with this probe and those obtained using a gamma attenuation technique and comparing the resulting values of average void fraction. The comparison indicated that the probe measurements were consistently lower than the gamma attenuation measurements; the deviation varied from 22% to 57% with an average of 35%. The deviation was

attributed to the wetting characteristics of water which resulted in a delay of signal as the needle entered the air bubbles. Some improvement was achieved by sharpening the probe tip and using a triggering device to reduce the effect of bubble deflection and deformation. However, the measured void fraction was still consistently low especially at low liquid velocities where the possibility of bubble deflection was high.

Similarly, Malnes [29] employed a conductivity probe for void fraction measurement in steam-water as well as air-water systems; however, the reliability of the results was not tested by any comparative measurements. As indicated by Herringe and Davis [30], all of these experiments were conducted at relatively low velocities, that is, below 1.5 m/sec for the air-water system and below 3 m/sec for the steam-water system.

Lecroat and Porte [31] conducted experiments similar to those performed by Malnes [29] in a flowing air-water system for velocities of up to 30 m/sec but were unable to detect clearly defined phase changes.

Burgess and Calderbank [32] showed that uncertainties in the conductivity probe measurements may arise due to the varying and unknown positions at which the probe contacts the bubble frontal surfaces. In other words, the bubbles whose axes and velocity vectors are not coincident with the probe axis may yield inaccurate results. To reduce these uncertainties, they recommended that two conditions should be satisfied: First, the probe must be capable of resolving the position

at which it is struck by the bubble relative to the bubble centerline. In particular, it should be able to record only those encounters when the bubble and probe axes of symmetry are coincident within fine limits. Second, the instant when the probe tip enters the bubble must be accurately determined, bearing in mind that the wetting characteristic of the liquid creates a delay time in the probe response to an approaching bubble. To achieve these aims, Burgess and Calderbank developed a sophisticated three-dimensional conductivity probe with five channels. They reported that their technique was able to sense the approach angle of the bubble local interface as well as to measure the bubble size and velocity.

Jones and Delhaye [25] reviewed the recent development of different types of conductivity probes with different relative position and shape of electrodes and discussed the problem associated with the electrochemical effect. In general, the conductivity probes have proven to be attractive because of their fast response and relative simplicity of operation. However, the considerable flow disturbance caused by these probes represents a serious drawback. This disturbance produces accelerations in the flow field which, by changing the relative gas and liquid velocities, affect the void fraction.

(2.1.2) Hot-Film Anemometer

The hot-film anemometer basically consists of a glass cylinder of a small diameter covered with a platinum coating and

connected at either end to conducting leads. To use the probe, its resistance should be set by means of an electric current at a value corresponding to a desired probe temperature. The probe temperature changes due to the power dissipation (heat transfer) which depends upon the phase in contact with the probe. If the probe resistance changes from the preset value as a result of temperature change, the control unit will respond to change the current, to maintain a constant probe temperature.

Hsu et al. [33] developed a hot-film anemometer which could be used for flow regime recognition and void fraction measurement in two-phase flow. Jones [22] used a 50 micrometer hot-film anemometer to measure void fraction radial profiles in an air-water flow system. He compared the centerline void fraction, as measured using the anemometer, with that measured by an x-ray attenuation method. A very large discrepancy between the two measurements was found especially at low liquid velocities.

The major advantage of the hot-film anemometer over the needle-type conductivity probe is that it is self contained and does not require a secondary electrode. In addition to the flow disturbance introduced by this device, the probe's extreme fragility, short lifetime and high initial cost represent its main disadvantages.

(2.1.3) Optical Probe

An optical probe can be used to measure the local void fraction and interface passage frequencies in two-phase flow. It makes use of the fact that the two phases have different refractive indices to the incident light beam. Jones and Delhaye [25] presented a detailed description of the different types of optical probes. As a typical example of these probes, the glass rod system which was developed by Miller and Mitchie [34] is described below.

The glass rod optical probe consists of a glass rod of 2 millimeter diameter reduced to 0.3 millimeter diameter at one end. The small tip of the rod is ground, polished and bent to form a right-angled cone. The other end of the rod is branched; while a light beam from a quartz-iodine lamp is focused on one of these branches, a phototransistor is located at the other branch. Light is transmitted parallel to the rod axis towards the tip of the probe. When the beam strikes the surface at an angle of 45°, it either emerges from the probe or is reflected back, depending upon the refractive indices of the probe and surrounding materials.

Miller and Mitchie tested the adequacy of their probe for void fraction measurement in an air-water system by comparing the measured average values of void fraction with those obtained by the "quick-closing valves" technique. The comparison showed that the optical probe indicated consistently lower values especially at high liquid velocities and for small pipe diameters. This can be attributed to the bubble deflection and to

the fact that small bubbles could not be resolved.

Jones and Delhaye [25] presented a detailed description of the different optical probes used in two-phase flow measurements. They also reported the results of the comparative study performed by Galaup [35] which demonstrated a reasonable agreement between radial void profile measurements in air-water flow using an optical probe, a conductivity probe and a hot-film anemometer.

Herringe and Davis [30] presented a direct quantitative comparison of three void fraction measuring techniques in an upward vertical air-water flow and discussed their suitability for different applications. In general, this study indicated that there was a significant difference in the results obtained from the hot-film anemometer, conductivity probes and optical probe. The comparison showed also that the single-needle conductivity probes caused the least flow disturbance with the least apparent bubble deflection and were capable of resolving the smallest bubbles. Under high void fraction conditions, however, these probes were found unsatisfactory and this necessitated the use of a two-needle conductivity probe. The hot-film anemometer was found unsuitable because it caused too much bubble deflection and did not respond to small bubbles and, thus, indicated values of average void fraction very much smaller than those obtained with other probes. The optical probe gave values of local and average void fraction

which were comparable with those obtained by the other probes. However, the water and air levels were not defined by the response of the optical probe as accurately as with the other probes.

(2.1.4) Quick-Closing Valves Technique

The total liquid volume contained in a conduit in which a two-phase mixture flows may be obtained by direct measurement. This technique requires two quick-closing valves to be installed at each end of the test section. The valves must not disturb the flow when open and must be able to be closed rapidly and simultaneously. After closing the valves, the volume or mass of liquid in the test section is measured directly and compared to the total volume of the test section to yield the average volumetric liquid fraction. The main advantage of this technique over many others is that it can be used with high accuracy even in complex geometries; Schraub et al. [36], for example, applied it successfully to measure the void fraction in a nine-rod bundle. Moreover, due to its fundamental nature, it can be used in calibrating and testing other void fraction measuring techniques. The main disadvantage of this technique is that it gives only values of void fraction averaged over the whole conduit and cannot be used to measure its detailed distribution or time variation.

This technique has been widely used in adiabatic systems particularly at low pressures (see for example Quandt [37]). Its successful application to void fraction measurement in

boiling systems was also reported by Agostini et al. [38].

(2.1.5) Radiation Attenuation and Scattering Techniques

The desire to measure the void fraction accurately in visually opaque systems without disturbing the flow promoted the use of radiation diagnostic techniques. These techniques make use of the fact that the two phases have different attenuation and scattering capabilities of incident radiation. A detailed review of the radiation attenuation techniques was presented by Schrock [39]. Some types of radiation which have been used in the field of two-phase flow are given below.

(2.1.5.1) X-Ray Attenuation Technique

The use of an x-ray tube as a source of radiation for the measurement of void fraction in two-phase flow has been tried by many investigators [40-42]. The advantage of x rays lies in the lack of the bulky source holders and the repeatability and long-term stability of the source strength. The main disadvantage is its short-term unsteadiness due to the alternating applied voltage. To reduce the induced fluctuations in the beam strength, Jones [40] employed special filters in the high-voltage side of the x-ray transformer power supply.

With the proper selection of the tube wall thickness, x-ray tube operating conditions and beam collimation, Pike et al. [41] concluded that the x-ray attenuation technique could be used successfully for void fraction measurement in steam-

water flow. By employing mock-ups of lucite and air, they indicated, however, that the error in measuring void fraction could be as high as 20%.

Smith [42] used a dual-beam x-ray tube where a reference beam acted to compensate for the inherent variation in the x-ray intensity at the source. To test the adequacy of this technique, Smith employed water and aluminum mock-ups and concluded that density changes of durations less than 100 microseconds could be recorded with acceptable accuracy. For non-uniform radial void distributions, however, void fraction measuring errors of the order of 30% were reported.

(2.1.5.2) Gamma-Ray Attenuation and Scattering Techniques

Gamma-ray and x-ray attenuation techniques employ essentially the same fundamental concept. However, since a gamma-ray beam may be obtained from nuclear disintegration of natural radioactive isotopes, its strength is expected to be time dependent. While short-lived sources require frequent calibration, long-lived sources of acceptable activities must be massive and, thus, are hazardous to handle. The main disadvantage of the gamma attenuation technique is due to the long range of gamma rays in hydrogeneous materials which puts a lower limit on the medium thickness and an upper limit on the value of void fraction. In addition, considerable attenuation takes place in the walls of the flow container. However, the high penetrating capability of a gamma-ray beam in hydrogeneous materials

permits its use to measure the void fraction in complex geometries [43].

Perkins et al. [44] stated that the gamma attenuation technique could be used with a reasonable accuracy in void fraction measurement for homogeneously-distributed voids with attenuation paths greater than 1 in. equivalent thickness of water and values of void fraction greater than 0.25. For systems of smaller void fraction, smaller path length or preferential radial void distribution,this technique may not offer sufficient accuracy. However, the gamma attenuation technique has been developed and the accuracy with which the void fraction can be measured has been improved considerably since then.

A series of tests on lucite mock-ups was conducted by Cook [45] to measure the void fraction in various simulated phase radial distributions using the gamma attenuation technique. His results indicated that the error between the measured and actual void fraction increased as the channel spacing was increased and as the distance between the radioactive source and channel was decreased; errors of up to 93% were observed in simulated annular flow.

Hooker and Pooper [46] performed an error analysis for the gamma attenuation technique and concluded that below 10% void fraction, the error in measuring void fraction became very large; for a higher void fraction, the maximum

error was reported to be less than 5% void. Malnes [29] indicated, however, that these conclusions did not agree with lucite calibration and suggested that an error of 10% void would be more realistic.

Petrick and Swanson [47] carried out a comparison between "one-shot" and traversing gamma attenuation techniques by using lucite mock-ups. They concluded that in the range of void fraction between 0.16 and 0.61, the average deviation for the "one-shot" technique was 36.5% whereas it was 7.3% for the traversing technique. Similarly, Richardson [48] calibrated these techniques against lucite blocks and reported an error of the order of ± 20% for both techniques with inhomogeneous configurations.

Gardner et al. [49] tested their "one-shot" gamma attenuation technique using lucite cylinders which simulated two extreme phase radial distributions; one type had a single hole machined in the tube center whereas the other was a solid circular rod placed at the tube center. The error in measuring the void fraction was reported to be within 10% for the first type and as high as 37% for the second type.

Le Vert and Helminski [50] suggested to use a dual-energy gamma attenuation technique instead of the conventional single-energy technique. Their analysis showed that the suggested technique would reduce the void fraction error arising

from the inherent fluctuations in two-phase flow. However, it is worth noting the added complexity which may result due to the inability to differentiate between the scattered high-energy photons and unscattered low-energy photons. This raises the question of whether there is a gain in the accuracy of the new technique over the single-energy technique.

Heidrick et al. [51] described a technique, based on the use of three gamma beams, to determine the density and phase radial distributions in two-phase flow. This technique involved the assumption of a three-parameter model to describe the phase radial distribution in the stratified, annular and bubbly flow regimes. To examine the adequacy of the proposed technique, they used lucite mock-ups in simulating the stratified and annular flow regimes. A comparison between the actual and measured densities indicated good agreement; the worst deviation was reported to be 25% at a density value of 0.1 milligram/m^3.

Kennett et al. [52] discussed the advantage of using a high-energy gamma scattering technique over the low-energy gamma attenuation technique. They proposed to extract a collimated gamma beam of energy as high as 9 Mev from a nuclear reactor. Their analysis demonstrated that the bias in void fraction measurement could be reduced by a factor of 10 with the suggested technique.

(2.1.5.3) Beta-Particle Attenuation Technique

Perkins et al. [44] reported the possible use of beta particles for void fraction measurement in two-phase flow. Unlike gamma rays, beta particles do not penetrate matter as well and, hence, their range in hydrogeneous materials is relatively very short. As a typical example, several millimeters of water can completely stop a beam of beta particles of energy 2 Mev. Nevertheless, there are two main advantages in using beta particles instead of gamma rays as a diagnostic tool for void fraction measurement. First, as indicated by Perkins et al. [44], beta particles can provide higher sensitivity (as much as 70 times more) and, second, shielding is not a major obstacle as in the case of long-lived gamma-ray sources. However, the high attenuation suffered by beta particles in heavy intensive materials represents a major disadvantage. This puts an upper limit on the thickness of the medium and container and a lower limit on the value of void fraction.

In addition, a massive radioactive source is required to supply a strong beam of high intensity. This is essential to provide a sufficiently high particle flux at the test detector in order to give statistically good results. This, in turn, enhances the fraction of the beta particles absorbed in the source material itself, that is, the self shielding effect. Hence, an optimum source size should be determined in order to maximize the source strength.

(2.1.5.4) Neutron Attenuation and Scattering Techniques

The use of neutrons for void fraction measurement in nuclear reactors was first suggested by Untermyer [53]. Following Untermyer's suggestion, Thie et al. [54] measured the cadmium ratios of cobalt wires which were placed at various locations in the reactor core and related these ratios to the local values of void fraction. Later, Untermyer [55] employed a fast-neutron detector, placed above the reactor vessel and in-line with the coolant channels, to monitor the steam output in boiling reactor channels by detecting the changes in the fission neutron flux.

Sha and Bonilla [56] used a neutron beam emitted by a radioactive isotope to measure values of void fraction of up to 0.25 in a multi-rod test section. They indicated that the neutron attenuation technique was sensitive enough to detect void fraction values as small as 0.03. By dissolving boron in the boiling water, the thermal neutron attenuation coefficient was greatly increased; thus, sensitivities of over 20 times that of a typical gamma attenuation technique could be obtained.

Moss and Kelly [57] developed a neutron radiographic technique which made use of the neutrons extracted from a nuclear reactor. They reported that this technique was able to measure water film thicknesses of up to 0.125 in. with an accuracy of 0.006 in.

Of all possible radiation attenuation techniques, Harms et al. [58] showed that the neutron attenuation technique provided higher accuracy within a wider range of void fraction. Furthermore, the constraints on the medium and wall thicknesses, discussed in the previous two subsections, could be much reduced using the neutron attenuation technique. They employed lucite mock-ups to test the adequacy of the neutron attenuation technique and concluded that this technique could be used over a range of 0.03 to 0.70 void fraction with an accuracy of about 6 to 7%.

The experimental bias in void fraction measurement, introduced by the inherent fluctuations in two-phase flow, was investigated by Harms and Forrest [59]. Their analysis demonstrated that these fluctuations could result in a substantial error (more than 40%) in the measured void fraction. As indicated by Harms and Forrest [59], this type of void fraction error is common to all radiation attenuation techniques. In order to minimize this error, Hancox et al. [60] suggested a gating technique to obtain discrete transmittance measurements over time intervals much smaller than the dominant period of medium fluctuations. To evaluate the effectiveness of the suggested gating technique, Hancox et al. [60] employed lucite mock-ups to simulate an idealized slug flow with a range of slug residence time of 0.1 to 0.8 sec. They found that the deviation between the actual and measured void fraction was much reduced as the gating period was decreased from 0.5 sec to

0.05 sec.

As indicated by Younis et al. [61], a neutron beam extracted from a nuclear reactor has an additional advantage of having relatively smaller variance-to-mean ratio if compared with the radiation emitted by radioactive isotopic sources. This was shown to result in a much smaller void fraction bias due to statistical fluctuations of the radiation source.

Instead of placing the neutron detector in line with the incident beam axis, as in the attenuation technique, it may be positioned with its axis perpendicular to that of the neutron beam to count the number of neutrons scattered off the beam path. Using the epithermal and fast neutrons extracted from a swimming pool reactor, Rousseau et al. [62] showed that the flux of the scattered neutrons in a given solid angle was strongly dependent on the average void fraction in the test section. They concluded that the neutron scattering technique was more accurate than gamma multi-beam techniques for void fraction measurement in hydrogeneous media. The attenuation techniques, however, allow the determination of phase radial distributions in the flow conduit which is not possible with the scattering technique.

Recently, Banerjee et al. [63] investigated the feasibility of using the fast-neutron scattering technique for void fraction determination in two-phase flow. They placed shaped aluminum test sections, of 1 in. and 2 in. I.D., containing water in the path of a fast neutron beam extracted from McMas-

ter's nuclear reactor. These test sections were designed to simulate the annular, core (inverse annular) and stratified flow regimes. By comparing the measured values of void fraction with the corresponding actual values, Banerjee et al. [63] found that the core and annular water distributions gave values of void fraction slightly lower than the actual values. Furthermore, it was found that in the stratified flow regime, the measured void fraction was not entirely independent of the position of voids in the test section. Banerjee et al. [63] stated that this effect could be corrected by positioning two neutron detectors opposite each other and averaging the count-rates.

Banerjee et al.[63] then went on to perform a series of experiments in which a test section (1.5 in. I.D.) containing an air-water mixture was placed in the fast-neutron beam. Except for two experimental runs, excellent agreement was obtained between the values of void fraction measured by the neutron scattering technique and the quick-closing valves technique.

In spite of the inability of the fast-neutron scattering technique to determine the detailed phase radial distribution, it has an apparent advantage over the thermal-neutron attenuation technique of yielding higher count-rates and, hence, better counting statistics in thick hydrogeneous media.

(2.1.6) Miscellaneous Techniques

(2.1.6.1) High-Speed Photography and Holographic Techniques

A detailed review of the application of the photographic technique in two-phase flow was given by Arnold and Hewitt [64]. Visual examination of high-speed motion pictures has been one of the major techniques of flow regime characterization. Although this technique can provide useful qualitative information about the flow structure, it cannot be used to determine the void fraction as accurately as most of the other techniques. This is because of the uncertainties involved in counting and measuring the gas bubbles and the difficulty that arises in interpreting two-dimensional photographs of the three-dimensional phenomena.

Feldberg et al. [65] employed a laser holographic technique to determine the bubble concentration of a boiling water in a vertical channel. This technique has an additional disadvantage that the system vibrations and external disturbances have very important effects on the contrast and resolution of the holographic image.

(2.1.6.2) Dissolved Radioactive Tracer Technique

If a pulse of radioactive tracer of short half life is injected into the liquid phase of a two-phase flow mixture, the intensity of the emitted radiation will depend on the amount of liquid in the mixture. Dengler [66] applied this technique to measure the void fraction of a boiling water in a vertical channel and reported an accuracy of 10%. However, the accuracy

of the technique depends on the amount of radioactive material present in the gas phase or adhering to the channel wall as well as the attenuation of radiation in the liquid phase.

If the motion of the radioactive tracer is followed along the flow channel, the average velocity of the liquid phase can be determined. This technique may give approximately the true value of mean velocity of the liquid. However, the use of this velocity in calculating the void fraction necessitates the assumption that the two phases are travelling separately but each with a respective constant velocity. This assumption may lead to inaccurate values of void fraction. Furthermore, the tracer technique can only be used in closed systems where it is possible to recover the radioactive material. It has an additional disadvantage in that it introduces a high background radiation and, thus, requires shielding of the whole experimental apparatus.

(2.1.6.3) Gamma-Neutron Reaction Technique

If a section of a channel containing two-phase flow, with D_2O as the liquid phase, is bombarded with gamma rays, neutrons will be emitted as a result of gamma-neutron reaction. Assuming that the gamma flux is constant, the neutron flux is proportional to the amount of D_2O present and, thus, to the liquid fraction. This technique was used by Rouhani [67] for void fraction measurement in two-phase flow. He then calibrated this technique by employing channels containing D_2O with alumi-

num wires as voids and reported an accuracy of 2.5% void.

In addition to the shielding problem associated with this technique, its range of application is limited because of the high cost of D_2O. Moreover, the analysis of the results is relatively complicated due to the fact that both gamma photons and neutron particles are attenuated along their paths.

(2.1.6.4) Pressure Drop Technique

Nassos [68] described a technique for void fraction determination in two-phase flow which was based on pressure drop measurements. He tested this technique against his conductivity-probe technique and reported good agreement between the two techniques although the acceleration component of pressure drop was assumed negligible. The maximum and average deviations between the two sets of void fraction measurements were about 9% and 7%, respectively. It is important to realize that this technique, similar to the quick-closing valves technique, only gives an average value of void fraction between the pressure taps without any inference about the detailed void distribution.

From the above, it is evident that an attenuation technique using a narrow neutron beam should be the most suitable technique for the measurement of void fraction radial profiles in the 3/4 in. I.D. test tube used in this study. Considerable research is further required to investigate the possibility of using the neutron beam, extracted from McMaster's 2 MW Swimming Pool Reactor, to measure the radial void profiles,

to characterize the flow regime and to test the flow development in an air-water two-phase flow system. This, then, constitutes one of the main objectives of this research.

(2.2) Two-Phase Flow Models

Many methods and techniques have been used to analyze the problem of two-phase flow. Interest in this problem continues to increase and new developments in the field are still forthcoming. Numerous publications dealing with both the experimental and the theoretical aspects of two-phase flow have appeared in the literature. However, not all of this substantial effort has contributed significantly either towards the understanding of the physical processes involved or towards providing the designer with design information of sufficient accuracy, reliability and generality.

Two-phase flow is such an exceedingly complex physical situation and, as such, modelling has yet not met with as much success as that for single-phase flow. In single-phase flow, empirical correlations are well established; in two-phase flow, the correlations and understanding, in general, are relatively poor. The commonly-used equations for two-phase flow often contain implied or unrecognized assumptions which are likely to result in a misleading description of the system behaviour. Most of the data and correlations have been developed to satisfy the immediate needs of a particular design and contributed little to a better understanding of the basic

mechanisms governing two-phase flow.

During the last decade, considerable effort has been expended to put the study of two-phase flow phenomena on a firmer theoretical foundation. Much of this effort has been directed towards the investigation of such fundamental aspects as the distribution of the phases over the flow cross-section, the relative motion of one phase with respect to the other and the inherent discreteness and unsteadiness characterizing the two-phase flow systems. In the following subsections, the different analytical models dealing with these fundamental aspects will be reviewed and, where possible, evaluated.

(2.2.1) Flow Parameters

There are two important effects which must be considered in any analysis of two-phase flow. The first is the non-uniformity in mixture velocity and void fraction distributions across the flow conduit. The second is the non-equality of the local velocities of the phases, i.e., the relative velocity of one phase with respect to the other. There have been numerous publications which ignore or consider either one or both of these effects.

The most drastic simplification is the use of the homogeneous model [69] in which the two phases are assumed to be homogeneously mixed and moving with identical velocity which

is uniformly distributed across the flow tube. This means that both effects are neglected. The obvious advantage of the homogeneous model is that it treats the two-phase flow as a mixture of fluids with appropriately averaged properties and, thus,makes the system analytically tractable.

From the continuity equation of the homogeneous mixture, the following relation between the cross-section average void fraction, $\langle\alpha\rangle$, and the apparent volumetric flow concentration, β, can be derived:

$$\langle\alpha\rangle = \beta \ , \tag{2.1}$$

where

$$\beta = \frac{Q_g}{(Q_g+Q_\ell)} \ , \tag{2.2}$$

where Q_g and Q_ℓ are the gas and liquid volumetric flowrates, respectively.

The assumption of zero relative velocity between the phases is only valid when the flow velocity is very high relative to the drift velocity between the phases. The assumption of uniform distribution of void fraction over the cross-section of the conduit is reasonable only for the fog flow regime. Since this flow is encountered only under special circum-

stances, the homogeneous model is very limited in its application to the two-phase flow systems in general. Therefore, although the model is simple, it does not provide accurate predictions of two-phase flow phenomena and more sophisticated models are required.

The influence of either one or both of these two effects has been presented by a number of investigators. The effect of local relative velocity was first considered by Behringer [70] for bubbly flow. Neglecting the effects of the radial distributions of mixture velocity and void fraction, Behringer modified equation (2.1) to give

$$\langle\alpha\rangle = \frac{Q_g}{A\, v_g} , \tag{2.3}$$

where the gas local velocity, v_g, is given by

$$v_g = \frac{Q_g+Q_\ell}{A} + v_\infty , \tag{2.4}$$

and v_∞ is the terminal rise velocity of a single bubble in an infinite medium which represents the gas velocity relative to the cross-sectional average mixture velocity.

Bankoff [71] was the first to consider the effect of the radial distributions of mixture velocity and void frac-

tion in bubbly two-phase adiabatic flow. He treated the two-phase flow as a continuous medium whose density is a function of the radial position across the flow tube. By assuming both the velocity and void radial distributions to be of power-law form, he derived the following expression for the cross-sectional average void fraction:

$$\langle\alpha\rangle = K\,\beta \ , \qquad (2.5)$$

where K is a flow parameter which can be related to the exponents in the void and velocity radial profiles. Consequently, the system pressure, the mass flowrates and the mixture quality are expected to have some effect on the parameter, K. Bankoff arrived at the conclusion that K may take a value between 0.6 and 1.0 for all the reasonable velocity and void radial profiles.

By analyzing existing experimental data using his model, Bankoff suggested that the flow parameter, K, was dependent upon the system pressure, P, according to the relation

$$K = 0.71+0.0001\,P \ , \qquad (2.6)$$

where P is in p.s.i.a. units. As indicated by Zuber [72], Armand [73] obtained equation (2.5) empirically and examined the pressure dependence of the parameter, K, where he found equation (2.6) to be in good agreement with his data.

It is noteworthy that Behringer's model, equation (2.3), is expected to be successful in correlating the experimental data only when the effect of velocity and void radial distri-

butions is negligible. On the other hand, Bankoff's model, equation (2.5), yields good agreement only when the effect of the local relative velocity between the phases is negligible. Similarly, the homogeneous model, equation (2.1), can only be valid when both effects are negligible.

Griffith and Wallis [74] modified Behringer's analysis for the slug flow regime. They expressed the terminal rise velocity, v_∞, which represents the velocity of the slug bubbles with respect to the liquid ahead of them, by the Dimitrescu-Taylor bubble velocity, i.e.,

$$v_\infty = 0.35(g\Delta\rho D/\rho_\ell)^{1/2} , \qquad (2.7)$$

where g is the gravitational acceleration, D is the tube diameter and $\Delta\rho$ is the difference between the liquid and gas densities, i.e., $\Delta\rho = \rho_\ell - \rho_g$. Bartolomei and Georgescu [75] derived the following correlation for v_∞ which fitted their experimental data for an adiabatic system:

$$v_\infty = (0.65+0.0034\ P)\left(\frac{D}{6.3}\right)^{0.2} , \qquad (2.8)$$

where P is in bars and D is in cm.

Nicklin et al. [76], Neal [77] and Nobel [78] took account of the distribution effect of the mixture velocity in the slug flow regime by introducing a distribution parameter, c', into equation (2.4) which then becomes

$$v_g = c'\left(\frac{Q_\ell+Q_g}{A}\right) + 0.35(gD\Delta\rho/\rho_\ell)^{1/2} . \qquad (2.9)$$

Nobel [78] examined the various models for slug flow and suggested that c' varies with the flow conditions and is approximately equal to the reciprocal of the local void fraction at the terminus of the slug flow bubble. Nicklin et al. [76] argued that because the bubble is located in the high-velocity region and moves faster than the average flow, the distribution parameter, c', should be taken equal to 1.2 which is approximately equal to the maximum-to-average velocity ratio in turbulent flow. This means that Nicklin et al. did not take the effect of the radial void distribution into consideration in calculating the value of c'. Substituting for v_g from equation (2.9) into equation (2.3) yields the following relation between $\langle\alpha\rangle$ and β:

$$\langle\alpha\rangle = \frac{\beta}{[1.2 + \frac{0.35}{\langle j_m\rangle}\sqrt{gD\,\frac{\Delta\rho}{\rho_\ell}}]}\,, \qquad (2.10)$$

where $\langle j_m\rangle$ is the mixture cross-section average velocity defined by

$$\langle j_m\rangle = \frac{Q_\ell + Q_g}{A}\,. \qquad (2.11)$$

Neal [77], on the other hand, expressed the distribution parameter, c', as the reciprocal of Bankoff's flow parameter, K. He also accounted for the effect of the relative velocity between the phases by adding, without proof, the second term in the right-hand side of equation (2.9). Later, Neal and Bankoff [79] extended the model of Bankoff to treat the cases where the effect of local relative velocity is not small by

assuming that the local phase velocities are proportional instead of being equal.

Zuber and Findlay [17] extended Neal's analysis to all flow regimes. In addition to the distribution parameter, C_o, defined by equation (1.5-a), they introduced the local drift velocity, V_{gj}, in analogy to the kinetic theory of gases, equation (1.6). Then from the basic field definitions, they derived the following relationship between the cross-sectional average void fraction and the volumetric flux densities:

$$\langle j_g \rangle / \langle \alpha \rangle = C_o \langle j_m \rangle + \bar{V}_{gj} , \qquad (2.12)$$

where $\langle j_g \rangle$ is the cross-sectionally averaged volumetric flux density of the gas phase. The local values of the volumetric flux densities of the gas phase, j_g, and of the liquid phase, j_ℓ, are related to the local respective phase velocities, v_g and v_ℓ, by

$$j_g = \alpha v_g , \qquad (2.13\text{-a})$$

and

$$j_\ell = (1-\alpha) v_\ell . \qquad (2.13\text{-b})$$

By definition, the local flux density of the mixture can be written as

$$j_m = j_g + j_\ell . \qquad (2.14)$$

The relative velocity between the phases, v_r, is defined as

$$v_r = v_g - v_\ell , \qquad (2.15)$$

which upon substituting from equations (1.6), (2.13) and (2.14) yields

$$v_r = V_{gj}/(1-\alpha) \quad . \tag{2.16}$$

Equation (2.12) can also be written in the form

$$\beta/\langle\alpha\rangle = C_o + \bar{V}_{gj}/\langle j_m\rangle \quad , \tag{2.17}$$

which is of the same form as equation (2.10) given by Nicklin et al. for the slug flow regime. It should be also mentioned that equations (2.12) and (2.17) are valid for all flow regimes. In equation (2.17), β is the volumetric apparent flow concentration which is defined by equation (2.2) as the ratio of the gas and the mixture volumetric flowrates. This is equivalent to the ratio between the gas and mixture volumetric flux densities, i.e.,

$$\beta = \langle j_g\rangle/\langle j_m\rangle \quad . \tag{2.18}$$

The various models presented here can be obtained from Zuber's equation by making the appropriate simplifications. Equation (2.17) reduces to equation (2.1) of the homogeneous model if the concentration and/or the velocity radial profiles are assumed uniform and the local phase velocities are assumed equal, i.e., $C_o = 1$ and $\bar{V}_{gj} = 0$. If, instead, only the effect of the non-uniform velocity and concentration radial distributions is neglected, C_o will be equal unity and Zuber's general equation (2.17) will reduce to Behringer's equation

(2.3) with $\bar{V}_{gj} = v_{\infty}$. Similarly, neglecting the effect of the local relative velocity, i.e., setting $\bar{V}_{gj}$ equal to zero, equation (2.17) simplifies to Armand's expression (equation (2.5) with C_o equal to the inverse of Bankoff's parameter, K. This is only possible for very large flowrates or relatively small mean drift velocity, i.e., for small $\bar{V}_{gj}/\langle j_m \rangle$. At low volumetric flowrates, this ratio can not be approximated by zero and the independence of the $\langle \alpha \rangle/\beta$ ratio of the flowrate assumed by Bankoff does not hold. If the mean drift velocity for the slug flow regime is taken equal to the Dimitrescu-Taylor velocity, equation (2.12) yields equation (2.9) with $C_o = c'$. Similarly, on setting $\bar{V}_{gj}$ equal to Dimitrescu-Taylor velocity and $C_o = 1.2$, equation (2.17) simplifies to equation (2.10) derived by Nicklin et al. [76].

Equation (2.12) or (2.17) can be used to calculate the average void fraction for given values of gas and mixture volumetric flux densities if the flow parameters, C_o and $\bar{V}_{gj}$, are known. Zuber and Findlay [17] showed that for vertical upward flow, both C_o and $\bar{V}_{gj}$ depend only on the type of flow regime, that is, they remain essentially constant for a given flow regime.

From equation (2.12), it is clear that the easiest way to determine C_o and $\bar{V}_{gj}$, for a specific flow regime, is to plot the experimentally measured values of the mean gas velocity, $\langle j_g \rangle/\langle \alpha \rangle$, versus the values of the mixture volumetric flux density, $\langle j_m \rangle$. The slope of the resulting straight line

is equal to C_o and its intercept is equal to $\bar{V}_{gj}$. As indicated by Zuber and Findlay [17], an abrupt change of the slope or the intercept of this straight line may be interpreted as an indication of a change in flow regime.

Assuming various radial profiles for the mixture velocity and void fraction and using equation (1.5-a), Zuber and Findlay [17] computed the possible values of the distribution parameter, C_o. For fully-established radial profiles and vanishingly small void fraction at the tube wall, they concluded that C_o could range from 1.15 to 1.5 for bubbly flow and become close to unity in annular flow. In general, for a wide range of flow conditions and for all flow regimes, they stated that a value of $C_o = 1.13$ would give quite good agreement with experimental data. Similarly, various expressions for the mean drift velocity, $\bar{V}_{gj}$, were given by Staub et al. [80] for different flow regimes.

Furthermore, Zuber and Findlay [17] estimated the values of the flow parameters which fitted the experimental data obtained by Petrick [81] and by Bailey et al. [82]. They found that each set of data was well represented by a straight line on the $\langle j_g \rangle / \langle \alpha \rangle$ versus $\langle j_m \rangle$ plot. Nassos [68] arrived at the same conclusion when he employed a vertical upward air-water loop to determine the flow parameters for bubbly flow. He estimated a value of 1.1 for the distribution parameter, C_o, which indicated flat mixture velocity and void fraction radial profiles. However, this was not consistent with the experimentally measured void fraction radial profiles which were readily

described by one-third or one-fourth power-law distributions. This discrepancy may be attributed to uncertainties incorporated in the void measuring technique which was employed by Nassos [68].

The analysis presented by Zuber and Findlay [17] has led to greater generality and better physical representation of the problem of two-phase flow. However, their method of flow parameters estimation requires the measurement of several radial void profiles which is, obviously, not desirable from the standpoint of the designer who may only be interested in evaluating these parameters for a specific flow condition. Hence, it is much preferable to have an alternative method which enables the designer to estimate the parameters by performing a single experiment where the radial void profile is measured. Equation (1.5), which defines the flow parameters, indicates that one can readily estimate these parameters if the radial distributions of the mixture velocity and void fraction are available.

Hancox [16] employed the experimental measurements performed by St. Pierre [83] for radial void profiles together with hypothetical radial velocity profiles to evaluate the distribution parameter, C_o. To make the analysis of dynamic boiling-flow systems, with a change of flow regime, mathematically tractable, Hancox [16] used a continuous functional relationship to describe the variation of C_o with the average void fraction, $\langle\alpha\rangle$, for the entire range of $\langle\alpha\rangle$ from zero to unity.

From the above discussion, it is evident that a single value of C_o or $\bar{V}_{gj}$ for all flow regimes is not a reasonable

assumption. Based on the fact, mentioned in section (1.2), that small errors in the flow parameters may lead to substantial errors in the predicted void fraction, one can conclude that there is a real need to obtain accurate estimates of these parameters. This conclusion stresses the importance of developing adequate mathematical models and experimental techniques to enable research workers to determine these flow parameters with acceptable accuracy under the given flow conditions.

(2.2.2) Transient Response of Void Fraction

As mentioned earlier, the volumetric concentration of one or the other phase in a two-phase flow system is very important. In the calculation of the total pressure drop, knowledge of the void fraction is essential in determining the gravitational or static head contribution. In the operation of boiling water nuclear reactors, the vapour volumetric concentration is of considerable interest mainly because of void-reactivity coupling.

Several investigators have been primarily concerned with the prediction of the transient response of void fraction to specific perturbations in heat flux and/or inlet flow. These types of perturbations are of great importance because they are realistic and may occur in nuclear reactors during normal operation as well as under accident conditions. Many of the techniques presented in that context were either questionable or used an incomplete set of equations to describe the behaviour of the two-phase flow system. These analyses were formulated in terms of the continuity, momentum and energy conservation laws of the two-phase mixture [84]. In the conservation equations, the radial distributions of the mixture velocity and void fraction were either ignored or incompletely taken into consideration. Birkhoff [85] examined the cross-sectionally averaged form of the conservation laws and indicated the mathematical implications of the one-dimensional formulation, that is, of not considering the distribution effects.

Some of the previous analyses have replaced the mass conservation equation needed to describe the diffusion of one phase into the other with an additional empirical void fraction relationship. Empirical relations were also employed for the wall shear stress and for the axial variation of the liquid phase enthalpy. Alternatively, the latter empirical relation was replaced with the assumption of thermal equilibrium between the phases [86]. There are two significant deficiencies in the above procedure. First, as noted by Zuber and Staub [87], the replacement of the second continuity equation with an empirical equation for the void fraction along with the one-dimensional assumption leads to errors in the momentum and energy equations. Secondly, as indicated by Ahmad [88], experiments have shown that in a boiling subcooled liquid, vapour and subcooled liquid exist simultaneously in the flow tube. This indicates that the assumption of thermal equilibrium between the phases is not realistic for some systems of practical interest.

For multi-phase or multi-component systems of n phases or components, it is well known [89] that n continuity equations must be used. It is usual to sum these n equations to provide a continuity equation for the entire mixture and, then, to express the remaining (n-1) equations as diffusion equations for the phases or components. With the exception of the work reported by Van Der Walle and Lamein [90], this was never done in the anslysis of two-phase flow before Zuber and Staub [87]

presented their propagation model. Van Der Walle and Lamein considered a diffusion equation for the vapour phase in addition to the continuity equation for the two-phase mixture. Obviously, it is essential to know the diffusion coefficient in order to use the void diffusion equation. However, it was found [15] that experimental data on the diffusion coefficient for boiling two-phase mixtures are almost non-existant.

As indicated by Spinks [91], Kanai et al. formulated the problem of void transient response in terms of the mixture continuity, momentum and energy equations. They also assumed that the velocity slip ratio depends only on the void fraction and not on the velocity as well. Hudson et al. [92] used the small perturbation theory and developed equations for the void amplitude and phase lag. Their analysis was based on the one-dimensional form of the conservation laws for the mixture, i.e., they neglected the effects of radial void and velocity profiles. St. Pierre [83] and Christensen [93] determined the void response to heat flux modulation for boiling water at near thermal equilibrium conditions.

Staub and Zuber [94] and Zuber et al. [95] presented a comprehensive analysis of the void response to heat and flow perturbations which led to greater generality and better physical representation than could be achieved with one-dimensional models. They formulated the problem in terms of the cross-sectionally averaged form of the mixture conservation laws in addition to the void propagation equation. The void propagation

equation is an independent equation which is analogous to the diffusion equation for the vapour phase. It can be obtained by manipulating the continuity equation of the gas or vapour phase.

Zuber [96] showed that the kinematic wave theory, or the propagation model, can be used to predict the change of vapour volumetric concentration as the flow passes through the tube. Such a theory was first developed by Lighthill and Whitham [97,98] to analyze flood waves and traffic flow on highways. It was also applied by Takeda [15] and by Wallis [69] to analyze the transient response of a dispersed gas-solid and of a gas-liquid two-phase flow, respectively. The void propagation equation was applied by Staub and Zuber [94,99] to predict the steady-state axial void distribution and the void response to both flow and power oscillations in a boiling forced flow with either axially uniform or quadratic-power input. They assumed that the phases were in thermal equilibrium and, then, obtained an expression for the vapour generation function from the mixture energy conservation equation. In their analysis, Staub and Zuber [94] assumed that the flow parameters, C_o and $\bar{V}_{gj}$, exhibit a tendency to remain constant along the flow tube. Using an x-ray beam, Zuber et al. [95] measured the steady-state axial distribution of average void fraction as well as the void response to oscillatory heat input at constant inlet flow and negligible inlet subcooling.

The data so obtained were shown to be in satisfactory agreement with the corresponding analytical prediction.

Hancox and Nicoll [24,100] adopted Zuber's cross-sectionally averaged form of the conservation laws and extended his analysis to include flows with non-zero inlet subcooling and developing void and velocity radial profiles. They assumed negligible local drift velocity and used constitutive equations to describe the wall shear stress and void-velocity radial distributions. They developed a semi-empirical relation for the vapour generation function employing a simplified model similar to that presented by Larsen and Tong [101]. In this analysis,the influence of the non-uniform radial distributions of void and velocity was taken into account by means of the distribution parameter, C_o, which was assumed to be a function of $\langle\alpha\rangle$.

Gonzalez and Lahey [102] and Hopkinson [103] discussed the transient behaviour of two-phase flow systems. Gonzalez and Lahey considered the case of a heated channel with an exponential decay in the inlet flowrate and a constant heat flux in both time and space. This is, in fact, representative of a pump rundown type of accident in nuclear reactors. Assuming that the phases were in thermal equilibrium, they developed a solution for the system flow and quality at each point in space and time during the exponential flow decay transient.

Shiralkar et al. [18] extended Zuber's propagation model to study the general case of non-saturated conditions, that is, subcooled inlet flow. They used their improved model to obtain a solution for the variation of the vapour volumetric fraction during exponential flow and power transients. They assumed constant values for the flow parameters, C_o and $\bar{V}_{gj}$, over the entire flow tube. According to Zuber and Findlay [17], this assumption holds only if the flow regime does not change during the transient. Thus, their analysis was strictly valid for a given flow regime and did not account for the changes in the flow regime that occurred along the heated channel.

In the analyses developed by Zuber, Gonzalez and Shiralkar, their partial differential equations were solved using the method of characteristics which was found suitable for these types of partial differential equations.

Nassos [68] presented a detailed investigation of the propagation of density disturbances vertically upwards in an atmospheric air-water bubbly flow. A square-wave pattern was imposed on a solenoid value controlling a secondary air flow to generate a regular sequence of density disturbances at low frequencies. He then compared the experimentally measured wave velocities with those predicted from the kinematic wave theory and obtained a fairly good agreement. At low mixture velocities, however, there was a tendency for the experimental values to be greater than the predictions. On the other hand, for large mixture velocities, the reverse trend occurred. Moreover, a plot of the local wave velocity as a function of the radial position showed flat

profiles; the wave velocity was found to decrease only quite close to the tube wall. This justified the use of cross-sectionally averaged values of the wave velocity. In addition, the experimental data indicated that the wave velocity was relatively independent of the axial location along the flow tube.

The steady-state experiments performed by Nassos [68] and by Malnes [29] showed that the cross-sectional average gas velocity, $\langle j_g \rangle$, was a function of the cross-sectional average void fraction, $\langle \alpha \rangle$, and mixture velocity, $\langle j_m \rangle$. This dependence means that the wave velocity, which is equal to the tangent to $\langle j_g \rangle - \langle \alpha \rangle$ curves at constant $\langle j_m \rangle$, is also a function of both $\langle \alpha \rangle$ and $\langle j_m \rangle$. Hence, the void disturbances may either spread or steepen and it is even possible for void fraction discontinuities to develop similar to shock waves in gas dynamic flow.

Nassos [68] also found that the experimentally measured decay rates of perturbation waves were considerably higher than the corresponding values which were predicted from the kinematic wave theory. He attributed the discrepancy to the axial turbulent diffusion of the gas which was not considered by the theory. He, then, introduced an axial diffusion term into the gas continuity equation by replacing the average gas velocity by $\langle j_g \rangle - k \frac{\partial \langle \alpha \rangle}{\partial z}$, where k was defined as the turbulent diffusion coefficient for the axial gas transport. This analysis demonstrated that, in some cases, a void perturbation could become more concentrated due to the formation of a shock wave and then spread out when the diffusion effect became dominant.

(2.2.3) Two-Phase Slip Models

In vertical two-phase flow systems, the average velocities of the phases are not equal. Consequently, the two-phase mixture in motion in a vertical tube is not of the same overall composition as that admitted to or released from the tube even under steady-state conditions. This phenomenon has been identified by the term gas or vapour slip. In general, the phase of lower density tends to slip past that of higher density. This means that in the case of a gas-liquid system, the gas phase travels a little faster than the homogeneous mean and occupies a smaller part of the tube cross-section. Conversely, the liquid phase travels a little slower than the mean and occupies a larger part of the tube cross-section than would otherwise be expected. Furthermore, since the concentration of the gas phase is usually highest at the tube center where the velocity is highest, the average velocity of the gas phase would be greater than that of the liquid phase. The slip in a two-phase flow system can, then, be considered as a result of two effects; the difference in the gravitational forces acting upon the phases, i.e., local slip and the existence of void and velocity gradients.

To account for the slip phenomenon, an important parameter, called the velocity slip ratio and denoted by S, is defined as the ratio of the weighted mean velocities of the phases. Therefore,

$$S = \frac{\bar{v}_g}{\bar{v}_\ell} , \qquad (2.19)$$

where

$$\bar{v}_g = \frac{\langle v_g \alpha \rangle}{\langle \alpha \rangle} , \qquad (2.20\text{-a})$$

and

$$\bar{v}_\ell = \frac{\langle v_\ell (1-\alpha) \rangle}{\langle (1-\alpha) \rangle} . \qquad (2.20\text{-b})$$

The slip ratio can be used to relate the void fraction to the flowrates of the phases in two-phase flow systems. Because of the important role that void fraction has in these systems, considerable effort has been devoted to study both void fraction and slip ratio.

Several models have been developed to predict the magnitude of the slip ratio in both boiling and adiabatic systems. By neglecting the effect of the local relative velocity between the phases, Bankoff [71] interpreted the occurrence of the slip as a result of the gas migration to the stream center where the resistance to the flow is minimum and the velocity is maximum. Thus, the gas phase will be transported at a faster rate than it would otherwise if the distributions of the phases were uniform across the flow tube. This means that, according to Bankoff's model, the mean velocity of the gas phase is greater than that of the liquid phase due to the distribution effects alone although at any point the liquid and gas move at the same velocity. Bankoff derived the following expression for the slip ratio:

$$S = \frac{1 - \langle\alpha\rangle}{K - \langle\alpha\rangle} , \qquad (2.21)$$

where K is a flow parameter which is given as a function of system pressure by equation (2.6).

It is evident from equation (2.21) that in order to have a positive real value of the slip ratio, the average void

fraction should be smaller than K. This prediction is in good agreement with Armand's experimental measurements [73] for air-water and steam-water mixtures in forced flow through circular ducts. According to equation (2.21), the slip ratio approaches the value of the reciprocal of the flow parameter, K, as the average void fraction becomes vanishingly small.

As shown by Isbin et al. [104], Govier et al. [105], Thom [106] and Meyer [107], the slip ratio can be used to express the dependence of the void fraction upon the characteristics of the flow system. They proposed the following relation:

$$S = \frac{x}{\langle\alpha\rangle}\left(\frac{1-\langle\alpha\rangle}{1-x}\right)\frac{\rho_\ell}{\rho_g}, \qquad (2.22)$$

where x is the mass quality of the two-phase mixture. Therefore,

$$x = \frac{Q_g\rho_g}{Q_g\rho_g+Q_\ell\rho_\ell}. \qquad (2.23)$$

Combining equations (2.2), (2.22) and (2.23), the slip ratio can be also expressed as

$$S = \frac{\beta}{\langle\alpha\rangle}\left(\frac{1-\langle\alpha\rangle}{1-\beta}\right). \qquad (2.24)$$

Equations (2.22) and (2.24) demonstrate that if the slip ratio is known, the void fraction can be directly determined from the flowrates of the phases. It is also interesting to note that equation (2.24) can be derived from Bankoff's model, equation (2.21), by substituting Armand's expression, equation (2.5).

In his variable-density model, Bankoff [71] neglected the effects of the buoyant forces and assumed that the phases moved with the same local velocity. Such an assumption is not valid in many practical situations. Neal and Bankoff [79] modified this model to treat the case when local slip was appreciable by replacing Bankoff's assumption with one that assumed that the local velocities were proportional. That is,

$$v_g = q\, v_\ell \,, \tag{2.25}$$

where q is greater than unity. This led to the following expression for the slip ratio:

$$S = q\left(\frac{1-\langle\alpha\rangle}{\frac{1}{C_o} - \langle\alpha\rangle}\right). \tag{2.26}$$

Similarly, Levy [21] presented a two-phase flow model, based upon mixing length theory, where he assumed that the local gas velocity was proportional to the local stream velocity, that is,

$$v_g = q'\, j_m \,, \tag{2.27}$$

where q', again, is greater than unity. He then derived the following equation:

$$S = \frac{1-\langle\alpha\rangle}{q'K-\langle\alpha\rangle} \,. \tag{2.28}$$

For the slug flow regime, Neal [108] developed the expression

$$S = \left(\frac{1-\langle\alpha\rangle}{K-\langle\alpha\rangle}\right)\left(1 + KC'\left\{\frac{\Delta\rho}{\rho_\ell F_{r\ell}}\right\}^{1/2}\right) , \tag{2.29}$$

where $F_{r\ell}$ is the Froude number based upon the liquid superficial velocity and is, then, given as

$$F_{r\ell} = \frac{\langle j_\ell \rangle^2}{gD} \quad . \tag{2.30}$$

The constant C' is a flow parameter which has a value of 0.35.

Equation (2.29) emphasizes that the slip in two-phase flow consists of two individual mechanisms. The first is due to the distribution effects whereas the second is due to the buoyancy effects. Equation (2.29) can also be put in the form

$$S = S_1 S_2 \quad , \tag{2.31}$$

where

$$S_1 = \frac{1-\langle\alpha\rangle}{K-\langle\alpha\rangle} \quad , \tag{2.32}$$

and

$$S_2 = 1 + KC' \left(\frac{\Delta\rho}{\rho_\ell F_{r\ell}}\right)^{1/2} \quad . \tag{2.33}$$

Here S_1 is the part of slip due to the spatial correlation between the void and velocity and S_2 is due to the buoyant forces. Neal's model tends to Bankoff's original model, equation (2.21), if the buoyant forces are assumed not to be large enough to affect the slip. For horizontal flow, the buoyant forces are at right angles to the flow direction and, hence, do not contribute to the slip. Then, both models become identical.

Griffith [109] derived the following equation for the slip ratio in two-phase slug flow:

$$S = 1 + \frac{V_b A}{Q_\ell} \quad , \tag{2.34}$$

where V_b is the velocity of the slug bubbles with respect to the liquid ahead of them which was expressed by Griffith as

$$V_b = 0.2 \left(\frac{Q_\ell + Q_g}{A}\right) + 0.35 \sqrt{gD} \quad . \tag{2.35}$$

Zuber and Findlay [110] defined a local drift velocity, equation (1.6), to account for the relative motion between the phases. Combining equations (2.13), (2.19) and (2.20), the slip ratio can be written as

$$S = \frac{\langle j_g \rangle}{\langle j_\ell \rangle} \left(\frac{1-\langle \alpha \rangle}{\langle \alpha \rangle}\right) \quad , \tag{2.36}$$

which upon substituting from equations (2.12) and (2.14), the following expression for slip ratio can be derived from Zuber's model:

$$S = (1-\langle \alpha \rangle) / \left(\frac{1}{C_o + \frac{\bar{V}_{gj}}{\langle j_m \rangle}} - \langle \alpha \rangle\right). \tag{2.37}$$

Equation (2.37) simplifies to Bankoff's expression, equation (2.21), if the Bankoff's flow parameter, K, is replaced by $\left(\frac{1}{C_o + \bar{V}_{gj}/\langle j_m \rangle}\right)$. Using equation (2.14), equation (2.12) can also be written in the form

$$\frac{\langle j_g \rangle}{\langle j_\ell \rangle} = \frac{C_o + \bar{V}_{gj}/\langle j_\ell \rangle}{\frac{1}{\langle \alpha \rangle} - C_o} \quad . \tag{2.38}$$

Substituting equation (2.38) into equation (2.36) yields

$$S = \left(\frac{1-\langle\alpha\rangle}{\frac{1}{C_o} - \langle\alpha\rangle}\right)\left(1 + \frac{\bar{V}_{gj}}{\langle j_\ell\rangle C_o}\right) , \qquad (2.39)$$

which tends to Neal's model, equation (2.29), for the slug flow regime if $\bar{V}_{gj}$ is equated to the Taylor rise velocity, $C'\sqrt{\frac{gD\Delta\rho}{\rho_\ell}}$, and C_o is taken as the reciprocal of Bankoff's parameter, i.e., $\frac{1}{K}$.

Brown et al. [111] proposed a model to predict the slip ratio in the cocurrent upward gas-liquid bubbly flow regime. The model was based on the assumption that the local slip velocity was constant and the radial distributions of liquid velocity and void fraction could be represented by the following equations:

$$\alpha = \alpha_c\left[1 - K_1 \left(\frac{r}{R}\right)^2\right] , \qquad (2.40\text{-a})$$

and

$$v_\ell = v_c\left[1 - K_2 \left(\frac{r}{R}\right)^2\right] . \qquad (2.40\text{-b})$$

They, then, arrived at the equation

$$S = \frac{v_\infty}{\bar{v}_\ell} + \frac{1-\langle\alpha\rangle}{K'-\langle\alpha\rangle} , \qquad (2.41)$$

where

$$K' = \frac{(2-K_1)(2-K_2)}{2\left(2-K_1-K_2+\frac{2}{3}K_1K_2\right)} . \qquad (2.42)$$

In his momentum exchange model, Levy [112] derived the following equation for the slip ratio:

$$S = \sqrt{\frac{\langle\alpha\rangle}{2} \quad (\rho_\ell/\rho_g)} \ . \qquad (2.43)$$

According to the above equation, the slip ratio may be expected to vary with the square root of the density ratio of the phases ; a dependence once proposed by Untermeyer [113]. Furthermore, as can be seen from equation (2.43), Levy's model demonstrates that at a certain system pressure, the slip ratio is not constant but increases with the void content. This is in agreement with the prediction of Martinelli and Nelson [114].

Zivi [115] and Thom [106], on the other hand, indicated that for a constant system pressure, the slip ratio could be taken as almost constant and independent of the two-phase quality. Zivi proposed the following expression for the slip ratio:

$$S = \left(\frac{\rho_\ell}{\rho_g}\right)^{1/3} \ . \qquad (2.44)$$

Thom showed that the slip ratio could be expressed as

$$S = \frac{1}{\varepsilon} \ (\rho_\ell/\rho_g) \ , \qquad (2.45)$$

where ε was called the slip factor and considered to be constant at any given system pressure. The values of the slip factor, ε, were determined by Thom [106] at different system pressures for steam-water flow in a 1 in. bore horizontal tube. At a pressure of 14.7 p.s.i.a., the value of ε was found to be 246. Furthermore, Thom [106] obtained a graphical correlation for the slip ratio by plotting the data of Haywood et al.

[116] and his own data [117]. Thom's graphical relationship can be approximated by

$$S = \left(\frac{\rho_\ell}{\rho_g}\right)^{0.2} , \qquad (2.46\text{-a})$$

which is valid for the pressure range

$$300 \text{ p.s.i.a.} \leq P \leq 3000 \text{ p.s.i.a.} \qquad (2.46\text{-b})$$

As reported by Thom [106], Petrick [118] suggested the following approximation for the slip ratio:

$$S = K'' v_i^{n'} , \qquad (2.47)$$

where v_i is the total inlet superficial velocity, and K" and n' are constants which depend only upon the system pressure. Ahmad [88] developed the following empirical correlation which gave the best fit of the experimental data in both subcooled and bulk boiling regions:

$$S = \left(\frac{\rho_\ell}{\rho_g}\right)^{0.205} \left(\frac{GD_e}{\mu_\ell}\right)^{-0.016} . \qquad (2.48)$$

Here G is the mass flux of the two-phase mixture in lb/ft^2 hr, D_e is the hydraulic diameter in ft and μ_ℓ is the liquid viscosity in lb/ft hr. Equation (2.48) is valid for system pressures higher than 140 p.s.i.a. and mixture mass fluxes greater than 3×10^5 lb/ft^2 hr.

Bartolomei and Georgescu [75] concluded, from their water-steam experiments, that at a pressure range of (200-500) p.s.i.a. and a mass flux range of $(3.5\text{-}9)\times10^5$ lb/ft^2 hr, the

dependence of slip ratio on quality was only observed at qualities less than .015. They also found that the slip ratio decreased with increasing pressure and mass flux. These observations agree with what Ahmad predicted by equation (2.48).

Premoli et al. presented a slip correlation which was reported by Hewitt and Semeria [119] as

$$S = 1 + E_1\sqrt{\xi}\left(\frac{1}{1+\xi E_2} - E_2\right)^{1/2} , \qquad (2.49)$$

where ξ is the ratio of the gas-to-liquid volumetric flowrates defined by

$$\xi = \frac{\beta}{1-\beta} , \qquad (2.50)$$

and the remaining parameters are

$$\left.\begin{aligned} E_1 &= 1.578\, R_e^{-.019}\left(\frac{\rho_\ell}{\rho_g}\right)^{0.22} , \\ E_2 &= 0.0273\, W_e\, R_e^{-.51}\left(\frac{\rho_g}{\rho_\ell}\right)^{0.08} , \\ R_e &= \frac{GD}{\mu_\ell} , \\ W_e &= \frac{G^2 D}{\sigma \rho_\ell} . \end{aligned}\right\} \qquad (2.51)$$

Here σ is the surface tension. In the limit when $E_2 = \frac{1}{1+\xi E_2}$, the slip ratio tends to unity.

Fohrman [120] empirically concluded that 75% of his data, which covered a viscosity range of (1.1-500) centipoise, could be correlated within ± 10% by the relation

$$S = 80\ \mu_\ell^{0.3}\ \left(\frac{\beta}{\beta + (1-\beta)\rho_\ell/\rho_g}\right)^{0.77}, \qquad (2.52)$$

where μ_ℓ is in centipoise. It is noteworthy that equation (2.52) does not appear to be correct in the limit for a vanishingly small gas flowrate.

Malnes [29] performed experimental measurements to determine the slip velocity ratio in the vertical upward bubbly flow regime for both atmospheric air-water flow and steam-water flow. These experiments covered water superficial velocities of 0.2 to 2.0 m/sec, air superficial velocities of 0.023 to 2.70 m/sec, void fractions of 0.05 to 0.65 and tube diameters of 2.63 to 5.12 cm for the air-water flow system. For the steam-water flow system, he considered a liquid velocity range of 0.647 to 1.520 m/sec and a pressure range of 20.3 to 59.6 $N/m^2 \times 10^{-5}$. Malnes used different slip models to fit his experimental data and found the following models to be most practical:

$$S = (1-\langle\alpha\rangle)\ \left|\frac{0.249}{\langle j_\ell\rangle} + \frac{0.817}{0.913-\langle\alpha\rangle}\right|, \qquad (2.53)$$

with a standard deviation of 6.4% for air-water flow and

$$S = (1-\langle\alpha\rangle)\ \left|\frac{0.196}{\langle j_\ell\rangle} + \frac{0.970}{0.900-\langle\alpha\rangle}\right|, \qquad (2.54)$$

with a standard deviation of 6.5% for steam-water flow.

(2.2.4) Turbulence Theory in Two-Phase Flow

The models developed for two-phase flow from fundamental turbulence theory have been based on adapting single-phase turbulence theory to two-phase flow systems [20,21,121-126]. Beattie [20] applied the Prandtl's mixing length theory to two-phase flow. In doing so, he assumed that the turbulence existed predominantly in the continuous phase and that the discrete phase contributed negligibly to the Reynold's shear stress. He also assumed a linear relationship between the local void fraction and continuous phase velocity. There appears to be no justification for such a relationship. Furthermore, he neglected the viscous effects which might lead to errors near the tube wall.

By assuming a linear relation between the mixing length and the distance from the tube wall, with a universal proportionality constant, and a uniform radial shear stress distribution, Beattie [20] was able to predict the void and velocity radial profiles for both annular and bubbly flows. The last two assumptions limit Beattie's theory to the wall region. However, as he indicated, inaccuracies due to the two assumptions would cancel each other out and the resulting radial

profiles would apply for most of the tube. These assumptions are still most critical at the tube center where the shear stress should drop to zero. Accordingly, the radial velocity profiles predicted by this theory would not exhibit a zero gradient at the center-line as required for axi-symmetric flow.

Levy [21] treated the two-phase flow as a continuous medium where the turbulent exchanges of momentum and density were assumed to be equal. He,then,applied Prandtl's mixing length model, as modified by Van Driest [127], to obtain an expression for the radial shear stress distribution. The shear stress equation was then integrated to yield the velocity and density radial profiles of the two-phase mixture in the bubbly flow regime. In doing so, Levy [21] used the velocity-density relation derived by Pai [128] in his treatment of the mixing of two gases. Pai arrived at this relation by introducing a diffusion equation and combining it with the continuity and momentum equations. For the annular flow regime, Levy [122] approximated the velocity and density of the two-phase mixture in the core and film regions by their average values. He, then, used a general expression for the Reynold's turbulent shear stress to predict the film thickness.

Tippets [123] studied the interface instability in annular two-phase flow and derived an expression for the film thickness. Levy [122] tried to apply Tippets' expression to the CISE data

but the test results could not be correlated. Levy suggested that the disagreement between Tippets' model and the experimental data resulted from neglecting the mass-transfer component of shear stress.

Calvert and Williams [124] derived an expression for the radial velocity distribution in the film region in an upward cocurrent annular two-phase flow. First, the turbulent shear stress was related to the velocity gradient, by means of Prandtl's mixing length theory, and substituted into the momentum equation. Then by integrating the resulting differential equation, the film velocity radial distribution was obtained. Similarly, Seban and Faghri [125] derived the radial velocity distribution in a turbulent falling film. While Calvert and Williams assumed a simple linear relation between the mixing length and the distance from the tube wall, Seban and Faghri used three different models for the mixing length which were more sophisticated.

Deissler's expression for eddy diffusivity near a solid wall was utilized by Dukler [129] to determine the radial velocity profile in a vertically falling liquid film and, then, to calculate the film thickness. The effect of a counter-current and cocurrent central gas flow was also considered. As indicated by Dukler, combined mechanisms of laminar and turbulent flow should be considered in the liquid film. In the region close to the wall, where the turbulence is damped and the eddy diffusivity becomes relatively small,

the shear stress is proportional to the velocity gradient. At progressively greater distances from the wall, the turbulent momentum exchange effects become more predominant, that is, the eddy diffusivity becomes progressively larger relative to the fluid viscosity. Dukler's approach was adopted by Hewitt [130] to study the case of upward cocurrent annular two-phase flow. Anderson and Mantzouranis [126] used Von Karman's universal velocity radial distribution in the film region of the annular flow regime. Integrating that velocity distribution, they were able to obtain a relation between the film thickness and the film flowrate.

In most of the models mentioned above [20,21,122-124], the mixing length parameter, as determined for single-phase flow, was assumed valid for two-phase flow systems. In single-phase flow systems, the mixing length parameter is exclusively a function of the distance measured from the wall, i.e., it is assumed independent of flowrate and fluid properties. Levy [21] argued that there was no reason to suspect a different behaviour in two-phase flow. The validity of such an assumption will be examined later in this study.

(2.3) Summary and Discussions

From the previous review, it is evident that although the problem of two-phase flow has been studied for a long time, a satisfactory understanding of two-phase flow and boiling

phenomena has yet not been achieved. This is mainly because of the fact that two-phase flow has a complex structure which is generally heterogeneous and usually exhibits large statistical fluctuations. In the present study, an attempt is made to emphasize the important role played by the distribution effects and the discrete nature of two-phase flow. It is hoped that this investigation will provide a clearer insight into the problem and invite more effort to be directed towards a better description of two-phase flow and boiling phenomena.

It can also be concluded that there is a real need to obtain good estimates of the flow parameters which are required in the solution of the void propagation equation. Thus, one can predict the transient response of the average void fraction in a two-phase flow system to different types of perturbations. One of the possible methods which can be used to estimate these parameters requires that fundamental data be obtained about the radial distributions of the mixture velocity and void fraction. While the radial void profile can be measured with a reasonable accuracy, there seems to be no adequate experimental technique which can be used to measure the mixture velocity radial profile in two-phase flow. The conventional techniques which have been employed to measure the radial velocity profile in single-phase flow, e.g., a pitot tube, are not recommended for two-phase flow [29].

The main objective of this work was, then, to develop

an instrumentation technique and a mathematical model and to apply them to determine these profiles. Among the different possible techniques reviewed, the neutron attenuation technique was selected to provide an accurate measure of the radial void profiles without disturbing the flow. On the other hand, Prandtl's mixing length turbulent model was applied together with the momentum conservation equation to calculate the mixture velocity radial profiles. Furthermore, the time-variation of the average void fraction was measured and compared with the corresponding values predicted by the void propagation model.

In the next chapter, the two-phase flow loop, designed to achieve these goals, will be described in detail together with the instrumentation used. Then the design and preparation of the neutron beam port to satisfy, most closely, our objectives are discussed and the types of problems involved are indicated. The safety consideration of working around the neutron beam will be discussed next. Chapter(4) will be devoted to perform some preliminary tests of the neutron attenuation method. First, the neutron beam is calibrated for the working fluids and, then, the sources of error associated with the void fraction measurements are evaluated. Second, the adequacy of the neutron attenuation technique as a diagnostic tool for radial void profile measurements, flow regime identification and flow development testing will be examined.

Chapter (5) will present and evaluate the possible methods which can be used to estimate the fundamental flow parameters. Next a comparison between the results obtained in this study with existing models and correlations, which have been used by various designers to describe two-phase flow behaviour, is performed. In Chapter (6), the void propagation equation is used to predict the void transient response to perturbations in the inlet gas flowrate. Then an analysis is presented to examine the possibility of using steady-state values of the flow parameters, as estimated for fully-developed flow, to predict the behaviour of two-phase flow under dynamic developing-flow situations. Finally, Chapter (7) will review the results obtained in the present study, summarize the pertinent conclusions and then recommend some areas for useful future work.

CHAPTER (3)

EXPERIMENTAL FACILITIES

(3.1) Introduction

The experimental loop was built as a facility for basic research in two-phase flow in the regions where the flow regimes have become fully developed. It was an open (atmospheric pressure), once-through, air-water system. The test tube was made of lucite with three stainless steel sections. This permitted the simultaneous visual observation of the flow regimes through the lucite section and neutron transmission measurement through one of the stainless steel sections.

As outlined in Chapter (1), the experimental investigation carried out in the present study is a part of an overall program to study the formation and propagation of void perturbations in two-phase flow systems. The experimental data obtained for air-water mixtures flowing cocurrently in a vertical circular tube included the following measurements:

(i) gas and liquid flowrates,

(i) pressure drop per unit tube length,

(iii) steady-state void fraction profiles across the flow tube,

(iv) time-variations of the void fraction at the center-line of the tube at two axial locations, and

(v) transient responses of the cross-sectional average void fraction to sudden changes in the inlet gas flowrate.

The adiabatic experimental system was selected since it was expected that it would be sufficient to satisfy the objectives of the course of study presented here. In spite of its simplicity and low cost, it was expected to provide useful experimental data and beneficial insight into two-phase flow phenomena. One further advantage of this system over one involving a boiling liquid is that it requires less time to return to an initial condition after a transient experiment has been performed. However, as mentioned in Chapter (1), it is recognized that construction of a boiling rig is required to test the different aspects of heated systems which is the main objective of the overall program.

(3.2) Air-Water Loop

(3.2.1) General Description

The experimental loop had to accommodate the defined range of air and water flowrates and should be leak tight. It was used to study two-phase flows of air volumetric flux of up to 32 m/sec and water volumetric flux of up to 80 cm/sec. A schematic layout of the test loop is presented in figure (3.1). It basically consisted of an air supply and its metering system, a water supply and its metering system, a liquid-gas mixing unit, a test section and a two-phase separating unit. A detailed description of these components will be presented below.

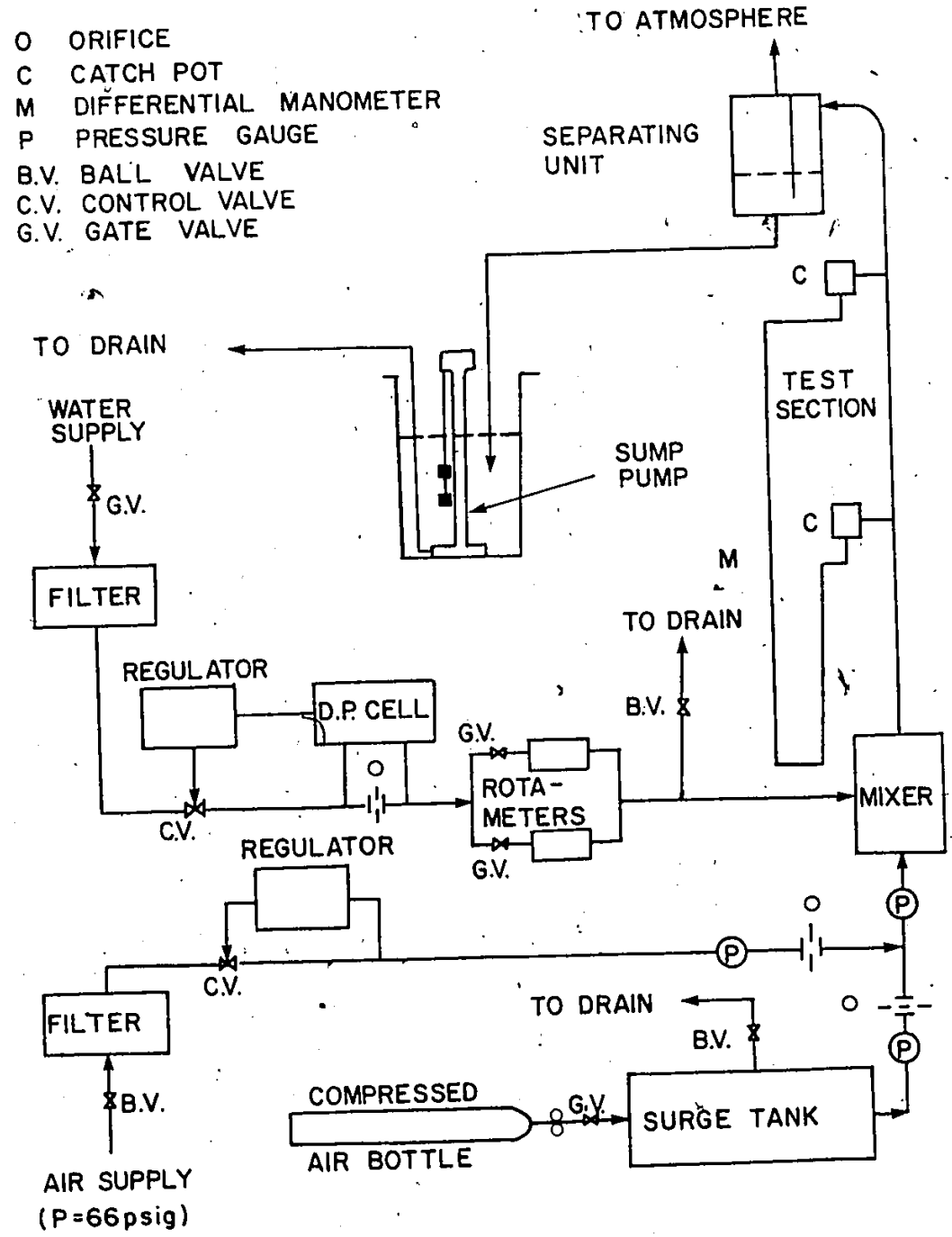

Figure (3.1): Schematic layout of the test loop.

(3.2.2) Air/Water Supply

The two-phase flow mixture was generated by mixing separate sources of air and water. Air was supplied to the loop mainly from the air supply on site at a pressure of 66 p.s.i.g. Because of the limited amount of air which could be obtained from this supply, three compressed air bottles were manifolded to provide additional air when required. This proved to be necessary to generate fully-developed annular flow at different water flowrates. Air passed through a 5 micron filter to remove entrained water, oil and dust particles. A sonic, or critical flow, orifice was used to measure the air flowrate. At the sonic orifice, the upstream pressure was controlled by a control valve(*) and a pressure regulator (0-100 p.s.i.g.). Depending upon the range of desired air flowrates, two interchangeable control valves were used (1/4 in. or 1/2 in.). This control system provided stable operating conditions for air velocities of 0.1 to 32 m/sec in the test section (air mass flowrates from 0.034 to 11 gm/sec).

Water from the main water supply was filtered through a 5 micron filter. Its flowrate was automatically controlled by one of two control valves (1/4 in. and 1/2 in.) which was regulated by a differential controller (0-100 in. water). This differential controller used the pressure drop across a 1/4 in. orifice as its measurement. The actual flowrates of water were

---

(*) The details of the equipment are given in Appendix (A).

measured by two calibrated rotameters mounted on a control panel. The range of water flowrates was 8.6 to 230 gm/sec which provided water velocities between 3 and 80 cm/sec in the test section.

(3.2.3) Flowrate Measurement

The water flowrate was measured by one or both of the rotameters. This system allowed an accurate measurement of water flowrate over a wide range. The smaller rotameter had a maximum flowrate of 0.6 Imp. gpm whereas that of the larger one was 4 Imp. gpm. They were calibrated on site by collecting and measuring the volume of the discharged water over fixed periods of time. The calibration curves are given in figure (3.2-a).

The air flowrate was measured by means of sonic orifices which were fabricated from brass, in the department's machine shop, according to ASME specifications [131]. These orifices were selected mainly because of their advantage of eliminating the effects of downstream pressure oscillations on the metering and control system. The mass flowrate of air through these orifices, $\dot{m}$, may be predicted from the expression [132]

$$\dot{m} = \frac{C\, A_0 P_1}{\sqrt{T}} \text{, if } P_2/P_1 \leq 0.53 \text{ ,} \qquad (3.1)$$

where A_0 is the cross-sectional area of the orifice throat, P_1 and P_2 are the upstream and downstream pressures, respective-

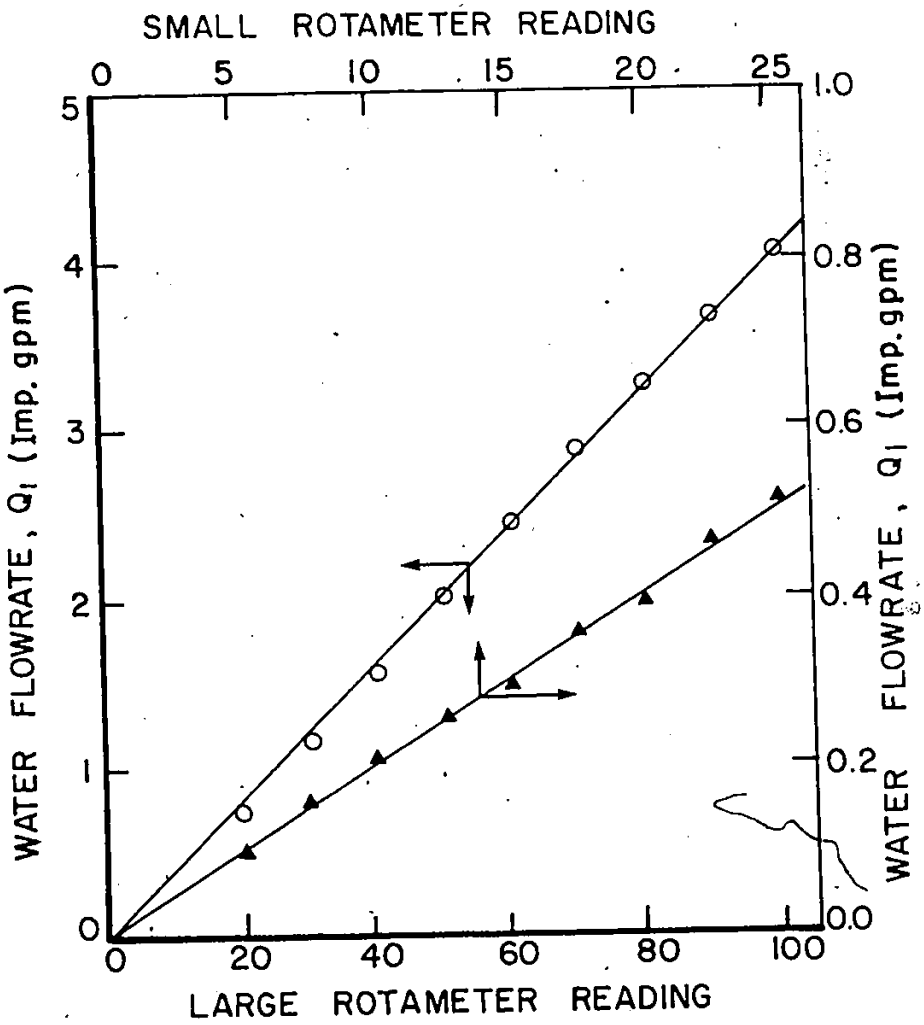

Figure (3.2-a): Calibration curves of the water rotameters.

ly, T is the absolute air temperature and C is a calibration constant which should be near unity for a well-designed orifice.

To cover the desired range of air flowrates, with the range of upstream pressures that could be applied, four critical orifices were manufactured with throat diameters of 0.0135, 0.019, 0.125 and 0.2 in. These orifices were held between brass flanges. The upstream pressure was measured using an accurate 10 in. diameter pressure gauge of 0.5 p.s.i. graduations and 0-500 p.s.i. range. A less accurate pressure gauge was located downstream to ensure that the pressure ratio was actually below the critical value.

The two smaller orifices were calibrated using a wet test meter. The two larger ones were calibrated using the department's calibration facility with two calibrated flow nozzles (diameters 0,516 and 1,25 in.). The calibration curves are shown in figure (3.2-b).

(3.2.4) Air-Water Mixer

The metered air and water streams were introduced into a mixing unit to provide the desired two-phase flow mixtures. The details of the mixing unit/test tube assembly are given in figure (3.3) and summarized in table (3.1). The mixing unit was specifically designed for given flow regimes in an attempt to stabilize any given flow regime quickly. This is because only a relatively short entrance section of 40 in. long could be accommodated upstream of the neutron port level on the

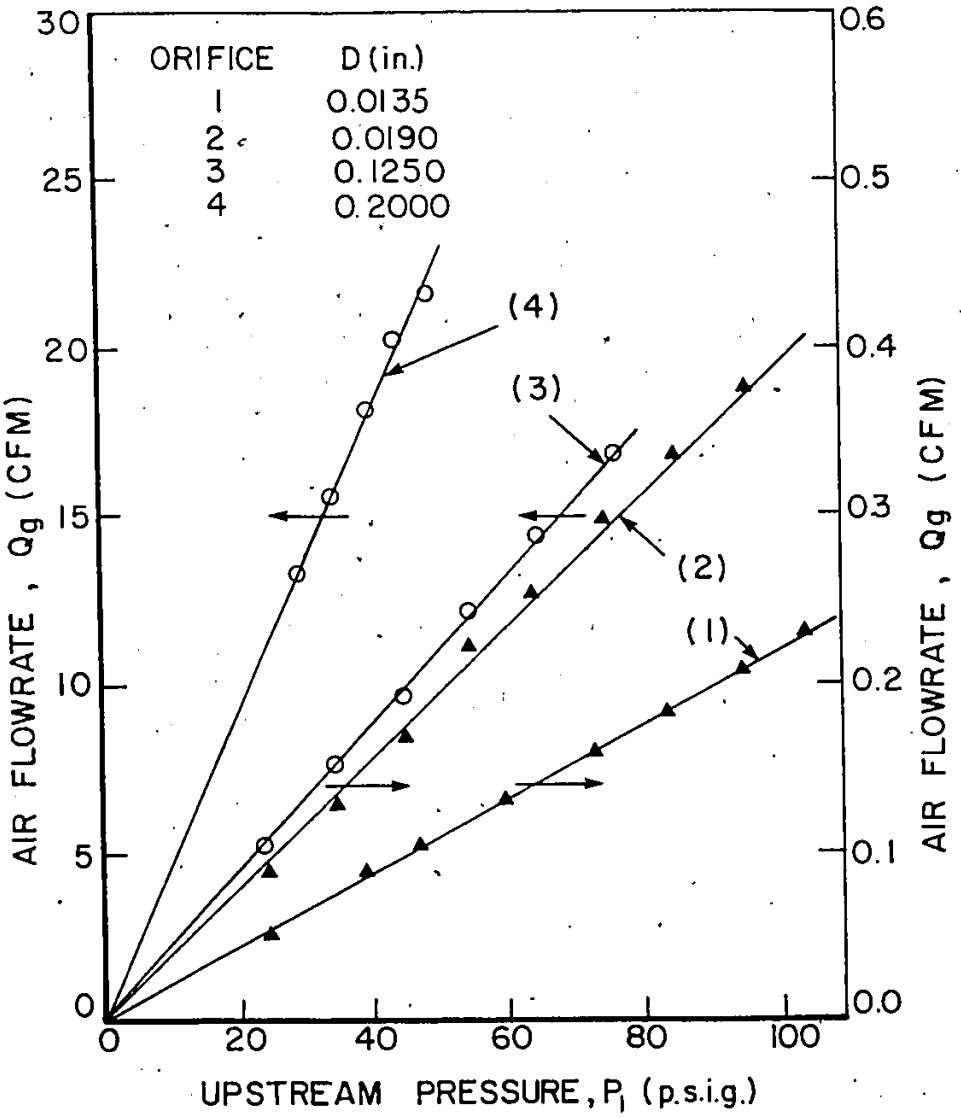

Figure (3.2-b): Calibration curves of the sonic orifices.

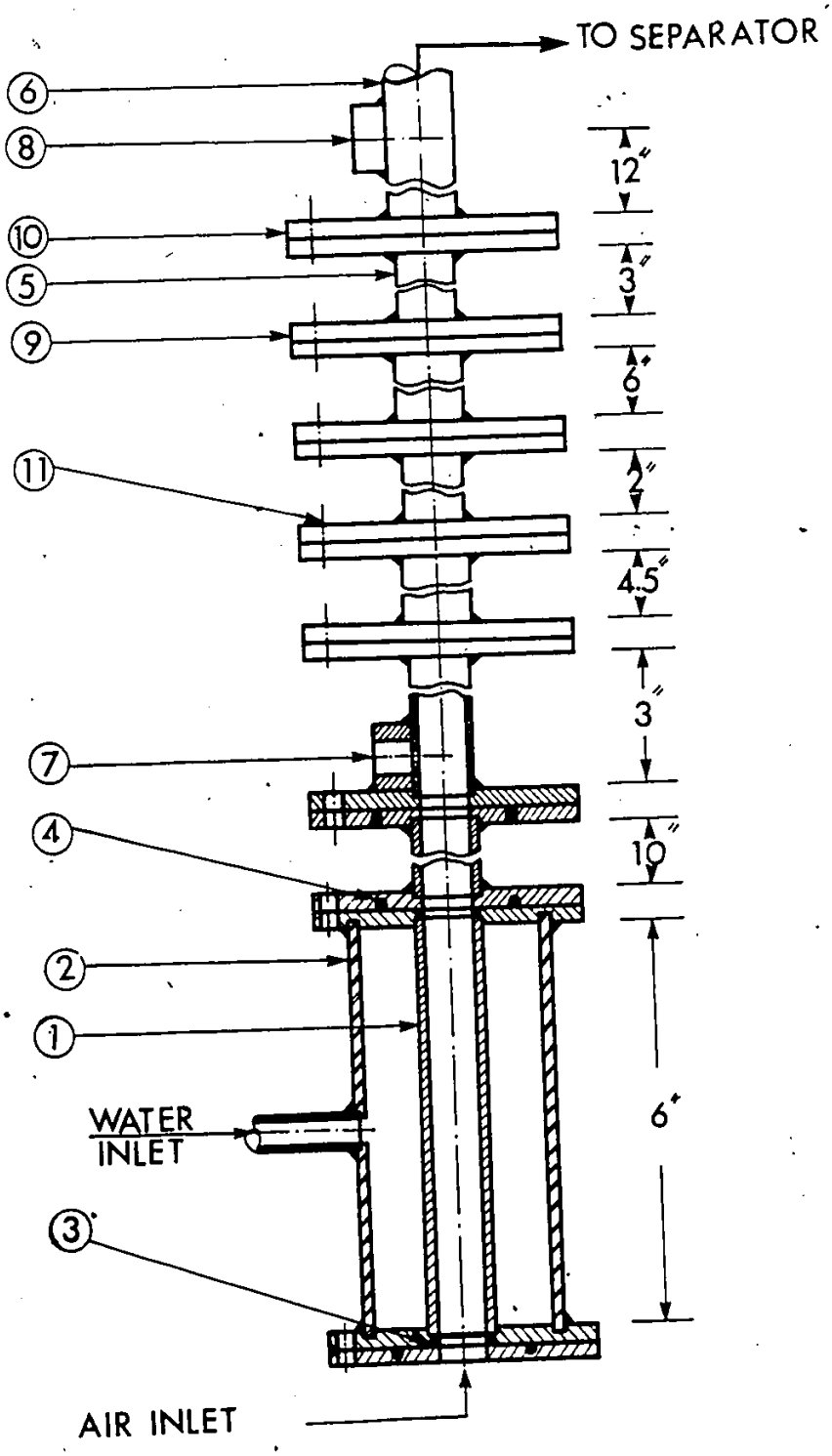

Figure (3.3): Mixing unit/test tube assembly.

Component No.	Component Specifications
(1)	Mixer Inner Sintered Tube (3/4 in. I.D. by 1 in. O.D.)
(2)	Mixer Outer Tube (3 in. O.D. by 1/8 in. Thick)
(3)	Rubber O-Ring (1 in. D. by 1/16 in. Thick)
(4)	Rubber O-Ring (2 in. D. by 1/16 in. Thick)
(5)	Stainless Steel Tube (3/4 in. I.D. by .045 in. Thick)
(6)	Lucite Tube (3/4 in. I.D. by 1 in. O.D.)
(7)	Stainless Steel Pressure Tap (1/2 in.-to-1/6 in. D.)
(8)	Lucite Pressure Tap (1/2 in.-to-1/16 in. D.)
(9)	Stainless Steel Flange (4 in. D. by 1/4 in. Thick)
(10)	Lucite Flange (4 in. D. by 1/4 in. Thick)
(11)	Steel Bolts and Nuts (1/4 in. D.)

Table (3.1): Summary of the component specifications of the mixing unit/test tube assembly.

nuclear reactor. The mixer consisted of two concentric cylinders of 6 in. long. The inner cylinder was made of a 3/4 in. I.D. by 1 in. O.D. porous (sintered) stainless steel tube having a 40 micron pore size; hence, it was of the same internal diameter as the test section and formed a continuous channel with it. It was easily removed for cleaning and/or replacement although this was minimized since the fluids were filtered upstream of the mixer with 5 micron filters. A 3 in. I.D. by 6 in. long cylinder was located concentrically around the inner porous tube. The two fluids were introduced into the mixing unit in a different manner depending on the flow regime desired.

In the bubbly flow regime, water stream was injected through the walls of the central tube of the mixing unit. In order to obtain small air bubbles characterizing bubbly flow, the air stream was injected through a sintered cap, of 5 micron pore size and 5/8 in. diameter, located concentrically inside the inner tube.

Similarly, in the annular flow regime, water was also injected through the periphery of the porous tube. The air, on the other hand, was allowed to flow directly to the bottom of the 3/4 in. I.D. central tube of the mixer from a 3/4 in. elbow. It was found that the injection of water uniformly on the wall to the continuously flowing air stream ensured an evenly distributed film of water at the wall and fully-developed annular flow was established very quickly.

Since the slug flow regime was expected to be an intermediate situation between the above two flow regimes, both mixing configurations were tried. It was found that it was much easier to get slug flow with the second configuration with smaller air flowrates than with the first with larger air flowrates. However, as indicated by Griffith and Wallis [74], entrance effects can persist for great lengths, e.g., for a length of 300 tube diameters, in developing the slug flow regime. For this reason, fully-developed slug flow was not expected to be achieved at the level of the extracted neutron beam. However, experimentation with this flow regime provided a good test to evaluate the neutron attenuation technique as a method to establish if the flow was fully developed or not.

(3.2.5) Flow Development

It was assumed that fully-developed bubbly and annular flows could be established in the bottom 30 in. (40 tube diameters) of the test section. Although it may be desirable to provide a longer flow-developing section, this was prevented by the location of the neutron beam port and, thus, the void fraction measurements were made at this level. As will be demonstrated later, the statistical fluctuations inherent in the transmitted neutron intensity, after passing through the flow tube, were used to show that the flow was fully developed at the 30 in. level when the flow was in the bubbly or annular flow regime. On the other hand, fully-developed slug flow

was not achieved within this short entrance section and, consequently, its study was not attempted.

(3.2.6) Test Section

As has been mentioned, the main objectives of the experimental work were to simultaneously measure the axial pressure drop, the radial void profiles and the flowrates, and to identify the flow regimes present under these flow conditions. To satisfy these objectives, the test flow tube (figure (3.3) and table (3.1)) was comprised of 3/4 in. I.D. by 1 in. O.D. lucite tubing which contained three stainless steel sections (3/4 in. I.D. by .045 in. wall). These materials were used, first, to allow visual observation of the flow regime and, secondly, to provide a material which exhibited relatively low neutron attenuation and induced gamma radiation. Lucite is also easily machined and compatible with the fluids and temperature levels employed. Unfortunately, it attenuates thermal neutrons appreciably. During the early part of the program, an aluminum test section was used because of its even lower attenuation characteristics. However, the chlorine in the tap water caused excessive pit corrosion of the aluminum and so it had to be replaced by stainless steel.

The stainless steel and lucite sections of the test tube were connected by means of 4 in. diameter flanges. The bores of these sections were accurately matched to minimize flow disturbances; this was especially important when operating in the annular flow regime. The connecting flanges were sealed

with interlocking rubber O-rings; thus, the transition from lucite to stainless steel was made with essentially a continuous inside tube wall.

The test section was supported along its length by means of steel clamps, brackets and tubes which ensured that the test section was straight, vertical and free to move vertically and horizontally. As indicated by Butterworth [133], if the flow tube deviates even slightly from the vertical, appreciable asymmetry can develop in the flow. Hence, the supporting clamps were carefully adjusted until the tube was vertical,as indicated by a vertical cathetometer. Flexible lines were used to connect the test tube with the other fixed lines to allow movement of the test tube and to provide mechanical isolation from vibration.

The test tube could be moved vertically for a distance of about 17 in. in two steps by raising the mixing unit, the test tube and the separating unit. This was done in order to check the development of the flow. Furthermore, the test section was easily moved horizontally to allow the measurement of radial void profiles at any axial position. This movement was measured by means of a 3 in. diameter dial gauge of 0.001 in. graduations, 0.1 in. per revolution and 2 in. total range.

The pressure drop over the test section was measured by 85 cm. differential manometers using Meriam fluid (tetrabromoethane, S.G. = 2.95) which is immiscible with water. The lines connecting the pressure taps were kept filled with water

by employing dash pots at the pressure tap locations. These dash pots were constructed from 2 3/4 in. I.D. by 2 3/4 in. long lucite cylinders; they were connected to the test section by 1/2 in. pipes. Their construction allowed any gas which entered them to be separated easily from the liquid; thus, the connecting lines to the manometer were kept free of gas and a constant head of water was maintained over the manometer legs. The pressure tappings in the test section were 32 1/2 in. apart and 1/16 in. diameter. They were made with a sharp high-speed drill and checked to ensure that no burr existed on the fluid side of the tube. Catch pots were also provided to collect the Meriam fluid in case a sudden surge should blow out the manometer. The differential manometer could be read with an accuracy of ±1 millimeter of Meriam fluid.

(3.2.7) Separating Unit

The two-phase mixture was then conveyed by a lucite tube into the side of an 8 in. diameter by 14 in. long lucite cylinder equipped with a 6 in. by 6 in. impingement baffle. The gas was exhausted to atmosphere through an upper outlet; the liquid was drained from a lower one to a polyethylene tank from which it was pumped to the drain. To minimize any disturbance to the flow, the connecting lucite tube was bent, by heating, on a long-radius 90°-bend.

(3.3) Void Fraction Measuring System

(3.3.1) Introduction

A collimated neutron beam, extracted from McMaster's 2 MW Swimming Pool Nuclear Reactor, was used in this study for void fraction measurement. The intensity of the transmitted beam, after it passed through the flow tube, was measured by means of a BF_3 detector placed in line with the beam. The signal generated in the neutron detector was amplified in two stages: First, by a pre-amplifier and then by a linear amplifier. The signals were counted using a dual counter/timer where the count-rates were displayed and then printed by a digital printer connected to the counter. The count-rates were also recorded on a magnetic tape which was connected to a digital ratemeter through an auto-recycle control and magnetic tape interface. The magnetic tape system allowed the collection and analysis of a statistically sufficient amount of data. Figure (3.4) shows a block diagram of the counting system.

(3.3.2) Conditioning of the Neutron Beam

The measurement of void fraction was based on the attenuation of thermal neutrons by water; thus, it was necessary to obtain a well-defined intense beam of thermal neutrons and, at the same time, to ensure that the system was safe for personnel in the area. The following requirements for this beam were specified at the outset:

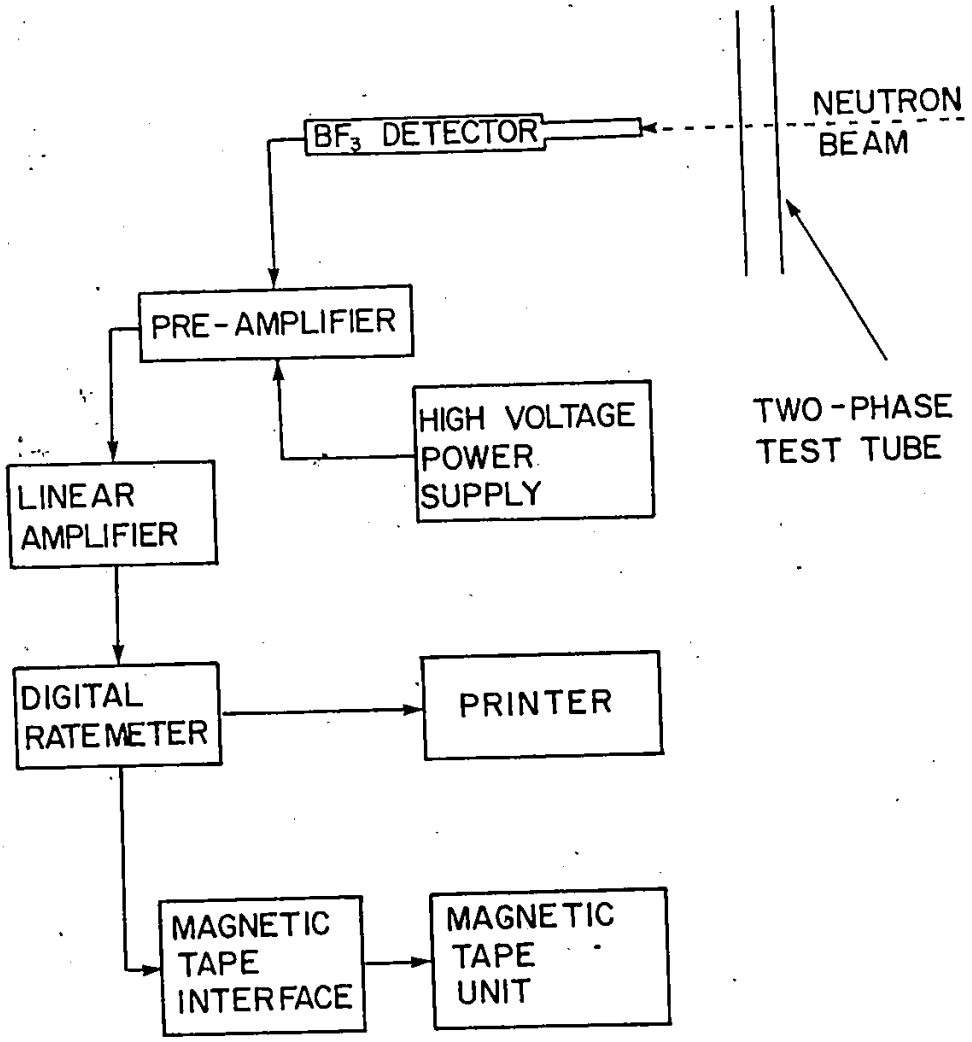

Figure (3.4): Block diagram of the counting system.

(i) The beam should be comprised of essentially only thermal neutrons; gamma radiation should be eliminated and fast neutrons should be thermalized.

(ii) Since local measurements of void fraction were desired, the dimensions of the neutron beam must be small. At the same time, the number of neutrons to be counted must be sufficient to provide good counting statistics over a very short time period (say about 0.01 sec). Hence, the beam size is related to the operating power level of the reactor.

(iii) The system must not constitute any safety hazard to personnel around the reactor.

The McMaster reactor has a number of beam ports located in the concrete structure which contains the light water. The conditioning of the beam was achieved by placing shielding materials in the beam tube, as shown in figure (3.5) and table (3.2). The beam tube was made of aluminum (1 in. I.D. stepped to 2 in.) and centrally located in the beam port where it was held by means of torus-shaped shielding blocks. These blocks were made of borated high-density concrete, encased in aluminum cylinders and employed both to support the beam tube and to provide the required shielding.

Primary and secondary lead polyethylene shielding slugs (6 in. long each) were plugged inside the beam tube in order to attenuate the leaking gamma radiation. To reduce the fast neutron background and to enhance the thermal neutron flux,

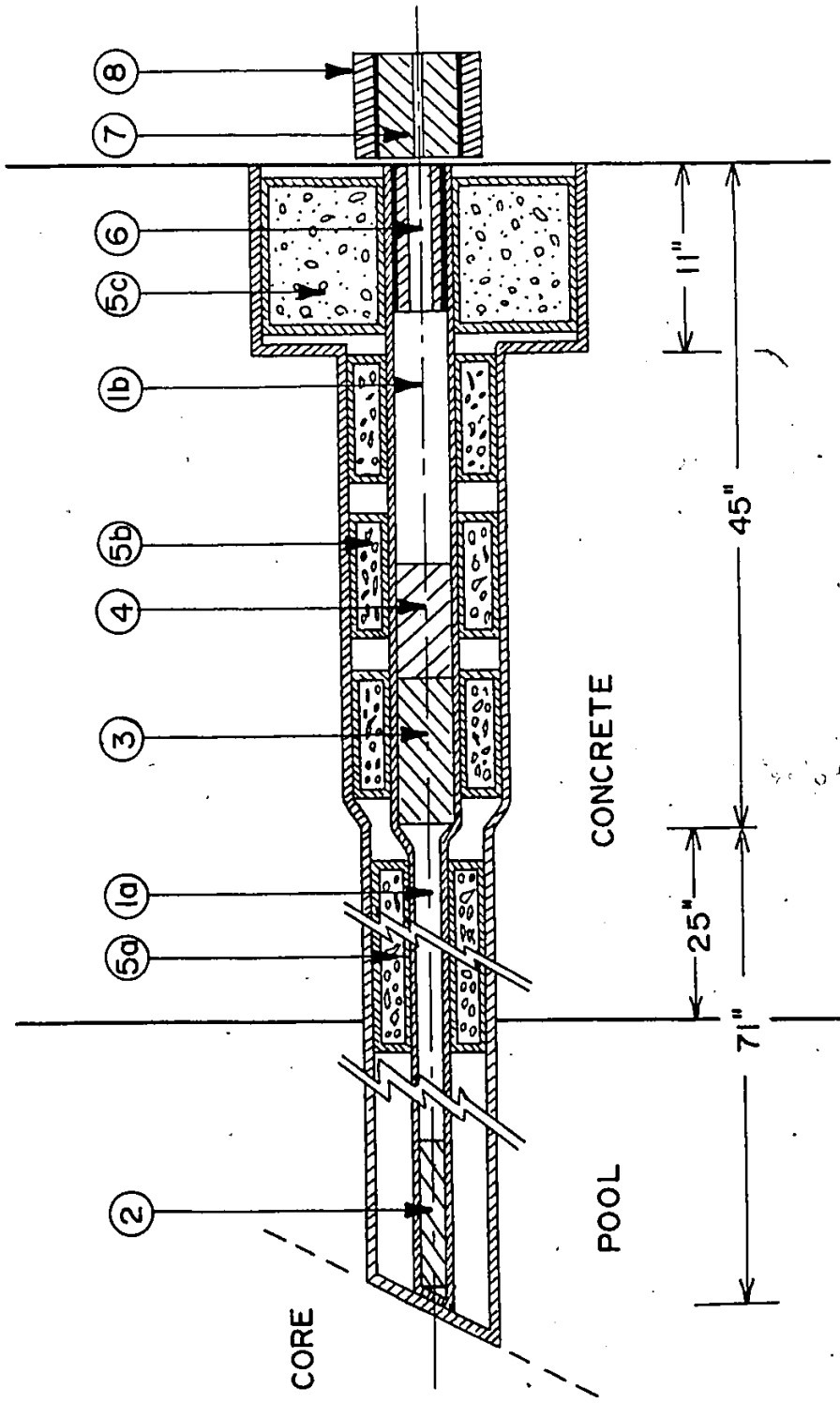

Figure (3.5): Schematic diagram of the neutron beam tube.

Component No.	Component Specifications
(1)	Aluminum Beam Tube a - 1 in. I.D. b - 2 in. I.D.
(2)	Lead Polyethylene Primary Shield (1 in. D. by 6 in. Long)
(3)	Lead Polyethylene Secondary Shield (2 in. D. by 6 in. Long)
(4)	Quartz Crystal Secondary Shield (2 in. D. by 4.5 in. Long)
(5)	Borated Concrete Shielding Blocks a - 6 in. O.D. by 2 in. I.D. by 8 in. Long b - 7 in. O.D. by 3 in. I.D. by 8 in. Long c - 12 in. O.D. by 3 in. I.D. by 10 in. Long
(6)	Boron Polyethylene Collimator (2 in. O.D. by 1 in. I.D. by 6 in. Long)
(7)	Boron Polyethylene Auxiliary Collimator (3 in. O.D. by 4 in. Long and 1/4 in. by 1/2 in. Hole)
(8)	Boron Polyethylene Shutter (4 in. Thick by 4.5 in. Wide)

Table (3.2): Summary of the component specifications of the neutron beam tube.

two different shielding materials were tried: First, graphite slugs and then a natural quartz crystal. These materials were placed next to the secondary shielding blocks (see figure (3.5)) where the radiation damage would not be excessive to the crystal.

To evaluate the effect of using the graphite slugs, the intensity of the emerging thermal neutron flux together with the gamma and fast neutron backgrounds were measured for different graphite thicknesses; table (3.3) summarizes the results of these measurements. As the graphite thickness increases, the emerging fast neutrons are reduced due to their slowing down and the thermal neutron flux also decreases due to out scattering by graphite; on the other hand, the gamma background remains the same. Thus, with this configuration, only a limited improvement in the desired beam characteristics was achieved and an alternative configuration had to be sought.

In the second configuration, use was made of the fact that some crystals (such as bismuth, lead and quartz) attenuate fast neutrons more readily than slow neutrons [134]. At room temperature, quartz was found superior to most of the other crystals as a thermal neutron filter [134]; hence, it was chosen to condition the neutron beam. Table (3.3) also summarizes the results of the corresponding measurements of thermal neutron flux together with gamma and fast neutron backgrounds which were obtained with a 4 1/2 in. long quartz crystal at different reactor output powers. It is evident that while the thermal neutron flux was increased by a factor of about 71, the gamma

Filter Material	Filter Thickness (in.)	Reactor Power (MWT)	Neutron Background (mrem/hr)	Gamma Background (mrem/hr)	Thermal Flux (C/cm^2sec)
Graphite	6	1.5	1000	300	570
	12	1.5	300	300	47
	18	1.5	50	300	32
Quartz Crystal	4.5	0.1	20	22	-
	4.5	0.5	100	100	12923
	4.5	1.0	175	130	26249
	4.5	1.5	200	150	40701

Table (3.3): Performance of the two possible configurations for neutron beam thermalization.

and neutron backgrounds were reduced by factors of 2 and 5, respectively. In summary, the second configuration allowed a beam of thermal neutrons of large area and high intensity to be brought out of the reactor without the need for extensive shielding around the experimentation area.

To reduce the undesirable neutron scattering by the components surrounding the test section, the neutron beam was collimated by a boron polyethylene collimator of 1 in. I.D. by 2 in. O.D. by 6 in. long. Boron was selected because it has an exceptionally high absorption capability for thermal neutrons and relatively soft gamma rays emitted in the absorption process (0.42 Mev). The physical and nuclear properties of boron polyethylene and lead polyethylene were provided by the manufacturers [135].

In order to measure radial void profiles in the 3/4 in. I.D. test section, it was essential to have a beam of much smaller size than 1 in. diameter. Due to the low intensity of the extracted neutron beam and the need to measure its transmitted intensity over short periods of time, the smallest collimated beam that could be used effectively in this application was found to require the dimensions 1/4 in. wide by 1/2 in. high. This was achieved by using a boron polyethylene collimator encased in a 3 in. O.D. by 4 in. long aluminum cylinder. This auxiliary collimator was placed in one of three

3 in. diameter holes provided by a beam shutter. The shutter was made by encasing a 4 in. thickness of boron polyethylene in a stainless steel container; this shutter effectively cut the neutron beam while not in use. To define the neutron beam incident on the detector, a collimator was made of .075 cm thick cadmium sheet and attached to the detector. The detector collimator together with the auxiliary beam collimator acted to precisely define the position of the neutron beam and to adjust the location of the test section relative to the beam.

(3.3.3) Neutron Detection

The fraction of thermal neutrons transmitted through the two-phase flow mixture can be determined by counting the number of neutrons incident on the test section and then those transmitted through it. This can be achieved by placing a neutron detector in line with the extracted neutron beam. The neutron detector should be relatively insensitive to other types of radiations and should respond quickly to changes in thermal neutron flux.

There are different types of detectors which are commonly used to measure thermal neutron fluxes, e.g., BF_3 detectors, chambers coated with B^{10}-enriched solid boron and fission chambers [136]. Each type has its advantages and disadvantages. The fission fragments produced in the fission chambers have large kinetic energies; thus, they produce a large specific ionization and permit monitoring low neutron intensities and discriminating against extremely high gamma fields. The BF_3

detectors, on the other hand, show relatively less discrimination between gamma rays and neutrons. The boron-coated detectors have an advantage over the BF_3 detectors in that they can be filled with more efficient counting gas. However, the sensitivity of a BF_3 detector can be appreciably improved by using a B^{10}-enriched pressurized BF_3 gas and/or increasing the detector size. The main disadvantage of the boron-coated detectors is that the lithium and alpha particles, which are produced, have very small ranges in solid boron; this limits their use to the measurement of high neutron fluxes only.

From table (3.3), it is evident that the conditioned neutron beam has a moderately intense thermal neutron flux with low gamma background. Consequently, based upon the above discussion and the fact that BF_3 detectors have been used satisfactorily in many similar situations of moderate neutron fluxes with gamma fields below 100 rem/hr [135], a BF_3 detector was chosen to be used in this work. It consisted of a 1 in. diameter stainless steel cylinder provided with a concentric electrode and filled with 96% B^{10}-enriched dry boron trifluoride gas at a pressure of 40 cm Hg. The extremely large absorptivity of boron for thermal neutrons, its simple energy dependence in the thermal energy range and its large specific ionization allowed thermal neutron detection even in the presence of gamma radiation.

The detector was encased in a sleeve made of 0.075 cm thick cadmium sheet to which the detector collimator was at-

tached. The sleeve acted to reduce the undesirable interference with the background radiation. The detector was mounted on a stand which provided three-dimensional adjustment of the detector to permit its precise alignment relative to the neutron beam.

To evaluate the contribution of all types of radiations emerging from the beam port other than thermal neutrons, the beam intensities were measured before and after passing through a .075 cm thick cadmium sheet. The results of these measurements at different applied voltages between the detector wall and the central electrode are summarized in table (3.4). The following two observations can be made:

(i) The detector should be operated at about 1400 volts which is clearly within the range of the detector plateau.

(ii) The fraction of the beam which penetrates the thin cadmium sheet at this operating voltage is only .025% of the incident beam; this indicates that the recorded count-rates are mostly due to thermal neutrons.

(3.3.4) Safety Consideration

The main aspect of personnel safety which was considered in this work was the precaution against radiation exposure. Recommendation from the resident Health Physics staff dictated much of the safety precautions. The maximum permissible exposure dose-rate should not exceed 5 rem/year [137]; thus, the equivalent maximum dose-rate is 2.5 mrem/hr for a person

Applied Voltage (Volt)	Unattenuated Beam Intensity (C/sec)	Transmitted Beam Intensity (C/sec)
0	0	0
200	9304	1
400	12580	2
600	26579	4
800	60013	5.5
1000	72138	7.5
1200	80565	11.5
1400	81571	19
1600	82554	38
1800	83550	175

Table (3.4): Effect of placing a 0.075 cm thick cadmium sheet in the beam path at different applied voltages.

whose work may involve continuous exposure to radiation. Under accident condition, however, an exposure of 25 rem or less to the whole body is believed to have no significant effects provided that it occurs only once in a lifetime. Table (3.3) shows that direct exposure to the beam must be completely avoided. Consequently, an additional shield, called the beam catcher, should be installed behind the experimental loop and the counting system to protect workers and persons passing by. The beam catcher was made of borated concrete and it was used to act as a final shield against any leaking gamma or neutron radiation.

As has been mentioned, the interference of the background radiation with neighbouring experiments was minimized by using the primary and secondary shieldings, the quartz crystal and the primary and auxiliary collimators. The effect of the existence of the stainless steel test section in the path of the emerging beam on the level of background radiation was evaluated and found to be unimportant. The background increased by only about 10% at a distance of 6 in. from the test section and remained essentially unchanged at all distances greater than 1 1/2 ft.

In summary, it can be concluded that the shielding facility proved to be sufficient to satisfy the requirements of low background interference with other experiments and to provide a safe working environment.

CHAPTER (4)

PRELIMINARY STUDIES OF NEUTRON ATTENUATION METHOD

(4.1) Introduction

Before using the extracted neutron beam as a diagnostic tool in two-phase flow, some preliminary studies had to be carried out. First, the neutron beam had to be calibrated, i.e., its attenuation parameters and secondary scattering effects for the tube wall and the working fluid had to be evaluated. Second, the effect of the statistical fluctuations of the neutron beam on the accuracy of the void fraction measurement had to be determined. This was necessary in order to ensure good counting statistics and correct sampling time so that the resulting bias in the void fraction measurement was minimized [61]. After this preliminary experimental work, the actual neutron transmittance measurements were carried out in a flowing two-phase fluid system . This was done to evaluate the accuracy of this diagnostic tool for the measurements of radial void profiles, to test its ability to recognize flow regimes and to evaluate its potential to test for fully-developed flow.

(4.2) Neutron Attenuation Parameters and Buildup Factor Measurements

The neutron attenuation parameters for the materials which are to be used must be evaluated. The attenuation para-

meter is defined as the probability per unit neutron path length that the neutron will undergo a collision with one of the material nuclei. Since there is a possibility for the scattered neutron to undergo further scattering processes and return back to the detector path, the neutron buildup factor is introduced to account for the effect of these secondary scattering events. Thus, this factor may be defined as the ratio of the actual neutron flux encountered by the detector to that which would be encountered with simple exponential attenuation describing single collision events.

In order to use the neutron attenuation technique, the attenuation parameters and buildup factor must be determined for the conduit material and the working fluid. The following alternative methods of obtaining these data were considered:

(i) Use the published data [138,139] for these parameters for thermal neutrons in the materials under study.

(ii) Use the values recently measured by the Canadian Westinghouse research group for neutrons extracted from the same beam port as that used in the present study [140].

(iii) Design a special test section of the same material, geometry and orientations as that to be used in the two-phase flow experiments and then determine directly these parameters for the neutron beam which is to be used in the present investigation.

While the neutron attenuation parameter for a material depends only on its nuclear structure and the neutron energy, its buildup factor depends on the medium configuration as well. Since the neutron beam was not comprised of only thermal neutrons, but was expected to have an epithermal component superimposed on its thermal spectrum, the use of the published information for specific neutron energies would lead to appreciable errors. Furthermore, since the water used in this study was taken directly from the city mains, it contained some impurities. These impurities might exhibit appreciable attenuation of thermal neutrons, the accounting of which would be difficult. In addition, the published data as well as the Westinghouse measurements were obtained for planar geometry and, therefore, would not account correctly for the buildup factor in the circular tube used in these experiments. Hence, the attenuation parameters and buildup factor could only be reliably estimated from direct measurements using the actual material with the correct geometry (configuration and known dimensions) and the actual neutron beam which was available.

A special apparatus, as shown in figure (4.1) and with dimensions indicated in table (4.1), was constructed. It consisted of an aluminum tube (1 in. O.D. by 0.117 in. wall) into which an aluminum rod was inserted to form a uniform annulus between the rod and the inside tube wall. Nine

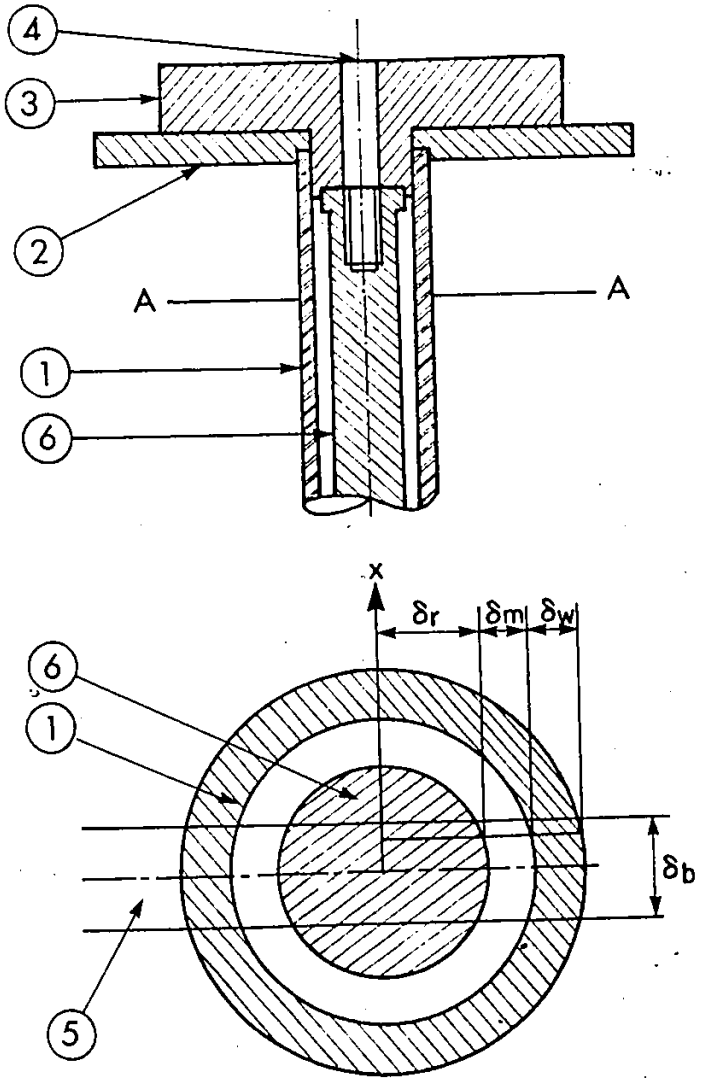

SECTION A-A

Figure (4.1): Schematic diagram of the test section used in neutron attenuation parameters and buildup factor experiments.

Component No.	Component Specifications
(1)	Aluminum Test Tube (1 in. O.D. by 0.117 in. Wall)
(2)	Aluminum Flange (4 in. D. by 1/4 in. Thick)
(3)	Aluminum Base Plate (3 in. D. by 1/2 in. Thick)
(4)	Central Hole (1/4 in. D.)
(5)	Neutron Beam (1/4 in. Wide by 1/2 in. High)
(6)	Aluminium Rod (D_r in. D.)

Rod No.	Dr (in.)
1	0.742
2	0.731
3	0.712
4	0.692
5	0.661
6	0.620
7	0.560
8	0.485
9	0.373

Table (4.1): Summary of component specifications of the test section used in neutron attenuation parameters and buildup factor experiments.

aluminum rods of different diameter were used to provide a range of water thicknesses (table (4.1)). The tolerances on the rod diameter and the tube inside diameter were 0.0005 in. and 0.001 in., respectively. This meant that the maximum error on the smallest water thickness was about 6.3% (0.0015 in.). Concentricity of the rod was ensured to be within 0.001 in. by the hole in the base plate of the rod and by the bolt fixing the rod to the base plate. Neutron transmittance measurements were taken near the bases of the rods where the geometry was best known.

The collimated neutron beam was used to measure the chordal transmittance function through the central portion of the test tube. The chordal transmittance function, T, is defined as the ratio of the intensity of the transmitted beam to that of the unattenuated beam. Both the transmitted and unattenuated intensities were measured in these particular experiments over time periods of 40 sec. Such long counting periods were used in order to reduce the experimental error due to the statistical fluctuations of the neutron beam [61]. The general expression of the chordal transmittance function for a neutron beam of width δ_b at the cross-section A-A, figure (4.1), can be written as

$$T = \frac{1}{\delta_b} \int_{\frac{-\delta_b}{2}}^{\frac{\delta_b}{2}} K_r(x) K_m(x) K_w(x)\, dx \,, \qquad (4.1)$$

where K_r, K_m and K_w are, respectively, the rod, medium and wall transmittance kernels which are given by

$$K_r = \exp(-\mu_r \delta_r) \quad , \tag{4.2-a}$$

$$K_m = B(\delta_m)\exp(-\mu_m \delta_m) \quad , \tag{4.2-b}$$

and

$$K_w = \exp(-\mu_w \delta_w) \quad . \tag{4.2-c}$$

Here the μ's and δ's are, respectively, the attenuation parameters and chordal thicknesses at a distance x from the tube center and $B(\delta_m)$ is the medium buildup factor. The chordal thicknesses are related to the rod diameter, D_r, and the tube inside and outside diameters, D_i and D_o, by

$$\delta_r = \sqrt{D_r^2 - 4x^2} \quad , \tag{4.3-a}$$

$$\delta_m = \sqrt{D_i^2 - 4x^2} - \delta_r \quad , \tag{4.3-b}$$

and

$$\delta_w = \sqrt{D_o^2 - 4x^2} - \sqrt{D_i^2 - 4x^2} \quad . \tag{4.3-c}$$

Since the chance of secondary scattering events increases with the medium thickness and attenuation capability [137], the effect of these events can be considered negligible for the aluminum rods and tube wall. Hence, their buildup factor can be set equal to unity. Furthermore, the gas phase is assumed to exhibit a relatively negligible neutron attenuation. Now consider the following four sets of experiments:

(4.2.1) Aluminum Attenuation Parameter Experiments

The attenuation parameter of aluminum, μ_{al}, was determined by carrying out five chordal transmittance measurements, four of which with the aluminum rods No. (6) to (9) located at the tube center and the fifth with the tube only. The mathematical model given by equation (4.1), with μ_r and μ_w as identical to μ_{al} and δ_m equal to zero, was then used to fit the experimental transmittance measurements, $\underline{T}_{meas.}$ This was done by using a non-linear least-squares program(*) based on Marquardt's algorithm [141] which minimized the weighted sum of squares, SS, given by [142]

$$SS = (\underline{T}_{meas.} - \underline{T}_{expect.})' \underline{V}^{-1} (\underline{T}_{meas.} - \underline{T}_{expect.}), \qquad (4.4)$$

where $\underline{V}$ is the variance-covariance matrix for the measurements. The best estimate of μ_{al} was found equal to 0.0846 cm^{-1}. Table (4.2) summarizes the results of the experimental measurements of the transmittance function together with the corresponding expected values.

(4.2.2) Water Attenuation Parameter Experiment

To determine the water attenuation parameter, μ_m, the annulus formed by the aluminum tube/rod combination was filled with water and the transmittance function was measured. Because the water thickness was not great, .035 in. with No. (2) rod, there was negligible secondary scattering effect and, hence, the buildup factor was expected to be very close

(*) The details of all computer programs used in this study are documented in the Department of Chemical Engineering.

Transmittance	D_{al} (in.)				
	0.620	0.560	0.485	0.373	0.000
$T_{expect.}$	0.8273	0.8348	0.8460	0.8604	0.9503
$T^{(*)}_{meas.}$	0.8277	0.8340	0.8458	0.8610	0.9505

$^{(*)}$Variance = 3.206×10^{-7}

Table (4.2): Measured and expected values of the chordal transmittance for aluminum attenuation parameter experiments.

to unity. At the same time, the relative measurement accuracy of the water thickness was high. With μ_{al} known from the previous subsection, the water attenuation parameter was found from equation (4.1) to be 5.19 cm^{-1}.

(4.2.3) Water Buildup Factor Experiments

It has been customary to express the buildup factor in terms of a power series expansion, the first term of which is set equal to unity to represent the transmitted neutrons which reach the detector without scattering. The higher-order terms, on the other hand, represent the fraction of neutrons scattered back to the beam path, i.e.,

$$B(\delta_m) = 1 + \sum_{i=1}^{r} a_i \delta_m^i , \qquad (4.5)$$

where the r coefficients, $\underline{a}$, must be estimated by performing a least-squares fitting procedure of the transmittance data. Equation (4.5) is empirical without any fundamental basis but has been proven to be very satisfactory [58,60].

Equations (4.1) and (4.5) may be combined to give the following model for the chordal transmittance function:

$$T = f_o + \sum_{i=1}^{r} f_i a_i , \qquad (4.6)$$

where f_o and f_i's are functions of the beam size and energy, rod diameter, tube dimensions and neutron attenuation parameters for aluminum and water. The number of coefficients, r, must be sufficient to ensure that the resulting transmittance model (equation (4.6)) is statistically adequate.

Equation (4.6) demonstrates that the transmittance model is linear in the parameters, $\underline{a}$. Since this model incorporates the empirical expression for the buildup factor, its adequacy needs to be tested. This test was performed by evaluating the variances of the experimental measurements of the transmittance function under several conditions. This was done here by performing five replicated experiments at each of ten different experimental conditions; nine different water thicknesses obtained by inserting different aluminum rods in the tube and one experiment when the tube was filled with water only were used.

The homogeneity of variance of the experimental transmittance data was tested by means of Bartlett's test [142,143], as outlined in Appendix (B). With n = 10 and p = 5, the value of Λ was calculated to be 36.8 while $\chi^2_{.95}(9) = 16.919$ [142]; this showed that the hypothesis that the variance was homogeneous should be rejected. It is known, however, that it is usually possible to transform the experimental data by making

$$T' = T^k \quad , \qquad (4.7)$$

so that the variances of the transformed data are homogeneous. In this case, a number of values of k were tried and k = 2/3 was found to be satisfactory to ensure that homogeneous variances existed (Λ = 5.8 which was less than $\chi^2_{.95}(9)$). The least-squares estimates of the parameters, $\underline{a}$, were determined by using the weighted function Z given by

$$Z = T'/s' \quad , \tag{4.8}$$

where $(s')^2$ is the estimate of the variance on T'.

Three different models of the form presented by equation (4.6) were tried with r equal to 3, 4 and 5, respectively. To differentiate between these models and to check their adequacy to fit the experimental data, an ANOVA test was applied for each case and the results are presented in table (4.3). The terminology used in this table is similar to that usually defined and used in the literature, e.g., [142]. For the 95% confidence limit, it was shown [142] that the criterion for model adequacy can be written as

$$(MS)_L/(MS)_{PE} \leq F_{.05}(d_L, d_{PE}) \quad , \tag{4.9}$$

where the subscripts L and PE stand for the lack of fit and pure error residual terms, respectively, MS is the mean-square, d is the degree of freedom and $F_{.05}$ is the F-distribution function evaluated at the 95% probability with d_L and d_{PE} degrees of freedom. The results which are summarized in table (4.3) indicate that the fourth and fifth-order models are adequate based on the lack of fit test.

To differentiate between these two models, an extra-term test was carried out. It has been shown [142] that an extra term is needed to be added to the fourth-order model if the following condition is satisfied:

$$\frac{(SS)_{R4} - (SS)_{R5}}{s_4^2} > F_{.05}\ (1, d_{R4}) \quad , \tag{4.10}$$

Source		Total	Model (Discrepancy)	Residual	Pure Error Residual	Lack of Fit Residual
SS	3rd Order Model	2.133×10^{7}	2.1326×10^{7}	3.6195×10^{3}	40.000	3.5795×10^{3}
	4th Order Model	2.133×10^{7}	2.133×10^{7}	55.2258	40.000	12.2258
	5th Order Model	2.133×10^{7}	2.133×10^{7}	52.2228	40.000	12.2228
d	3rd Order Model	50	3	47	40	7
	4th Order Model	50	4	46	40	6
	5th Order Model	50	5	45	40	5
MS	3rd Order Model	4.266×10^{5}	7.442×10^{6}	7.7	1.0	511.361
	4th Order Model	4.266×10^{5}	5.3325×10^{6}	1.135	1.0	2.0376
	5th Order Model	4.266×10^{5}	4.266×10^{6}	1.16	1.0	2.4446

Table (4.3): ANOVA table for the transmittance models for water buildup factor experiments.

where $(SS)_{R4}$ and $(SS)_{R5}$ denote the sum of squares of the residuals of the fourth and fifth-order models, respectively, and s_4^2 is the estimated variance of the fourth-order model. The ratio on the left-hand side was found to be equal to 3.06×10^{-3} while $F_{.05}(1,45)$ was 4.08. This analysis proved that an additional term to the fourth-order model should not be included; the small value of the left-hand side of equation (4.10) meant that the extra residual sum of squares, accounted for by adding the extra term, was not significant if compared to the estimated variance. Since the transmittance model was adequate, the residual mean-square could be used as an estimate of the variance.

As an additional test for the adequacy of the model, the dependence of the residuals on the system independent variable (rod diameter) was investigated, as shown in figure (4.2). Since the residuals are randomly distributed about zero, the model is shown to be adequate in all respects. Table (4.4) shows the measured and expected values of the chordal transmittance after being transformed according to equations (4.7) and (4.8).

The best least-squares estimates of the model parameters were found to be

$$\underline{a} = -.144, 4.044, -6.426 \text{ and } 4.378 \ . \qquad (4.11)$$

Figure (4.3) shows the variation of water buildup factor with water thickness, as given by equation (4.5) after substituting the estimated values of the parameters, $\underline{a}$. The figure

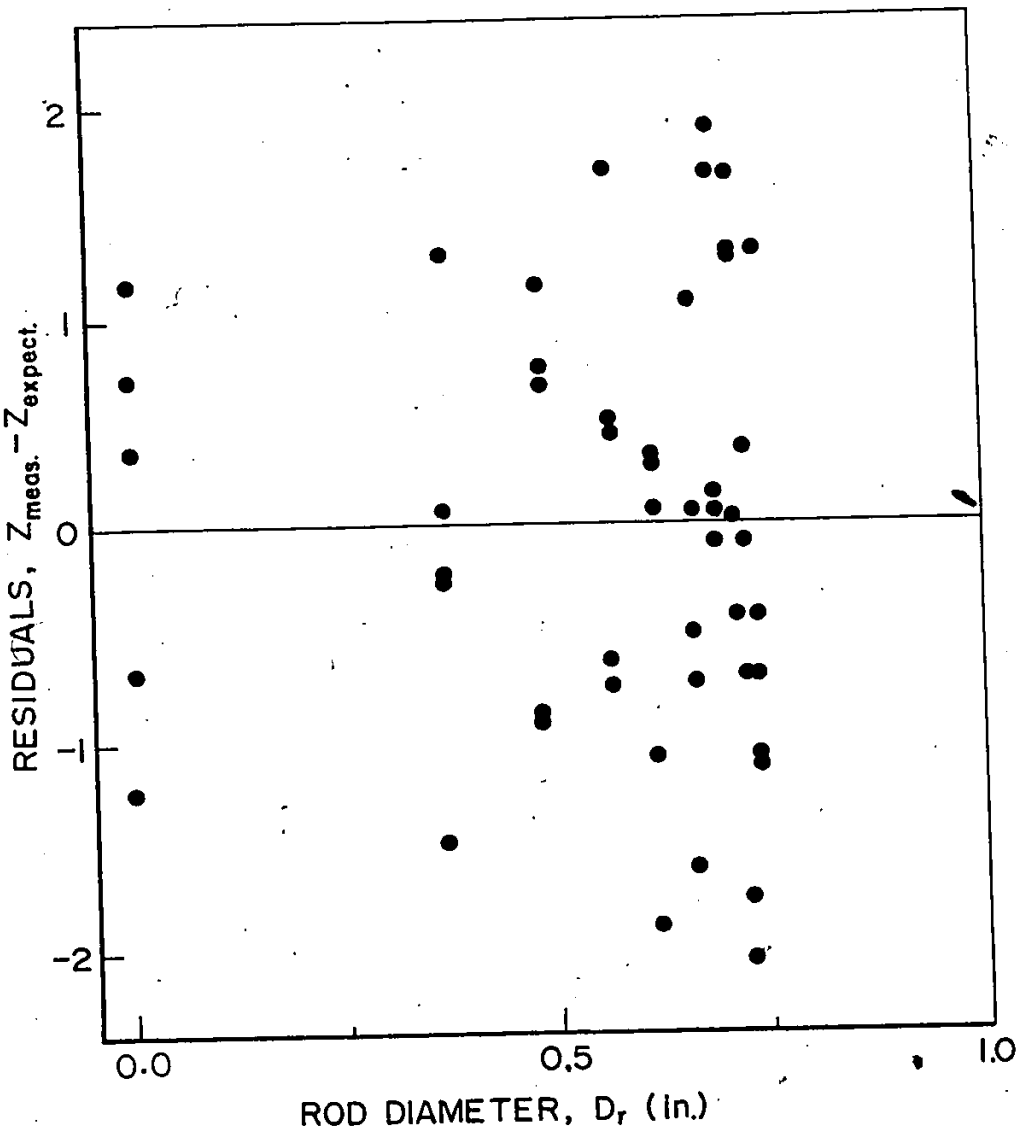

Figure (4.2): Dependence of the residuals on the rod diameter in water buildup factor experiments.

Test No.	D_{al} (in.)	$Z_{expect.}$	$Z^{(*)}_{meas.}$				
			1	2	3	4	5
1	0.742	1195.00	1194.58	1196.30	1194.27	1193.86	1193.91
2	0.731	990.20	989.76	988.40	988.13	989.53	990.55
3	0.712	861.50	862.79	862.79	860.80	861.48	863.14
4	0.692	625.80	625.95	625.86	627.46	627.68	625.51
5	0.661	628.60	628.10	629.67	628.68	626.99	627.82
6	0.620	406.00	405.09	406.30	406.07	404.87	406.31
7	0.560	312.40	311.61	312.85	311.75	314.08	312.83
8	0.485	222.40	221.45	221.48	223.57	223.14	223.07
9	0.373	130.40	130.14	130.44	131.67	128.86	130.18
10	0.000	44.14	42.89	43.47	44.84	44.50	45.32

(*) Variance = 1.135

Table (4.4): Measured and expected values of the transformed chordal transmittance for water buildup factor experiments.

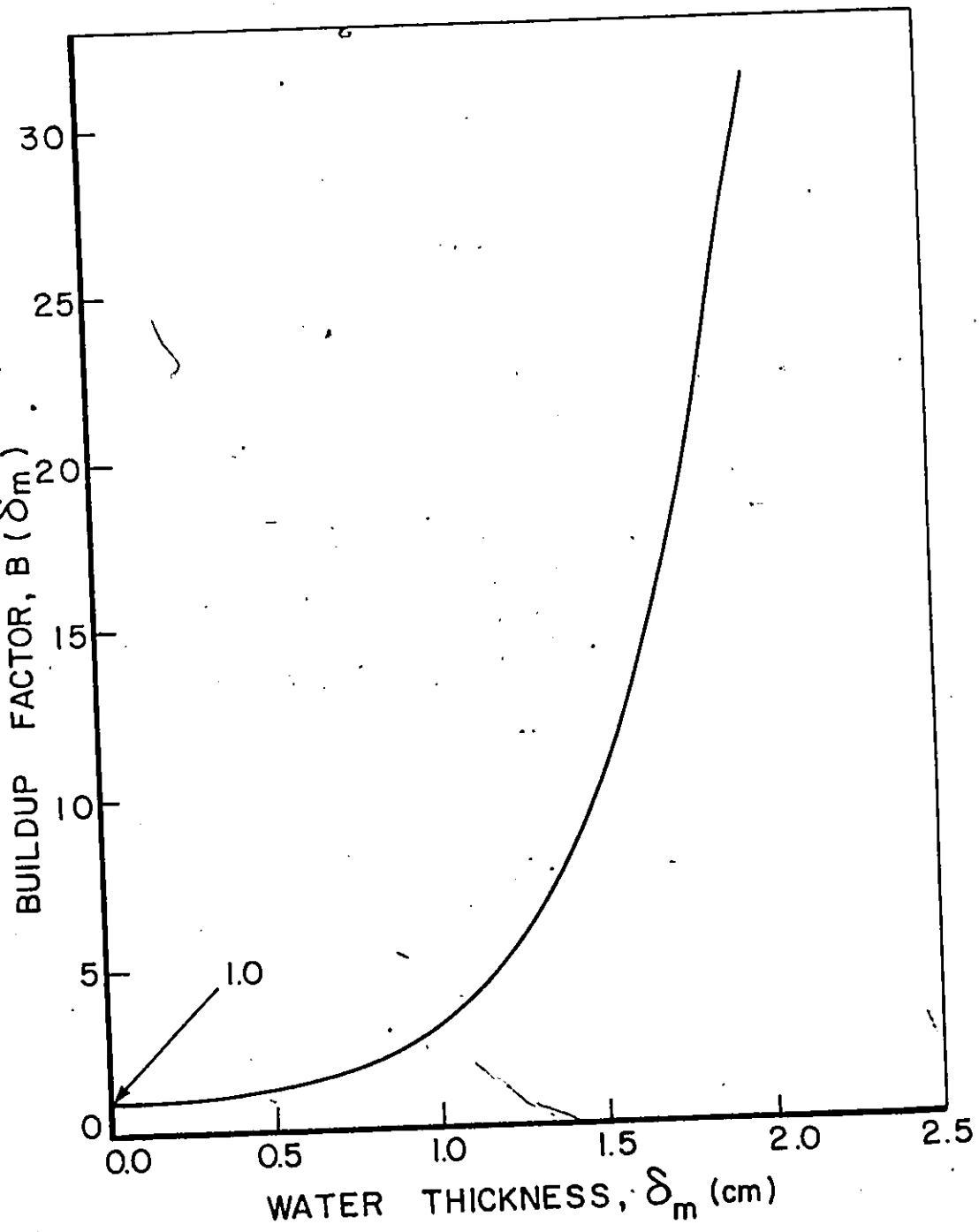

Figure (4.3): Water buildup factor.

demonstrates that this factor remains almost unity until the thickness of water exceeds 0.3 cm. This supports the assumption made concerning the insignificance of neutron secondary scattering events in water medium of small thicknesses.

(4.2.4) Stainless Steel Attenuation Parameter Experiments

As mentioned in subsection (3.2.6), aluminum was found to be incompatible with water from the main supply because of the impurities in it. Consequently, a 304 stainless steel test tube of .75 in., I.D. by .045 in. wall was used. For such a thin tube, the buildup factor can be assumed unity without significant error [136,137]. In these experiments, ten chordal transmittance measurements were made using the four aluminum rods numbered (6) to (9). The details of these experiments are given below.

(i) one measurement with the empty stainless steel tube,

(ii) four measurements with the four aluminum rods in the empty tube,

(iii) four measurements with the four rods in the tube containing water in the annular space, and

(iv) one measurement with the tube completely filled with water.

The general expression for the chordal transmittance given by equation (4.1) was used to predict the transmittance functions in all of the above cases, after making the appropriate simplifications as follows: For the first case, the rod

and water transmittance kernels, K_r and K_m, were put equal to unity. In the second case, the water transmittance kernel was equated to unity whereas in the fourth case, the rod transmittance kernel was taken as unity and the rod diameter, D_r, was substituted by zero. Knowing the water and aluminum attenuation parameters and the water buildup factor from the previous experiments, a non-linear model with one parameter remained, that is, the attenuation parameter for stainless steel, μ_w. Using the non-linear least-squares program, a best estimate of this parameter was found to be equal to 1.08 cm^{-1}. In table (4.5), the measured and expected values of the transmittance function are given.

(4.3) Sources of Error in Void Fraction Measurement

The effect of the statistical fluctuations of the neutron source on the accuracy of the void fraction measurements is investigated in this section. In the general application of radiation transmittance techniques, the usual experimental strategy is to measure the transmitted radiation over a sufficiently long period of time. This is done in order to minimize any statistical sampling variation due to source fluctuations. If, however, the medium density is also fluctuating which is the case in two-phase flow systems, the experimentally measured void fraction can be significantly in error [59]. One alternative strategy is to use a gating technique for the measurement of the transmitted radiation [60]. In this technique,

Transmittance	D_{al} (in.)									
	.000	.373	.485	.560	.620	.620(*)	.560(*)	.485(*)	.373(*)	.000(*)
$T_{expect.}$	.7671	.6634	.6602	.6576	.6559	.5893	.5061	.4068	.3151	.0014
$T_{meas.}^{(**)}$	.7702	.6624	.6585	.6546	.6539	.5961	.5001	.4232	.2996	.0016

(*) These runs were carried out with water filling the annular space.

(**) Variance = 6.879×10^{-5}.

Table (4.5): Measured and expected values of the chordal transmittance for stainless steel attenuation parameter experiments.

the continuous detector signal is sampled for discrete intervals of time much less than the dominant period of void fluctuation. This method is very effective in providing useful additional data about the voided system. However, this mode of operation requires an evaluation of the effect of the probability distribution of the radiation source on the void fraction measurement.

Although all radiation sources fluctuate with time, most of the published work using radiation attenuation methods has assumed a stationary source. For certain radiation sources, this assumption may lead to serious experimental errors in the measured void fraction [61]. It is more appropriate to consider the transmittance as a random variable to which a probability distribution function has been assigned. Figure (4.4) shows the time-variation of the intensity of the unattenuated neutron beam, as measured for a sampling period of 10 milliseconds. This figure clearly demonstrates that the radiation source used for void fraction measurement is not stationary with time, but has a time-fluctuating intensity.

If $p(T)$ is the probability density function (PDF) designated for the transmittance function, the corresponding void fraction PDF, $p(\alpha)$ can be expressed as [144]

$$p(\alpha) = p(T) \cdot |dT/d\alpha| \ . \qquad (4.12)$$

This equation is based on the premise that the probability of the void fraction lying between α and $\alpha+d\alpha$ is the same as

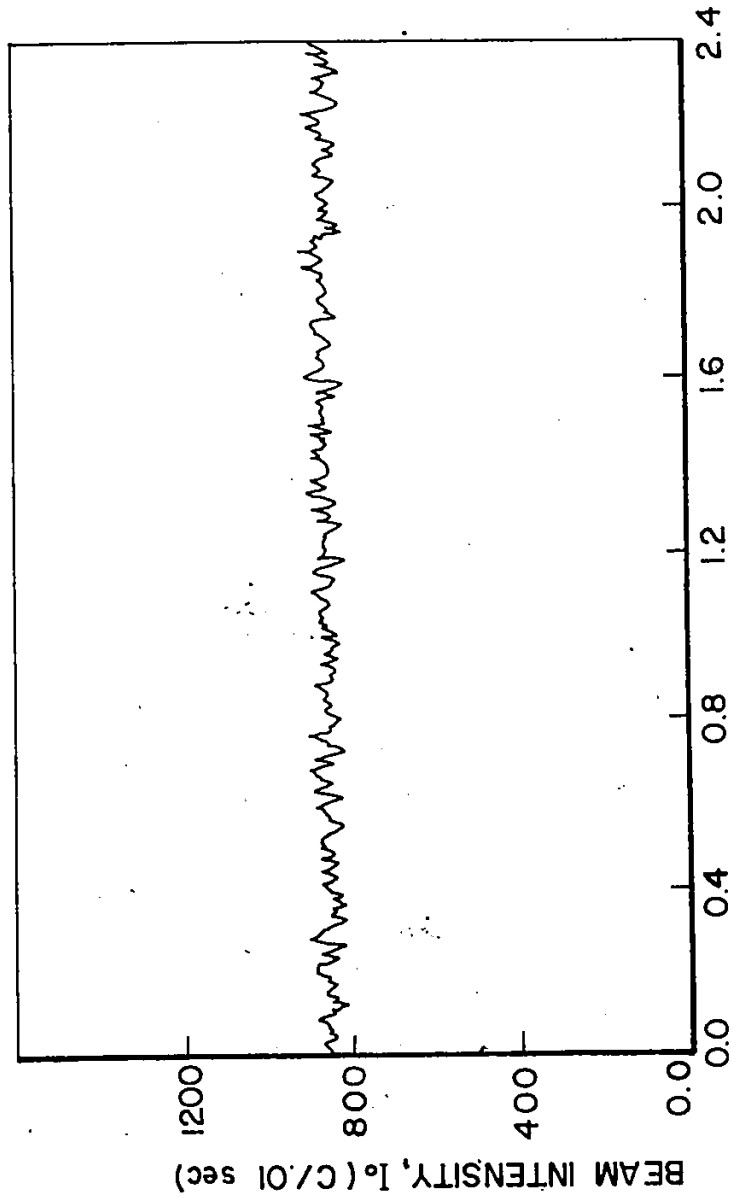

Figure (4.4): Time-variation of the intensity of the unattenuated neutron beam measured for a sampling period of 10 milliseconds.

the probability of the transmittance being between T and T+dT. For simplicity, consider the transmission of a neutron beam through a two-phase flow system possessing a steady-state uniform void fraction, α. The fluid is assumed to be contained between two thin planar panels each of thickness δ and separated by a distance x_m. The transmitted beam intensity is, then, given by

$$I(\alpha) = I_0 \exp(-\mu_w \cdot 2\delta) \exp[-\mu_m x_m (1-\alpha)] , \qquad (4.13)$$

where I_0 is the intensity of the unattenuated beam. In equation (4.13), the neutron attenuation in the gas phase is assumed negligible and the medium is considered thin enough so that the secondary scattering events contribute negligibly to the transmitted beam.

The beam intensity transmitted through a completely empty channel can be derived directly from equation (4.13), with $\alpha=1$, as

$$I(\alpha=1) = I_0 \exp(-\mu_w \cdot 2\delta) . \qquad (4.14)$$

Now define the transmittance function, $T(\alpha)$, as the ratio between the transmitted intensities with and without the two-phase mixture flowing in the channel, respectively. That is,

$$T(\alpha) = I(\alpha)/I(\alpha=1) . \qquad (4.15)$$

Substituting equations (4.13) and (4.14) into equation (4.15) yields

$$T(\alpha) = \exp[-\lambda(1-\alpha)] , \qquad (4.16)$$

where λ is the thickness of the medium in units of mean free path, i.e., $\lambda = \mu_m x_m$. Differentiating equation (4.16) and substituting into equation (4.12) give

$$p(\alpha) = \lambda T \, p(T) \quad . \tag{4.17}$$

These probabilistic considerations have been shown [61] to account for the anomalous results which have been reported in the literature; such as void fractions which are less than zero and greater than unity. These values of void fraction were experimentally obtained when a gating period of 100 milliseconds was used [139]. The corresponding probabilities for these events are clearly given by the following expressions:

$$P_r(\alpha<0) = \int_{-\infty}^{0} p(\alpha) \quad d\alpha \quad , \tag{4.18-a}$$

and

$$P_r(\alpha>1) = \int_{1}^{\infty} p(\alpha) \quad d\alpha \quad . \tag{4.18-b}$$

Figure (4.5) presents the relation between an arbitrary transmittance PDF and the associated void fraction PDF for a typical value of void fraction, $\alpha=0.3$, and medium thickness, $\lambda=1$. It is evident from figure (4.5) that such a relationship is not linear and, hence, the means of the two distributions do not coincide. The distortion effect generated by the non-linearity factor, λT, in equation (4.17) on the void fraction PDF is also clear.

The correct expression for the actual void fraction

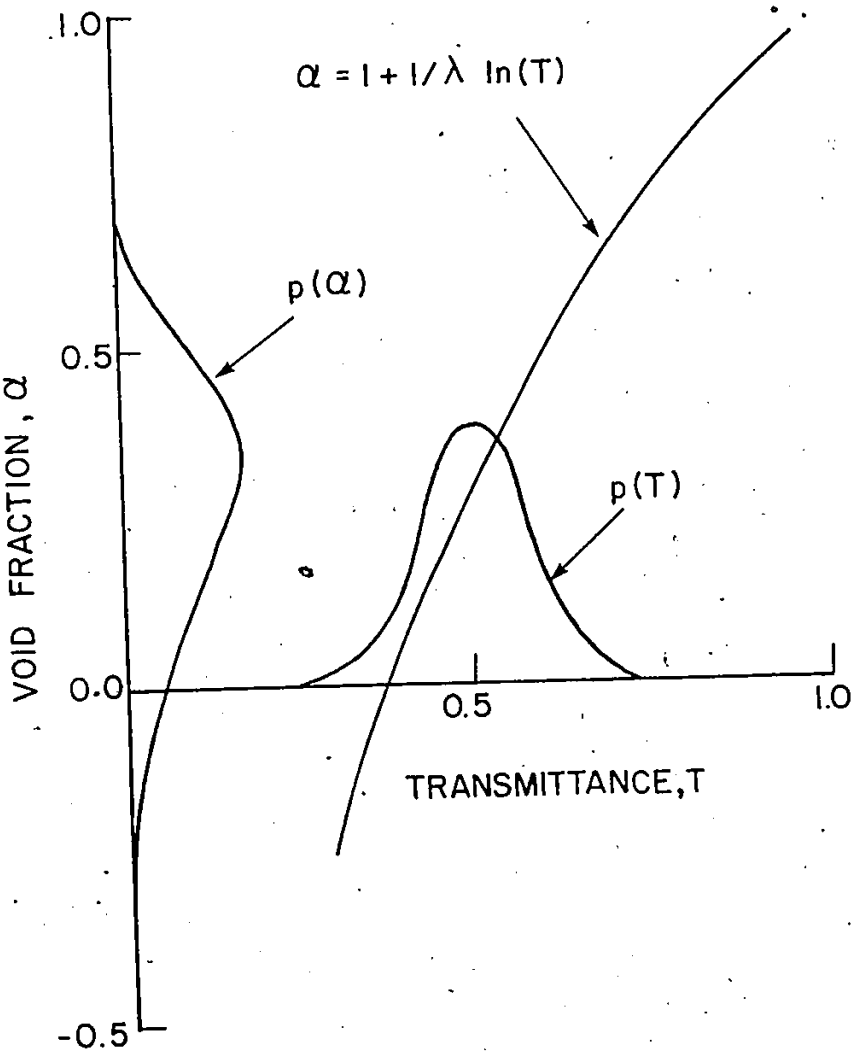

Figure (4.5): Graphical illustration showing the relation between an arbitrary transmittance PDF and the associated void fraction PDF for a typical value of void fraction, $\alpha = 0.3$, and medium thickness, $\lambda = 1$.

is given by

$$\alpha_0 = 1 + \frac{1}{\lambda} \ell n(\hat{T}) \quad . \tag{4.19}$$

Here $\hat{T}$ is the expected value of transmittance which is defined as

$$\hat{T} = \int_0^\infty T \; p(T) dT \quad , \tag{4.20}$$

which upon substituting into equation (4.19) yields

$$\alpha_0 = 1 + \frac{1}{\lambda} \ell n\{\int_0^\infty T \; p(T) dT\} \quad . \tag{4.21}$$

On the other hand, the expected value of void fraction is given by

$$\hat{\alpha} = \int_{-\infty}^\infty \alpha \; p(\alpha) d\alpha \quad . \tag{4.22}$$

By the appropriate substitution of equations (4.12) and (4.16) into equation (4.22) and making use of the normalization property of the probability density function, $p(T)$, the following expression can be obtained:

$$\hat{\alpha} = 1 + \frac{1}{\lambda} \int_0^\infty \ell n(T) p(T) dT \quad . \tag{4.23}$$

The distinction between α_0 and $\hat{\alpha}$, as can be seen from equations (4.21) and (4.23), is attributed to the nonlinear relationship between the transmittance and void fraction, equation (4.16). The expected value of void fraction,

however, corresponds to that which would pertain if the neutron source was stationary; since in its formulation, all fluctuations in the transmitted neutron beam are attributed to fluctuations in the medium. When the source is not stationary, some bias in the value of α will result.

This bias may be evaluated as follows: Define the fractional experimental bias in void fraction measurement as

$$\frac{\Delta\alpha}{\alpha_0} = \frac{\hat{\alpha} - \alpha_0}{\alpha_0} , \qquad (4.24)$$

which upon substituting for α_0 and $\hat{\alpha}$ from equations (4.21) and (4.23) gives

$$\frac{\Delta\alpha}{\alpha_0} = \frac{\lambda + \int_0^\infty \ell n\,(T)\cdot p(T)\,dT}{\lambda + \ell n\{\int_0^\infty T\cdot p(T)\,dT\}} - 1 . \qquad (4.25)$$

Equation (4.25) demonstrates that the dynamic characteristics of the extracted neutron source may present a serious source of error in void fraction measurements. In order to evaluate this error and examine its implication on experimental measurements, the PDF associated with the unattenuated neutron intensity of the extracted beam was required. This was measured for sampling periods of 1, 10, 100 and 1000 milliseconds(*). Figure (4.6) shows a typical histogram of the transmittance function measured for a sampling time of 10 milliseconds together with the corresponding probability density function. From a consideration of several suitable functions with appropriate shapes,

(*) The details of all transmittance measurements performed in this study are documented in the Department of Chemical Engineering.

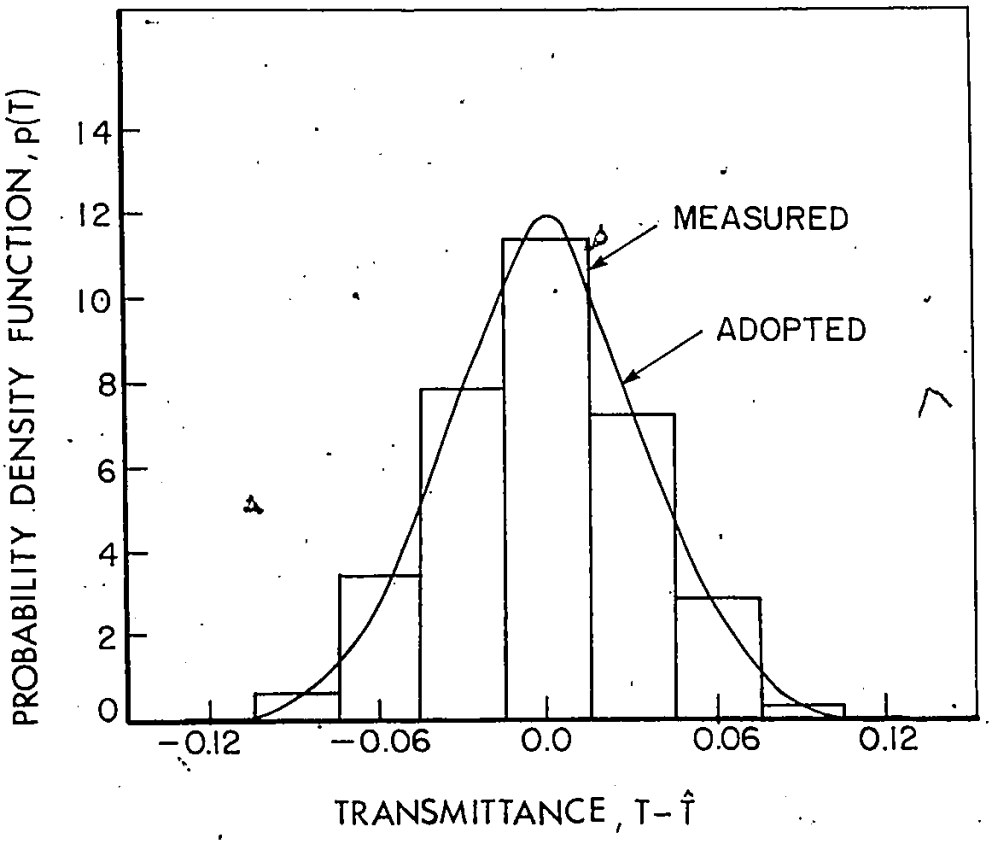

Figure (4.6): Probability density function of the transmittance measured for a sampling time of 10 milliseconds.

it was found that the following distribution provided an excellent least-squares fit of the transmittance PDF:

$$p(T) = \frac{1}{\sqrt{2\pi}\ \sigma_T} \exp\left[-\frac{1}{2}\left(\frac{T-\hat{T}}{\sigma_T}\right)^2\right] , \qquad (4.26)$$

where σ_T is the standard deviation of the distribution function; its value was estimated from the data as 0.0346. Note that this analysis indicates that the measurements are normally distributed. Table (4.6) gives the resulting experimental bias in void fraction measurements for different values of void fraction, medium thickness and sampling period.

An experimental confirmation of the mathematical formalism given above was presented previously [61]. The experimental and predicted values of void fraction bias were found to be in good agreement. It is noteworthy that for all the cases considered in table (4.6), the resulting error was always negative. In other words, in all these cases, the expected value of void fraction was smaller than the void fraction value corresponding to the expected transmittance. This can be attributed to the distortion incorporated in the void fraction PDF as a result of the non-linearity relationship between α and T. Furthermore, it can be concluded that the experimental error becomes significant only at low values of void fraction, for small counting periods and for low medium thicknesses. This result can be attributed to the fact that the radiation

α_0 \ λ	0.05	0.1	0.5	1.0	3.0	5.0
0.2	-64.194	-32.097	-6.420	-3.210	-1.070	-0.642
0.4	-32.097	-16.049	-3.210	-1.605	-0.535	-0.321
0.6	-21.398	-10.699	-2.140	-1.070	-0.357	-0.214
0.8	-16.048	-8.024	-1.605	-0.802	-0.267	-0.160
1.0	-12.839	-6.419	-1.284	-0.642	-0.214	-0.128

Table (4.6-a): Percentage error in void fraction measurements due to neutron beam fluctuation for a sampling period of 0.001 sec (full width-to-mean of 0.224).

α_0 \ λ	0.05	0.1	0.5	1.0	3.0	5.0
0.2	-5.986	-2.993	-0.599	-0.299	-0.100	-0.060
0.4	-2.993	-1.497	-0.299	-0.150	-0.050	-0.030
0.6	-1.995	-0.998	-0.200	-0.100	-0.033	-0.020
0.8	-1.497	-0.748	-0.150	-0.075	-0.025	-0.015
1.0	-1.197	-0.599	-0.120	-0.060	-0.020	-0.012

Table (4.6-b): Percentage error in void fraction measurements due to neutron beam fluctuation for a sampling period of 0.01 sec (full width-to-mean of 0.0692).

α_0 \ λ	0.05	0.1	0.5	1.0	3.0	5.0
0.2	-0.6327	-0.3164	-0.0634	-0.0318	-0.0107	-0.0065
0.4	-0.3163	-0.1582	-0.0317	-0.0159	-0.0053	-0.0032
0.6	-0.2109	-0.1054	-0.0211	-0.0106	-0.0035	-0.0021
0.8	-0.1581	-0.0791	-0.0158	-0.0079	-0.0026	-0.0016
1.0	-0.1265	-0.0633	-0.0127	-0.0063	-0.0021	-0.0013

Table (4.6-c): Percentage error in void fraction measurements due to neutron beam fluctuation for a sampling period of 0.1 sec (full width-to-mean of 0.0225).

α_0 \ λ	0.05	0.1	0.5	1.0	3.0	5.0
0.2	-0.0678	-0.0340	-0.0069	-0.0036	-0.0013	-0.0008
0.4	-0.0339	-0.0170	-0.0034	-0.0018	-0.0006	-0.0004
0.6	-0.0226	-0.0113	-0.0023	-0.0012	-0.0004	-0.0003
0.8	-0.0169	-0.0085	-0.0017	-0.0009	-0.0003	-0.0002
1.0	-0.0135	-0.0068	-0.0014	-0.0008	-0.0002	-0.0001

Table (4.6-d): Percentage error in void fraction measurements due to neutron beam fluctuation for a sampling period of 1.0 sec (full width-to-mean of 0.00736).

source used in this investigation had a small full width-to-mean probability density function. It is to be noted that Lo [139] found that the neutron source fluctuations contributed negligible error in void fraction measurements if the counting period was at least 20 milliseconds.

This is not always the case for other types of radiation sources. For an isotopic gamma radiation source [61], for example, it was found that the probability density function associated with the source intensity was much wider. The corresponding errors were found at least one order of magnitude larger than those obtained using neutrons from a reactor. As indicated in table (4.6), the full width-to-mean ratio measured for the radiation source in use was found to decrease as the counting period increased. It can be concluded, then, that void fraction bias can be much reduced by increasing the counting period. This explains the reason why the intensity of radiation sources has usually been measured over a considerable time. However, in two-phase flow systems, the inherent void fluctuations were found [60] to introduce an experimental error in the void fraction, as interpreted from the mean transmittance measurements. In order to reduce the resulting bias, it was recommended [60] that a gating technique be used in which the continuous detector signal was sampled over short discrete time intervals. Using this technique, Harms and Forrest [59] calculated the percentage errors in measuring the void fraction due to medium fluctuations.

From a comparison of the magnitude of these errors [59] with those summarized in table (4.6), it can be concluded that the experimental error arising from medium fluctuations is much larger than that arising from the statistical characteristics of the neutron source. Although the error arising from medium fluctuations may be reduced considerably by using the gating technique with short sampling times, a compromise is required since very small counting times can lead to a high measurement bias due to source fluctuations. Furthermore, the counting period is limited by the intensity of the extracted neutron beam and the medium attenuation capability.

In this investigation, the solution to this problem was to use the gating technique with a counting period of 10 milliseconds. While it was found that this counting period provided sufficient counts to yield reasonable counting statistics under all void fraction conditions investigated, it was also found that the medium fluctuation error was small [59] and the void fraction bias arising from source fluctuations was acceptable (table (4.6)).

(4.4) Flow Regime Recognition and Flow Development Testing

In the study of two-phase flow, the concept of "flow regime" has been introduced as a convenient classification of the various possible interface configurations between the phases. A change of flow regime implies changes in velocity

and/or void fraction radial profiles as well as the geometry of the interface between the phases. This explains the change of the values of flow parameters, C_o and $\bar{V}_{gj}$, as defined in Chapter (1), in the regions where a change of flow regime was visually observed [17]. For the same reason, it is also expected that the values of these parameters change as the flow is developing along the flow tube. Consequently, the transient response of void fraction to changes in flowrate, for example, should depend, to a large extent, on the type of flow regime and on the developing condition of the flow. This emphasizes the overriding importance of defining the flow regime and checking the flow development before performing any experiments to determine the flow parameters or to measure the void response to flow perturbations.

(4.4.1) Flow Regime Recognition

In two-phase flow, the flow regime can not be described simply, as for the case of single-phase flow, to be either laminar, transitional or turbulent. In a two-phase flow system, the relative amount of phases, their diffusion in one another and the existence, area and location of the interface between them are of fundamental importance in defining the flow regime. Consequently, much time and effort have been spent in the delineation of two-phase flow regimes

for various types of fluids, channel geometries and flow conditions.

(4.4.1.1) Flow Regimes in Vertical Upward Cocurrent Two-Phase Flow

In vertical upward cocurrent gas-liquid flow, the following three main flow regimes are usually observed:

(i) Bubbly Flow Regime

In this regime, the gas phase is distributed in discrete bubbles within a liquid continuum. The gas bubbles are small compared to the tube diameter and rise with different velocities, depending upon their position and size, but faster than the local liquid phase. Bubbly flow is steady and usually occurs at very low gas qualities.

(ii) Slug Flow Regime

When the gas quality is increased beyond some critical value, the small bubbles coalesce to form large bubbles which are usually bullet shaped with a cross-sectional diameter almost equal to the tube diameter. Slug flow is unsteady and characterized by large bubbles separated by liquid slugs which may contain small dispersed gas bubbles. When the separation between two adjacent bubbles is large, all bubbles have smoothly rounded heads and rise with uniform velocity. This type of flow is termed as fully-developed slug flow. When this separation becomes smaller than some critical value, the trailing bubble rises faster and the two bubbles

may coalesce. In this case, the nose of the bubble is distorted and becomes eccentric on one side. These are the characteristics of the developing slug flow.

It is noteworthy that slug flow was not observed at any time in the experiments performed by Staub and Zuber [145] which involved two-phase flow systems with heat addition. Vapour slugs were seen only in adiabatic sections following the heated part of the flow channel. The same observation was confirmed by Baker [146], by Hsu and Graham [147] and by Gouse and Hwang [148]. The probable reason is that slug flow requires considerable time and distance to develop. In boiling systems, the vapour flowrate usually changes so fast that slug flow does not have a chance to develop before a new flow regime manifests itself.

(iii) Annular Flow Regime

Annular flow consists of two adjacent and parallel streams. One stream is made up of a thin liquid layer (or film) flowing along the channel wall and presents a more or less continuous, but wavy, interface to the second stream. The second stream flows in the central core of the channel and consists of a gas containing drops of liquid of various size. The liquid annulus on the wall is relatively

thin and very wavy; sometimes it contains very small gas bubbles. The entrained liquid in the core develops because, in annular flow, the gas velocities in the core are fairly large and the resulting large shear force on the wavy liquid film causes liquid to be continuously sheared from it. At the same time, there is a continuous deposition of liquid droplets from the core to the film. Hence, under steady-state condition, these processes lead to a steady-state concentration of liquid in the core region. Many authors have distinguished between annular flow and annular dispersed flow, i.e., annular flow with liquid entrainment. Since the existence of annular flow without droplet entrainment is rare, such a distinction will not be made here.

Hewitt et al. [149] examined the nature of the core-film interface in annular flow and found that it was covered by a complex pattern of relatively slow-moving ripples. These ripples were found to be traversed by high-velocity, high-amplitude waves (or swells) of longer wave-length. Hence, any measurement of liquid film thickness usually means obtaining an average thickness unless an instantaneous measurement is possible.

Figure (4.7) shows a sketch of the bubbly, slug and annular flow regimes.

(4.4.1.2) Methods of Flow Regime Recognition

A possible way to determine the flow regime in a two-phase flow system is to use one of the published flow maps [10,74,146,150-154]. These flow regime maps are actually two-dimensional plots with flowrates of the phases on the axes or total mass flowrate on one axis versus gas quality on the other. Direct flow observation was used to show the approximate boundaries of the various flow regimes. In some maps, account was taken for channel geometry [10] or physical properties [74,146] by suitable adaptation of the parameters which were plotted.

The flow regime map for vertical flow is different from that of horizontal flow. For horizontal flow, the best-known and most widely-used flow regime map is that prepared by Baker [10] and modified by Scott [150]. Although Baker's chart serves as a useful qualitative guide to flow regimes in horizontal flow, the actual results can deviate significantly from it [155,156]. In their investigations of the vertical slug flow regime, Griffith and Wallis [74] and Moisses [151] presen-

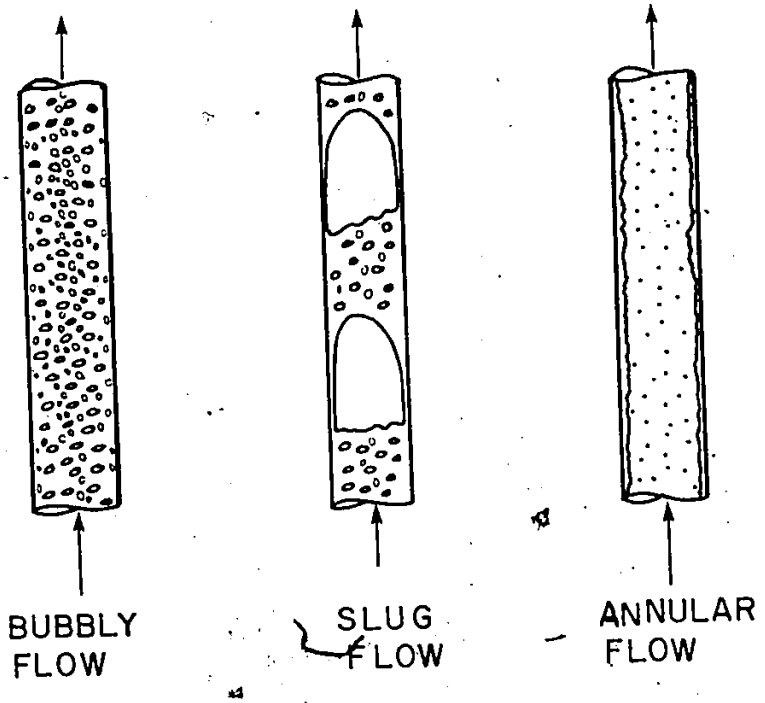

Figure (4.7): Sketch of the flow regimes in vertical upward cocurrent two-phase flow.

ted one of the first vertical flow regime maps. Similarly, Bennett et al. [152], Golan and Stenning [153] and Koslov [154] prepared different flow regime maps for vertical flow.

One of the most important variables determining the flow regime is the manner by which the two-phase flow is formed, i.e., the way by which the individual phases are introduced into the flow channel. Since this effect was usually neglected when reporting the results for flow regime mapping, the range of application of these flow regime maps is usually limited.

Many methods have been developed to determine the flow regime in two-phase flow systems. A review of these methods was given in detail by Hewitt and Hall-Taylor [157] and by Hewitt [158]. The most straightforward method is to visually observe the flow regime directly provided it is contained in a transparent test section. Obviously, this method can not be used for boiling flow in a heated metal channel. This has led to the search for alternative techniques for flow regime recognition in opaque channels.

An obvious method is to try to relate the flow regime to one of the measured variables in two-phase flow such as pressure gradient or void fraction or to their time-variations. As an example, the use of pressure fluctuations in two-phase flow for flow regime identification was demonstrated by Webb [159]. Jones and Zuber [160], on the other hand, used

the void fluctuations, as measured by an x-ray technique, to determine the flow regime. Similarly, Merilo et al. [161] used the fluctuations in the conductivity of the two-phase flow mixture for flow regime discrimination.

It is the objective of the next subsection to examine the possibility of using the neutron radiation source as a diagnostic tool for flow regime categorization.

(4.4.1.3) Identification of the Flow Regime Using the Neutron Attenuation Technique

In this investigation, the test system was located so that the neutron beam traversed the central portion of the uppermost stainless steel section in the test channel (about 40 tube diameters from the exit of the mixing section). The gas and liquid flowrates were adjusted to produce one of the three flow regimes mentioned above. The actual regime was observed directly in a transparent lucite section. The intensity of the transmitted neutron beam was detected over a gating period of 10 milliseconds and recorded continuously on a magnetic tape. The transmittance functions were then calculated and analyzed to determine the corresponding probability density functions for the transmittance and void fraction.

If the transmittance PDF is known, the corresponding void fraction PDF can be determined using the relation expressed by equation (4.12) in the previous section. The transmittance, T, through a medium of total thickness ℓ and neutron

attenuation parameter μ_m can be related to the medium void fraction, α, by

$$T = B(\delta_m)\exp(-\mu_m\delta_m) \quad , \tag{4.27}$$

where

$$\delta_m = \ell(1-\alpha) \quad . \tag{4.28}$$

The values of the medium attenuation parameter and buildup factor were predetermined using the experiments described in section (4.2). In equation (4.27), the wall transmittance kernel is included in the transmittance function. In other words, the function T is defined in equation (4.27) as the ratio between the transmitted intensities with and without the two-phase mixture flowing in the tube, respectively. The measurements of the transmittance functions over the central portion of the tube were performed using the 1/4 in. wide collimated neutron beam. Within this region, the cylindrical curvature of the tube could be neglected without significant error. Hence, the medium thickness and void fraction were assumed to be spacially constant within the width of the neutron beam.

Differentiating equation (4.27) with respect to α yields

$$\frac{dT}{d\alpha} = \ell\ F(\delta_m)\exp(-\mu_m\delta_m) \quad , \tag{4.29}$$

where

$$F(\delta_m) = \mu_m\ B(\delta_m) - \frac{dB}{d\delta_m} \quad . \tag{4.30}$$

The second term on the right-hand side of equation (4.30) can be obtained by differentiating equation (4.5) with respect to δ_m as

$$\frac{dB}{d\delta_m} = a_1 + 2a_2\delta_m + 3a_3\delta_m^2 + 4a_4\delta_m^3 , \qquad (4.31)$$

which upon combining with equation (4.5) and substituting in equation (4.30) gives

$$F(\delta_m) = b_0 + b_1\,m + b_2\delta_m^2 + b_3\delta_m^3 + b_4\delta_m^4 . \qquad (4.32)$$

Here the $\underline{b}$ coefficients are given by

$$\left.\begin{aligned} b_0 &= \mu_m - a_1 \\ b_1 &= \mu_m a_1 - 2a_2 \\ b_2 &= \mu_m a_2 - 3a_3 \\ b_3 &= \mu_m a_3 - 4a_4 \\ b_4 &= \mu_m a_4 \end{aligned}\right\} . \qquad (4.33)$$

Equation (4.29) is then substituted into equation (4.12) to obtain the following relationship between the void and transmittance probability density functions:

$$p(\alpha) = \ell\, p(T)F(\delta_m)\exp(-\mu_m\delta_m) . \qquad (4.34)$$

In figure (4.8), the void probability density functions determined for the bubbly, annular and slug flow regimes are presented. This figure demonstrates the clear differences between the void probability density functions corresponding to the three flow regimes. In fact, the neutron attenuation

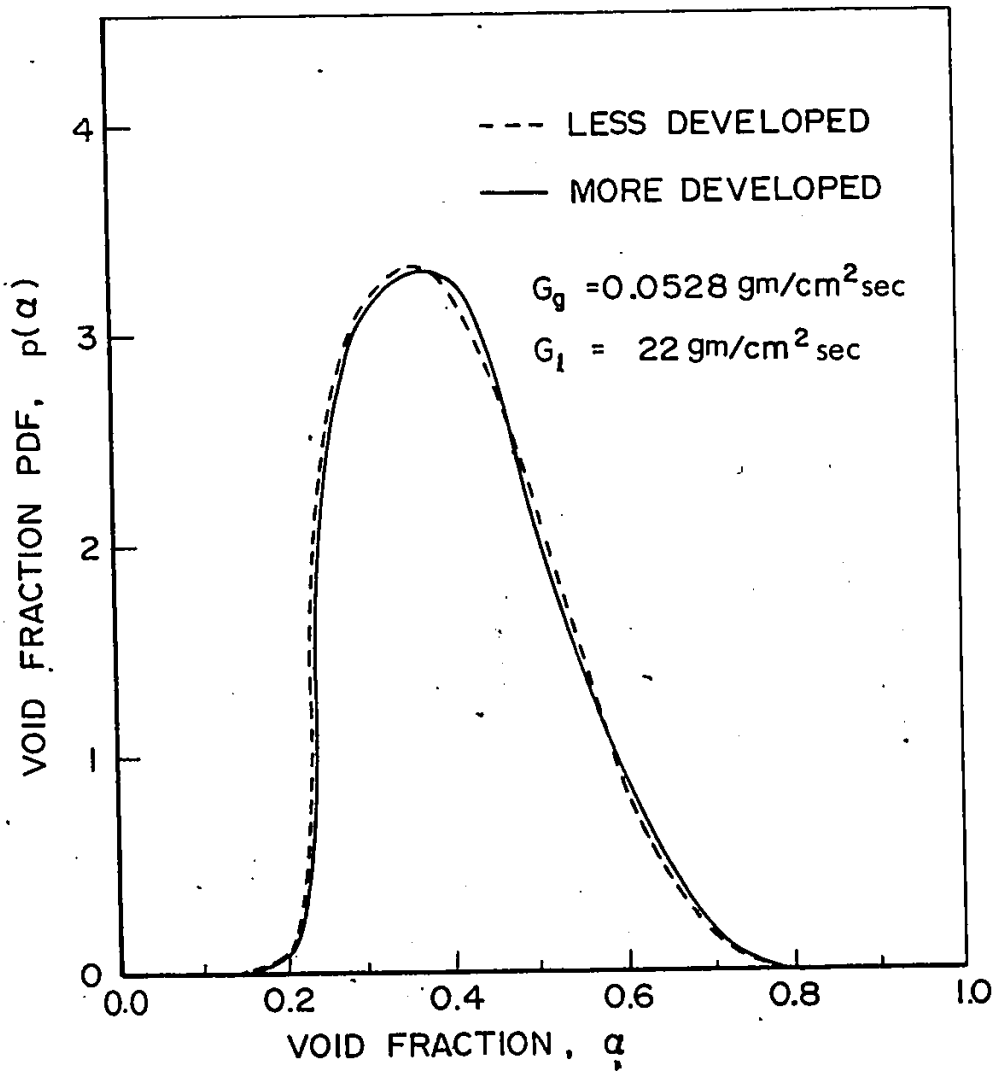

Figure (4.8-a): Void fraction PDF at two axial locations for the bubbly flow regime.

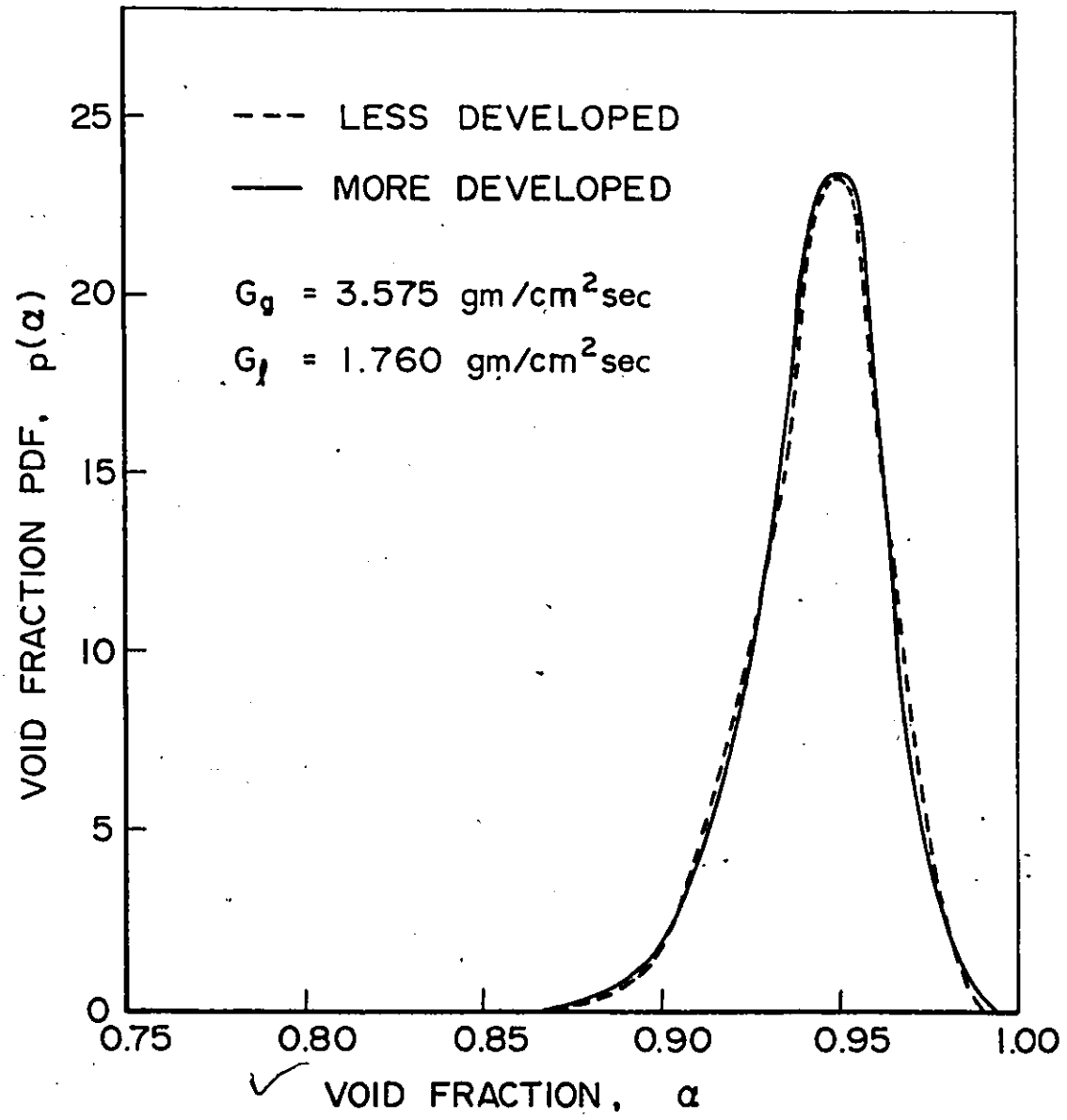

Figure (4.8-b): Void fraction PDF at two axial locations for the annular flow regime.

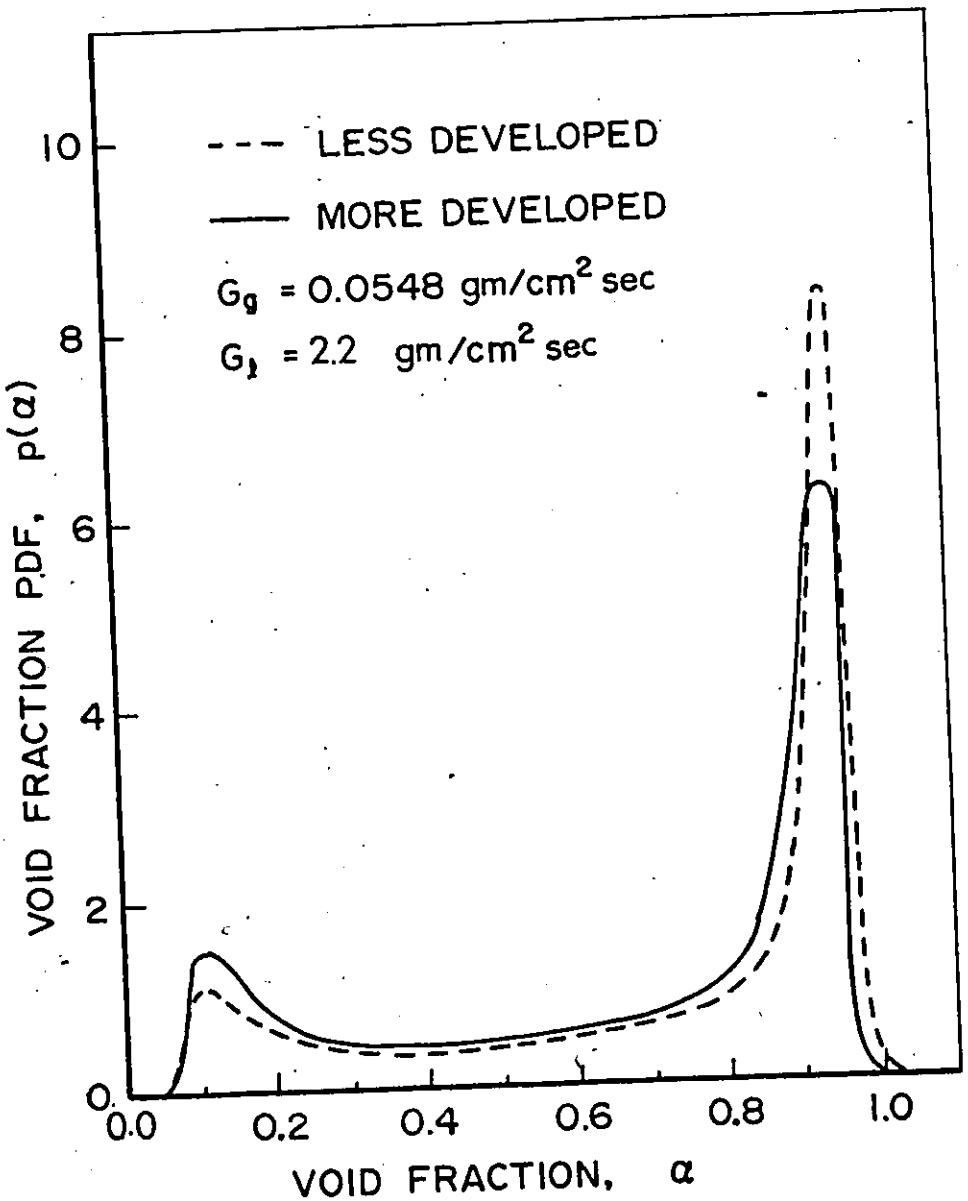

Figure (4.8-c): Void fraction PDF at two axial locations for the slug flow regime.

method provides a convenient characteristic "finger print" for each flow regime and, hence, suggests that it can be used very effectively to recognize flow regimes. This is especially important for non-transparent test sections where the visual observation method is not possible. The following characteristics distinguish the different flow regimes:

(i) Bubbly Flow

The corresponding void PDF is in the form of slightly-skewed normal distribution. It is relatively spread and its mean is located at a relatively low value of void fraction.

(ii) Annular Flow

The void PDF for this flow regime is characterized by a very narrow distribution, i.e., $p(\alpha)$ has a relatively small variance-to-mean ratio. It is located at a high value of void fraction and, similar to the case of bubbly flow, it is skewed but to the reverse side.

(iii) Slug Flow

This regime is characterized by large-amplitude void fraction fluctuations. The corresponding void PDF is bimodal; one peak is located at a low value of void fraction and the other is located at a high value. This emphasizes the expectation that the slug flow regime combines the features of the other two flow regimes. The large-amplitude void fluctuations are, in fact, due to the periodic oscillations of the slug flow between the bullet-shaped gas bubbles and the gas-dispersed liquid slugs. The gas bubbles can be thought to simulate the

annular flow regime and, hence, to be responsible for the peak located at a high value of void fraction. Similarly, the other peak on the void PDF can be considered as the contribution of the liquid slugs which have features similar to the bubbly flow regime. Furthermore, this analysis of the slug flow regime is supported by the similarity between the distribution skewness of the two peaks in slug flow and the corresponding distributions in annular and bubbly flows.

(4.4.2) Testing of the Flow Development

In any experimental investigation involving steady-state flow inside conduits, it is usually important to ensure that the flow is fully developed. This implies that the radial velocity profiles are fully established and, in the case of two-phase flow, the average void fraction and radial void profile are, on the average, essentially the same at all downstream axial positions. Since the void probability density function provides a convenient way to characterize the flow at any axial position, it does seem reasonable to consider using this measurement to test whether the flow has become fully developed. This information was particularly important for the experimental loop which was used here since the highest level at which the transmittance measurements could be made was only 40 in. above floor level.

To test this hypothesis experimentally, the entire test rig was raised 9 in. and the transmittance measurements were

repeated through the central portion of the next stainless steel test section. The corresponding void probability density functions are shown in figure (4.8). Comparing the corresponding probability density functions, it can be seen that while those for bubbly and annular flows are almost identical at the two axial locations, a substantial change occurs in that of the slug flow regime. These measurements indicate that the bubbly and annular flow regimes were fully developed by the point at which the bulk of the measurements were made. On the other hand, slug flow needs a much longer tube to develop; this conclusion agrees with many previous investigations, e.g., [74]. Due to the fixed location of the neutron beam, the required length for slug flow development was not available and, hence, the study of slug flow could not be carried further. Thus, this study was limited to bubbly and annular flows. Since it has been observed that slug flow may not occur in boiling systems or perhaps fast-changing flow systems, this limitation is not a serious one.

However, the void PDF for slug flow can still be employed to extract some useful information about the flow. By definition, the ratio of the areas under the two peaks of the void PDF represents the probability ratio of liquid slug and gas bubble occurrence in the path of the neutron beam, i.e.,

$$\frac{P_r \text{ (liquid slug)}}{P_r \text{ (gas bubble)}} = \frac{A_1}{A_2} , \qquad (4.35)$$

where A_1 and A_2 are the areas under the peaks of the void PDF at the low and high values of void fraction, respectively. From figure (4.8-c), it is clear that such a ratio is changing as the slug flow is developing along the test section.

As a summary of the results presented in this section, it is evident that the time-fluctuation of the transmitted neutron beam through the two-phase flow channel presents an excellent tool for flow regime recognition. Furthermore, the measurements of this fluctuation at two axial positions have also been shown to provide a way to check the flow development along the test section. These measurements have indicated that both bubbly and annular flows develop much faster than slug flow.

(4.5) Testing Experiments of the Adequacy of Neutron Diagnostic Technique for Void Fraction Measurement

The adequacy of neutron attenuation method for void radial profile measurement in two-phase flow was tested in both the bubbly and annular flow regimes. This test was carried out by integrating the radial void profile, as measured using the neutron beam, and comparing the resulting cross-sectional average void fraction with that obtained directly by a trapping method. This trapping method has become a standard, well-established, accurate method in measuring the average overall void fraction in isothermal, two-component, two-phase flow [157]. It involves using quick-closing shut-off valves at two locations

in the conduit and measuring the trapped liquid volume as described below.

(4.5.1) Experimental Details

For this trapping experiment, the experimental system, as shown in figure (3.1), was modified as follows: The lucite test tube was replaced by a stainless steel tube (type 304, 0.618 in. I.D. by 0.75 in. O.D.) in order to accommodate the high-pressure shock which the tube experienced when the quick-shutting valves were suddenly closed. The two shut-off valves were installed so that the face-to-face distance between them was 18.25 in.; the lower valve was located about 7.5 in. below the neutron beam level. The valves were air-activated ball valves. The hole through each valve was exactly 0.618 in. I.D. so that this opening exactly matched the tube cross-section; hence, there was smooth uninterrupted flow through them. The two valves were closed essentially simultaneously by having a single switch activate two identical solenoid valves; these valves allowed high-pressure air to be admitted to the piston-closing mechanism which was installed on each valve. To prevent undesirable sudden increases of the system pressure when closing the valves, a third solenoid valve was installed in a bypass line off the main air-supply line. The signal closing the shut-off valves opened this bypass valve to allow the air to flow into a surge tank and then to atmosphere. The main air and water supply were closed shortly thereafter.

(4.5.2) Experimental Procedure

The experimental procedure of obtaining the void profile across the tube was essentially the same for all experiments. First, the beam port was opened and the intensity of the unattenuated neutron beam, I_0, was measured and recorded on a magnetic tape. The measurement of I_0 was performed for a relatively long counting period of 20 sec in order to minimize the effects of the statistical fluctuations of the neutron source. The shut-off valves on the test channel were fully opened. The liquid and gas flowrates were adjusted to the required values to provide a desired flow regime. After steady-state conditions were established(*), as indicated by the stability of the pressure drop manometer, the intensity measurements of the transmitted neutron beam were begun. Before measuring the time-averaged transmitted beam intensity across the flow tube, the time-variation of the transmitted beam intensity was measured at the central portion of the stainless steel tube. These measurements had to be performed in order to ensure that the desired flow regime was generated in the tube with the adjusted gas and liquid flowrates.

As mentioned in subsection (3.3.2), the collimated neutron beam was required to be 1/4 in. wide in order to provide the required intensity. Note that this dimension is large relative to the tube diameter and this has created a problem since

(*) At low-to-medium flowrates, steady-state was established very quickly; however, for high flowrates, several minutes were required.

a radial void fraction distribution is desired. This problem was overcome by taking six overlapping chordal measurements of the transmitted beam intensity across the tube radius. Since the neutron beam was fixed, the flow tube was moved in the horizontal direction in steps of 0.0368 in. between each chordal measurement. Each chordal intensity measurement was repeated ten times in order to get an estimate of the variances of the experimental measurements. The gating technique together with the sampling period recommended in section (4.3) were used in measuring the transmitted beam intensity in order to reduce the measuring bias of void fraction.

After all neutron intensity measurements were completed, the manometer was isolated from the system. The two shut-off valves were then closed simultaneously by activating the appropriate solenoid valves. At the same time, the bypass line on the air was opened; the gas and liquid supply lines were turned off immediately after. The section including the two shut-off valves was removed from the test rig and was drained into a graduated cylinder in order to measure the volume of the collected liquid. The liquid adhering to the tube was removed by passing a small piece of cloth through the separated section; its volume was determined by weighing that piece before and after it was passed through the tube. The total volume of the liquid contained between the two valves was, then, calculated by adding the volume of the drained liquid to that of the adhering liquid.

The whole procedure was repeated for different gas and liquid flowrates. Table (4.7) summarizes the range of gas and liquid flowrates used in this experimental investigation for both the bubbly and annular flow regimes. The steady-state experimental measurements of the transmittance function across the flow tube are tabulated in Appendix (H) for these flow regimes.

(4.5.3) Treatment of Data and Results

(i) Characterization of the Flow Regime

The measured time-variation of the transmitted beam intensity at the central portion of the stainless steel tube was used to characterize the flow regime. This was done by calculating and comparing the void fraction PDF for each experimental run with those determined for the three major flow regimes in a similar transparent lucite test tube, i.e., figure (4.8). Figure (4.9) presents the void fraction PDF for typical runs of the bubbly and annular flow regimes.

(ii) Time-Average Radial Void Profile

At steady-state, the transmittance, T, of the neutron beam through a chordal position centered at a distance L from the centre of the flow tube is given in Appendix (C) as

$$T = \int_{L-\delta_b/2}^{L+\delta_b/2} K(x)\,dx \ , \qquad (4.36)$$

where the neutron transmittance kernel, K(x), is given by

$$K(x) = B(\delta_m)\exp[-(\mu_w\delta_w + \mu_m\delta_m)] \ . \qquad (4.37)$$

Here δ_w and δ_m are, respectively, the wall thickness and the equivalent thickness of liquid intercepting the beam path

Flowrate (gm/cm^2 sec)	Experiment No.							
	1	2	3	4	5	6	7	8
G_g	.0384	.0384	.0384	.04875	.04875	.0581	.0581	.0581
G_ℓ	72.0	86.2	106.2	86.2	115.3	89.1	100.8	116.2

a - Bubbly Flow

Flowrate (gm/cm^2 sec)	Experiment No.			
	1	2	3	4
G_g	4.5796	4.5796	4.5796	4.5796
G_ℓ	5.8711	7.8281	9.3938	13.6992

b - Annular Flow

Table (4.7): Summary of the gas and liquid flowrates used in the holdup experiments for both the bubbly and annular flow regimes.

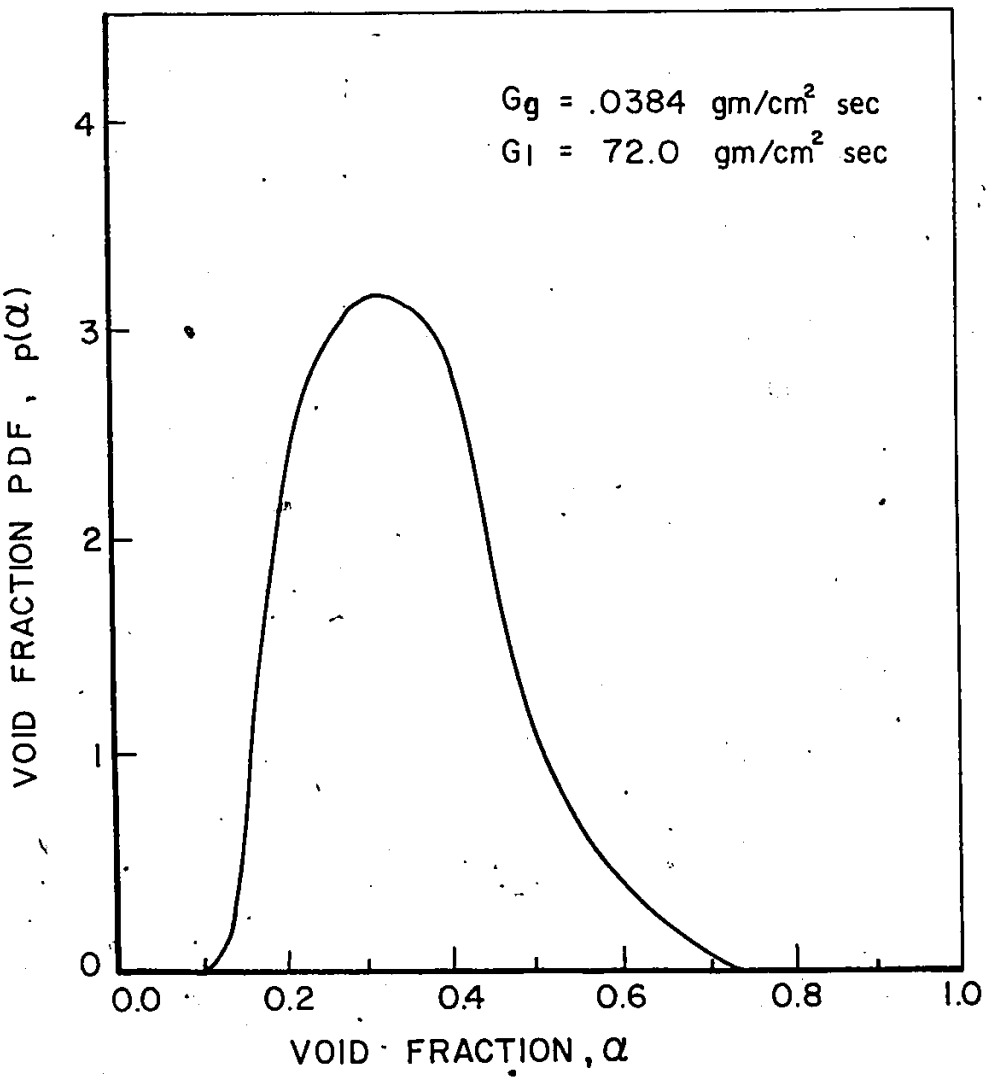

Figure (4.9-a): Void fraction PDF for a typical experimental run of the bubbly flow regime.

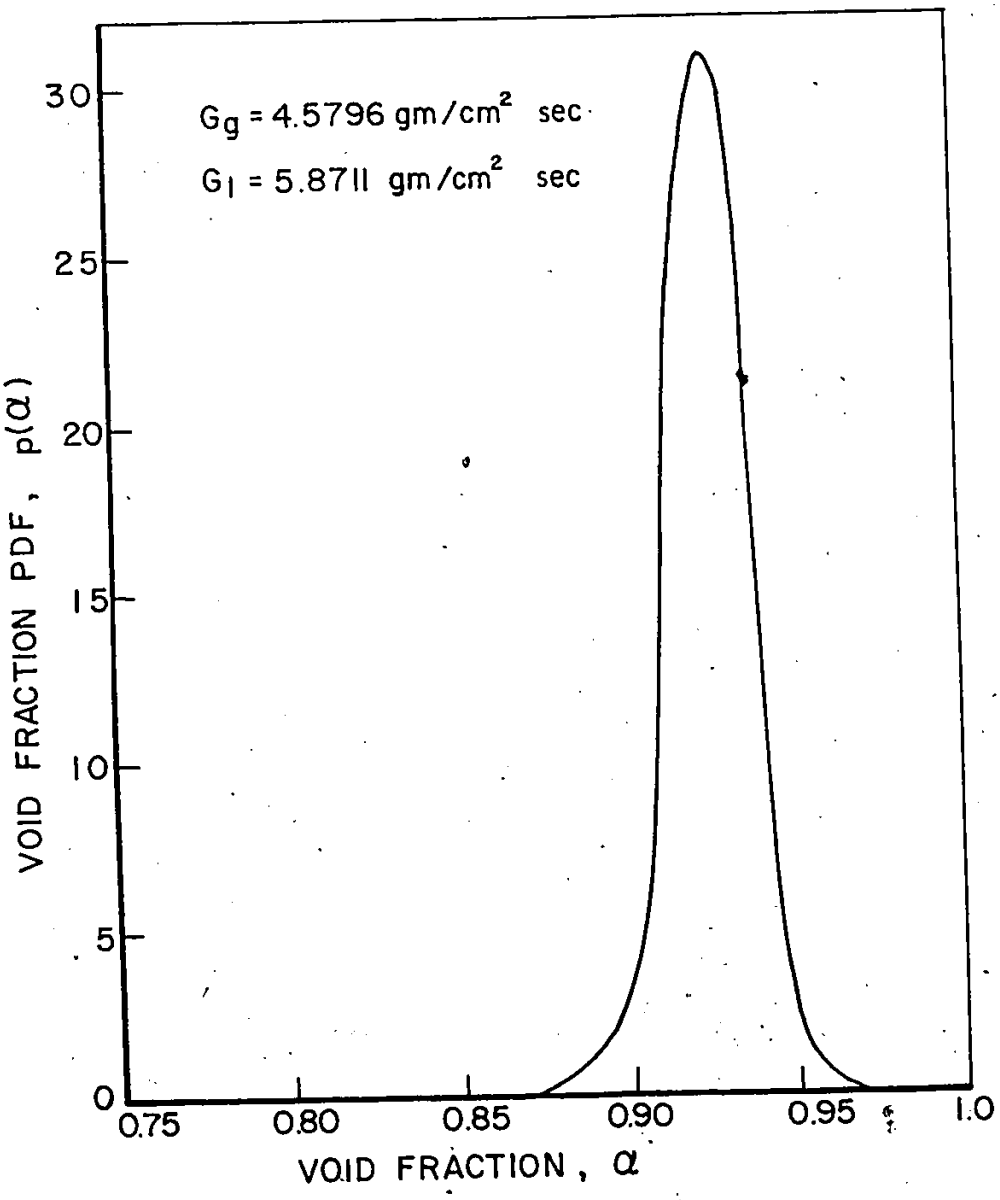

Figure (4.9-b): Void fraction PDF for a typical experimental run of the annular flow regime.

at a chordal position x from the tube center. These thicknesses are shown in Appendix (C) to be related to the tube inside and outside diameters as

$$\delta_w = \sqrt{D_0^2 - 4x^2} - \sqrt{D_i^2 - 4x^2} \ , \qquad (4.38\text{-a})$$

and

$$\delta_m = [1-\bar{\alpha}(x)] \sqrt{D_i^2 - 4x^2} \ . \qquad (4.38\text{-b})$$

In equation (4.38-b), $\bar{\alpha}(x)$ is the average value of void fraction along the chordal position under consideration which is given by

$$\bar{\alpha}(x) = \frac{1}{\delta_t} \int_{-\frac{\delta_t}{2}}^{\frac{\delta_t}{2}} \alpha(x,y)dy \ , \qquad (4.39)$$

where

$$\delta_t = \sqrt{D_i^2 - 4x^2} \ . \qquad (4.40)$$

In equation (4.39), $\alpha(x,y)$ is the time-averaged local void fraction at the point (x,y). Mathematical models for $\alpha(x,y)$ in the bubbly and annular flow regimes may be assumed to be of the following forms:

(a) <u>Bubbly Flow</u>

$$\alpha(x,y) = \alpha_c[1 - (\frac{2\sqrt{x^2+y^2}}{D_i})^n] \ . \qquad (4.41)$$

(b) <u>Annular Flow</u>

$$\alpha(x,y) = \alpha_c[1-(\frac{\sqrt{x^2+y^2}}{a})^n] \ , \quad \text{for } \sqrt{x^2+y^2} \leq a \ , \qquad (4.42\text{-a})$$

and

$$\alpha(x,y) = 0 \ , \quad \text{otherwise} \ . \qquad (4.42\text{-b})$$

where a is the radius of the central core region. As indicated in Appendix (C), the void fraction models given by equations (4.41) and (4.42) are physically reasonable and both qualitatively and quantitatively in good agreement with the important features of the flow behaviour. Furthermore the symmetry assumed in these models is in agreement with the observations made by Staub and Zuber [145] for bubbly flow and by Gill et al. [162] and Isbin et al. [163] for annular flow.

The parameters n and α_c, representing a void index and the value of the center-line void fraction, respectively, may be estimated by using a least-squares procedure based on Marquardt's algorithm [141]. Before applying the least-squares method, the homogeneity of variance of the transmittance data was checked by Bartlett's test, as outlined in Appendix (B). For the bubbly and annular flow regimes, it was found that all the experimental runs almost satisfied Bartlett's test for 0.95 χ^2 distribution.

The least-squares method was, then, used to minimize the sum of squares of the differences between the sixty transmittance measurements and the corresponding expected values, equation (4.4). These expected values were calculated in the following way: Equation (4.41) or (4.42), depending upon the flow regime, was substituted into equation (4.39) and then, with $\bar{\alpha}(x)$, equations (4.38), (4.37) and (4.36) were

solved in order. Note that in the annular flow regime, an additional knowledge of the mean film thickness is needed to solve the equations (4.36) to (4.42). A detailed analysis of the radial velocity profile together with the method of calculating the mean film thickness in annular flow will be presented in the next chapter.

The adequacy of the assumed void models was tested by applying an ANOVA lack of fit test to each experimental run. This test showed that

$$(MS)_L/(MS)_{PE} < F_{.05}(d_L, d_{PE}) \quad , \qquad (4.43)$$

in all cases considered for both flow regimes. The analysis of variance for two typical runs, one for each flow regime, is summarized in table (4.8). With the 0.95 F-distribution, $F_{.05}(4,54)$, having a value of 2.55 [142], the adequacy of the models for these two runs is demonstrated in table (4.8). As an additional test of model adequacy, the residuals (experimental minus expected values) were plotted as a function of the tube chordal position, such as indicated in figure (4.10), and as a function of the liquid flowrate, as shown in figure (4.11). In all cases, the residuals were shown to be randomly distributed about zero. Thus, the models were shown to be adequate in all respects.

Typical measurements of the chordal transmittance function together with the corresponding expected values are shown in figure (4.12) for both flow regimes. The corresponding

Flow Conditions	Source	Total	Model (Discrepancy)	Residual	Pure Error Residual	Lack of Fit Residual
Bubbly Flow (gm/cm^2 sec) $G_g = 0.0384$ $G_\ell = 72.0$	SS	3.738×10^4	3.731×10^4	63.475	54.0	9.475
	d	60	2	58	54	4
	MS	622.927	1.866×10^4	1.091	1.0	2.369
Annular Flow (gm/cm^2 sec) $G_g = 4.5796$ $G_\ell = 5.8711$	SS	2.788×10^6	2.787×10^6	60.933	54.0	6.933
	d	60	2	58	54	4
	MS	4.646×10^4	1.394×10^6	1.051	1.0	1.733

Table (4.8): ANOVA table for the radial void profile models for two typical runs of the bubbly and annular flow regimes.

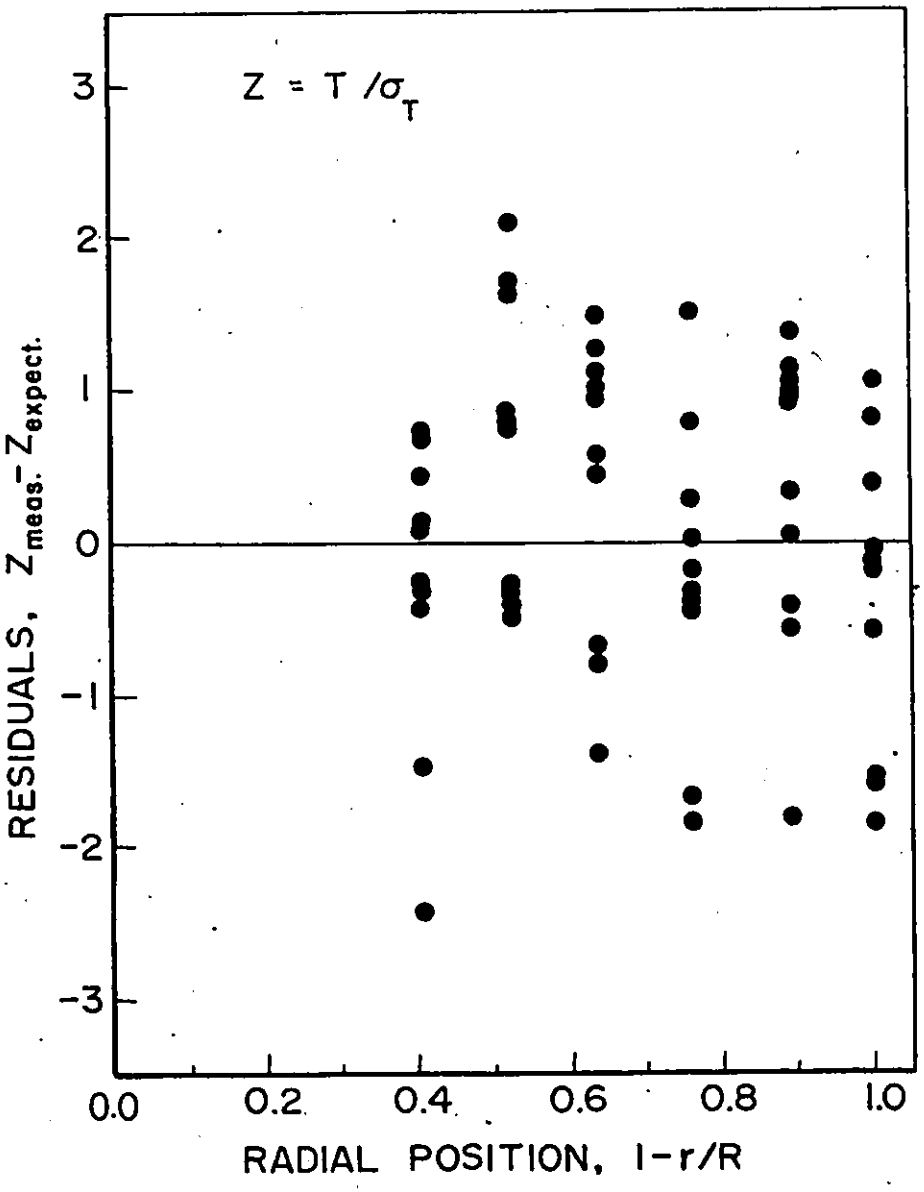

Figure (4.10-a): Dependence of the residuals on the radial position for a typical experimental run of the bubbly flow regime.

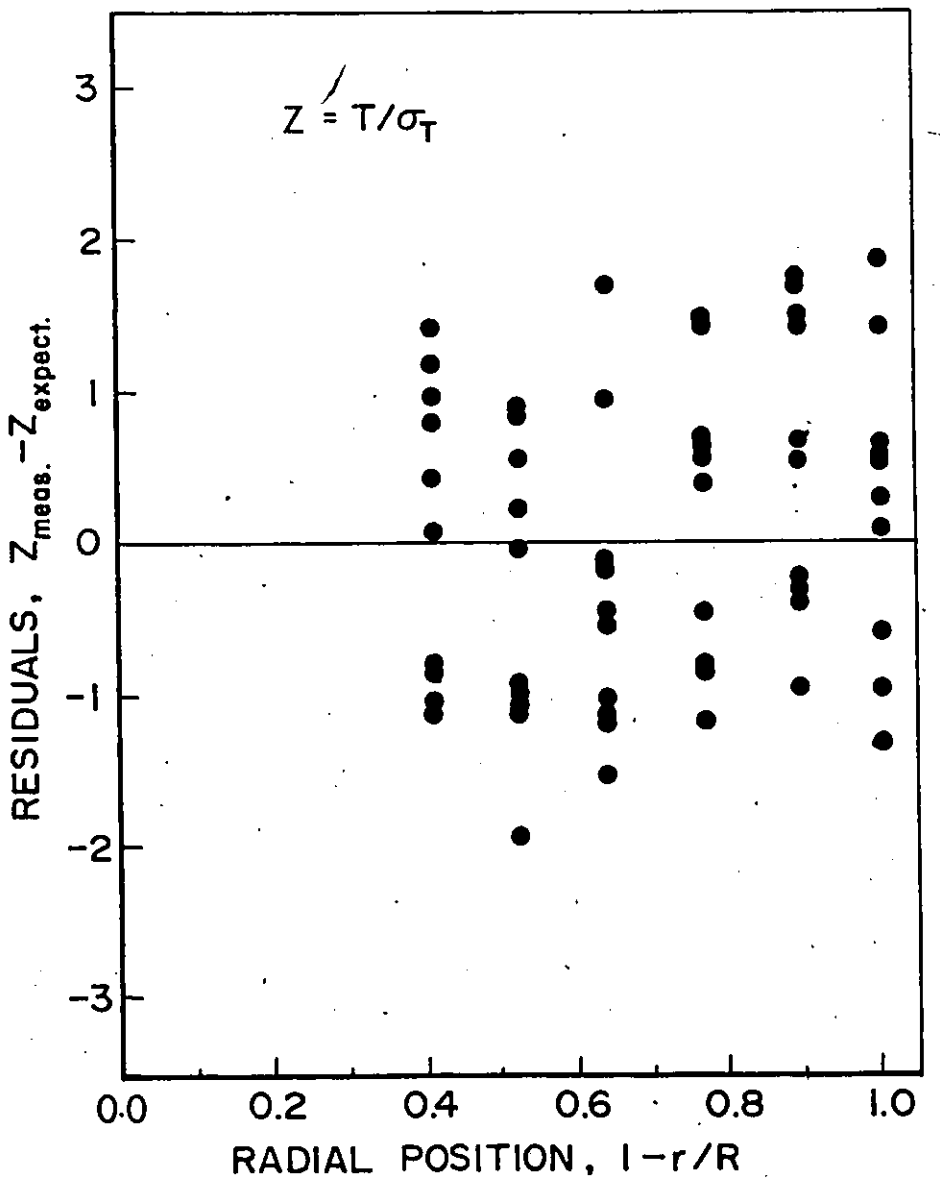

Figure (4.10-b): Dependence of the residuals on the radial position for a typical experimental run of the annular flow regime.

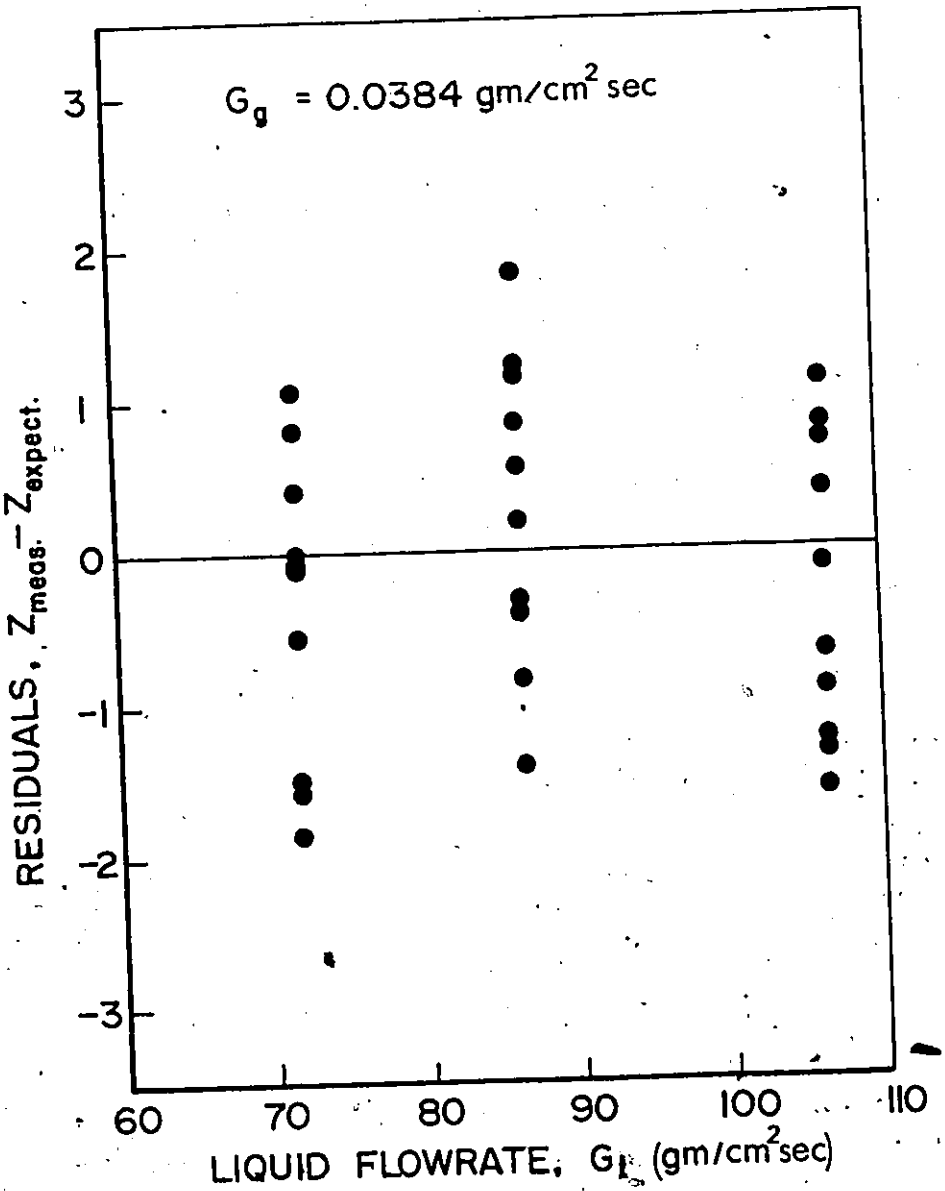

Figure (4.11-a): Dependence of the residuals at tube center on the liquid flowrate for the first three experimental runs of the bubbly flow regime.

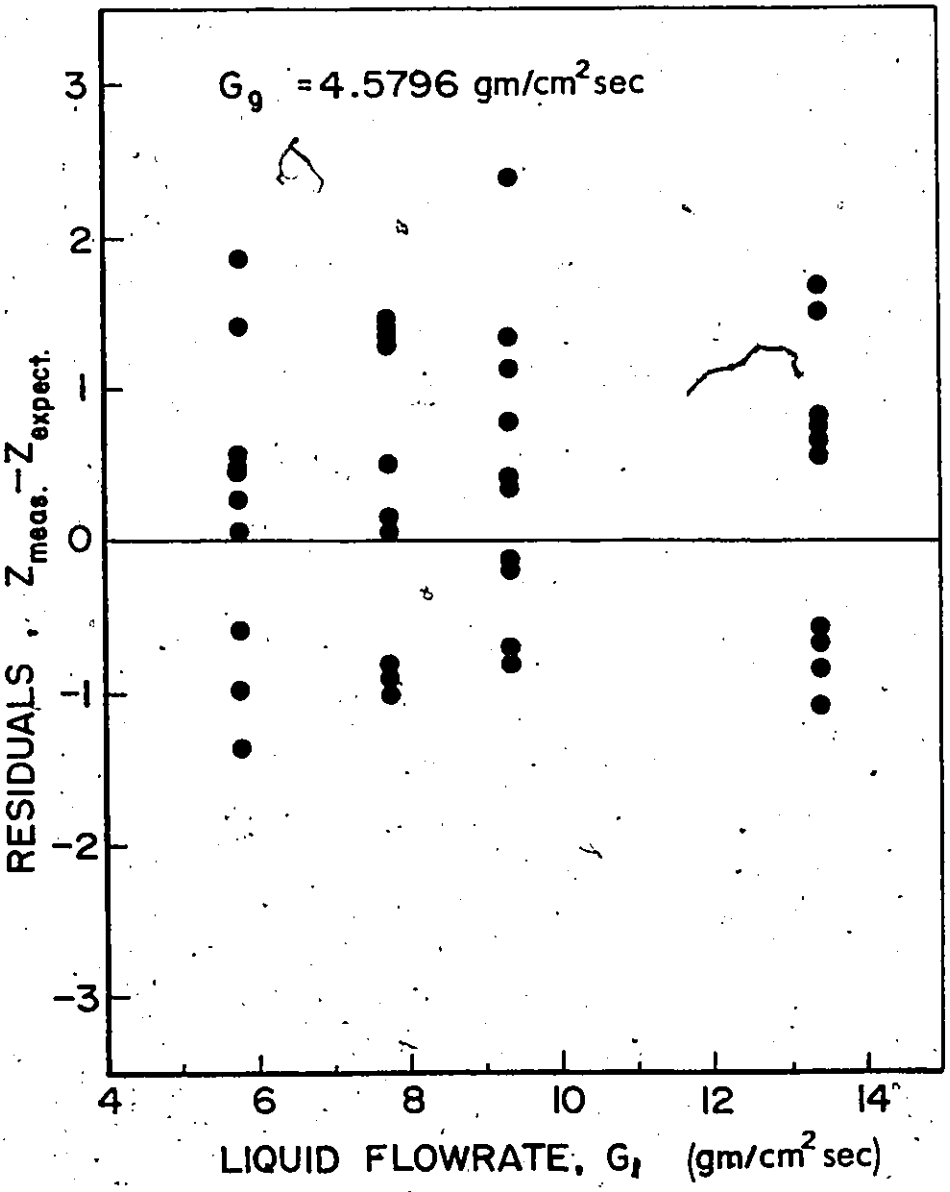

Figure (4.11-b): Dependence of the residuals at tube center on the liquid flowrate for the annular flow regime.

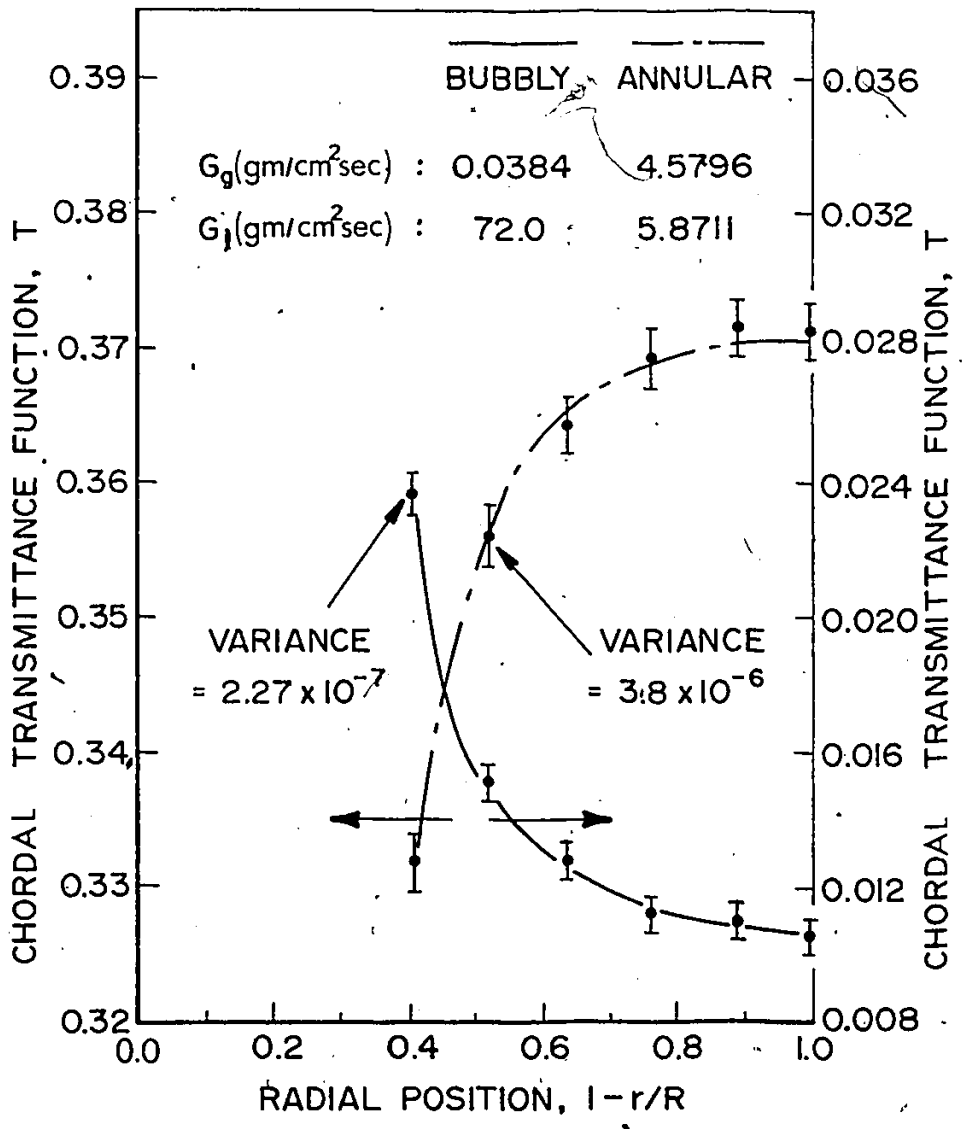

Figure (4.12): Typical radial distributions of the chordal transmittance function for the bubbly and annular flow regimes.

radial void profiles are given in figure (4.13). It is noted that the radial void profile for annular flow supports the studies made by Adorni et al. [165] and by Gill et al. [166] which showed that the droplet volume concentration was relatively constant across the core. The apparent differences between the chordal transmittance radial distributions in the bubbly and annular flow regimes suggest a possible alternative method for flow regime classification.

(iii) Cross-Sectional Average Void Fraction

The cross-sectional average void fraction was easily determined by integrating the radial void profile given by equation (4.41) or (4.42). Thus,

$$\langle\alpha\rangle_n = \frac{1}{A}\int_A \alpha(x,y)\,dA \quad , \tag{4.44}$$

which upon substituting for $\alpha(x,y)$ gives

$$\langle\alpha\rangle_n = \frac{n\alpha_c}{n+2} \quad , \tag{4.45-a}$$

for bubbly flow, and

$$\langle\alpha\rangle_n = \frac{a^2}{R^2}\left(\frac{n\alpha_c}{n+2}\right) \quad , \tag{4.45-b}$$

for annular flow.

It was shown in subsection (4.4.2) that when operating in the bubbly and annular flow regimes, the flow became fully developed very quickly. In particular, it was shown that the flow was fully developed and, hence, the radial void profile could be

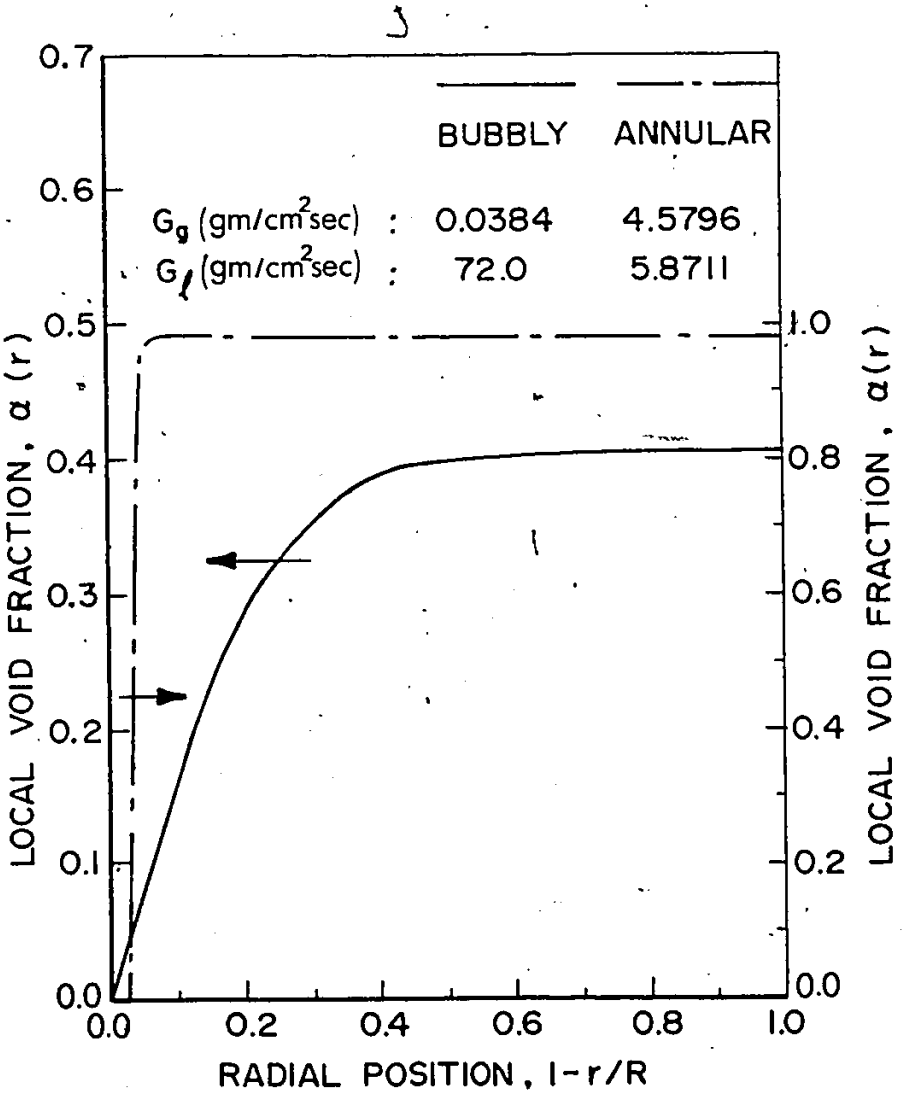

Figure (4.13): Typical radial void profiles for the bubbly and annular flow regimes.

assumed independent of axial position over the 18.25 in. length of the test section between the two quick shut-off valves. It was, thus, possible to test the radial void profile models directly by comparing the cross-sectional average void fraction, as predicted by equation (4.45), with that measured by the trapping technique. In this experiment, the cross-sectional average void fraction was obtained from the relation

$$\langle\alpha\rangle_t = 1 - V_m/V_e \,, \qquad (4.46)$$

where V_m and V_e are, respectively, the volume of the collected water and the empty tube volume contained between the valves. Figure (4.14) shows a comparison between the two methods for the average void fraction determination in bubbly and annular flows. The highest percentage deviation between the two methods was found to be 6.3% and -2.56% for the bubbly and annular flow regimes, respectively.

To examine the reproducibility of the void fraction data obtained by the trapping method, the same measurement was repeated five times, under the given air and water flowrates, for three experimental runs of bubbly flow and two runs of annular flow. It can be easily seen from figure (4.14-a) that most of the experimental data fall within the confidence limit for the bubbly flow regime. On the other hand, for the annular flow regime, the neutron attenuation method always indicated values of the average void fraction

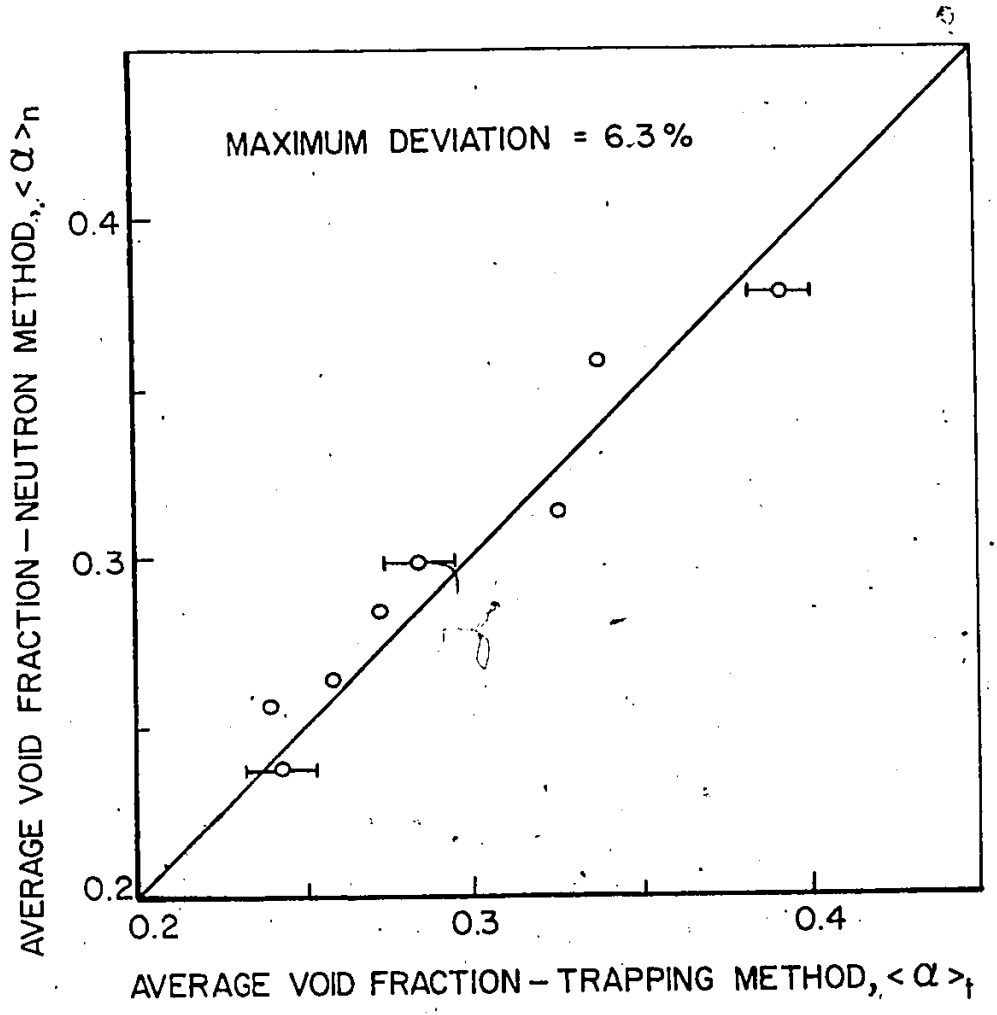

Figure (4.14-a): Comparison between the neutron attenuation and trapping methods for the average void fraction determination in the bubbly flow regime.

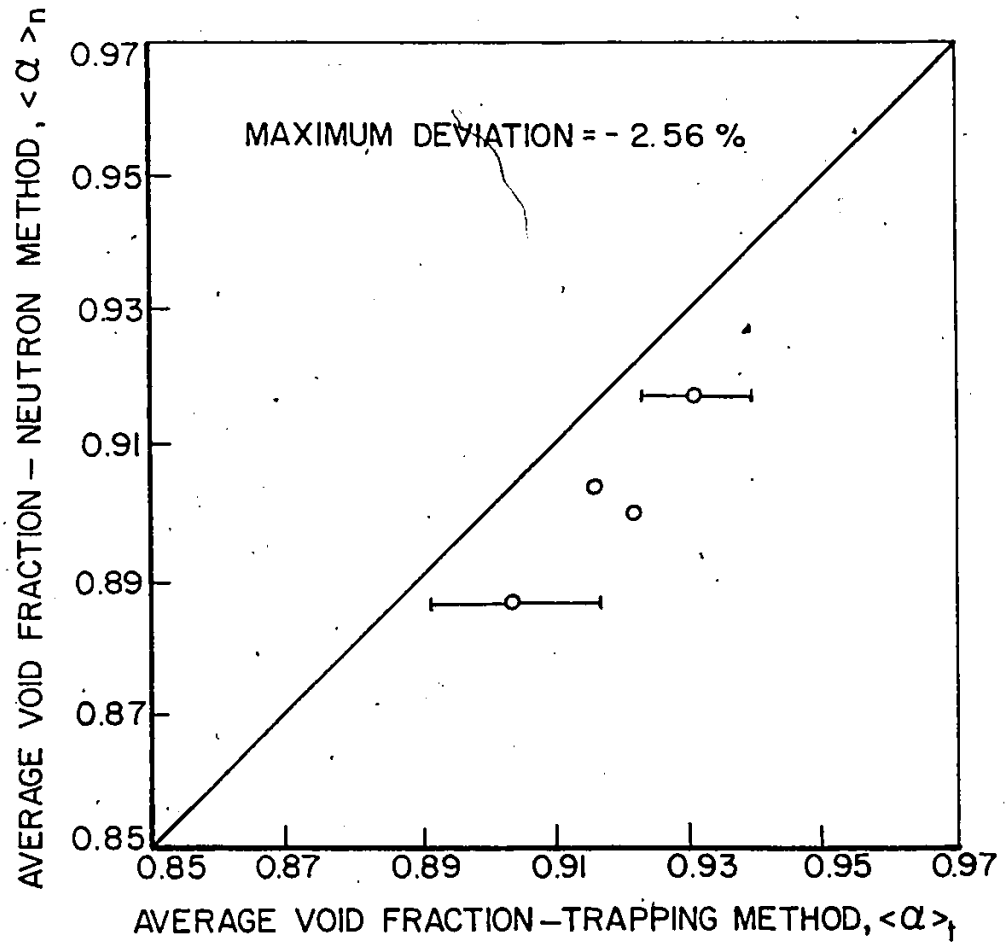

Figure (4.14-b): Comparison between the neutron attenuation and trapping methods for the average void fraction determination in the annular flow regime.

which were slightly lower than that measured by the trapping technique. This difference, however, can be attributed to the difficulty of removing all of the trapped water in the case of annular flow.

In summary, these results indicate that the neutron attenuation technique and procedure, as described here, provide an accurate way to obtain radial profiles of void fraction in the water-air flow system employed.

CHAPTER (5)

FLOW PARAMETERS

(5.1) Introduction

In Chapter (1), it was demonstrated that there is a real need to obtain accurate estimates of the fundamental flow parameters, C_o and $\bar{V}_{gj}$. These parameters were shown to be required in order to predict the transient behaviour of two-phase flow systems. This chapter presents and evaluates the possible methods which can be used to estimate the flow parameters.

(5.2) Experimental Work

As mentioned in Chapter (4), the strategy here is to assume a model for the void fraction radial profile (equation (4.41) or (4.42)), to measure the transmittance function at different chordal locations across the tube and then to fit the corresponding experimental data to obtain a best estimate of the model parameters, α_c and n. The detailed analysis was given previously in Chapter (4).

The transmitted beam intensity was measured at eleven chordal positions over the cross-section of the uppermost stainless steel section by moving the two-phase flow tube relative to the fixed neutron beam. In order to scan the radial void distribution across the 3/4 in. I.D. tube with the 1/4 in. wide neutron beam, the chordal measurements were carried out by moving the tube a distance of 0.05 in. between each measurement. The gating technique together with the sampling period recommended in section (4.3) were used in measuring the transmitted beam intensity in order to reduce the measuring bias of

void fraction. The transmittance data were stored on a magnetic tape and then analyzed by means of a computer program.

The experimental procedure was very similar to that described in section (4.5), except that the liquid was not trapped and measured in this case. The procedure was repeated for different gas and liquid flowrates while maintaining the same two-phase flow regime. The experimental runs were carried out in groups by varying the flowrate of one phase while maintaining the flowrate of the other constant. Table (5.1) shows the experimental range of the gas and liquid flowrates used in the bubbly and annular flow regimes. The steady-state experimental measurements of the transmittance function across the flow tube are tabulated in Appendix (H) for these flow regimes. It should be mentioned here that the study of the slug flow regime was not attempted since it was found that such a flow regime needed a much longer flow tube to become fully developed.

(5.3) Treatment of Data

(5.3.1) Void Fraction Radial Profiles

An analysis of the transmittance data similar to that presented in section (4.5) was used in order to estimate the void profile parameters. Figure (5.1) presents typical void fraction radial profiles for the bubbly and annular flow regimes. From figure (5.1), it can be concluded that the void profile changes from a parabolic profile for bubbly flow to a much flatter one for annular flow. Consequently, the exponent, n, in the void profile models is expected to be much higher for annular flow than for bubbly flow.

Experiment No.	Flowrate (gm/cm^2 sec)	
	G_g	G_ℓ
1	0.016	13.87
2	0.016	26.84
3	0.016	58.47
4	0.016	81.85
5	0.023	18.98
6	0.023	42.52
7	0.023	58.47
8	0.023	81.85
9	0.033	42.52
10	0.033	58.47
11	0.033	81.85

Table (5.1-a): Summary of the gas and liquid flowrates for the bubbly flow regime.

Experiment No.	Flowrate (gm/cm^2 sec)	
	G_g	G_ℓ
1	2.61	2.66
2	3.11	2.66
3	3.58	2.66
4	4.00	2.66
5	2.61	5.32
6	3.11	5.32
7	3.58	5.32
8	4.00	5.32
9	2.61	7.97
10	3.11	7.97
11	3.58	7.97
12	4.00	7.97
13	2.61	10.63
14	3.11	10.63
15	3.58	10.63
16	4.00	10.63

Table (5.1-b): Summary of the gas and liquid flowrates for the annular flow regime.

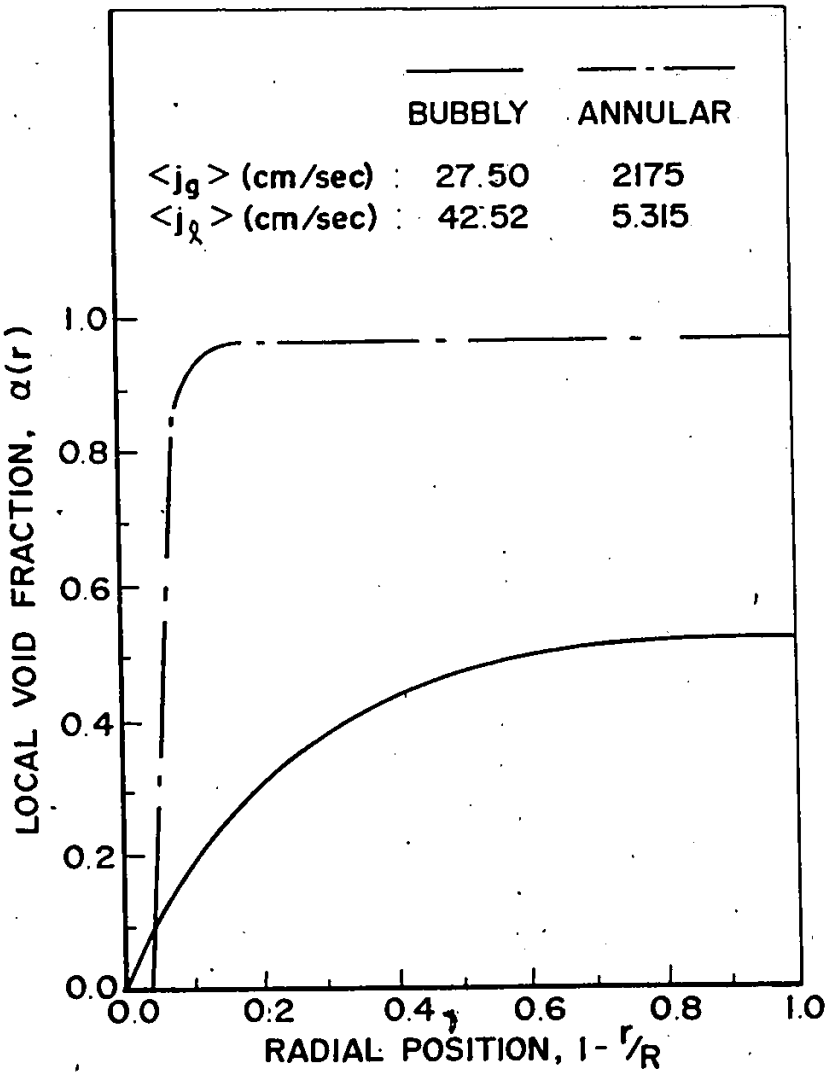

Figure (5.1): Typical void fraction radial profiles for the bubbly and annular flow regimes.

(5.3.2) Testing of the Pressure Drop Measurements

In order to test the adequacy of the method described in Chapter (3) for pressure drop measurement along the test tube, the experimental results were compared with those predicted from one of the existing correlations. For the annular flow regime, the CISE correlation [167] as reported by Levy [122], was used, viz,

$$(-\frac{\partial \bar{P}}{\partial z}) = g\rho_a + \frac{0.42}{D^{1.2}} (\frac{\sigma}{73})^{0.4} [\frac{(G_\ell+G_g)^2}{\rho_a}]^{0.75}, \qquad (5.1)$$

where ρ_a is an average mixture density defined as

$$\frac{1}{\rho_a} = \frac{1}{(G_\ell+G_g)} (\frac{G_\ell}{\rho_\ell} + \frac{G_g}{\rho_g}) . \qquad (5.2)$$

In equation (5.1), all units are in the cgs system.

For the bubbly flow regime, the approach based upon the similarity principles and presented by Dukler et al. [168] was used. For the sake of completeness, this approach is given here in detail. Starting with the requirement of dynamic similarity for two-phase flow, Dukler et al. derived the following equation for the frictional pressure drop component:

$$(-\frac{\partial \bar{P}}{\partial z})_f = \frac{2(G_\ell+G_g)^2 \lambda f}{g D \rho_{ns}}, \qquad (5.3)$$

where ρ_{ns} is the density of the two-phase no-slip homogeneous mixture which can be written in the form

$$\rho_{ns} = \rho_{\ell}(1-\beta) + \rho_g\beta \quad . \tag{5.4}$$

In equation (5.3), λ is a dimensionless group defined by

$$\lambda = \frac{\rho_{\ell}(1-\beta)^2}{\rho_{ns}(1-\langle\alpha\rangle)} + \frac{\rho_g\,\beta^2}{\rho_{ns}\langle\alpha\rangle} \quad , \tag{5.5}$$

and f is the friction factor given as

$$f = f_o\left(1 - \frac{\phi}{1.281+.478\phi+.444\phi^2+.094\phi^3+.00843\phi^4}\right) \quad , \tag{5.6}$$

where

$$\phi = \ell n(1-\beta) \quad . \tag{5.7}$$

Here f_o is the single-phase friction factor evaluated at the mixture Reynolds number, that is,

$$f_o = .0014 + \frac{.125}{(Re_{TP})^{.32}} \quad , \tag{5.8}$$

where

$$Re_{TP} = \frac{(G_{\ell}+G_g)D\lambda}{\mu_{ns}} \quad , \tag{5.9}$$

and μ_{ns} is the viscosity of the no-slip homogeneous mixture which is defined by

$$\mu_{ns} = \mu_{\ell}(1-\beta) + \mu_g\beta \quad . \tag{5.10}$$

To account for the acceleration component of the pressure drop, Dukler et al. multiplied the frictional pressure drop by the factor $1/(1-e)$ where e is given by

$$e = \frac{(G_{\ell}+G_g)G_g\bar{P}}{gP_1P_2\bar{\rho}_g} \quad , \tag{5.11}$$

where P_1 and P_2 are the upstream and downstream absolute pressures, respectively, and $\bar{\rho}_g$ is the gas density calculated at the average value of the absolute pressure along the flow tube, $\bar{P}$. It is clear from equation (5.11) that an iterative procedure is needed to calculate the acceleration correction factor. However, if the pressure drop is much less than the downstream pressure, which was found to be the case ((P_1-P_2) was of the order of 10^5 dyne/cm^2 whereas P_2 was of the order of 10^6 dyne/cm^2), it can be assumed that $\bar{P} \simeq P_1$ and equation (5.11) can be approximated by

$$e \sim \frac{(G_\ell+G_g)G_g}{g\,P_2\,\rho_g} \quad . \qquad (5.12)$$

To calculate the total pressure drop along the vertical two-phase flow tube, an additional term should be included to account for the gravitational component; thus,

$$\left(-\frac{\partial \bar{P}}{\partial z}\right) = \langle\rho\rangle g + \left(-\frac{\partial \bar{P}}{\partial z}\right)_f / (1-e) \quad , \qquad (5.13)$$

where

$$\langle\rho\rangle = \rho_\ell - (\rho_\ell-\rho_g)\langle\alpha\rangle \quad . \qquad (5.14)$$

Figure (5.2-a) shows the variation of the measured values of pressure drop per unit tube length, $\left(-\frac{\partial \bar{P}}{\partial z}\right)$, with the gas volumetric flux density at a constant liquid flowrate for typical experimental runs of bubbly and annular flows. The corresponding predicted values, as calculated using Dukler et al.'s approach [168] for bubbly flow and CISE formula [122] for

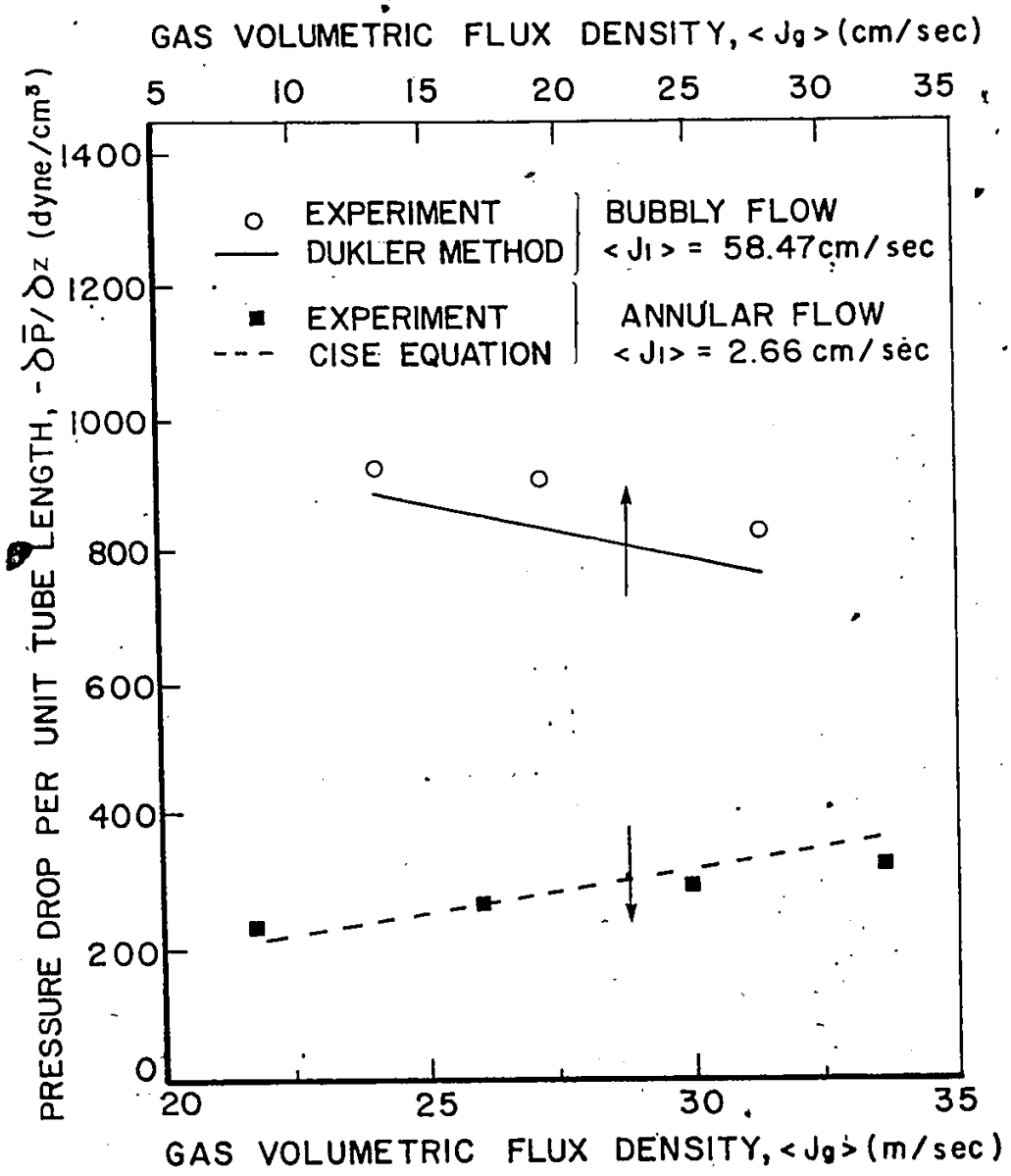

Figure (5.2-a): Variation of the pressure drop per unit tube length with the gas volumetric flux density at a constant liquid flowrate.

annular flow, are also shown in figure (5.2-a). Similarly, the variation of $(-\frac{\partial \bar{P}}{\partial z})$ with the liquid volumetric flux density at a constant gas flowrate for the typical runs of the two flow regimes is shown in figure (5.2-b).

Figure (5.2-a) indicates different trends for the dependence of the pressure drop on the gas volumetric flux density for the different flow regimes. In the bubbly flow regime, as the gas flowrate increases, the pressure drop decreases. This can be attributed to the reduction in the static head component of the pressure drop due to the reduction in the flow density. Although the frictional pressure drop component increases with gas flowrate, its rate of increase is much less than the rate of decrease of the static component. On the other hand, in the annular flow regime, the static head component becomes relatively less important and the increase in the frictional pressure loss causes the total pressure drop to increase with the gas flowrate. At a constant gas flowrate, the total pressure drop is found to increase with the liquid volumetric flux density for both regimes (figure (5.2-b)) because of the increase of the static and frictional components of the pressure drop.

In figures (5.3-a) and (5.3-b), the deviations between the measured and predicted values of the pressure drop for all the experimental runs are shown for the bubbly and annular flow regimes, respectively. These plots indicate fairly good agreement between the measured and predicted pressure drop. The maximum deviation is less than 10% in the bubbly flow

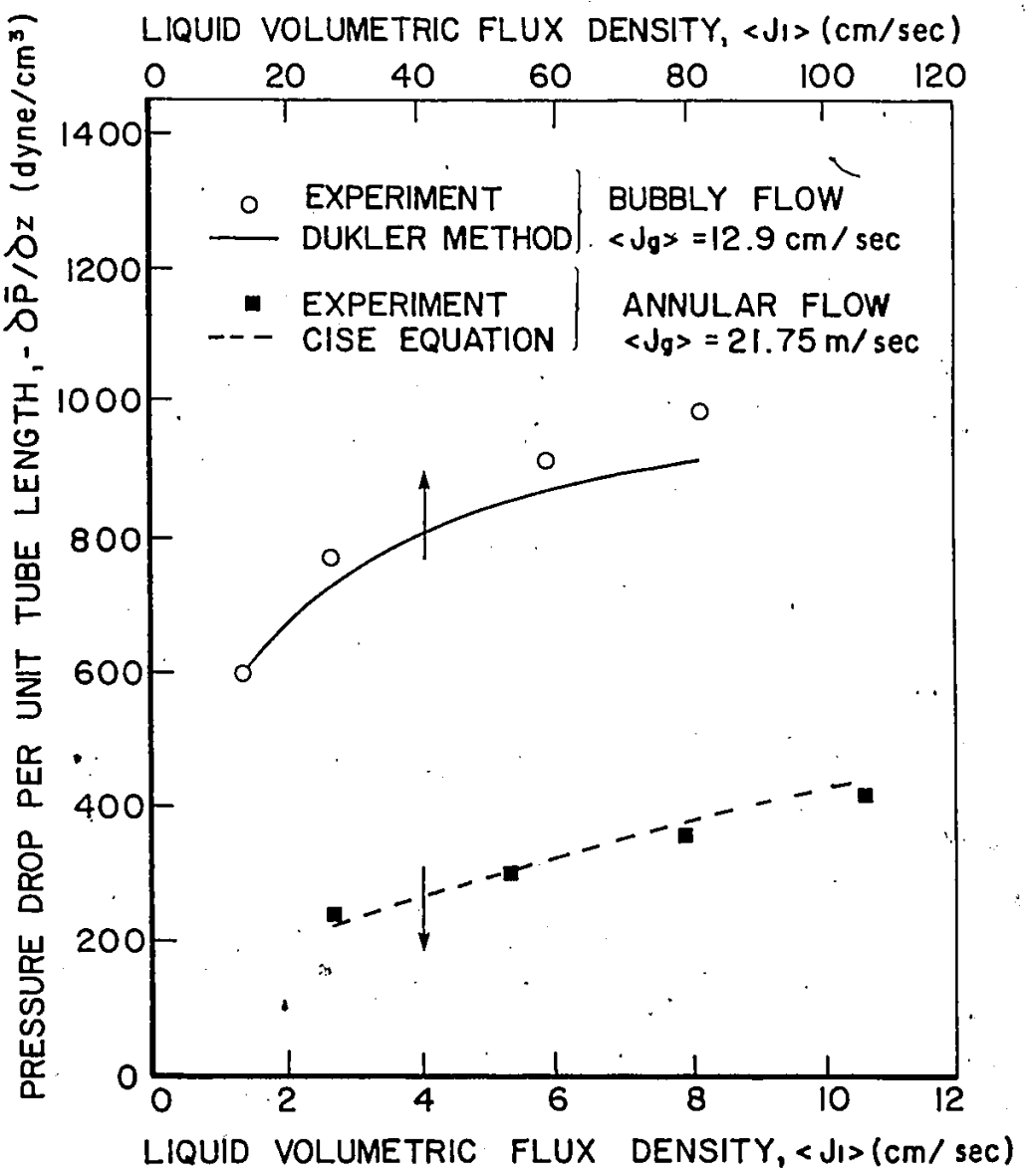

Figure (5.2-b): Variation of the pressure drop per unit tube length with the liquid volumetric flux density at a constant gas flowrate.

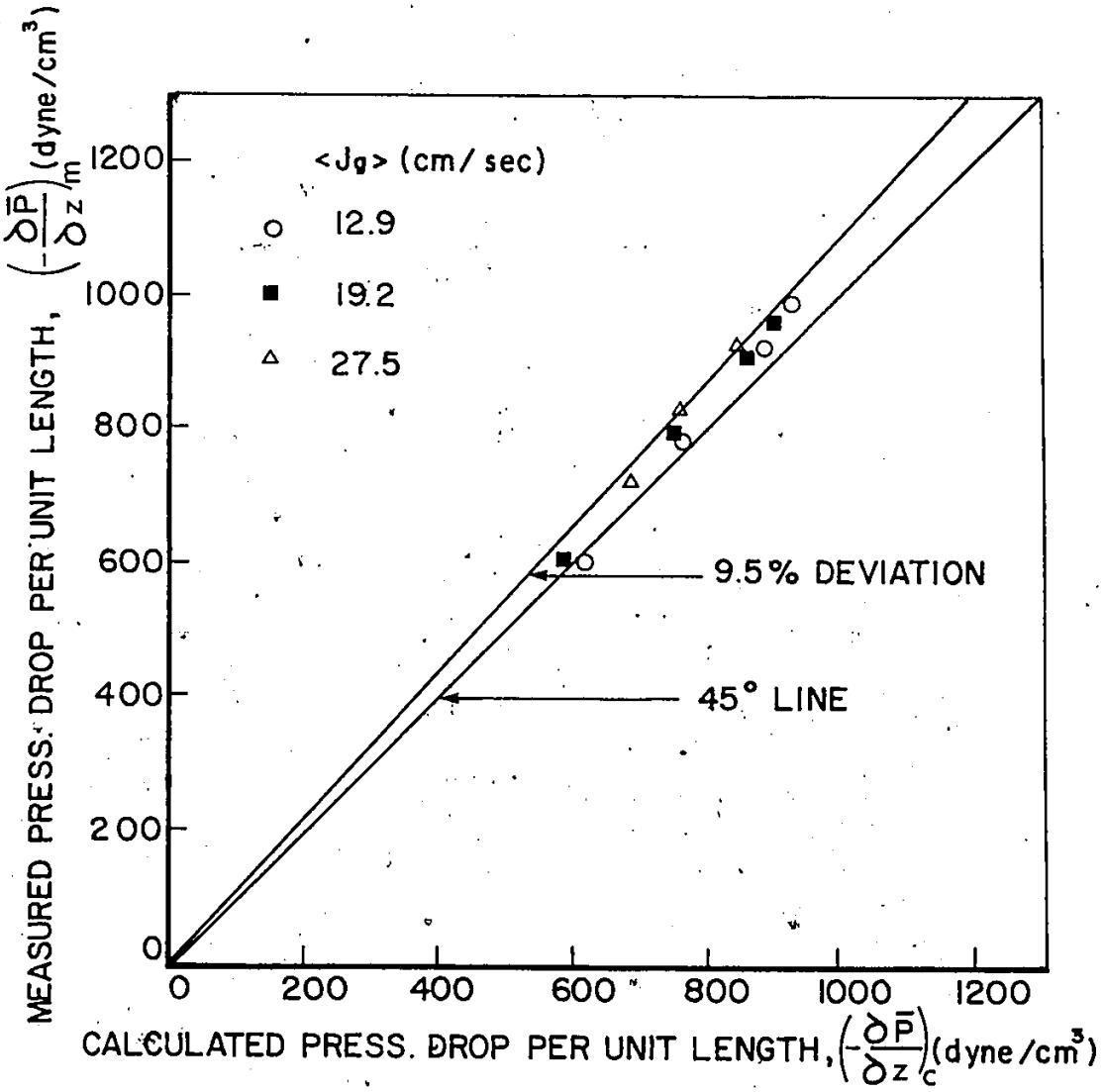

Figure (5.3-a): Comparison between the measured and calculated values of pressure drop per unit tube length for the bubbly flow regime.

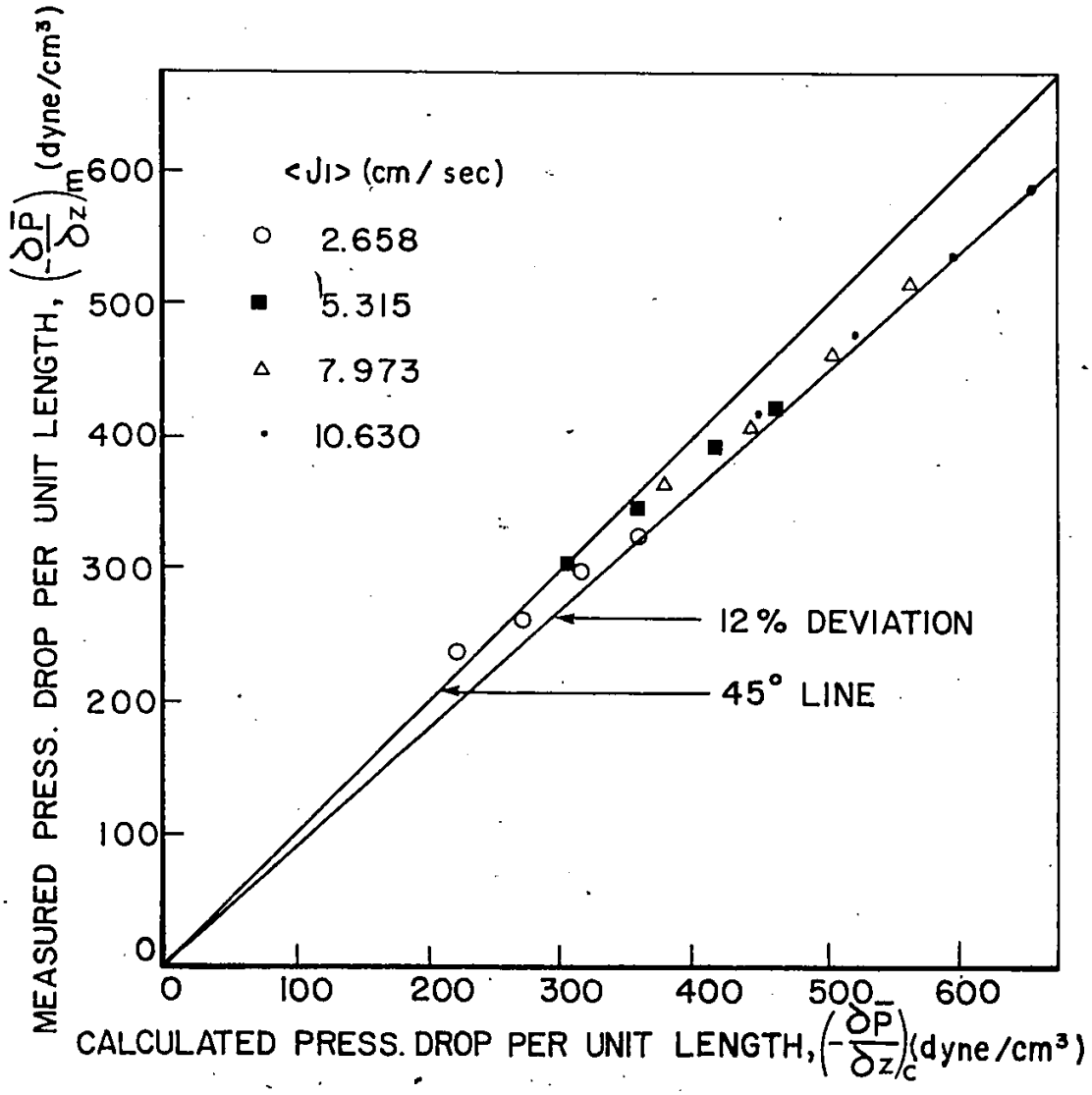

Figure (5.3-b): Comparison between the measured and calculated values of pressure drop per unit tube length for the annular flow regime.

regime and about 12% for the annular flow regime.

(5.4) Results and Discussions

(5.4.1) Bubbly Flow

The relation between the cross-sectional average void fraction, $\langle\alpha\rangle$, and the apparent volume concentration, β, is plotted in figure (5.4-a). According to the analysis presented by Bankoff [71], the slope of the straight line which best fits the experimental data is equal to the flow parameter, K (equation (2.5)). The estimated value of K is 0.807 which is in good agreement with the published values [73]. The 45° line shown in figure (5.4-a) represents the expected behaviour of the homogeneous model with K = 1.

Figure (5.4-b) shows a plot of the relation between the gas weighted mean velocity, $\langle j_g\rangle/\langle\alpha\rangle$, and the mixture average velocity, $\langle j_m\rangle$. As indicated in Chapter (2), Zuber and Findlay [17] derived, from the basic field definitions, the following relationship between $\langle j_g\rangle/\langle\alpha\rangle$ and $\langle j_m\rangle$:

$$\langle j_g\rangle/\langle\alpha\rangle = C_o\langle j_m\rangle + \bar{V}_{gj} \quad . \qquad (5.15)$$

This equation suggests that the slope and intercept of the straight line which is fitted to the experimental data, shown in figure (5.4-b), represent an estimate of C_o and $\bar{V}_{gj}$, respectively. The values of these flow parameters, averaged for the bubbly flow regime, were estimated as $C_o = 1.138$ and $\bar{V}_{gj} = 6.25$ cm/sec which are in good agreement with the limits specified by Zuber and Findlay [17]. Again the 45° line shown in figure (5.4-b) repre-

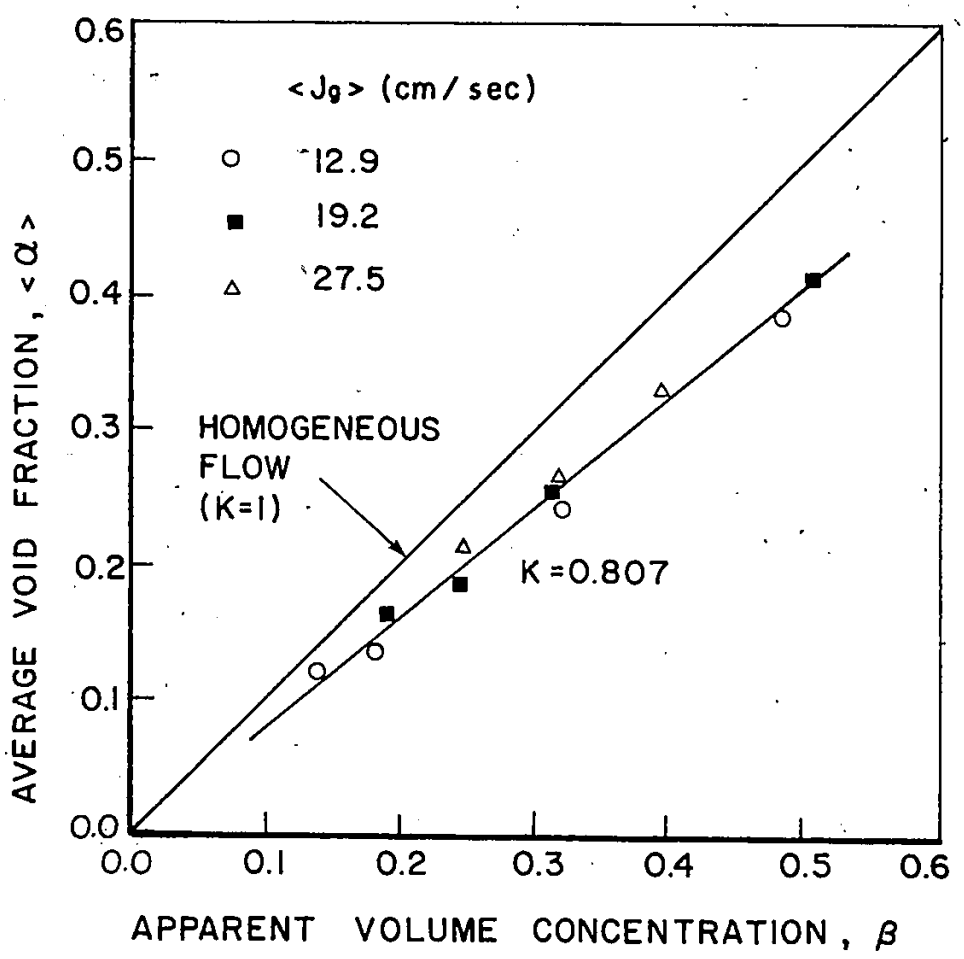

Figure (5.4-a): Average void fraction - apparent volume concentration relation for the bubbly flow regime.

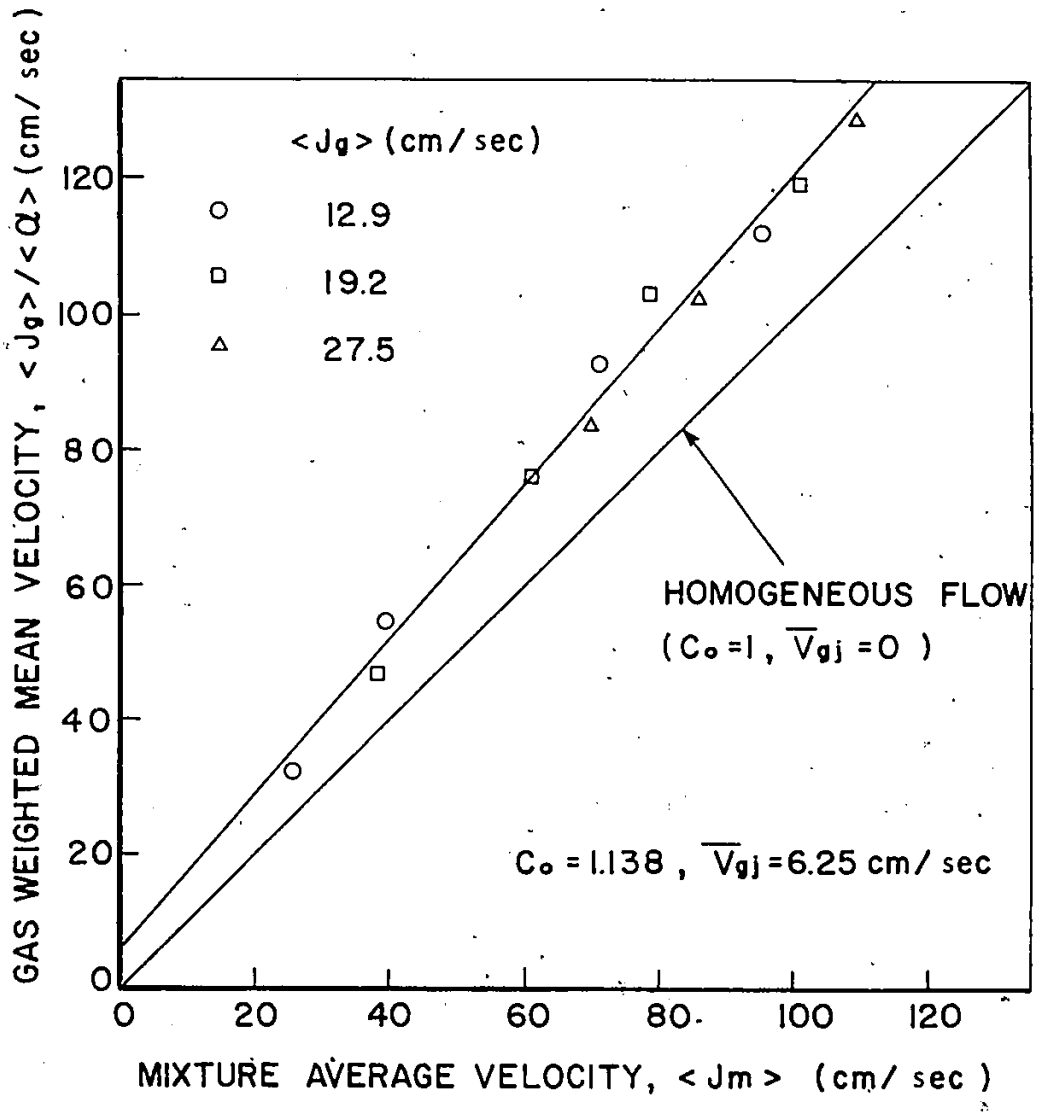

Figure (5.4-b): Gas weighted mean velocity-mixture average velocity relation for the bubbly flow regime.

sents the homogeneous model ($C_o = 1$ and $\bar{V}_{gj} = 0$).

Figure (5.4-b) indicates that the experimental data are well represented by the fitted straight line. The deviations between the straight line and the data do not exhibit a systematic trend and therefore can be attributed to experimental uncertainties. This observation is similar to that made by Zuber and Findlay [17] when they plotted the experimental data obtained by Petrick [81] and Bailey et al. [82] on $\langle j_g \rangle / \langle \alpha \rangle - \langle j_m \rangle$ planes. Moreover, figure (5.4-b) emphasizes the conclusion made by Zuber and Findlay [17] that the flow parameters do not depend on the flowrates of the phases and remain essentially constant for a given flow regime. One can conclude, then, that the estimated values of the slope and intercept are good representation of the flow parameters averaged for the bubbly flow regime. In other words, the estimated values of the flow parameters can be used without introducing appreciable errors to predict the cross-sectional average void fraction from equation (5.15) for the specified experimental apparatus. The root-mean squares of deviations between the predicted and measured values of the cross-sectional average void fraction was calculated as 5.21% which is reasonably good.

To emphasize the adequacy of the method presented above to determine the flow parameters, some of the steady-state measurements performed by Malnes [29] for air-water bubbly flow, in a 2.63 cm I.D. tube at atmospheric pressure, were used. In selecting these data, the consistency of the conditions under which

they were obtained was considered. Table (5.2) summarizes the selected steady-state measurements of the cross-sectional average void fraction together with the flow conditions at which they were obtained. Figure (5.5) shows the relation between $\langle j_g \rangle / \langle \alpha \rangle$ and $\langle j_m \rangle$ together with the straight line which was fitted to the experimental data. From the slope and intercept of the fitted straight line, the distribution parameter and mean drift velocity were best estimated as 0.851 and 29.64 cm/sec, respectively.

It is evident from figure (5.5) that most of the experimental data are well described by the fitted straight line which emphasizes the adequacy of this method to estimate the flow parameters. It is also important to realize that in contradiction to Bankoff's observation [71] and the present results, the distribution parameter determined by Malnes is smaller than unity. This can be attributed to the different phase injection system which was employed by Malnes in performing his experiments. In the present work, air was introduced to the flow tube through the bottom end of the mixing section whereas the liquid phase was injected through the walls of this section. On the other hand, in the experimental apparatus used by Malnes [29], air was injected through the periphery of the mixing section into the continuously flowing liquid phase. This explains the peaks which were indicated by Malnes' radial void profiles near the wall region. As indicated by equation (1.5-a) which defines the distribution parameter, C_o, peaked values of void fraction

Experiment No.	Volumetric Flux Density (cm/sec)		Average void Fraction, $\langle\alpha\rangle$	Pressure (Atmosphere)	Temperature (°C)
	$\langle j_g \rangle$	$\langle j_\ell \rangle$			
R-72	8.95	58.50	0.1015	1.238	33.0
R-73	14.25	58.50	0.1475	1.228	33.0
R-74	19.95	58.50	0.2060	1.210	33.0
R-75	25.80	58.50	0.2500	1.204	33.0
R-76	31.80	58.80	0.3010	1.194	33.0
R-77	37.90	58.80	0.3360	1.190	33.0
R-78	44.60	58.80	0.3690	1.184	33.5
R-82	8.90	100.00	0.0707	1.249	33.5
R-83	14.10	99.50	0.1150	1.241	33.5
R-84	19.50	102.00	0.1560	1.237	33.5
R-85	25.20	100.80	0.1920	1.237	34.0
R-86	31.20	100.80	0.2240	1.224	34.0
R-87	43.50	102.00	0.2770	1.210	34.0
R-88	56.00	100.50	0.3440	1.201	34.0
R-89	75.00	100.80	0.4120	1.197	34.0
R-90	88.60	100.50	0.4440	1.190	34.0
R-93	13.90	149.50	0.0875	1.263	34.0
R-94	19.35	149.00	0.1100	1.256	34.0
R-95	24.90	149.50	0.1390	1.249	34.0
R-96	30.60	149.00	0.1700	1.247	34.0
R-97	36.40	149.50	0.1950	1.243	34.0
R-129	13.73	149.50	0.0836	1.259	31.0
R-130	24.60	149.30	0.1400	1.249	31.0
R-131	36.10	149.50	0.1920	1.240	31.5
R-132	47.90	149.50	0.2370	1.233	31.5

Table (5.2): Steady-state air-water measurements performed by Malnes for bubbly flow in a 2.63 cm I.D. tube at atmospheric pressure [29].

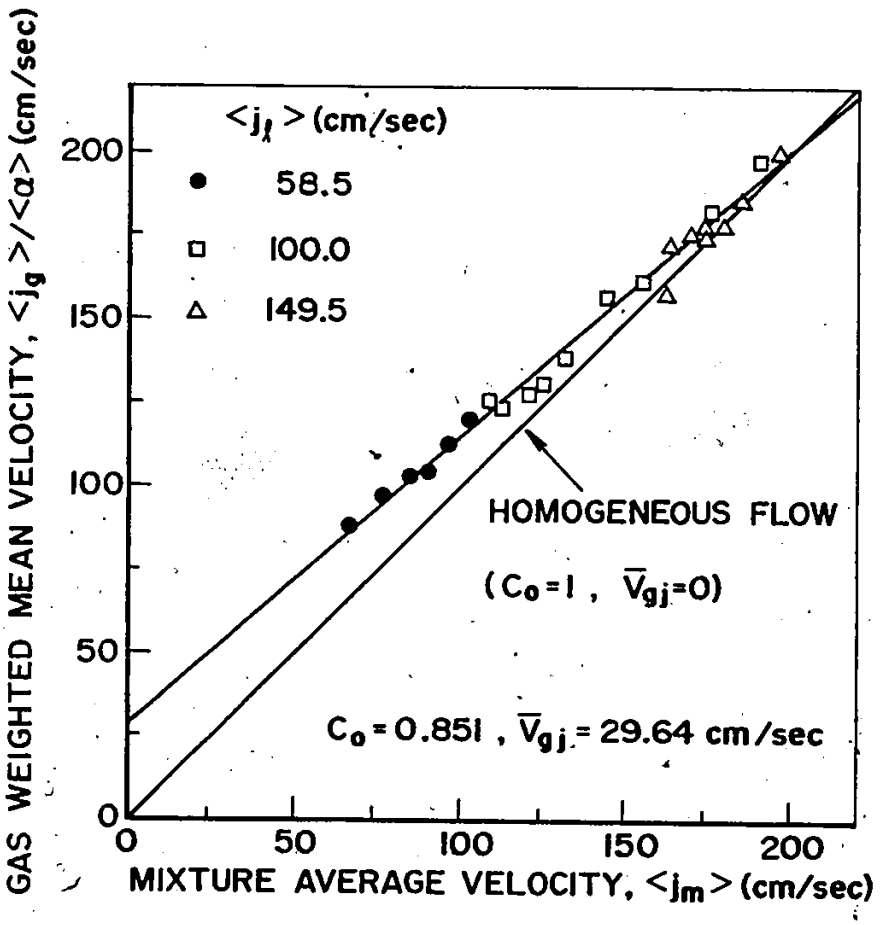

Figure (5.5): Gas weighted mean velocity-mixture average velocity relation for Malnes' data [29].

in the low-velocity region near the tube wall would result in a value of C_o smaller than unity.

(5.4.2) Annular Flow

A similar plot of the relation between $\langle j_g \rangle / \langle \alpha \rangle$ and $\langle j_m \rangle$ is shown in figure (5.6) for the annular flow regime. The slope and intercept of the fitted straight line yield values of flow parameters of $C_o = 1.082$ and $\bar{V}_{gj} = 120.04$ cm/sec which are in good agreement with Zuber and Findlay's limits [17]; the 45° line shown represents the case where the homogeneous model is assumed to be valid ($C_o = 1$ and $\bar{V}_{gj} = 0$).

Figure (5.6) indicates an extremely good fitting of the experimental data to the straight line which demonstrates the adequacy of the present method to estimate the flow parameters in annular flow. It also emphasizes the conclusion that these flow parameters remain essentially constant as long as the flow regime is unchanged. To test the adequacy of the estimated values of the flow parameters to predict the cross-sectional average void fraction, these values were substituted into equation (5.15) together with the measured values of $\langle j_g \rangle$ and $\langle j_m \rangle$ listed in table (5.1-b). The root-mean squares of deviations between the predicted and measured values of the cross-sectional average void fraction was found to be 0.70% which is, as expected, very low.

(5.5) Alternative Method

As shown in the previous section, a plot of the relation between $\langle j_g \rangle / \langle \alpha \rangle$ and $\langle j_m \rangle$ is required in order to evaluate the flow

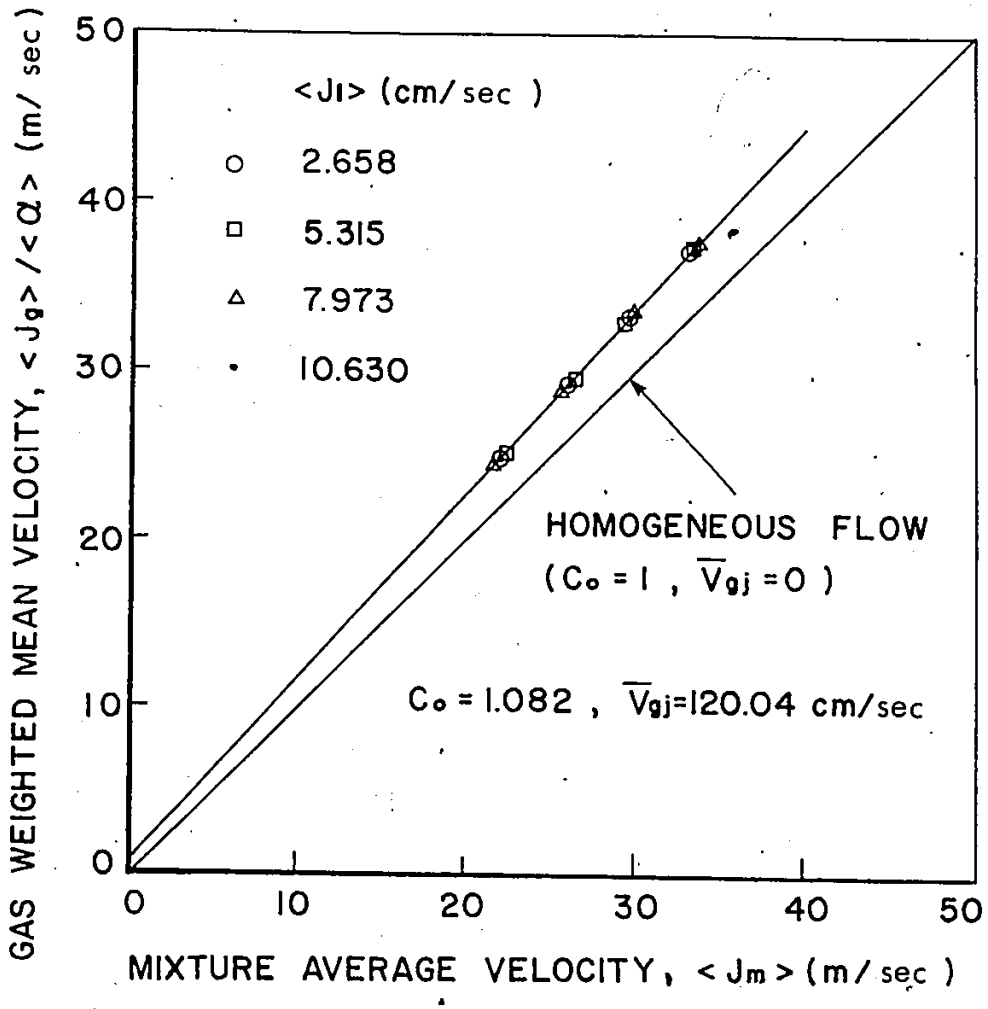

Figure (5.6): Gas weighted mean velocity-mixture average velocity relation for the annular flow regime.

parameters. This includes the measurements of several radial void fraction profiles which is, obviously, not desirable from the standpoint of the designer who would need these parameters to predict the transient behaviour of two-phase flow in situations where the flow regime remained unchanged during the transient. It is much preferable, then, to have an alternative method which enables the designer to evaluate the flow parameters by performing a single experiment in which the radial void profile is measured.

Equations (1.5-a) and (1.5-b), which define the flow parameters, indicate that these parameters may be readily evaluated if the radial profiles of mixture velocity and void fraction are available. While the radial void profile can be measured using the neutron attenuation technique, to the author's knowledge, no adequate method has been developed to measure the mixture velocity radial profile in two-phase flow. The conventional techniques which have been employed to measure the radial velocity profile in single-phase flow, e.g., a pitot tube, are not recommended for two-phase flow [29]. Consequently, a model, based on the mixing length theory, was developed to predict the radial profile of mixture velocity in two-phase flow.

(5.5.1) Mixing Length Model

The problem is to be viewed in cylindrical coordinates with the flow direction being the positive z-axis. Let u, v and w be the instantaneous velocity components at any point in the r, z and θ directions, respectively. The flow is assumed to be fully developed. Like single-phase turbulent flow, the two-phase flow is characterized by irregular velocity fluctuations superimposed on the mean stream velocity. In fact, the velocity, void fraction and pressure at a fixed point in space

do not remain constant with time, but exhibit very irregular fluctuations of high frequency. These fluctuations are caused by lumps or macroscopic packets of molecules (turbulent eddies) which have different sizes and continuously agglomerate or disintegrate.

In this analysis, as was done by Bankoff [71] and Levy [21], the two-phase flowing mixture is considered to be a pseudo-continuous medium; hence, the mixing length concept may be applied. Therefore, at any arbitrary time t, each of the velocity components, void fraction, density and pressure may be resolved into a constant mean (time-averaged) component and a fluctuating component; thus,

$$\left.\begin{aligned} v &= \bar{v} + v' \quad , \\ u &= \bar{u} + u' \quad , \\ w &= \bar{w} + w' \quad , \\ \alpha &= \bar{\alpha} + \alpha' \quad , \\ P &= \bar{P} + P' \quad , \\ \rho &= \bar{\rho} + \rho' \quad . \end{aligned}\right\} \tag{5.16}$$

The time-averaged component is defined, for example, for the v-component of velocity as

$$\bar{v} = \frac{1}{t_1} \int_{t}^{t+t_1} v \, dt \quad , \tag{5.17}$$

where t_1 is a sufficiently long time to ensure that these average values are completely independent of the time interval for the observations. According to the above definition, the average values of the fluctuating terms vanish, that is,

$$\bar{v}' = \bar{w}' = \bar{u}' = \bar{\alpha}' = \bar{\rho}' = \bar{P}' = 0. \qquad (5.18)$$

Based upon the pseudo-continuous two-phase flow assumption, the mixture density can be related to the void fraction as

$$\rho = \alpha\rho_g + (1-\alpha)\rho_\ell \ . \qquad (5.19)$$

Upon substituting for ρ and α from equation (5.16) into equation (5.19) and taking the time-average, one can write

$$\bar{\rho} = \bar{\alpha}\rho_g + (1-\bar{\alpha})\rho_\ell \ . \qquad (5.20)$$

Subtracting equation (5.20) from equation (5.19) yields

$$\rho' = -\Delta\rho\alpha' \ . \qquad (5.21)$$

Since the flow is fully developed and the tube is assumed of uniform diameter, then,

$$\bar{u} = 0. \qquad (5.22)$$

Assuming no spiraling effect, the azimuthal component can be considered equal to zero, that is,

$$\bar{w} = 0 \ . \qquad (5.23)$$

Using the above system of equations, it can be shown (Appendix (D)) that the continuity equation for the two-phase flow mixture becomes

$$\frac{1}{r}\frac{\partial}{\partial r}(r\bar{\rho}\bar{u}) + \frac{\partial}{\partial z}(\bar{\rho}\bar{v}) = 0, \qquad (5.24\text{-a})$$

and

$$\frac{1}{r}\frac{\partial}{\partial r}\left(r\overline{\alpha' u'}\right) + \frac{\partial}{\partial z}\left(\overline{\alpha' v'}\right) = 0. \qquad (5.24\text{-b})$$

Similarly, the momentum equation in the direction of flow is

$$\frac{1}{r}\frac{\partial}{\partial r}\left[r\left\{\bar{\rho}\,\overline{u'v'} - \Delta\rho\,\bar{v}\,\overline{\alpha' u'} - \mu\frac{\partial \bar{v}}{\partial r}\right\}\right] = \left(-\frac{\partial \bar{P}}{\partial z}\right) - \bar{\rho}g. \qquad (5.25)$$

Equations (5.24) and (5.25) are, in fact, the time-averaged equations of continuity and momentum for steady-state, fully-developed, turbulent two-phase flow. The equation of continuity (5.24-a) is the same as that for laminar flow, except that the time-averaged velocity and density components replace the instantaneous values; in addition, equation (5.24-b) governs the fluctuating components. Similarly, in the momentum equation, the velocity components, pressure and density are replaced by their time-averaged values; in addition, however, new terms arise which are associated with the turbulent void and velocity fluctuations.

The momentum equation can be integrated to yield

$$\left(\overline{\rho v' u'} - \bar{v}\Delta\rho\,\overline{\alpha' u'} - \mu\frac{\partial \bar{v}}{\partial r}\right) = \frac{1}{r}\int r\left[\left(-\frac{\partial \bar{P}}{\partial z}\right) - \bar{\rho}g\right]dr + c. \qquad (5.26)$$

The left-hand side of equation (5.26) represents the total shear stress acting on the fluid at the point in question; it consists of the following two distinct parts:

(i) The laminar shear stress, $\tau^{(\ell)}$, which is given by

$$\tau^{(\ell)} = -\mu\frac{\partial \bar{v}}{\partial r}, \qquad (5.27)$$

and

(ii) The turbulent shear stress, $\tau^{(t)}$, given as

$$\tau^{(t)} = \bar{\rho}\ \overline{v'u'} - \bar{v}\ \Delta\rho\ \overline{\alpha'u'} \quad . \tag{5.28}$$

This means that the superposition of the fluctuations on the mean motion gives rise to an additional shear stress which is usually called the Reynolds shear stress. It should be pointed out that while the laminar shear stress is actually a momentum transfer on the molecular scale, the turbulent shear stress is on a scale which is appreciable compared with the tube diameter.

In principle, the radial velocity profile may be calculated for any given flow situation from the momentum equation provided that the turbulent shear stress is known as a function of the system variables. Several empirical relations have been widely used. One of the best-known and accepted expressions was that based on the mixing length hypothesis developed by Prandtl [169]. By assuming that the eddies move in a flow field very much as molecules move about in a gas, Prandtl developed an expression for momentum transfer in a fluid. In this expression, the mixing length was introduced to play a role roughly analogous to that played by the mean free path in the kinetic theory of gases. In other words, the mixing length is, by definition, a measure of the distance moved by a lump or an agglomerate of fluid before mixing with another fluid lump. Then,

$$u' = v' = \ell_v \frac{d\bar{v}}{dr} \ , \tag{5.29-a}$$

and

$$\rho' = \ell_\rho \frac{d\bar{\rho}}{dr} \ , \tag{5.29-b}$$

where ℓ_v and ℓ_ρ are the mixing length for the velocity and density distributions. If the turbulent exchange processes for momentum and mass are assumed to be essentially the same, then, the mixing length for the velocity and density should be equal; and

$$\ell_v = \ell_\rho = \ell. \tag{5.30}$$

Combining equations (5.21), (5.28), (5.29) and (5.30), the turbulent shear stress, $\tau^{(t)}$, can be written as

$$\tau^{(t)} = \ell^2 \left(\frac{d\bar{v}}{dr}\right) \frac{d}{dr} \left(\bar{\rho}\bar{v}\right) . \tag{5.31}$$

This expression is identical to that used by Levy [21], by Pai [128] and by Hsu and Smith [170].

Combining equations (5.26), (5.28) and (5.31) and realizing that $\bar{v}$ is, in fact, the two-phase mixture velocity, j_m, the momentum equation can be written in the form

$$\ell^2 \left(\frac{dj_m}{dr}\right) \left(\frac{d\bar{\rho}j_m}{dr}\right) - \mu \left(\frac{dj_m}{dr}\right) = \frac{1}{r} \int r\left[\left(-\frac{\partial \bar{P}}{\partial z}\right) - \bar{\rho}g\right] dr + c . \tag{5.32}$$

Equation (5.32) is a quadratic equation in $\left(\frac{dj_m}{dr}\right)$; it can be integrated to give the radial velocity profile if the density radial distribution, the pressure gradient and the mixing length parameter, ℓ^2, are known.

From the velocity measurements in turbulent flow of a single fluid, Nikuradse [171] presented a graphical relation between the mixing length, ℓ, and the distance measured from the tube wall. He demonstrated that in single-phase flow, the

mixing length is only a function of the distance measured from the tube wall and is independent of the flowrate and fluid properties. Levy [21] argued that there is no reason to expect different behaviour in two-phase flow. A similar assumption was made by Beattie [20], Tippets [123], and Calvert and Williams [124] who used the mixing length, as determined for single-phase flow, in two-phase flow systems. In this work, the same assumption will be made; however, the sensitivity of the estimated values of flow parameters, C_o and $\bar{V}_{gj}$, to this assumption will be examined later.

Now consider the following flow regimes:

(i) Bubbly Flow Regime

In order to define the density radial distribution given by equation (5.20), the mathematical model proposed for the void fraction radial profile (equation (4.41)) is substituted to give

$$\bar{\rho} = \rho_\ell - \Delta\rho\alpha_c[1 - (\frac{r}{R})^n] \quad , \qquad (5.33)$$

where α_c and n are to be estimated from an independent set of transmittance experiments.

Assuming that the pressure gradient is uniform along the tube, the term $(-\frac{\partial\bar{P}}{\partial z})$ is, in fact, equal to the measured or calculated pressure drop per unit tube length. By inserting the value of the pressure drop and the radial density distribution (equation (5.33)) into the integrand in the right-hand side of equation (5.32), it can be analytically integrated.

The radial velocity profile can, then, be readily obtained by numerically integrating equation (5.32) using, for example, a fourth-order Runge-Kutta formulation [172]. In the cases presented here, the mixing length for the two-phase flow system is evaluated from the graphical relation prepared by Nikuradse [171] for single-phase turbulent flow. The boundary conditions expressing the no-slip condition at the wall and flow symmetry are, respectively,

$$\text{at } r = R \quad , \quad j_m = 0 \quad \text{and} \quad \bar{\rho} = \rho_\ell , \tag{5.34-a}$$

and

$$\text{at } r = 0 \quad , \quad \frac{d\bar{\rho}}{dr} = \frac{dj_m}{dr} = 0. \tag{5.34-b}$$

Knowing the radial velocity profile, as predicted from the mixing length model, and the radial void profile, as measured using the neutron attenuation technique, equation (1.5-a) can be used to estimate the distribution parameter. Similarly, one can use equation (1.5-b) to evaluate the mean drift velocity if an expression for the local drift velocity, V_{gj}, is available. Zuber and Findlay recommended the following constitutive re-

lationship for V_{gj} in bubbly flow [17]:

$$V_{gj} = 1.41 \left(\frac{\sigma g \Delta\rho}{\rho_\ell^2}\right)^{0.25} (1-\alpha)^{1.5} . \qquad (5.35)$$

(ii) Annular Flow Regime

Most of the analysis presented here is very similar to that given by Levy [122]. For the sake of completeness, the approach of Levy with some modification will be presented in detail. As has been mentioned earlier, annular flow can be considered to be made up of two distinct and adjacent regions; the film layer at the tube wall and the central core region. The radial distribution of void fraction in these two regions has been assumed to be of the form given in equation (4.42). Now consider these regions in turn.

(a) Film Region

For simplicity, it has been assumed that the film region is made up entirely of liquid. Then, the density in the film can be assumed to be equal to the liquid density and equation (5.32) can be simplified to

$$\rho_\ell \ell^2 \left(\frac{dj_m}{dr}\right)^2 - \mu_\ell \left(\frac{dj_m}{dr}\right) = \frac{1}{r} \int r\left[\left(-\frac{\partial \bar{P}}{\partial z}\right) - \rho_\ell g\right] dr + c \quad . \qquad (5.36)$$

In a way similar to that described for equation (5.32), this equation can be solved to yield the radial velocity distribution in the film region if the following boundary conditions are used:

$$\text{at } r = R \quad , \quad j_m = 0 \quad , \qquad (5.37\text{-a})$$

and

$$\text{at } r = a \quad , \quad j_m = v_i \quad . \qquad (5.37\text{-b})$$

The shear stress distribution in the film region is derived in Appendix (E) in the form

$$\tau = \frac{R}{r} \tau_w + \left[\rho_\ell g - \left(-\frac{\partial \bar{P}}{\partial z}\right)\right] \left(\frac{R^2 - r^2}{2r}\right) \quad , \qquad (5.38)$$

where τ_w is the wall shear stress which is given by

$$\tau_w = \frac{R}{2} \left[\left(-\frac{\partial \bar{P}}{\partial z}\right) - g\rho_c \frac{a^2}{R^2} - g\rho_\ell \left(1 - \frac{a^2}{R^2}\right)\right] \quad . \qquad (5.39)$$

In equation (5.39), ρ_c is the average density in the core region which is also derived in Appendix (E) as

$$\rho_c = \rho_\ell - \frac{n\Delta\rho\alpha_c}{n+2} \quad . \qquad (5.40)$$

The film flowrate per unit tube cross-section area can be defined as

$$G_f = \frac{1}{\pi R^2} \int_a^R \rho_\ell \, j_m \, 2\pi r \, dr \quad . \qquad (5.41)$$

The difference between the total liquid flowrate per empty tube area, G_ℓ, and this calculated G_f is the entrained liquid flowrate per unit tube area, G_e. That is,

$$G_e = G_\ell - G_f \ . \qquad (5.42)$$

It should be mentioned here that G_f should be less than or equal to G_ℓ. The average velocity in the film region can also be defined as

$$\bar{j}_f = \frac{G_f}{\rho_\ell} \left(\frac{R^2}{R^2-a^2}\right) \ . \qquad (5.43)$$

(b) Core region

The mixture density in the core region, which consists of a gas laden with liquid droplets entrained from the film region, can be obtained by combining equations (4.42) and (5.20) as

$$\bar{\rho} = \rho_\ell - \Delta\rho\alpha_c\left[1 - \left(\frac{r}{a}\right)^n\right] \ , \qquad (5.44)$$

which upon substituting in equation (5.32) and solving yields the radial velocity profile in the core region. The following boundary conditions are used:

$$\text{at } r = a \ , \quad j_m = v_i \ , \qquad (5.45\text{-a})$$

and

$$\text{at } r = 0 \ , \quad \frac{dj_m}{dr} = \frac{d\bar{\rho}}{dr} = 0 \ . \qquad (5.45\text{-b})$$

The first condition is, in fact, the no-slip condition at the core-film interface; the second condition is due to symmetry. The shear stress radial distribution is similarly derived for the core region in Appendix (E) as

$$\tau = \frac{a}{r}\tau_i - [(-\frac{\partial \bar{P}}{\partial z}) - g\rho_c](\frac{a^2}{r^2} - 1)\frac{r}{2} - \frac{g\Delta\rho\alpha_c}{(n+2)}(\frac{r^n}{a^n} - 1)r \quad , \quad (5.46)$$

where τ_i is the value of shear stress at the core-film interface which is given by

$$\tau_i = \frac{a}{2}[(-\frac{\partial \bar{P}}{\partial z}) - g\rho_c] \quad . \quad (5.47)$$

It should be mentioned here that the shear stress distribution in both the film and core regions is far from being uniform or even linear as has been considered by many investigators [20, 122, 124 and 129]. The non-linearity of the shear stress radial distribution for annular two-phase flow in circular pipes was also considered by a number of other research workers [157, 173-175]. Note also that in order to integrate equations (5.32) and (5.36), the mean film thickness has to be known a priori.

Film Thickness Determination

Because of the wavy interface of the film, the film thickness is a function of both axial position and time. At a certain level along the test tube, the equivalent film thickness, F, is, in fact, the time-average value. To determine F, equate the interface shear stress, as given by equation (5.47), with that given by the mixing length theory at r = a, i.e.,

$$\frac{a}{2}[(-\frac{\partial \bar{P}}{\partial z}) - g\rho_c] = [\ell^2(\frac{dj_m}{dr})(\frac{d\bar{\rho}j_m}{dr}) - \mu(\frac{dj_m}{dr})]_{r=a} \quad . \quad (5.48)$$

From equation (5.48), it can be seen that in order to determine the mean film thickness, the velocity and void radial profiles at least

near the core-film interface must be known. But, as mentioned above, to calculate the radial velocity profile, the mean film thickness must be known a priori. Furthermore, as shown in Appendix (C) and mentioned in section (4.5), the values of the void profile parameters, n and α_c, can be determined from the transmittance data only if the mean film thickness is known. Hence it was necessary to use an iterative procedure to determine the mean film thickness, the void profile parameters and the radial velocity profile. This iterative procedure was carried out as follows: First, a starting value was assumed for the mean film thickness and then the transmittance data were used to estimate the values of the void profile parameters. The radial velocity profiles in both the film and core regions were calculated using equations (5.32) and (5.36) and then the mean film thickness was determined using equation (5.48). The determined value of the mean film thickness was then compared with that assumed; if the difference was within a prescribed tolerance, the flow parameters were determined using the measured radial void profiles and the predicted radial velocity profiles. If not, the entire procedure was repeated with a new value of the mean film thickness. In each iterative step, the film flowrate had to be calculated to ensure that it did not exceed the total liquid flowrate. If it did, the film flowrate was assumed equal to the total liquid flowrate and the corresponding mean film thickness was then recalculated.

Two corrections have been suggested by Levy [122] and used in this analysis to account for the core inhomogeneity and for the rippling effect of the core-film interface; these

corrections are

(a) Homogeneity Correction

In the analysis presented here, the core flow has been assumed homogeneous while, in fact, there is a relative velocity between the gas phase and the entrained liquid droplets. To correct for this assumption, the mixing length, ℓ, in the core region is multiplied by a correction factor, R'. Levy [122] considered the correction factor, R', to be a function of the phase density ratio, ρ_ℓ/ρ_g.

(b) Interface Rippling Correction

The appearance of definite wave patterns on the film-core interface in vertical annular two-phase flow was observed by many investigators [37, 149, 157, 173 and 176]. At a low gas velocity, the characteristic wave-length is quite large; however, as the gas flowrate is increased, the wave-length decreases so that many individual waves can exist in the flow tube at the same time. These waves are expected to affect the turbulence characteristics in the core and, hence, the mixing length; thus, a correction factor for this effect is required in equation (5.47). Moreover, when the pressure drop, $(-\frac{\partial \bar{P}}{\partial z})$ is smaller than the gravity term, $g\rho_\ell$, there is more shear transmitted to the liquid film through the interface than it can dissipate along the tube wall. Consequently, the interface waves are expected to be larger and, hence, the mixing length will be larger at the interface. In this case, Levy [122]

suggested that the mixing length at the interface should be multiplied by the factor $[g\rho_\ell/(-\frac{\partial \bar{P}}{\partial z})]^{1/3}$ if $(-\frac{\partial \bar{P}}{\partial z})$ is less than $g\rho_\ell$; if it is greater, then, no correction need be applied.

As indicated in the previous subsection, the predicted radial velocity profile can be combined with the measured radial void profile to evaluate the flow parameters, using equation (1.5), once an expression for the local drift velocity, V_{gj}, is assumed. However, the annular flow regime is characterized by the existence of two distinct flow regions; namely: the film and core regions. Hence, there is no fundamental significance for V_{gj} and the mean drift velocity, $\bar{V}_{gj}$, for annular flow is merely a mathematical parameter which was shown in Chapter (1) to appear in the void propagation equation. Consequently, in annular flow, a constitutive relationship for V_{gj} in terms of the void fraction and physical properties, similar to that given by equation (5.35) for bubbly flow, cannot be formulated. On the other hand, the mean drift velocity can be evaluated for annular flow by substituting the measured values of $\langle\alpha\rangle$, $\langle j_m\rangle$ and $\langle j_g\rangle$, and the predicted values of the distribution parameter, C_o, into equation (5.15).

(5.5.2) Model Predictions

(5.5.2.1) Radial Velocity Profiles

Figure (5.7) presents typical radial velocity profiles for both the bubbly and annular flow regimes. It is evident from this figure that the radial velocity profiles in two-phase flow are more peaked than those usually obtained for single-phase flow.

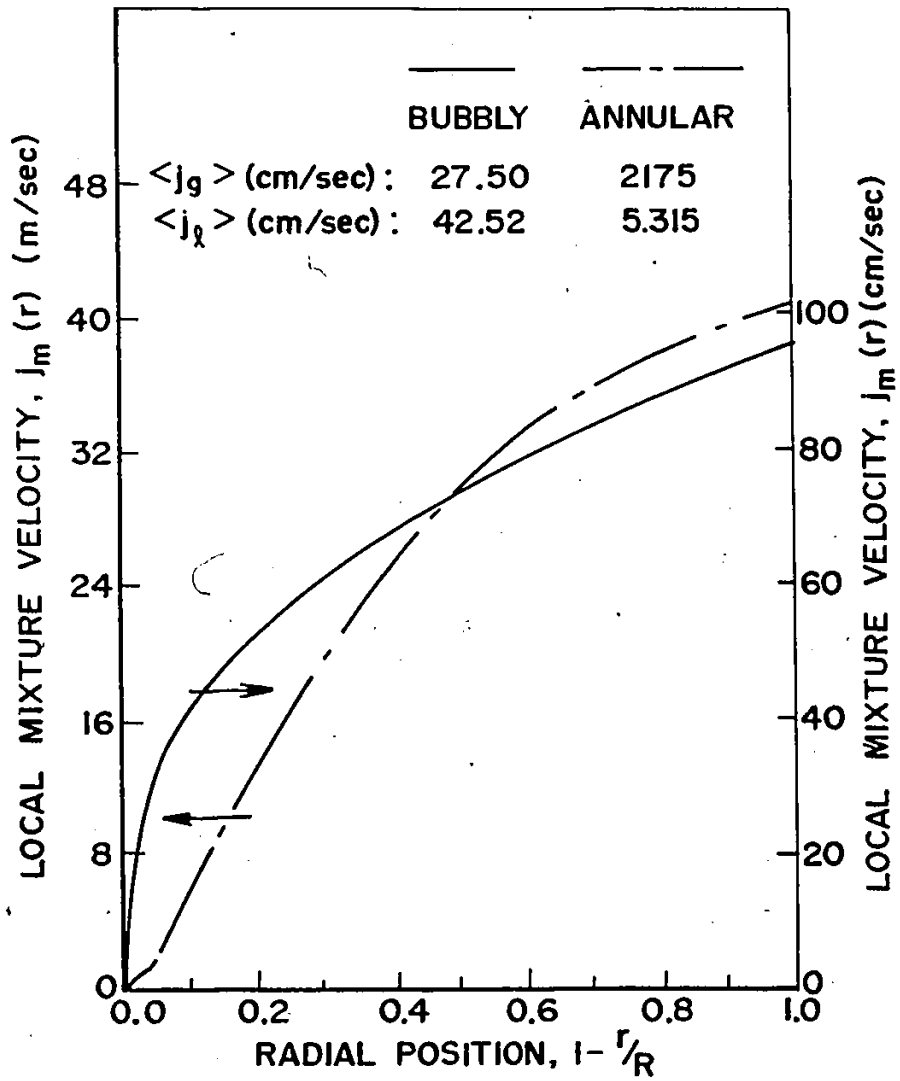

Figure (5.7): Typical mixture velocity radial profiles for the bubbly and annular flow regimes.

(5.5.2.2) Shear Stress Radial Distributions

As outlined in Appendix (E), the shear stress radial distribution may be calculated for any given liquid/gas flowrate and flow regime once the pressure gradient, mean film thickness and void profile parameters are known. Figure (5.8) shows the calculated shear stress radial distributions for typical cases of the bubbly and annular flow regimes. The peaked value in the calculated shear stress radial distribution for annular flow agrees with those predicted by the analysis presented by Calvert and Williams [124] and by Anderson and Mantzouranis [126] for that flow regime. The form of these distributions definitely disagrees with the constant or linear radial distributions for the shear stress which have been commonly assumed.

(5.5.2.3) Mean Film Thickness - Film Flowrate

The variation of the mean film thickness with the gas and liquid volumetric flux densities in annular flow is shown in figure (5.9-a). As expected, the mean film thickness increases as the liquid flowrate increases while maintaining a constant gas flowrate. This observation agrees with Levy's prediction [122] and the data presented by Gill et al. [177]. Similarly, the decrease of the mean film thickness with the gas flowrate agrees with the observations of many other investigators [37, 177, 178 and 179] and can be interpreted as follows: As the gas flowrate increases, the drag force exerted on the film layer by the fluid flowing in the core increases which, in turn, results in an increase in the film velocity as well as the fraction of li-

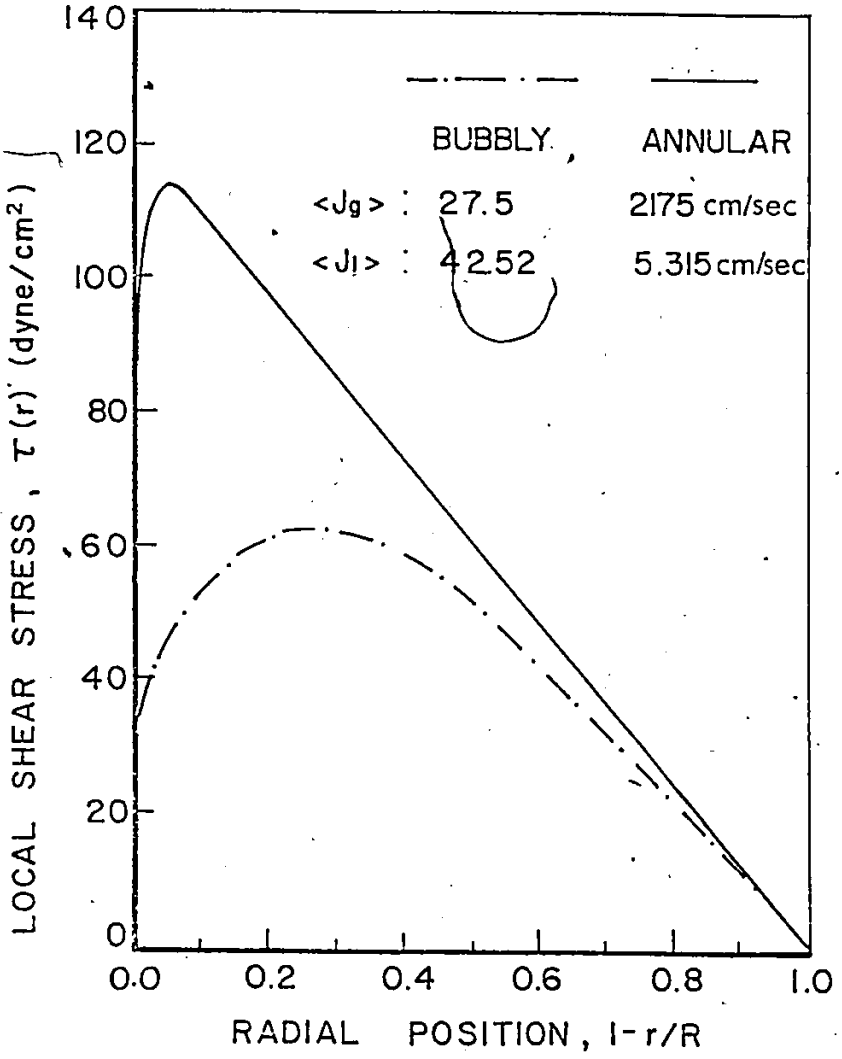

Figure (5.8): Typical shear stress radial distributions for the bubbly and annular flow regimes.

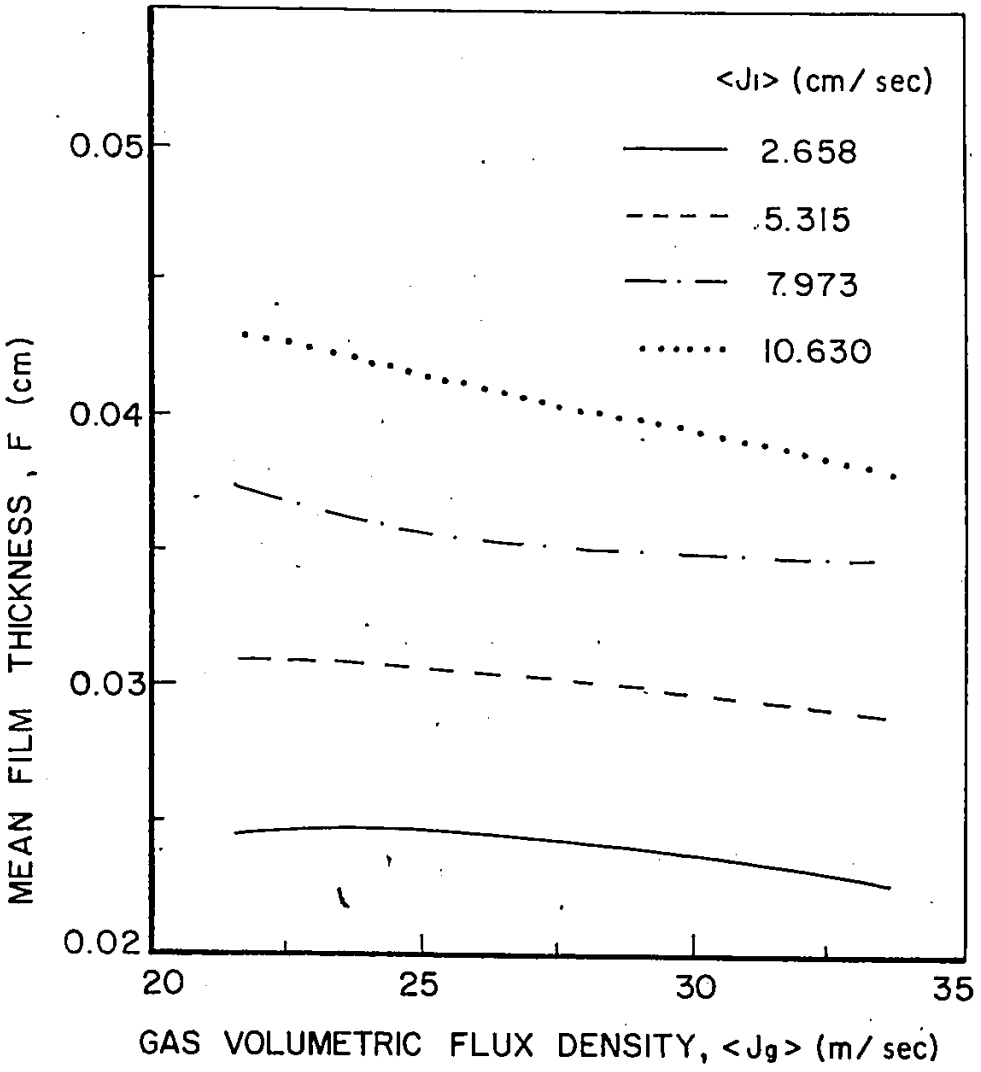

Figure (5.9-a): Variation of the mean film thickness with the gas and liquid volumetric flux densities.

quid entrained to the core. For a given total liquid mass flowrate, this can only arise by decreasing the mean film thickness.

Figure (5.9-b) presents the corresponding variation of the film flowrate with the gas and liquid volumetric flux densities; this figure demonstrates that the film flowrate increases with the gas and liquid flowrates. As has been mentioned, the increase of the film flowrate with the gas flowrate, in spite of the decrease in the mean film thickness, is attributed to the film velocity increase. The increase of the film flowrate with the liquid flowrate is easily understood.

(5.5.2.4) Flow Parameters

(i) Bubbly Flow

Figures (5.10-a) and (5.10-b) show the values of the flow parameters, C_o and $\bar{V}_{gj}$, which were obtained by combining the predicted radial velocity profiles and measured radial void profiles for bubbly flow. For the sake of comparison, the corresponding constant averaged values of C_o and $\bar{V}_{gj}$, which were obtained from figure (5.4-b), are also shown in these figures. It is evident from figures (5.10-a) and (5.10-b) that there are apparent systematic variations of the flow parameters with the gas and liquid flowrates. These variations are not consistent with the observation made in subsection (5.4.1) that the flow parameters are independent of the flowrates of the phases and remain essentially constant as long as the flow regime is unchanged. Hence, one can conclude that these variations are not true and result from shortcomings in the mixing length model.

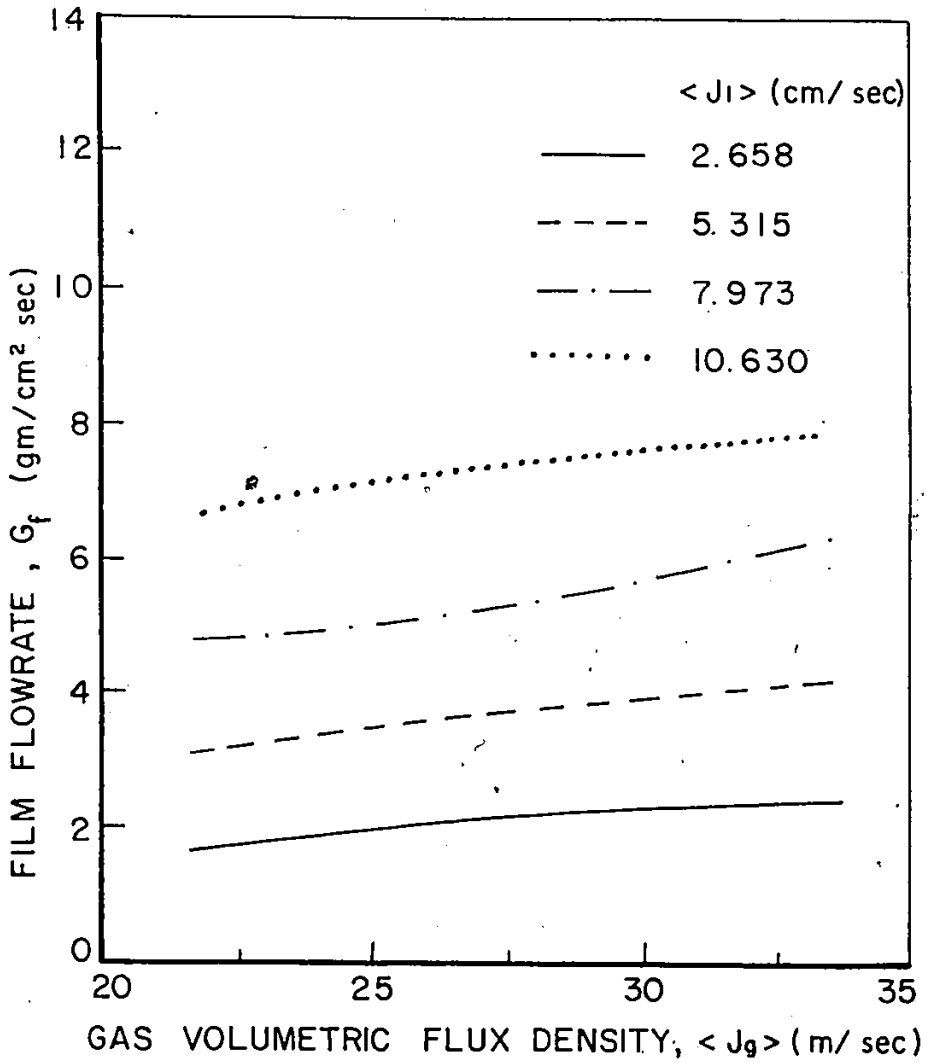

Figure (5.9-b): Variation of the film flowrate with the gas and liquid volumetric flux densities.

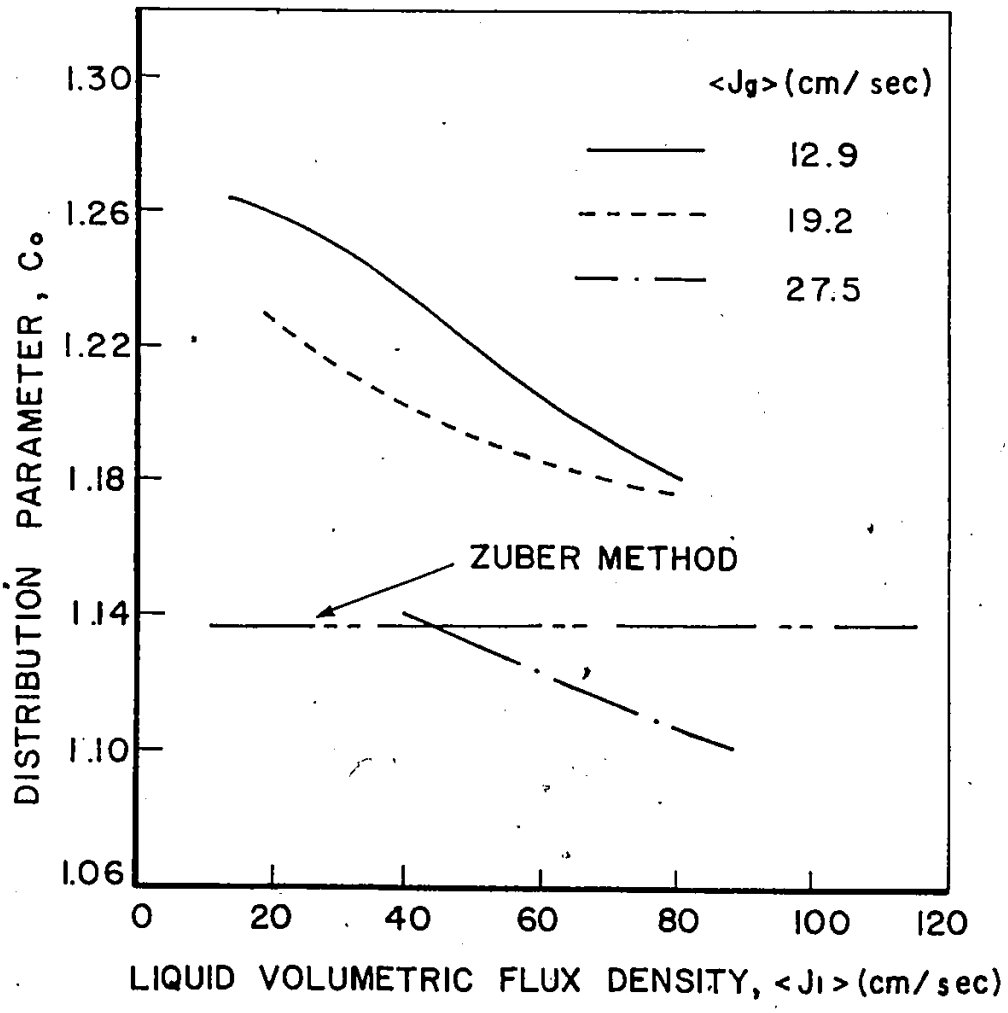

Figure (5.10-a): Dependence of the distribution parameter on the gas and liquid volumetric flux densities for the bubbly flow regime.

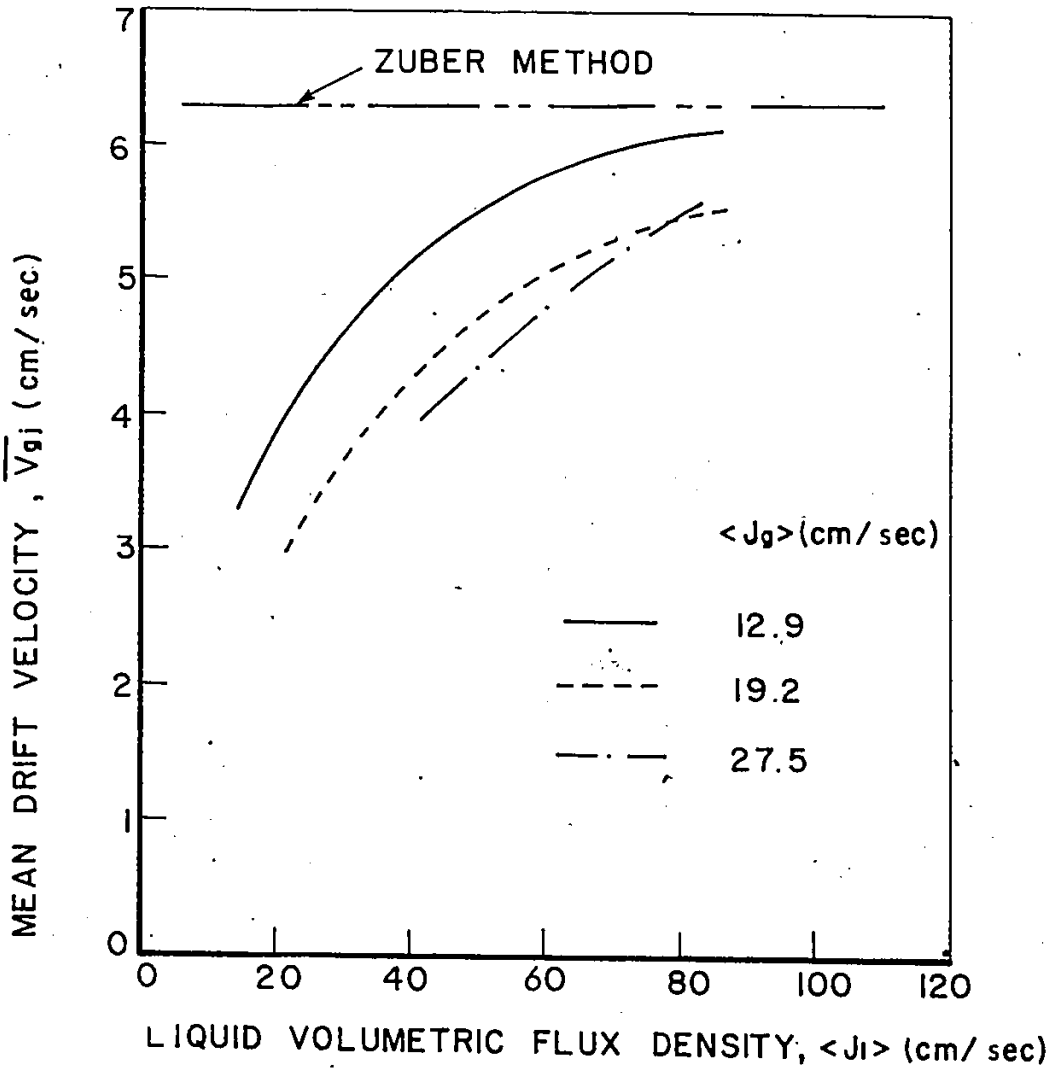

Figure (5.10-b): Dependence of the mean drift velocity on the gas and liquid volumetric flux densities for the bubbly flow regime.

Figure (5.10-a) also indicates that the percentage deviation between the values of the distribution parameter, C_o, as calculated from the mixing length model and determined indirectly from the void fraction measurements, varies from -2.84% to 11.00%. On the other hand, the corresponding deviations for the mean drift velocity, $\bar{V}_{gj}$, are shown in figure (5.10-b) to be much more significant and a deviation as high as -53.44% is observed. These substantial deviations in $\bar{V}_{gj}$ may be attributed to the use of the constitutive relationship for the local drift velocity which was recommended by Zuber and Findlay [17] and given by equation (5.35).

To examine further the adequacy of equation (5.35), equation (5.15) was used to evaluate $\bar{V}_{gj}$ by substituting the measured values of $\langle\alpha\rangle$, $\langle j_g\rangle$ and $\langle j_m\rangle$, and the constant averaged value of C_o, as determined from figure (5.4-b), that is, C_o = 1.138. Table (5.3) presents a comparison between these values of $\bar{V}_{gj}$ and those shown in figure (5.10-b). This table indicates that the values of $\bar{V}_{gj}$ which were predicted from the basic field relationship (equation (5.15)) are scattered wildly about the constant averaged value obtained from figure (5.4-b), that is, $\bar{V}_{gj}$ = 6.25 cm/sec. On the other hand, much closer agreement with this value is indicated when $\bar{V}_{gj}$ was calculated from its defining equation and the constitutive relationship for V_{gj} (equations (1.5-b) and (5.35), respectively). However, the latter values of $\bar{V}_{gj}$ exhibit an apparent systematic variation with the gas and liquid flowrates which was shown to be inconsistent with observations.

Experiment No.	Mean Drift Velocity, $\bar{V}_{gj}$ (cm/sec)	
	From Equations (1.5-b) and (5.35)	From Equation (5.15) with $C_o = 1.138$
1	3.293	3.016
2	4.416	9.125
3	5.718	11.245
4	6.061	1.388
5	2.910	3.231
6	4.498	4.756
7	5.018	14.540
8	5.419	4.231
9	4.084	3.574
10	4.775	3.983
11	5.576	3.628

Table (5.3): Comparison of the values of mean drift velocity calculated from its defining equation and the local constitutive relationship with those calculated from the basic field relationship with a constant value of the distribution parameter ($C_o = 1.138$).

The significant scattering of the values of $\bar{V}_{gj}$ which were predicted from equation (5.15) indicates that any small error introduced in estimating C_o is magnified through multiplication by the factor $\langle j_m \rangle$. Another important feature is demonstrated by equation (5.15); that is, the cross-sectional average void fraction, $\langle \alpha \rangle$, is relatively less sensitive to the mean drift velocity, $\bar{V}_{gj}$. To examine the sensitivity of the predicted cross-sectional average void fraction to errors introduced in the distribution parameter, C_o, differences of -5% and 10% were assumed in C_o and the resulting changes in $\langle \alpha \rangle$ were calculated from equation (5.15). This was based on the range of deviations which was found between the values of C_o, as calculated from the mixing length model and determined indirectly from the void fraction measurements. Similarly, differences of -5% and -50% were introduced in $\bar{V}_{gj}$ and the corresponding changes in $\langle \alpha \rangle$ were calculated. For comparison, $\bar{V}_{gj}$ was also changed by 10% although such a positive deviation is not expected (figure (5.10-b)). Typically, for the experimental run No. (1) (G_g = 0.016 gm/cm^2 sec, G_ℓ = 13.870 gm/cm^{2}sec), reducing $\bar{V}_{gj}$ by 5% and 50% increases the predicted value of $\langle \alpha \rangle$ by 0.86% and 9.29%, respectively, and an increase of 10% in $\bar{V}_{gj}$ introduces a reduction of 1.67% in $\langle \alpha \rangle$. On the other hand, a 5% reduction in C_o increases $\langle \alpha \rangle$ by 4.33% and a 10% increase in C_o introduces a 7.66% reduction in $\langle \alpha \rangle$. This analysis shows that equation (5.15) can be used to predict the cross-sectional average void fraction with a reasonable accuracy and does not reflect the errors which may be introduced in the predicted values of $\bar{V}_{gj}$.

Furthermore, it will be shown in the next chapter that the transient response of the cross-sectional average void fraction is independent of the mean drift velocity as long as the flow regime remains unchanged. This conclusion agrees with the assumption made by Hancox that the value of $\bar{V}_{gj}$ and its variation with $\langle\alpha\rangle$ are relatively small for bubbly flow and, hence, can be ignored in predicting the transient behaviour of two-phase flow [16]. However, this is only true if the observation made for steady-state flow is also valid under transient flow conditions. That is, the flow parameters must remain essentially constant for a specific flow regime and not vary with the flow-rates of the individual phases and, hence, with the cross-sectional average void fraction. It is worthy of note that Zuber and Staub [15] made a similar assumption in their analysis of transient response of forced-flow boiling systems.

To ascertain the adequacy of the estimated values of flow parameters to predict the cross-sectional average void fraction, $\langle\alpha\rangle$, the measured values of $\langle\alpha\rangle$ were compared with those predicted from equation (5.15). In predicting $\langle\alpha\rangle$, two different sets of flow parameters were used, namely: (i) the constant averaged values obtained from figure (5.4-b), that is, $C_o = 1.138$ and $\bar{V}_{gj} = 6.25$ cm/sec, and (ii) those presented in figures (5.10-a) and (5.10-b).

Table (5.4) shows this comparison and indicates an excellent agreement between the measured and predicted values of

Experiment No.	$\langle\alpha\rangle_{meas.}$	$\langle\alpha\rangle_{pred.}$ (Equation (5.15))	
		Constant Averaged C_o and $\bar{V}_{gj}$	C_o and V_{gj} From Equations (1.5) and (5.35)
1	0.3851	0.3511	0.3473
2	0.2372	0.2504	0.2371
3	0.1394	0.1473	0.1403
4	0.1199	0.1148	0.1108
5	0.4105	0.3855	0.3841
6	0.2553	0.2503	0.2436
7	0.1859	0.2022	0.1961
8	0.1605	0.1578	0.1536
9	0.3298	0.3195	0.3276
10	0.2696	0.2637	0.2705
11	0.2143	0.2100	0.2169

Table (5.4): Comparison between measured and predicted values of the average void fraction.

$\langle\alpha\rangle$. The root-mean squares of deviations between the measurements and predictions were calculated as 5.21% and 4.93% when the two described sets of flow parameters were used, respectively. This demonstrates that either set of the flow parameters can be used to predict the cross-sectional average void fraction in bubbly flow without introducing appreciable errors. The relatively smaller root-mean squares of deviations associated with the second set of flow parameters indicates that the mixing length model is adequate to predict the radial velocity profile for the purpose of evaluating the flow parameters. This conclusion is true in spite of the use of the constitutive relationship for V_{gj} and the systematic variations of the flow parameters with the gas and liquid flowrates which are not consistent with observations. However, it would be desirable to develop an adequate experimental technique to measure the radial distribution of the mixture velocity in two-phase flow. As indicated by Malnes [29], the conventional techniques which have been employed to measure the radial velocity profile in single-phase flow are not adequate to be applied in two-phase flow.

To examine further the adequacy of the mixing length model, the steady-state measurements performed by Nassos [68], for air-water bubbly flow in a 2.75 in. I.D. tube at atmospheric pressure, were used. This was achieved by combining Nassos' radial void profiles with the radial velocity profiles predicted

from the mixing length model to evaluate the distribution parameter. The estimated values of the distribution parameter are listed in table (5.5) together with the experimental range of gas and liquid flowrates and cross-sectional average void fraction. As shown by Nassos [68], these experimental data can be well represented by a straight line on a $\langle j_g \rangle / \langle \alpha \rangle$ versus $\langle j_m \rangle$ plot with an estimated slope of $C_o = 1.1$.

Table (5.5) indicates values of the distribution parameter which are always larger than the constant averaged value, that is, $C_o = 1.1$. The maximum deviation from this value was calculated as 19.16% which is significantly larger than the corresponding deviations obtained for the present work, as shown in figure (5.10-a). These relatively large deviations may be attributed to the uncertainty in the experimental conductivity-probe technique which was employed by Nassos to measure the void fraction. Burgess and Calderbank [32] showed that uncertainty in the measurements of a conductivity probe may arise due to the varying and unknown positions at which the probe contacts the bubble frontal surfaces. In other words, the bubbles whose axes and velocity vectors are not coincident with the probe axis may yield very inaccurate measurements. Moreover, it is worthy of note that Nassos [68] used an indirect calibration technique which had unknown but probably considerable error.

It should be also mentioned that the phase injection system used by Nassos in performing these experiments was simi-

Experiment No.	Flowrate ($gm/cm^2 sec$)		Average Void Fraction, $\langle\alpha\rangle$	C_o
	G_g	G_ℓ		
V-1	0.0014	17.034	0.017	1.3108
V-2	0.0051	29.506	0.051	1.2353
V-3	0.0105	38.023	0.099	1.2320
V-4	0.0142	36.806	0.123	1.2366
V-5	0.0142	22.509	0.142	1.2607
V-6	0.0141	15.513	0.168	1.2279
C-4	0.0450	76.045	0.207	1.1626
C-5	0.0369	76.045	0.190	1.1412
C-6	0.0190	76.045	0.109	1.1348
C-8	0.0337	45.627	0.188	1.1900
C-9	0.0064	45.625	0.053	1.1488

Table (5.5): Distribution parameters evaluated from Nassos' radial void profiles [68], and mixing length model in bubbly flow.

lar to that used by Malnes [29] where the gas phase was injected through the wall of the mixing section. However, the measured radial void profiles were found to increase monotonically from zero at the tube wall to maximum values at the tube center and, thus, did not exhibit local peaks near the wall region as indicated by Malnes' radial void profiles.

(ii) Annular Flow

Figures (5.11-a) and (5.11-b) show the values of the flow parameters which were calculated from the measured radial void profiles and predicted radial velocity profiles together with the corresponding constant averaged values estimated from figure (5.6). These figures indicate systematic variations of the flow parameters with the gas and liquid flowrates which contradict the observation made from figure (5.6) that these parameters remain unchanged in the annular flow regime. Hence, they are not true variations and actually represent the shortcomings of the model used to predict the radial velocity profiles.

However, figure (5.11-a) indicates that the deviation between the predicted values of the distribution parameter and the constant averaged value varies from -1.30% to 2.78%. This demonstrates the adequacy of the presented method to predict the distribution parameter in annular flow with a reasonable accuracy. On the other hand, much larger deviations are indicated by figure (5.11-b) between the predicted values of the mean drift velocity and the corresponding constant averaged value with a maximum deviation of -39.39%. These large deviations may be explained

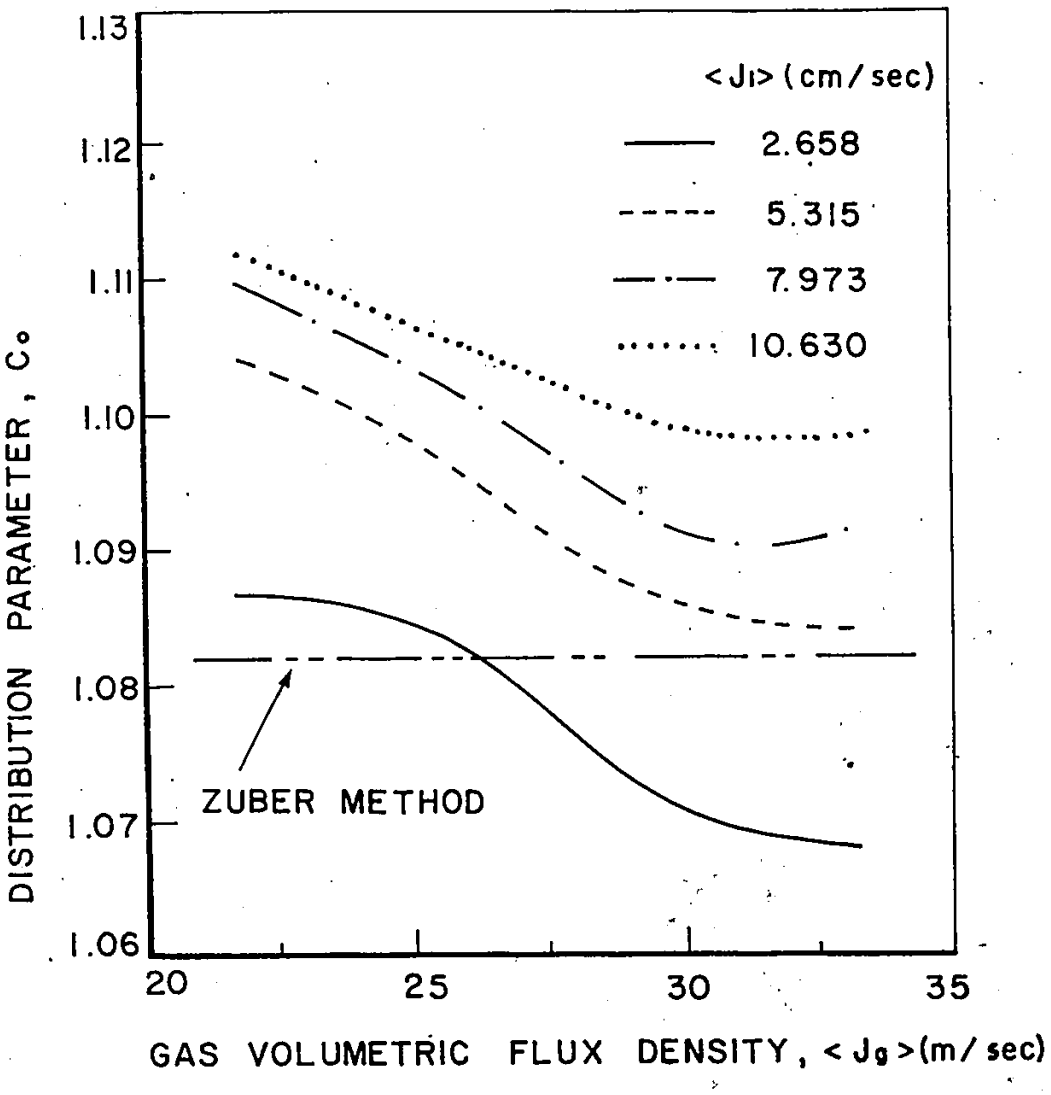

Figure (5.11-a): Dependence of the distribution parameter on the gas and liquid volumetric flux densities for the annular flow regime.

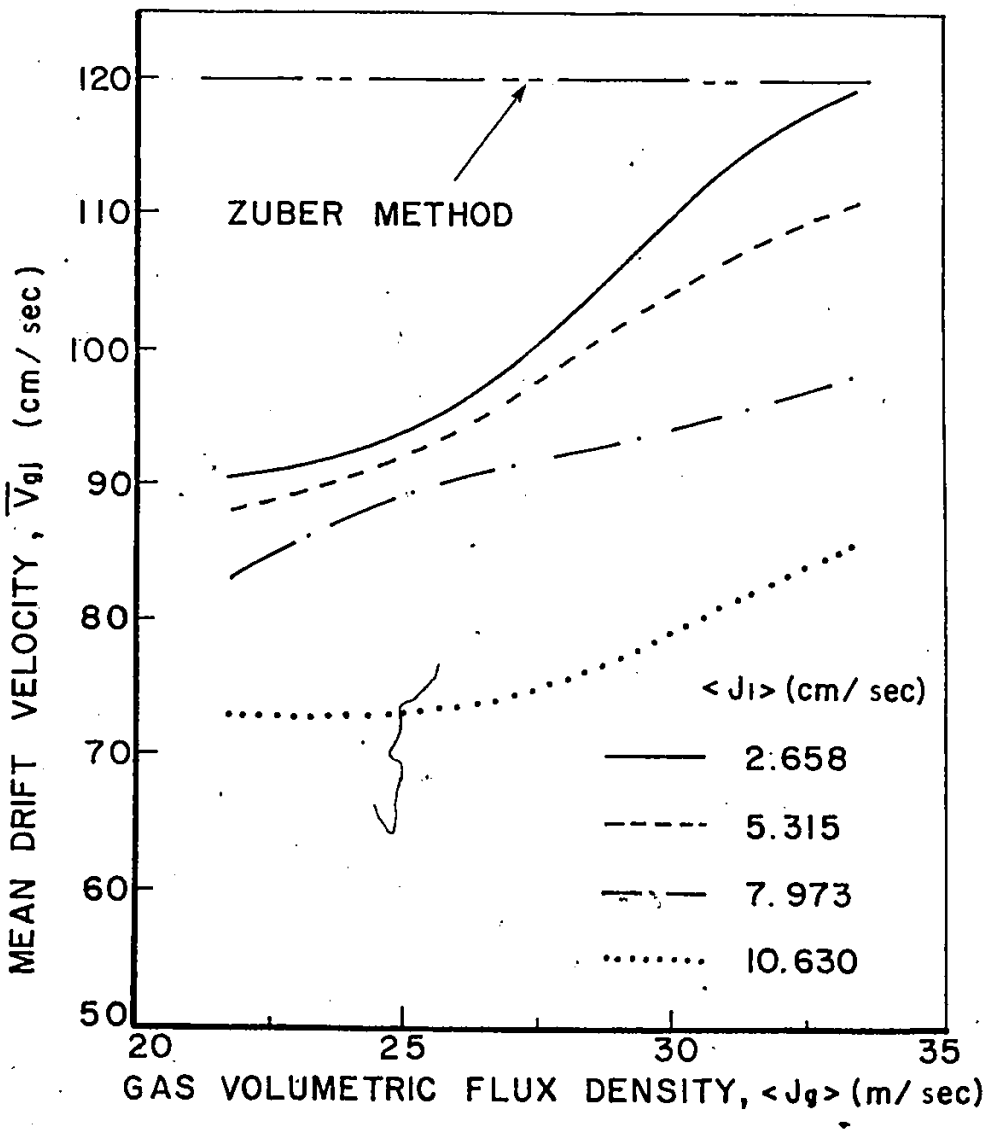

Figure (5.11-b): Dependence of the mean drift velocity on the gas and liquid volumetric flux densities for the annular flow regime.

by the fact that any uncertainty introduced in predicting the distribution parameter is magnified by a factor of $\langle j_m \rangle$ in equation (5.15); a factor which is apparently large in annular flow.

The sensitivity of the cross-sectional average void fraction, $\langle \alpha \rangle$, as predicted from equation (5.15), to the flow parameters, C_o and $\bar{V}_{gj}$, was investigated for a typical case of annular flow (G_g = 2.61 gm/cm^2 sec and G_ℓ = 2.66 gm/cm^{2}sec). It was found that changing the value of C_o by ± 5% introduces changes of -4.54% and 5.00% in $\langle \alpha \rangle$, respectively. On the other hand, 5% and 40% reductions in the value of $\bar{V}_{gj}$ only increase the predicted value of $\langle \alpha \rangle$ by 0.24% and 1.98%, respectively. This analysis confirms the conclusion made for bubbly flow, that is, the cross-sectional average void fraction, as predicted from equation (5.15), is more sensitive to the distribution parameter than the mean drift velocity. Hence, this equation can be used to predict the average void fraction without appreciable errors in spite of the uncertainties which may arise in the mean drift velocity.

Moreover, as has been indicated in the previous subsection, the transient response of the cross-sectional average void fraction, $\langle \alpha \rangle$, does not depend on the mean drift velocity as long as the flow regime remains unchanged during the transient. This is based on the assumption that under transient flow conditions, the flow parameters would remain essentially constant for a specified flow regime and would not change with $\langle \alpha \rangle$ as has been found for steady-state flow.

In summary, the calculations and observations presented above suggest that the experimental technique and model predictions are consistent with expectations and previous observations and predictions. Moreover, the mixing length model has been shown to be generally adequate to predict the radial velocity profiles in two-phase flow for the purpose of evaluating the flow parameters. To emphasize this conclusion and to check whether this model, as applied here, is valid for two-phase flow, a sensitivity analysis was performed. In this analysis, the errors introduced by the mixing length model into the prediction of two-phase flow parameters are evaluated.

(5.6) Sensitivity Analysis

The effect of using the single-phase mixing length in calculating the flow parameters, C_o and $\bar{v}_{gj}$, is tested by changing the mixing length and evaluating the resulting differences in these flow parameters. Furthermore, there is a question of which form of the two-phase mixture viscosity should be used in two-phase flow calculations. Two expressions are commonly assumed [21]; these are

$$\mu = \mu_\ell(1-\alpha) + \mu_g\alpha, \qquad (5.49\text{-a})$$

and

$$\mu = \mu_\ell\left[1 + 2.5\ \alpha\ \left(\frac{\Delta\rho}{\rho_\ell}\right)\right] . \qquad (5.49\text{-b})$$

While the first expression is based on a volumetric averaging, the second one is Einstein's formula modified to give a value for the mixture viscosity identical to that of the liquid phase when the densities of the two phases become identical.

Figure (5.12) shows the effect of changing the mixing length parameter, ℓ^2, by ± (20%, 40%, 60%, and 100%) and 200% on the flow parameters for typical experimental runs of the bubbly and annular flow regimes. Table (5.6) presents the effect of using the two expressions for the mixture viscosity on the values of C_o and $\bar{V}_{gj}$ for the two flow regimes. From these results, it can be clearly seen that neither the distribution parameter nor the mean drift velocity is sensitive to changes in the mixing length parameter. For the bubbly flow regime, a 200% increase in ℓ^2 produces only a -0.63% change in C_o and a 100% decrease in ℓ^2 produces a 6.4% change in C_o. The mean drift velocity is found to be insensitive to any change in ℓ^2 for bubbly flow. In annular flow, the influence of ℓ^2 on C_o is even much smaller and the highest percentage errors in calculating $\bar{V}_{gj}$ are equal to 3.22% and -3.62% for changes in ℓ^2 of 200% and -100%, respectively. The effect of using either expression for the two-phase mixture viscosity is found to be unimportant, as seen from table (5.6).

In summary, it can be concluded from the sensitivity analysis that the mixing length model is adequate to predict the radial velocity profiles in two-phase flow for the purpose of evaluating the flow parameters.

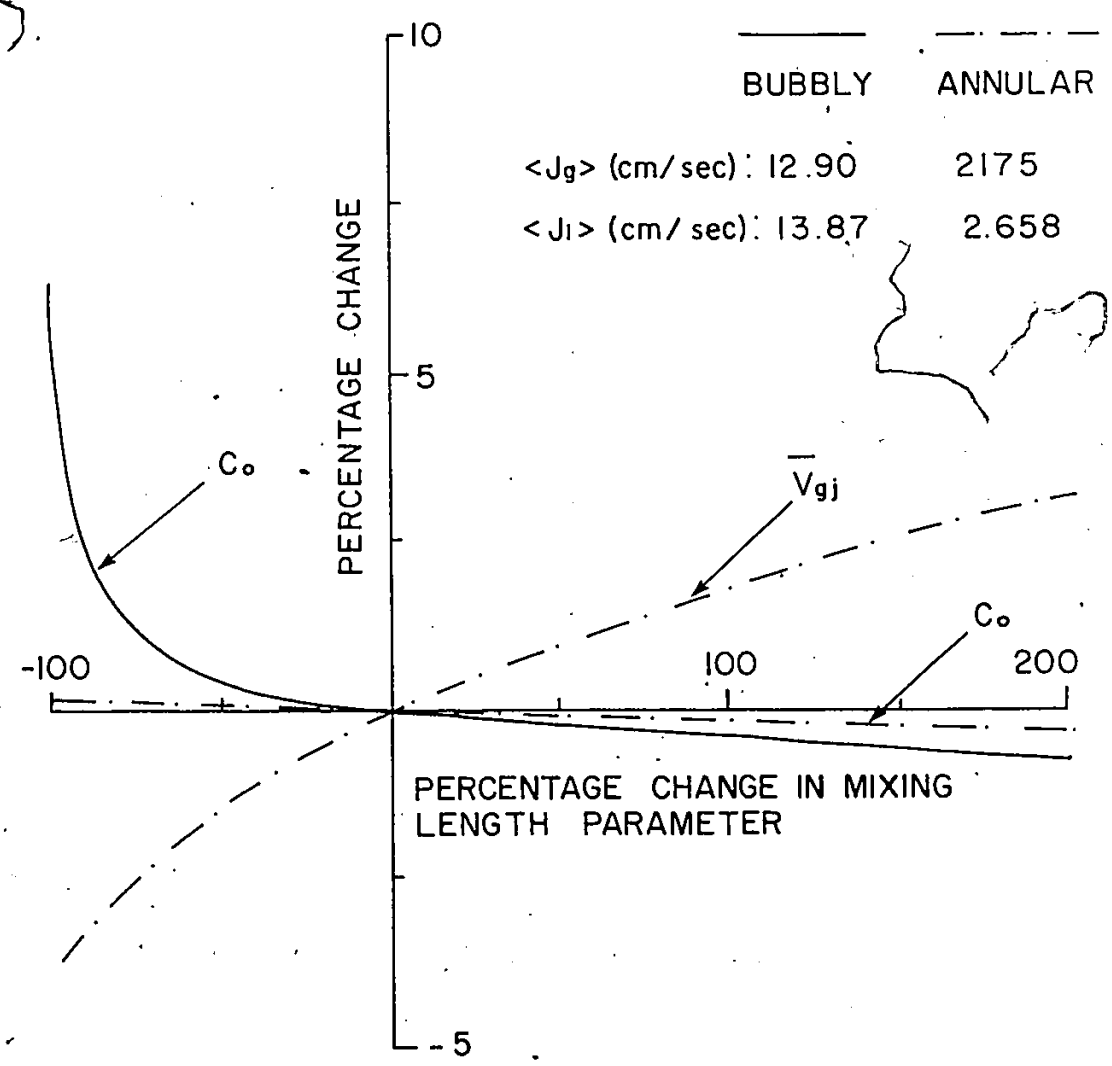

Figure (5.12): Effect of changing the mixing length parameter on calculating the flow parameters for typical cases of the bubbly and annular flow regimes.

Parameter	Flow Regime	Modified Einstein's Formula	Volumetric Average Formula	Difference	Percentage Relative Difference
C_o	Bubbly	1.263	1.262	-.00061	-.048
	Annular	1.089	∿ 1.089	.00003	.0028
$\bar{V}_{gj}$ (cm/sec)	Bubbly	3.302	3.302	0	0
	Annular	89.75	89.69	-.0633	-.071

Table (5.6): Effect of using different expressions for the mixture viscosity on the flow parameters for two typical cases of the bubbly and annular flow regimes.

(5.7) Comparison with Existing Models and Correlations

It is of interest to compare these experimental observations and analysis with correlations and analysis (modelling) presented by other investigators. There are many aspects of two-phase flow that are of prime importance to the designer; these are discussed and compared in turn.

(5.7.1) Average Void Fraction-Quality Relations

As has been mentioned, the knowledge of the steady-state average void fraction is important for the calculation of the mean density of a two-phase flow mixture. This information is needed for the estimation of the different components of the pressure drop in the two-phase flow system. It is also necessary in evaluating the reactivity of nuclear reactors when boiling occurs. For this reason, an adequate correlation is required to predict the average void fraction under any given flow condition. Consequently, many mathematical models and empirical correlations have been developed for such a purpose. Some of these models and correlations are given in detail in Appendix (F). Now consider the bubbly and annular flow regimes in turn.

(a) Bubbly Flow Regime

Table (5.7-a) summarizes the average void fraction measurements at different two-phase mixture qualities, x, for bubbly flow together with the corresponding predictions from a number of selected published correlations and models. The

Run No.	Quality ($\times 10^3$)	$\langle\alpha\rangle$ (measured)	Homogeneous Model		Levy's Model		Thom's Correlation		Styrikowich et al.'s Correlation		Lockhart-Martinelli's Correlation	
			$\langle\alpha\rangle$	$\%\Delta\langle\alpha\rangle$	$\langle\alpha\rangle$	$\%\Delta\langle\alpha\rangle$	$\langle\alpha\rangle$	$\%\Delta\langle\alpha\rangle$	$\langle\alpha\rangle$	$\%\Delta\langle\alpha\rangle$	$\langle\alpha\rangle$	$\%\Delta\langle\alpha\rangle$
1	1.1183	.3850	.4819	25.164	.1129	-70.671	.1779	-53.798	.3549	- 7.817	.2819	-26.788
2	.5783	.2370	.3246	36.966	.0739	-68.817	.1006	-57.568	.2317	- 2.226	.2046	-13.667
3	.2655	.1390	.1807	30.035	.0441	-68.285	.0488	-64.879	.1296	- 6.786	.1352	- 2.759
4	.1941	.1199	.1389	15.825	.0357	-70.255	.0362	-69.842	.1007	-16.040	.1134	- 5.432
5	1.2163	.4110	.5029	22.356	.1190	-71.036	.1905	-53.650	.3726	- 9.340	.2929	-28.740
6	.5433	.2550	.3111	21.993	.0709	-72.177	.0951	-62.722	.2218	-13.017	.1982	-22.279
7	.3952	.1860	.2472	32.903	.0575	-69.079	.0710	-61.845	.1759	- 5.405	.1678	- 9.802
8	.2823	.1600	.1900	18.753	.0459	-71.285	.0517	-67.659	.1360	-15.020	.1398	-12.614
9	.7780	.3298	.3927	19.086	.0896	-72.836	.1308	-60.346	.2831	-14.150	.2373	-28.057
10	.5669	.2696	.3199	18.650	.0729	-72.974	.0985	-63.419	.2282	-15.339	.2024	-24.939
11	.4043	.2140	.2515	17.517	.0584	-72.713	.0725	-66.125	.1790	-16.352	.1698	-20.642

Table (5.7-a): Comparison of the measured average void fraction with the corresponding values predicted from selected models and correlations for the bubbly flow regime.

Zuber-Findlay's Model		Kholodovski's Correlation		Armand's Correlation		Hancox' Model		Nishino-Yamazaki's Correlation		Yagi-Sasaki's Correlation	
$\langle\alpha\rangle$	$\%\Delta\langle\alpha\rangle$	$\langle\alpha\rangle$	$\%\Delta\langle\alpha\rangle$	$\langle\alpha\rangle$	$\%\Delta\langle\alpha\rangle$	$\langle\alpha\rangle$	$\%\Delta\langle\alpha\rangle$	$\langle\alpha\rangle$	$\%\Delta\langle\alpha\rangle$	$\langle\alpha\rangle \times 10^4$	$\%\Delta\langle\alpha\rangle$
.3231	-16.086	.3915	1.684	.4014	4.262	.4329	12.442	.3696	-3.999	.7748	-99.980
.2352	-.756	.2657	12.110	.2704	14.093	.2853	20.386	.2619	10.492	.2240	-99.991
.1414	1.739	.1496	7.627	.1506	8.319	.1624	16.854	.1568	12.838	.0518	-99.996
.1114	-7.058	.1156	-3.611	.1157	-3.518	.1296	8.063	.1238	3.260	.0281	-99.998
.3619	-11.943	.4113	.074	.4189	1.922	.4534	10.317	.3839	-6.585	.6097	-99.985
.2396	-6.026	.2568	.693	.2591	1.620	.2732	7.139	.2524	-1.025	.1338	-99.995
.1950	4.836	.2049	10.178	.2059	10.708	.2174	16.858	.2067	11.113	.0735	-99.996
.1532	-4.269	.1583	-1.059	.1583	-1.079	.1699	6.173	.1640	2.475	.0391	-99.998
.3067	-7.007	.3249	-1.471	.3272	- .802	.3479	5.489	.3089	-6.337	.1836	-99.994
.2546	-5.561	.2657	-1.448	.2665	-1.165	.2811	4.267	.2586	-4.096	.1009	-99.996
.2039	-4.738	.2098	-1.942	.2095	-2.108	.2210	3.278	.2098	-1.965	.0536	-99.998

Table (5.7-a) (continued)

average absolute percentage deviations between the present data and these predictions are given in table (5.7-b). In view of the results presented in tables (5.7-a) and (5.7-b), the following observations can be made:

(i) While the homogeneous model provides an upper limit of the average void fraction for a particular mixture quality, Levy's model and Thom's correlation give the lower limit. Under the usual condition of cocurrent upward flow, the average velocity of the gas phase is higher than that of the liquid phase. This explains why the homogeneous model predicts higher values of the average void fraction than those measured experimentally.

(ii) The homogeneous model, however, predicts values closer to the observed ones than either of these two models. Thom's assumption that the slip factor, ε, is independent of the system quality contradicts experimental observations [186] and, hence, limits the validity of his correlation. Levy's model predicts much lower values of $\langle\alpha\rangle$ than those measured; this observation agrees with a similar conclusion made by Madsen [186].

(iii) Although Styrikowich et al.'s and Lockhart-Martinelli's correlations also yield values of $\langle\alpha\rangle$ which are consistently lower than the present data, they are more capable of fitting these data than Thom's correlation and Levy's model.

Model or Correlation	Average Absolute Percentage Deviation $\lvert \%\Delta\langle\alpha\rangle \rvert$	
	Bubbly Flow	Annular Flow
Homogeneous Model	23.568	12.692
Levy's Model	70.921	7.748
Thom's Correlation	61.987	11.787
Styrikowich et al.'s Correlation	11.045	12.410
Lockhart-Martinelli's Correlation	17.793	7.547
Zuber-Findlay's Model	6.365	6.187
Kholodovski's Correlation	3.809	0.684
Armand's Correlation	4.509	8.639
Hancox' Model	10.115	12.620
Nishino-Yamazaki's Correlation	5.835	7.669
Yagi-Sasaki's Correlation	99.993	92.958
Turner-Wallis' Model	-	3.484

Table (5.7-b): Summary of the average absolute percentage deviations between the present average void fraction data and the predictions from selected models and correlations for the bubbly and annular flow regimes.

(iv) The average void fraction data are in good agreement with the predictions from Zuber-Findlay's and Hancox' models as well as Nishino-Yamazaki's, Kholodovski's and Armand's correlations.

(v) Although the correlation presented by Yagi and Sasaki was reported to yield reasonable predictions of $\langle\alpha\rangle$ at moderate pressures [104], it does not fit the current data at all.

(b) Annular Flow Regime

The measured values of $\langle\alpha\rangle$ for annular flow together with those predicted by the models and correlations given in Appendix (F) are summarized in table (5.7-c). The following observations are evident from tables (5.7-b) and (5.7-c):

(i) The homogeneous and Hancox' models as well as the correlations presented by Thom and Styrikowich et al. give the same trend as the experimental results; all data points fall consistently below the predictions from these models and correlations. In other words, these models and correlations present an upper limit to the average void fraction data.

(ii) Hancox' model becomes equivalent to the homogeneous model over the range of $\langle\alpha\rangle$ appropriate to the annular flow regime where the distribution parameter, C_o, approaches unity.

Run No.	Quality	<α> (measured)	Homogeneous Model		Hancox' Model		Thom's Correlation		Styrikowich et al.'s Correlation		Turner-Wallis' Model	
			<α>	%Δ<α>	<α>	%Δ<α>	<α>	%Δ<α>	<α>	%Δ<α>	<α>	%Δ<α>
1	.4962	.8850	.9988	12.856	.9984	12.812	.9948	12.404	.9974	12.699	.9136	3.233
2	.5398	.8918	.9990	12.018	.9987	11.986	.9956	11.640	.9980	11.907	.9230	3.502
3	.5752	.9025	.9991	10.705	.9990	10.691	.9962	10.382	.9981	10.592	.9301	3.055
4	.6017	.9053	.9992	10.373	.9990	10.349	.9966	10.084	.9983	10.272	.9350	3.282
5	.3300	.8715	.9976	14.465	.9970	14.399	.9896	13.552	.9950	14.170	.8653	-.716
6	.3697	.8816	.9980	13.198	.9974	13.134	.9913	12.438	.9960	12.975	.8793	-.266
7	.4038	.8903	.9982	12.122	.9977	12.062	.9924	11.470	.9963	11.905	.8898	-.055
8	.4303	.8940	.9984	11.679	.9980	11.632	.9932	11.096	.9970	11.520	.8973	.367
9	.2472	.8681	.9963	14.773	.9954	14.663	.9845	13.407	.9926	14.341	.8275	-4.682
10	.2811	.8771	.9970	13.662	.9961	13.566	.9869	12.523	.9940	13.327	.8447	-3.697
11	.3110	.8884	.9973	12.263	.9966	12.178	.9887	11.286	.9946	11.953	.8578	-3.449
12	.3349	.8896	.9976	12.142	.9970	12.072	.9898	11.267	.9951	11.858	.8671	-2.531
13	.1976	.8688	.9951	14.542	.9940	14.410	.9794	12.733	.9902	13.972	.7959	-8.396
14	.2268	.8790	.9959	13.301	.9950	13.196	.9827	11.793	.9920	12.854	.8155	-7.221
15	.2530	.8854	.9965	12.543	.9955	12.434	.9849	11.243	.9930	12.152	.8306	-6.192
16	.2741	.8866	.9968	12.432	.9960	12.338	.9865	11.266	.9935	12.056	.8414	-5.103

Table (5.7-c): Comparison of the measured average void fraction with the corresponding values predicted from selected models and correlations for the annular flow regime.

Kholodovski's Correlation		Zuber-Findlay's Model		Lockhart-Martinelli's Correlation		Nishino-Yamazaki's Correlation		Armand's Correlation		Levy's Model		Yagi-Sasaki's Correlation	
<α>	%Δ<α>	<α>	%Δ<α>	<α>	%Δ<α>	<α>	%Δ<α>	<α>	%Δ<α>	<α>	%Δ<α>	<α>	%Δ<α>
.8821	-.3230	.9387	6.068	.9678	9.359	.9656	9.113	.9764	10.323	.9760	10.279	.1362	-84.609
.8852	-.736	.9409	5.502	.9711	8.895	.9685	8.598	.9800	9.890	.9797	9.857	.1553	-82.583
.8878	-1.631	.9424	4.420	.9736	7.878	.9706	7.549	.9826	8.874	.9923	8.847	.1726	-80.871
.8896	-1.723	.9434	4.210	.9753	7.736	.9722	7.386	.9843	8.730	.9841	8.708	.1868	-79.367
.8811	1.100	.9376	7.582	.9507	9.093	.9518	9.211	.9589	10.030	.9536	9.416	.0411	-95.285
.8844	.312	.9399	6.615	.9557	8.408	.9557	8.407	.9649	9.453	.9606	8.958	.0476	-94.601
.8870	-.370	.9416	5.758	.9595	7.768	.9587	7.685	.9693	8.871	.9656	8.456	.0537	-93.972
.8890	-.558	.9427	5.444	.9621	7.616	.9609	7.480	.9722	8.752	.9690	8.388	.0588	-93.427
.8800	1.374	.9365	7.874	.9371	7.945	.9413	8.428	.9452	8.886	.9326	7.428	.0196	-97.742
.8835	.725	.9390	7.054	.9433	7.553	.9460	7.859	.9528	8.631	.9425	7.456	.0228	-97.402
.8862	-.244	.9407	5.891	.9481	6.716	.9497	6.898	.9583	7.873	.9496	6.892	.0258	-97.099
.8883	-.145	.9419	5.882	.9514	6.947	.9523	7.047	.9622	8.158	.9545	7.296	.0283	-96.819
.8790	1.172	.9353	7.657	.9253	6.504	.9325	7.331	.9348	7.602	.9129	5.076	.0115	-98.675
.8826	.407	.9380	6.714	.9327	6.106	.9380	6.707	.9433	7.310	.9254	5.277	.0134	-98.476
.8855	.007	.9399	6.157	.9382	5.965	.9421	6.407	.9495	7.242	.9344	5.537	.0152	-98.286
.8876	.115	.9412	6.157	.9421	6.265	.9451	6.600	.9539	7.592	.9406	6.094	.0167	-98.119

Table (5.7-c) (continued)

(iii) While Levy's model and Lockhart-Martinelli's, Nishino-Yamazaki's and Armand's correlations give the same trend as the above mentioned models and correlations, they predict closer values to the experimental data.

(iv) Of all the models and correlations which are considered here, only Turner-Wallis' model predicts lower values of $\langle\alpha\rangle$ at a low quality and higher values at a high quality.

(v) While Kholodovski's correlation is clearly the best, the Turner-Wallis' and the Zuber-Findlay's models are also good approximations to these data; Zuber and Findlay's model is less satisfactory than that of Turner and Wallis.

(vi) As in the case of bubbly flow, the correlation presented by Yagi and Sasaki is still unable to yield acceptable predictions of $\langle\alpha\rangle$ in the annular flow regime.

(5.7.2) Velocity Slip Ratio for Bubbly Flow

The velocity slip ratio of the two phases may be determined from the experimental average void fraction measurements using the relation

$$S = \frac{\beta}{\langle\alpha\rangle} \left(\frac{1-\langle\alpha\rangle}{1-\beta}\right) \quad . \qquad (2.24)$$

A comparison between the values of the slip ratio, as determined by using the measured values of $\langle\alpha\rangle$ in equation (2.24), with

those predicted from existing models and correlations is given in table (5.8-a). The average absolute percentage deviations between the present slip data and these predictions are summarized in table (5.8-b).

Except Zivi's and Thom's correlations (equations (2.44) and (2.45)), all the models and correlations which are considered here indicate that the slip ratio depends on the average void fraction. These two correlations, which are based on the assumption that S is a unique function of the system pressure, predict much larger values of the slip ratio than those obtained from the present experimental data. While Bankoff's predictions (equation (2.21)) present the closest agreement with these data, the model presented by Zuber and Findlay (equation (2.37)) yields a good approximation. Similarly, Premoli et al.'s correlation (equation (2.49)) provides an acceptable representation of the data; however, it is not as good as Bankoff's or even Zuber and Findlay's predictions.

The values of the slip ratio predicted by Levy's model (equation (2.43)) are much larger than those observed; the deviation becomes more significant at high values of $\langle\alpha\rangle$. On the other hand, Fohrman's correlation (equation (2.52)) yields values of S less than unity over the entire range of experimental conditions which were investigated in this study. The deviation between Fohrman's predictions and the present data decreases as the average void fraction increases. It is worthy of note, however, that Fohrman's equation does not appear to

Run No.	<α> (measured)	S (present data)	Thom's Correlation		Zivi's Correlation		Bankoff's Model		Zuber-Findlay's Model	
			S	%ΔS	S	%ΔS	S	%ΔS	S	%ΔS
1	.3850	1.480	3.777	128.087	9.400	534.966	1.373	-7.273	1.997	34.876
2	.2370	1.543	3.777	118.836	9.400	509.212	1.280	-17.033	1.564	1.329
3	.1390	1.360	3.777	148.340	9.400	591.347	1.241	-8.758	1.339	-1.537
4	.1199	1.175	3.777	187.348	9.400	699.941	1.234	5.026	1.288	9.608
5	.4110	1.445	3.777	133.747	9.400	550.721	1.396	-3.383	1.823	26.162
6	.2550	1.3126	3.777	157.256	9.400	616.167	1.289	-1.803	1.439	9.625
7	.1860	1.428	3.777	136.493	9.400	558.366	1.258	-11.886	1.353	-5.258
8	.1600	1.223	3.777	175.990	9.400	668.321	1.248	2.015	1.299	6.158
9	.3298	1.310	3.777	157.725	9.400	617.475	1.332	1.655	1.474	12.490
10	.2696	1.269	3.777	166.078	9.400	640.727	1.296	2.155	1.383	8.974
11	.2140	1.231	3.777	174.342	9.400	663.734	1.270	3.165	1.315	6.873

Table (5.8-a): Comparison between the slip data from the present investigation and the corresponding values predicted from selected models and correlations for the bubbly flow regime.

Premoli et al's Correlation		Levy's Model		Fohrman's Correlation		Homogeneous Model	
S	%ΔS	S	%ΔS	S	%ΔS	S	%ΔS
2.483	67.720	12.645	754.157	.423	-71.443	1.000	-32.453
1.940	25.694	9.921	542.982	.255	-83.503	1.000	-35.192
1.546	13.693	7.598	458.804	.140	-89.736	1.000	-26.455
1.435	22.155	7.057	500.515	.109	-90.686	1.000	-14.903
2.456	70.000	13.065	804.425	.451	-68.780	1.000	-30.777
1.831	39.516	10.291	684.044	.242	-81.548	1.000	-23.815
1.665	16.616	8.789	515.574	.189	-86.740	1.000	-29.964
1.525	24.645	8.152	566.283	.146	-88.056	1.000	-18.267
1.995	52.270	11.704	793.282	.320	-75.592	1.000	-23.676
1.796	41.537	10.582	733.825	.250	-80.292	1.000	-21.202
1.629	32.342	9.428	665.959	.193	-84.297	1.000	-18.755

Table (5.8-a) (continued)

Model or Correlation	Average Absolute Percentage Deviation, $\lvert \%\Delta S \rvert$
Thom's Correlation	153.113
Zivi's Correlation	604.634
Bankoff's Model	5.832
Zuber-Findlay's Model	11.172
Premoli et al's Correlation	36.926
Levy's Model	638.168
Fohrman's Correlation	81.879
Homogeneous Model	25.042

Table (5.8-b): Summary of the average absolute percentage deviations between the present slip data and the predictions from selected models and correlations for the bubbly flow regime.

be correct in the limit as the gas flowrate vanishes, i.e., as β and $\langle\alpha\rangle$ tend to zero. This may explain the large deviations at low values of $\langle\alpha\rangle$. It is interesting to note as well that the homogeneous model, which assumes negligible slip between the phases, gives better representation of the data than many of the models and correlations available in the literature although it is obviously incorrect.

Since in annular flow, the liquid travels as a film and as entrained droplets, a single value of the slip ratio in this regime has no general meaning and, hence, is of no real interest.

(5.7.3) Mean Film Thickness - Interfacial Shear Stress Relations

As mentioned earlier, the core-film interface in an annular upward two-phase flow usually appears wavy and, hence, one can treat the gas stream as flowing in a rough pipe with the interface replacing the wall. By analogy with single-phase flow, the friction factor, f_i, at the interface may be defined by

$$f_i = \frac{2\,\tau_i}{\rho_g\,\bar{v}_g^{\,2}} \,. \qquad (5.50)$$

In equation (5.50), the interface has been assumed to be stationary since in most practical cases, the gas velocity is much greater than the velocity at the interface. From the definition of the weighted mean gas velocity given by equations (2.13-a) and (2.20-a), equation (5.50) may be written in the form

$$f_i = \frac{2\tau_i \langle\alpha\rangle^2}{\rho_g \langle j_g \rangle^2} \quad . \qquad (5.51)$$

The interfacial friction factor has also been expressed by Wallis [188] as a function of the ratio of mean film thickness-to-tube radius by the relation

$$f_i = 0.005(1 + 150\ F/R) \quad . \qquad (5.52)$$

On the other hand, the rough-pipe correlation of Moody [189] can be approximated by the equation

$$f \sim 0.005(1 + 37.5\ k_s/R) \quad , \qquad (5.53)$$

where k_s is the equivalent grain size of "sand roughness". Equation (5.53) has been found to be valid over the range $0.002 < k_s/R < 0.06$ [188]. A comparison between equation (5.52) and equation (5.53) suggests that the interfacial friction factor in annular two-phase flow is higher than that for a rough pipe of "sand roughness" equal to the mean film thickness. Moreover, this comparison indicates that the wavy film-core interface is about equivalent to a "sand roughness" of four times the mean film thickness.

Similarly, Moeck and Stachiewicz [190] developed the following empirical correlation for the friction factor at the core-film interface:

$$f_i = 0.005[1 + 545(F/R)^{1.42}] \quad . \qquad (5.54)$$

Furthermore, Wallis [188] showed that Levy's interfacial friction function, F', [122] is, in fact, approximately related to the interfacial friction factor by

$$F' \sim \sqrt{f_i/8} \, . \tag{5.55}$$

He arrived at this conclusion by approximating Levy's correction factor, R', by

$$R' \sim \frac{1}{2} \sqrt{\rho_\ell/\rho_g} \, . \tag{5.56}$$

For the sake of comparison, the results from the current investigation were transformed into the appropriate form, using equations (5.51) and (5.55), and then superimposed on Levy's curve [122] which is reproduced in figure (5.13). Also plotted on the same figure are the corresponding predictions from Wallis' and Moeck's correlations (equation (5.52) and (5.54), respectively). Figure (5.13) demonstrates that while Moeck's correlation agrees quite well with the results of the current investigation, Levy's and Wallis' predictions are only in fair agreement with these results.

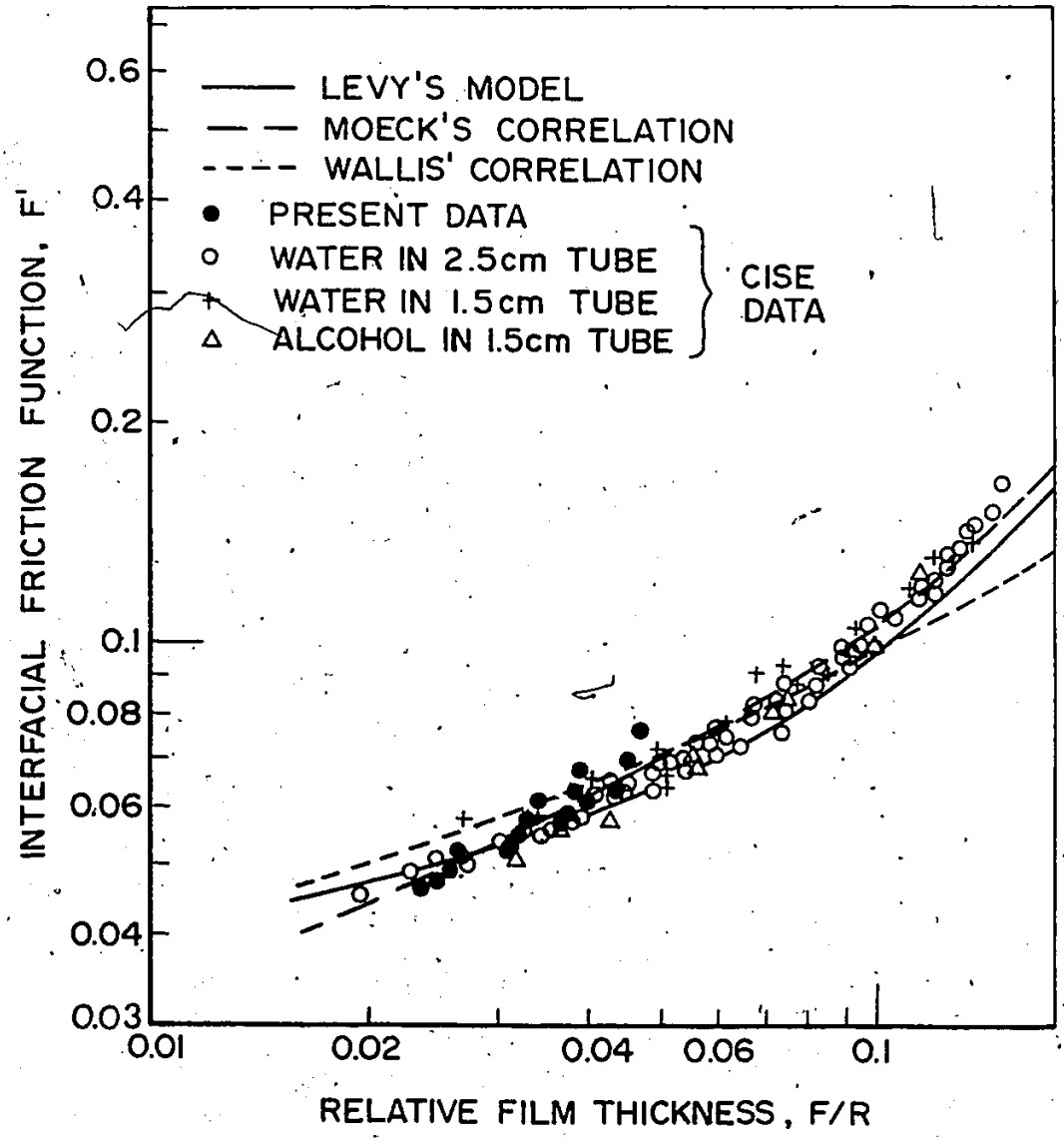

Figure (5.13): Comparison between the present results for the interfacial friction function and selected models and correlations.

(5.7.4) Mean Film Thickness - Film Flowrate Relations

In his analysis of liquid films, Kutateladze [191] assumed a logarithmic velocity profile across the film which upon integration yields the following expression for the dimensionless mean film thickness, F^+:

$$F^+(12+10\ \ell n\ F^+) - 156 = Re_f \ . \qquad (5.57)$$

Here the dimensionless mean film thickness and the film Reynolds number, Re_f, are defined as

$$F^+ = F\left(\frac{u^* \rho_\ell}{\mu_\ell}\right) \ , \qquad (5.58)$$

and

$$Re_f = \frac{4\Gamma_f}{\mu_\ell} \ , \qquad (5.59)$$

where Γ_f is the film mass flowrate per unit wetted perimeter. In equation (5.58), the term u* denotes the wall shear stress velocity given by

$$u^* = \sqrt{\tau_\omega/\rho_\ell} \ . \qquad (5.60)$$

Kutateladze approximated the film mass flowrate per unit wetted perimenter, Γ_f, for thin films by

$$\Gamma_f = \rho_\ell \int_0^F v\ dy \ , \qquad (5.61)$$

where v is the local film velocity at a distance y from the tube wall.

Kosky [192], on the other hand, proposed a simple alternative approach to that presented by Kutateladze. He considered two cases: One applicable to very thin films ($y^+ = y(\frac{\rho_\ell u^*}{\mu_\ell}) \leq 5$) and the other for thicker films ($y^+ > 5$). In the thin-film model, the dimensionless velocity, $v^+ = v/u^*$, was assumed linear and of the form

$$v^+ = y^+ \quad , \tag{5.62}$$

which is normally accepted for pipe flow. This assumption led to the following expression for the mean film thickness:

$$F^+ = \sqrt{Re_f/2} \quad . \tag{5.63}$$

For thicker films, Kosky employed Prandtl's $\frac{1}{7}$th power-law velocity radial profile, viz,

$$v^+ = 8.74(y^+)^{1/7} \quad , \tag{5.64}$$

in equation (5.61) and upon integration obtained

$$F^+ = 0.0504\ (Re_f)^{7/8} \quad . \tag{5.65}$$

Figure (5.14) shows a comparison of the mean film thickness-film flowrate results, as predicted from equations (5.57), (5.63) and (5.65), with the corresponding experimental data of a number of investigators [193-198]. To compare these predictions with the corresponding values determined by the methods employed in this investigation, the film flowrate per unit wetted perimeter is written as

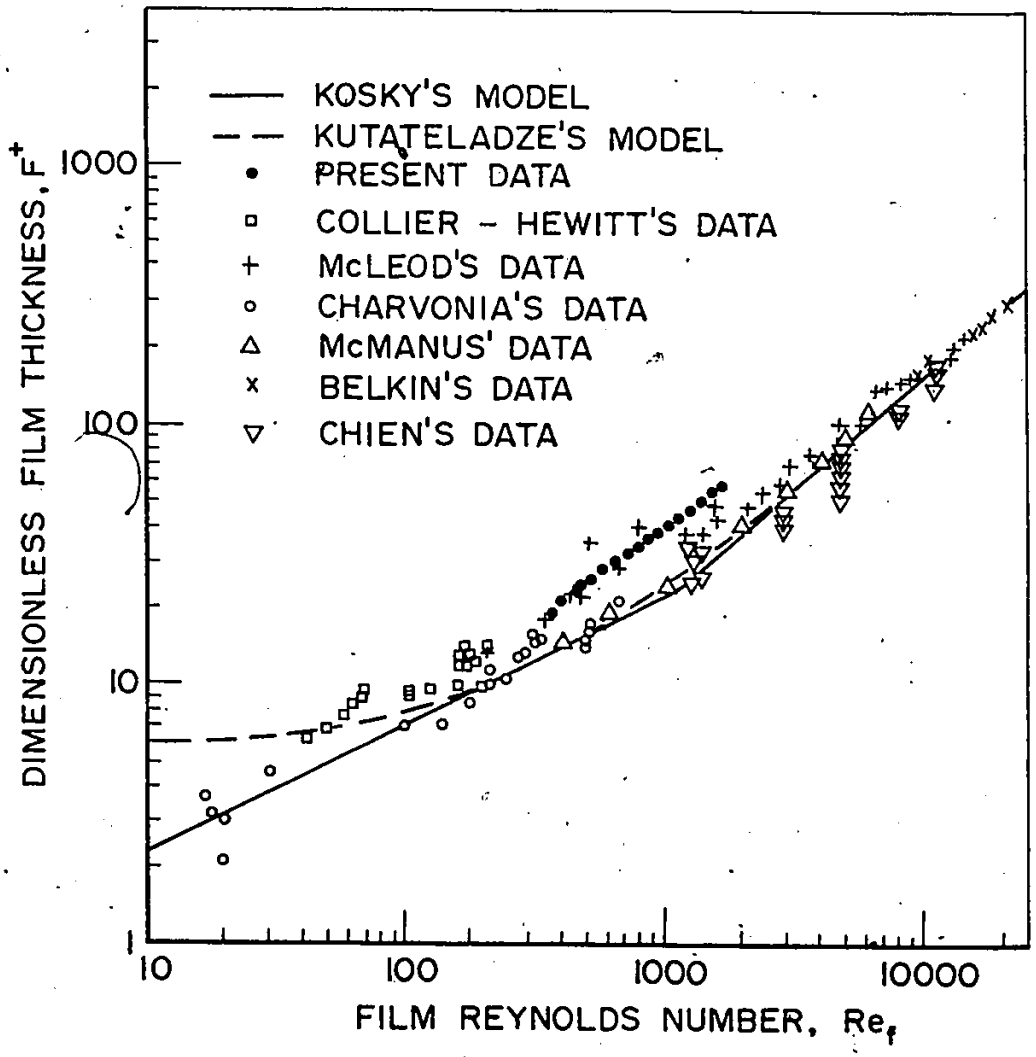

Figure (5.14): Comparison between the present results for the film thickness and selected data and models.

$$\Gamma_f = \frac{\rho_\ell}{2\pi R} \int_0^F 2\pi (R-y) v dy. \qquad (5.66)$$

If the film velocity radial profile indicated in section (5.5) is substituted into equation (5.66) and if the method of obtaining the mean film thickness, as recommended in the same section, is used, the resulting data points shown in figure (5.14) can be generated. Note that F indirectly relates to the experimental measurements of the radial void profile.

It is evident that all the data presented in figure (5.14), including those obtained in this investigation, lie above the curves predicted by Kosky and Kutateladze in the range of Re_f between 200 and 2000. The deviations may be attributed mainly to the wavy nature of the core-film interface; a fact which was not considered in deriving these models. Indeed, all of the models assume a smooth surface. Furthermore, the deviations between the values of F obtained in this investigation and those obtained from Kosky's and Kutateladze's models are also due to the different film velocity radial profiles employed. Finally, the simplifying assumption made in developing equation (5.61), concerning the neglect of the effect of the tube curvature, may also contribute partly to these deviations.

CHAPTER (6)

FLOW TRANSIENTS IN TWO-PHASE FLOW SYSTEMS

(6.1) Problem Definition

As mentioned in Chapter (1), the understanding of nuclear reactor behaviour under accident conditions is essential to study the reactor safety and controllability. The transient response of the average void fraction to perturbations in the input heat flux and/or inlet flow is of considerable interest because of its influence on neutron dynamics. These types of perturbations usually occur under accident conditions as well as in normal operation. In particular, among the most important accidents which may occur in boiling reactors are those caused by a pump failure or flow blockage where the coolant flow to the reactor core is reduced. Consequently, the accurate prediction of the dynamic characteristics of boiling reactors depends on the correct formulation of the void transient response to these perturbations.

It is customary to formulate the problem of void transient response in terms of a diffusion-type equation. Unfortunately, data on the effective diffusion coefficient in two-phase flow systems are not available in the literature [15]. Moreover, such a formulation has no real fundamental signifi-

cance and, hence, it is essentially not recommended for two-phase flow analysis. Hence, another approach must be sought. Zuber and Staub [15] have shown that the kinematic wave theory, expressed as a propagation equation, provides a convenient and fundamental method to analyze the dynamic behaviour of two-phase flow systems. The relation between the analysis formulated in terms of the kinematic waves and the standard formulation in terms of the diffusion equation has been discussed by Zuber [199].

It is worthy of note that the void propagation equation applies only to slow transients, as caused by a flow blockage or a pump failure, where compressibility effects can be ignored. In extreme situations, a loss-of-coolant accident, as caused by a main pipe failure in a pressurized system, can lead to fast transients where the compressibility effects may become important. Hence, the present analysis needs to be modified to account for the compressibility effects which could occur during severe accidents.

In this chapter, the void propagation equation will be derived from the continuity equations for the adiabatic gas-liquid flow system and then used to predict the transient response of the mixture average void fraction to perturbations in the gas inlet flow. The analysis presented here is most closely related to that given by Zuber and Staub [15] which has been based on the cross-sectionally averaged form of the mass conservation equations. The solution of the void propagation equation provides the desired information concerning the variation of the average void fraction with time and space along the test

section for any transient condition imposed on the system. Furthermore, the validity of the assumption usually made concerning the flow parameters, C_o and $\bar{V}_{gj}$, which are required in the formulation, will be tested. In summary, this assumption states that the parameter values obtained for steady-state, fully-developed flow are valid under transient developing-flow situations. That is to say that the steady-state flow parameters pertaining to the flow regime and the local average voidage condition apply in the transient system. The test involves the comparison of measured transient average void responses at an axial location along the flow tube with those predicted for the conditions of the experiments.

(6.2) Problem Formulation

The problem is formulated in terms of the equations of continuity for the liquid and gas phases. The continuity equation of the liquid phase is then transformed into the void propagation equation which is analyzed in terms of the kinematic waves. Appendix (G) contains the derivation of the void propagation equation for the adiabatic gas-liquid flow system under consideration.

Figure (3.3) shows the details of the flow system which has been used to study the transient response of the average void fraction to changes in the inlet gas flowrate. It consists of a mixing and a developing section of lengths L_1 and L_2, respectively.

In deriving the equations for this flow system, assume that the liquid phase is injected uniformly along the walls of the mixing section at a constant flowrate while the gas phase is introduced through its bottom end. At time t=0, a sudden change in the inlet gas flowrate is applied and it is required to predict the corresponding variation of the average void fraction with time and space along both the mixing and developing sections.

As shown in Appendix (G), the void propagation equation, as expressed in terms of quantities averaged over the tube cross-section, can be written in the form

$$\frac{\partial \langle \alpha \rangle}{\partial t} + U \frac{\partial \langle \alpha \rangle}{\partial z} = \Omega, \qquad (6.1)$$

where U is the velocity of the kinematic waves and Ω is the

characteristic reaction frequency. The void propagation equation demonstrates that the disturbances in the average void fraction, $\langle\alpha\rangle$, are propagated through the two-phase flow system at the velocity of the kinematic waves. This is derived in Appendix (G) as

$$\dot{U} = C_o\langle j_m\rangle + \langle\alpha\rangle\langle j_m\rangle \frac{\partial C_o}{\partial\langle\alpha\rangle} + \dot{\bar{V}}_{gj} + \langle\alpha\rangle \frac{\partial \dot{\bar{V}}_{gj}}{\partial\langle\alpha\rangle} . \quad (6.2)$$

Similarly, the characteristic reaction frequency is shown to be of the form

$$\Omega = \frac{\partial\langle j_m\rangle}{\partial z} - \frac{\langle\Gamma_\ell\rangle}{\rho_\ell} - C_o\langle\alpha\rangle \frac{\partial\langle j_m\rangle}{\partial z} , \quad (6.3)$$

where $\langle\Gamma_\ell\rangle$ is the liquid source term, that is, the rate of formation of liquid mass per unit mixture volume. As indicated by Zuber [84], this term is analogous to the source term in the continuity equation for a given species in a chemical reacting system. Consequently, in order to specify $\langle\Gamma_\ell\rangle$, it is necessary to specify the proper constitutive equation for this process. All the terms appearing in equations (6.1), (6.2) and (6.3) are in consistent units and have been defined previously.

Assuming that the liquid is distributed uniformly over the length L_1, the liquid source term can be written as

$$\langle\Gamma_\ell\rangle = \frac{Q'_\ell \rho_\ell}{L_1} , \quad \text{for } z \leq L_1 , \quad (6.4\text{-a})$$

and

$$\langle \Gamma_\ell \rangle = 0 \quad , \quad \text{for } z > L_1 \ , \tag{6.4-b}$$

where Q'_ℓ is the liquid volumetric flowrate per unit tube cross-sectional area. The rate of change of the average volumetric flux density of the mixture along the flow tube is derived in Appendix (G) in the form

$$\frac{\partial \langle j_m \rangle}{\partial z} = \frac{\langle \Gamma_\ell \rangle}{\rho_\ell} \ , \tag{6.5}$$

which upon integration yields

$$\langle j_m \rangle = Q'_g + \int_0^z \frac{\langle \Gamma_\ell \rangle}{\rho_\ell} \, dz \ , \tag{6.6}$$

where Q'_g is the gas volumetric flowrate per unit tube cross-sectional area.

Substituting for the liquid source term from equation (6.4) allows equation (6.6) to be written in the form

$$\langle j_m \rangle = Q'_g + \frac{Q'_\ell z}{L_1} \quad , \text{ for } z \leq L_1 \ , \tag{6.7-a}$$

and

$$\langle j_m \rangle = Q'_g + Q'_\ell \quad , \text{ for } z > L_1 \ . \tag{6.7-b}$$

Equation (6.7) states that the mixture average volumetric flux density increases linearly in the mixing section due to the liquid addition and then remains constant in the developing section, as would be expected. In view of equations (6,3), (6.4) and (6.5), the characteristic reaction frequency can be expressed as

$$\Omega = \frac{-C_o\langle\alpha\rangle Q'_\ell}{L_1} \quad , \quad \text{for } z \leq L_1 \; , \qquad (6.8\text{-a})$$

and

$$\Omega = 0 \quad , \quad \text{for } z > L_1 \; . \qquad (6.8\text{-b})$$

It is apparent from equations (6.2) and (6.6) that the velocity of the kinematic waves depends upon the average volumetric flux density of the mixture and, hence, upon the inlet conditions and the integrated effect of the liquid generation rate. On the other hand, the characteristic reaction frequency depends on the axial rate of change of the mixture average velocity and, hence, it depends on the local effects of the liquid generation rate (equations (6.3), (6.4) and (6.5)). Furthermore, it is important to note from equations (6.1), (6.2) and (6.8) that the transient response of the average void fraction depends upon the flow parameters, C_o and $\bar{V}_{gj}$. This emphasizes the fact that estimates of these parameters must be available for the system, a priori. Since it is difficult to obtain the flow parameters under unsteady-state conditions, their steady-state values will be assumed to be valid under transient conditions.

It is noted that the void propagation equation (6.1) is a first-order, non-linear partial differential equation of hyperbolic form [172]. It can be solved by standard methods to yield the time-variation of the cross-sectional average void fraction at any level along the mixing and developing sections. The calculation of the transient response of the average void fraction to perturbations in the gas inlet flowrate is carried out in two steps: First, the steady-state axial void distribution is determined before applying the change in the gas inlet

flowrate. Then this distribution is used as an initial condition to determine the time-variation of the average void fraction at different levels along the mixing and developing sections after the application of the flow disturbance.

Since equation (6.1) is first order in both the time and space variables, it is necessary to specify one initial condition for the dependent variable, $\langle\alpha\rangle$, at some time, t, and a boundary condition at some level, z. The appropriate boundary and initial conditions for the flow system under consideration are

(i) At z=0 and at any time t, $\langle\alpha\rangle = 1$. This is because the gas phase only enters through the bottom end of the mixing section.

(ii) At t=0, the average void fraction, $\langle\alpha\rangle$, has an initial axial distribution which is equivalent to the steady-state void distribution along the flow tube. Such a distribution has to be obtained by solving the void propagation equation starting with an arbitrary axial void distribution, say $\langle\alpha\rangle = 1$, and a sudden change in the liquid inlet flowrate from zero to Q_ℓ.

The boundary condition stated in (i) pertains for any initial condition that might be chosen.

(6.3) Solution of the Void Propagation Equation

(6.3.1) Method of Solution

(6.3.1.1) General Discussion

The void propagation equation has been recognized as a non-linear first-order partial differential equation of the hyperbolic type; the non-linearity arises because of the dependence of U and Ω on the average void fraction. There are two possible methods of solution: (i) one of the standard finite-difference methods and (ii) the method of characteristics. However, there are some severe computational restrictions involved in the use of the explicit finite-difference methods, namely: The problem of stability and convergence of computation and the excessive computer time required to achieve a given accuracy [172]. To remove some of these difficulties, a number of implicit finite-difference formulations have been developed. Hancox [16] solved the void propagation equation using an implicit finite-difference scheme to yield the void transient response to sinusoidal input power. However, some difficulties might be expected to arise in using such a scheme because of the concentration discontinuities which may result between pairs of mesh points. The method of characteristics avoids these difficulties and this is important in the present problem.

(6.3.1.2) Method of Characteristics

In the method of characteristics, the independent variables are transformed in such a way that the partial dif-

ferential equation is converted into a set of ordinary differential equations. It is known that the hyperbolic partial differential equation (equation (6.1)) possesses a set of characteristic curves in the $(t,z,\langle\alpha\rangle)$ space [172]. A characteristic curve is one whose tangent at every point has the direction vectors 1, U and Ω in the t, z and $\langle\alpha\rangle$ directions, respectively. Since the average void fraction is a function of both time and space, the total differential may be written as

$$d\langle\alpha\rangle = \frac{\partial\langle\alpha\rangle}{\partial t}\,dt + \frac{\partial\langle\alpha\rangle}{\partial z}\,dz. \qquad (6.9)$$

Equations (6.1) and (6.9) may be considered as simultaneous equations with the partial derivatives, $\frac{\partial\langle\alpha\rangle}{\partial t}$ and $\frac{\partial\langle\alpha\rangle}{\partial z}$, as the unknowns. In order that an infinite number of solutions exist for the partial derivatives, the determinant

$$\begin{vmatrix} 1 & U \\ dt & dz \end{vmatrix}$$

should be set equal to zero; thus,

$$\frac{dt}{dz} = \frac{1}{U}\ , \qquad (6.10)$$

which defines a set of characteristic curves labelled I. Similarly, in order for some solution to exist, the determinant

$$\begin{vmatrix} U & \Omega \\ dz & d\langle\alpha\rangle \end{vmatrix}$$

should be equal to zero. In other words,

$$\left.\frac{d\langle\alpha\rangle}{dz}\right|_I = \frac{\Omega}{U} \quad . \tag{6.11}$$

It is noteworthy that equation (6.11) can also be derived if one substitutes equation (6.10) into equation (6.9) to get

$$d\langle\alpha\rangle = \left(\frac{1}{U}\frac{\partial\langle\alpha\rangle}{\partial t} + \frac{\partial\langle\alpha\rangle}{\partial z}\right)dz \quad , \tag{6.12}$$

and then compares equation (6.12) with equation (6.1).

The method of characteristics is straightforward and systematic; it can be made as accurate as needed by constructing a finer mesh network of characteristics. The characteristic curves can be physically interpreted as follows: A characteristic curve represents the trajectory of an element of fluid which enters the system at a time equal to the intercept of that characteristic curve with the time-axis. Therefore, a disturbance in the composition of the feed will propagate along the characteristic curve with a velocity equal to U. This means that the characteristic curves represent the paths along which perturbations in the average void fraction propagate in the flow system. This, in turn, implies that the void concentration may be discontinuous across the characteristic curves. Because of these discontinuities, the derivatives of a function cannot be approximated by the difference quotients and extra caution should be exercised in solving the partial differential equation using one of the finite-difference methods. However, if the method of characteristics is used, one can readily avoid the regions of discontinuities because these discontinuities are propagated

along the characteristic curves of the system.

In summary, the void propagation equation can be transformed through the method of characteristics to two simultaneous ordinary differential equations; the solution is obtained by integrating equation (6.11) along equation (6.10) which describes the characteristic curves. Thus, the symbol $\left.\frac{d\langle\alpha\rangle}{dz}\right|_I$ in equation (6.11) indicates the derivative of $\langle\alpha\rangle$ with respect to z along the characteristic curves which are denoted by I and defined by equation (6.10). It is obvious that in terms of numerical computation, considerable simplification is achieved by employing the method of characteristics since this method gives rise to a set of ordinary differential equations. It has been shown by Lapidus [172], in his comparison between the method of characteristics and finite-difference approaches, that the former is slower for a given mesh size but much faster for a given accuracy.

(6.3.1.3) Details of Solution

Because of the advantages of the method of characteristics in this instance, this method will be used to solve the void propagation equation. For convenience in visualizing the system of equations, a two-dimensional plane diagram in the (t-z) space may be constructed. On this plane, a family of characteristic curves are plotted as a result of integrating equation (6.10) with the proper boundary conditions. A typical mesh layout for the method of characteristics is shown in figure (6.1) where

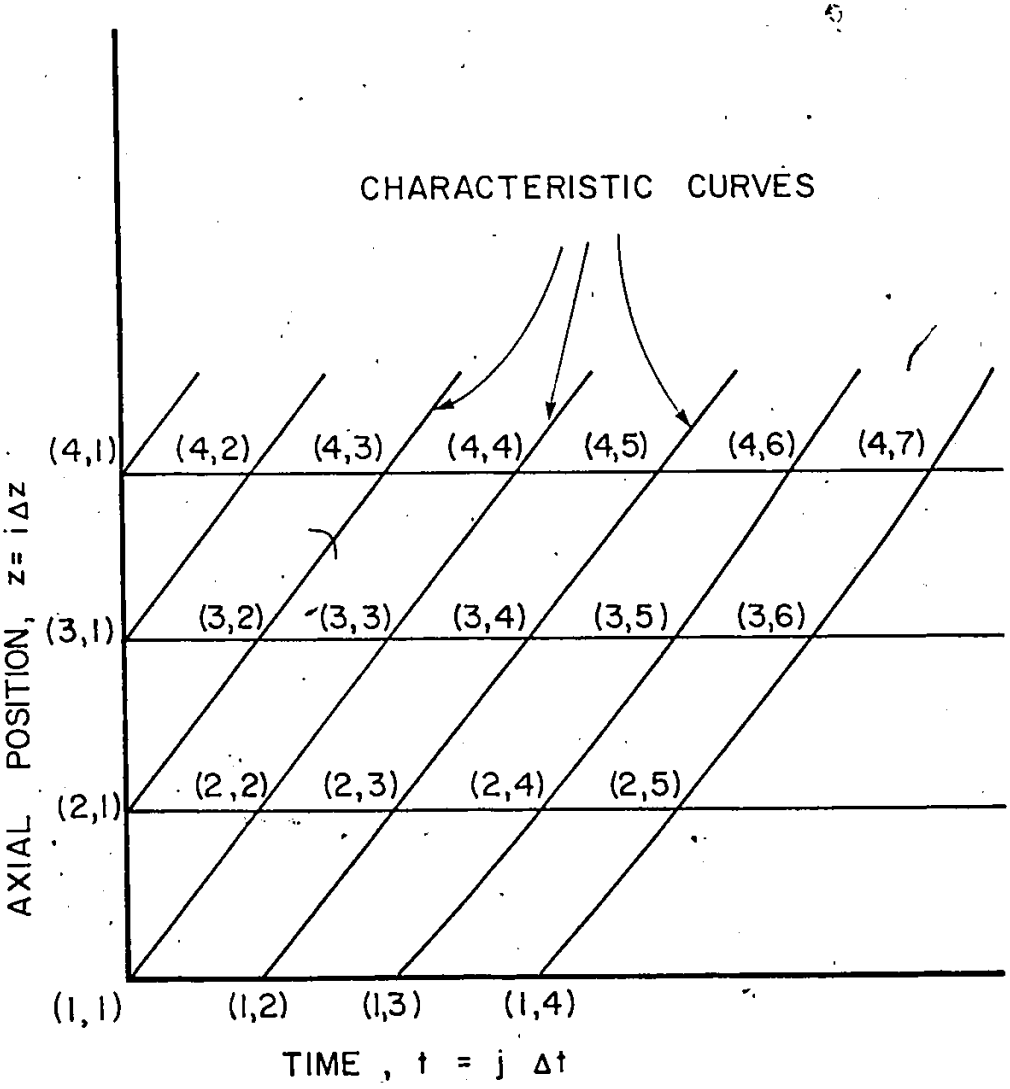

Figure (6.1): Mesh layout for the method of characteristics.

i and j indicate the number of finite steps in the distance and time variables, respectively. The resulting characteristic curves determine when a given variation in the average void fraction will reach a given point in the flow system. The integration of equation (6.11) along these characteristics yields the variation of the average void fraction with time and position after any perturbation occurs in the system.

In view of equations (6.2) and (6.8), the velocity of the kinematic waves, U, and the characteristic reaction frequency, Ω, depend on the cross-sectional average void fraction, $\langle\alpha\rangle$. Since this makes equations (6.10) and (6.11) non-linear, a numerical integration technique must be used. In the present study, the fourth-order, Runge-Kutta-Merson formulation [200] has been used to solve these equations simultaneously. In order to solve the void propagation equation to yield the time-variation of the average void fraction at specified levels along the flow tube, the z-axis is divided into N parts of a constant increment Δz. To define the boundary conditions needed to solve equation (6.10), which yields the equations of the characteristic curves, the t-axis is divided into corresponding divisions each of length Δt which is assigned the value

$$\Delta t = \Delta z / Q_g' \quad . \qquad (6.13)$$

(6.3.2) Behaviour of the Adiabatic Flow System

(6.3.2.1) General Discussion

In view of equations (6.2), (6.8), (6.10) and (6.11), it is evident that the changes in the average void fraction only occur in the mixing section; this is expected since this is the only region where liquid is added to the flowing two-phase mixture. Hence, in the flow-developing section, the average void fraction should remain constant and equal to its value at the exit of the mixing section. However, the void fraction distribution across the flow tube is expected to keep changing till the fully-developed flow condition is approached. On the other hand, the developing section introduces a transport delay to the void response which is equivalent to the time taken by the fluid elements to travel from the top end of the mixing section to the measuring location.

Furthermore, it is of interest to note that discontinuities have been introduced in $\langle \Gamma_\ell \rangle$ and, hence, in Ω, as indicated in equations (6.4) and (6.8), respectively. In order to avoid the effect of these discontinuities on the numerical solution, this solution has been obtained separately for the mixing and developing sections. Thus, the solution of the void propagation equation at the end of the mixing section may be used as a boundary condition for its solution in the developing section.

It is also evident from equations (6.1), (6.2) and (6.3) that in order to determine the void transient response, the flow parameters, C_o and $\bar{V}_{gj}$, should be known a priori. Since

there is no available information about these parameters for the case of unsteady developing flow, the only alternative at this time is to use those parameter estimates obtained for the same apparatus under steady-state, developed-flow conditions, as presented in Chapter (5). It is worthy of note that all previous investigations which have dealt with the problem of void transient response have assumed that the steady-state values of these parameters for fully-developed flow can be used for the dynamic systems [15,16 and 18]. However, there are still unanswered questions concerning the validity of such an assumption.

The next subsection is devoted to discuss the assumptions made concerning the flow parameters which are used to predict the void transient response for the flow system under consideration. The validity of these assumptions will be examined in subsequent sections.

(6.3.2.2) Flow Parameters Used in Predicting the Dynamic Response

For the flow system which has been considered in the present study, the average void fraction, $\langle\alpha\rangle$, starts with a value of unity at the bottom end of the mixing section and keeps changing in that section due to liquid addition. In the developing section, while $\langle\alpha\rangle$ remains constant and equal to its value at the exit of the mixing section, the void radial distribution keeps changing till the fully-developed flow condition is approached.

As indicated in Chapter (5), the flow parameters, C_o and $\bar{V}_{gj}$, were found to remain essentially constant under steady-state, fully-developed flow conditions for an unchanged flow regime. In the present investigation, it will be assumed that this is also valid under transient developing-flow conditions, that is, the flow parameters remain constant until a change in the flow regime occurs.

Therefore, in the case where the final condition at the measuring location is bubbly flow, the flow regime is expected to be annular at the beginning of the mixing section and then rapidly changes to bubbly flow in the rest of the tube. This means that the flow parameters, C_o and $\bar{V}_{gj}$, are expected to change due to the change of the flow regime and/or the void radial distribution. However, the region over which C_o and $\bar{V}_{gj}$ change from their values corresponding to one flow regime to those corresponding to the other flow regime can not be determined in a steady-state experiment. This is because the variation in the flow parameters depends on therate of change of the average void fraction along the mixing section and on how fast the change in flow regime occurs.

Thus, to make the problem mathematically tractable, it is required to have a continuous functional relationship for the flow parameters to describe their variation with the average void fraction, $\langle\alpha\rangle$. This relationship should cover the entire range of $\langle\alpha\rangle$ which is expected in the transient experiment. In this case, this range is from unity at the inlet to the values measured

at the given axial measuring station. In addition, this relationship should account for the fact that the flow may be still developing along the flow tube although the average void fraction has become constant.

These requirements delineate major shortcomings in the use of the void propagation equation to study and predict the transient behaviour in two-phase flow. One shortcoming is that the flow parameters are required but they can only be conveniently obtained under steady-state flow conditions. Note also that it is only possible to obtain these parameters over very limited ranges of average void fraction, that is, only in the bubbly and annular flow regimes since slug flow exists over the range of $\langle\alpha\rangle$ between these two flow regimes. It is known that considerable time or axial distance in a pipe is required to obtain steady-state slug flow conditions and sufficient time or distance is not available to develop these flow conditions during a transient. Hence, the values of the flow parameters can only be inferred over the intermediate region of $\langle\alpha\rangle$ from about 0.45 to 0.80 and this inference can only be obtained by interpolating the parameters between the bubbly and annular flow regimes.

In the present analysis, a continuous functional relationship will be assumed for the distribution parameter, C_o, which satisfies the limits when $\langle\alpha\rangle$ approaches zero or unity. However, the effect of this assumption on the predicted void transient res-

ponse will be assessed later by performing a sensitivity analysis and comparing the predicted responses with those experimentally measured. It is worthy of note that, for the same reasons described above, Hancox [16] similarly had to assume a continuous functional relationship for C_o in his analysis of dynamic boiling-flow systems and he did not test the validity of his assumed relationship.

For the experimental apparatus under consideration, the distribution parameter, C_o, should approach unity at the limits when the average void fraction, $\langle\alpha\rangle$, approaches zero or unity. This can be understood in view of equation (1.5-a) if one realizes that at both limits, the local void fraction tends to have flat radial distributions. Moreover, since the liquid is injected through the walls of the mixing section into the continuously flowing gas, the latter tends to concentrate in the high-velocity region near the tube center. As indicated in Chapter(5), this results in values of C_o greater than unity at the intermediate values of $\langle\alpha\rangle$ which are consistent with the observations made by Zuber and Findlay [17] and by Bankoff [71].

Styrikowich et al. [184] proposed to correlate the distribution parameter, C_o, to the average void fraction, $\langle\alpha\rangle$, by a model of the form

$$C_o = \frac{1 + \langle\alpha\rangle^m}{1 + \langle\alpha\rangle^{m+1}} \quad , \qquad (6.14)$$

which satisfies the requirements mentioned above. In the present

analysis, equation (6.14) will be used to interpolate between the values of C_o which were estimated for the bubbly and annular flow regimes under steady-state, fully-developed flow conditions. These values of C_o, as indicated by figures (5.9-a) and (5.10-a), were used to obtain a best estimate of 0.887 for the parameter, m, in equation (6.14). The estimation procedure used Marquardt's method [141] to minimize the sum of squares of the residuals between these values of C_o and those determined from equation (6.14).

Figure (6.2) shows the variation of the distribution parameter, C_o, with the average void fraction, $\langle\alpha\rangle$, as predicted from equation (6.14), together with those values of C_o which were obtained for the bubbly and annular flow regimes. For comparison, this figure also shows the corresponding functional relationship which was assumed by Hancox for C_o in a boiling flow system with a uniformly heated tube [16]. It is of interest to note that while equation (6.14) always predicts values of C_o greater than unity, the model assumed by Hancox indicates values of C_o less than unity at low values of $\langle\alpha\rangle$. This can be explained by the fact that in a heated tube, vapour bubbles are initially formed at the wall and remain in the wall region where the velocity is low. However, as the flow progresses downstream and the average void fraction increases, the vapour bubbles migrate to the central region of the tube where the velocity is high. Hence, for this type of flow, the distribution parameter has a value less than unity near the tube inlet and increases to

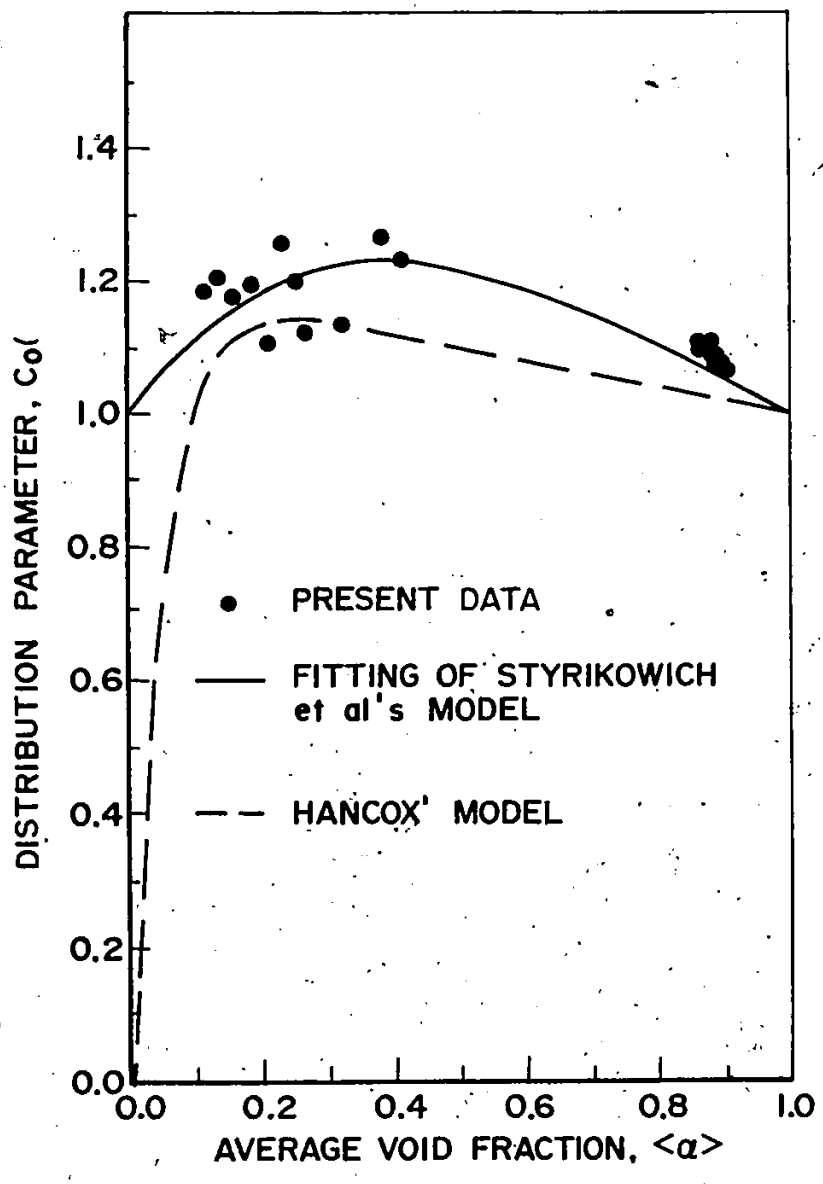

Figure (6.2): Variation of the distribution parameter with the average void fraction.

values greater than unity as the average void fraction increases.

Furthermore, as indicated by Hancox [16] and emphasized in Chapter (5), the value of the mean drift velocity, $\bar{V}_{gj}$, is relatively small for bubbly flow. Since the transition to the bubbly flow regime is expected to occur in a relatively short portion of the flow tube, $\bar{V}_{gj}$ and its variation with $\langle\alpha\rangle$ can be neglected in equation (6.2). The effect of this assumption will also be investigated when the comparison between the measured and predicted void transient responses is performed. Consequently, equation (6.2) can be reduced for this particular case to

$$U = \langle j_m \rangle \left(C_o + \langle\alpha\rangle \frac{\partial C_o}{\partial \langle\alpha\rangle}\right) \quad . \qquad (6.15)$$

On the other hand, in the case where the final flow condition at the measuring location is annular, the only flow condition which exists in the flow tube is that pertinent to annular flow. Consequently, the problems described above do not arise for this case since, as concluded in Chapter(5), the flow parameters remain essentially constant in this flow regime and do not depend on $\langle\alpha\rangle$. Thus, the constant averaged values of the flow parameters, that is, $C_o = 1.082$ and $\bar{V}_{gj} = 120.04$ cm/sec, can be used in this case to predict the void transient response. However, this is based on the assumption that the observation made for steady-state, fully-developed flow is also valid for the same apparatus under transient developing-flow situations; an assumption which needs to be tested. It is worthy of note

that Shiralkar et al. [18] and Staub et al. [80] made a similar assumption in their analyses of void transient response in boiling forced-flow systems.

Equation (6.2) can, then, be simplified to

$$U = C_o \langle j_m \rangle + \bar{V}_{gj} \quad , \qquad (6.16)$$

which, according to equation (5.15), indicates that the velocity of the kinematic waves is equivalent to the gas weighted mean velocity. Thus, one can conclude that as long as the flow regime is unchanged, the velocity of the kinematic waves does not depend on the mean drift velocity, $\bar{V}_{gj}$; a conclusion which is similar to that made by Zuber and Staub [15]. Moreover, it is evident from equation (6.3) that the characteristic reaction frequency, Ω, is also independent of $\bar{V}_{gj}$ for the experimental system under consideration. Hence, the transient response of the average void fraction in the present case should not depend on the value of the mean drift velocity.

(6.4) Sensitivity of Void Transient Response to Errors in the Distribution Parameter

Before any actual dynamic experiments are performed and the actual results are compared with those expected from the analysis, it is worthwhile assessing the sensitivity of the predicted void response to errors in the distribution parameter. This was achieved by solving the void propagation equation by the method of characteristics to predict the void transient response

to an arbitrary step change in the gas inlet flowrate. The predicted transient response of the cross-sectional average void fraction at a level of 36 in., is shown in figure (6.3) for a typical case of bubbly flow. This figure suggests that there are four variables which can be used to characterize the void transient response; viz,

(i) The starting value of the steady-state average void fraction, $\langle\alpha\rangle_1$.

(ii) The new value of the steady-state average void fraction that occurs after the application of the flow perturbation. This can be represented by the total change in the average void fraction, $\Delta\langle\alpha\rangle$, from the initial to the final condition.

(iii) The time t_1 at which the average void fraction starts to change at that particular axial location, that is, the time taken by the flow system before it responds to the flow perturbation.

(iv) The rise time Δt, that is, the time required by the system to reach 99.5% of the new steady-state value of the average void fraction.

These four variables were used to characterize the void transient response for any given simulated dynamic experiment. Thus, it was possible to test the sensitivity of this response to the accuracy of the estimated values of distribution parameter.

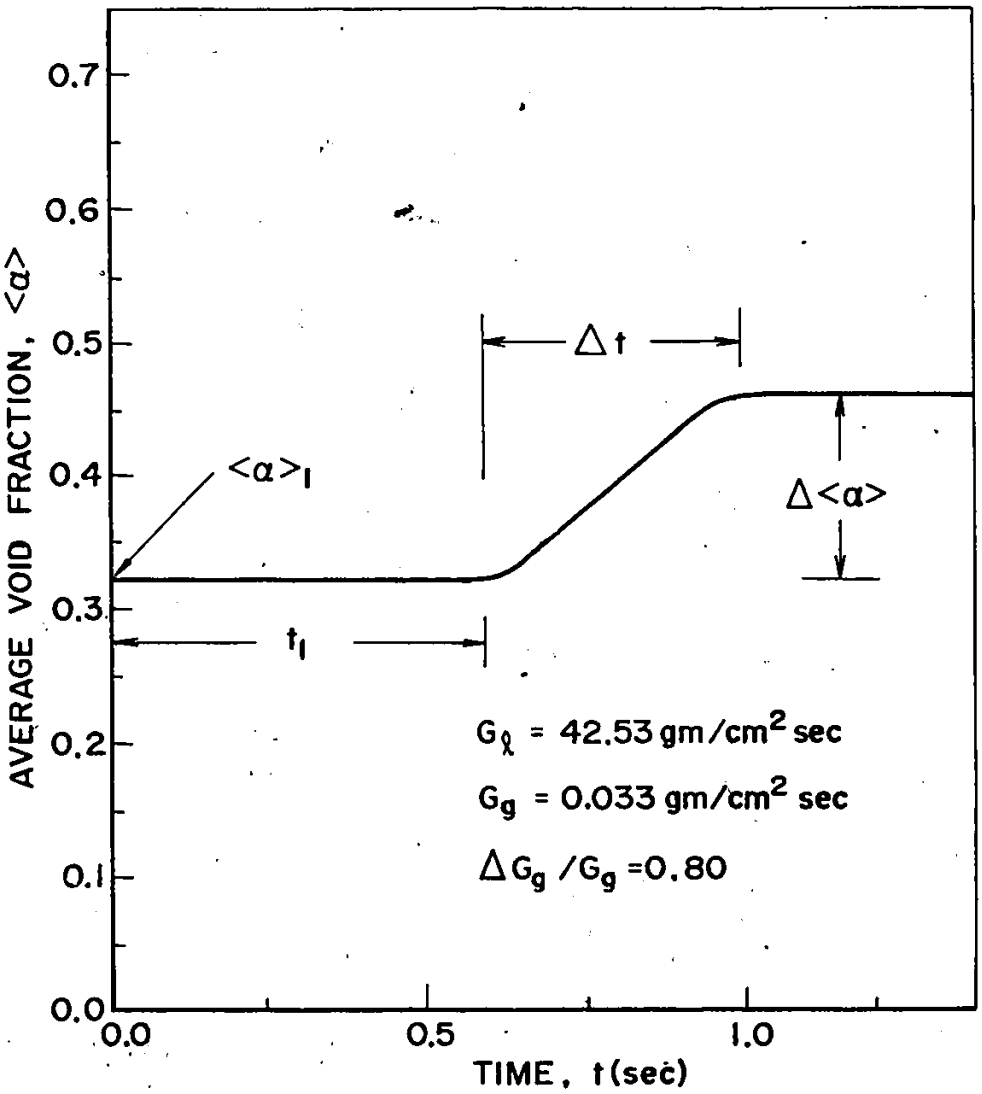

Figure (6.3): Transient response of the average void fraction to an arbitrary step change in the gas inlet flowrate for a typical case of bubbly flow.

This would show if a comparison between measured and predicted void transient responses can be used to check the applicability of the parameter values, as estimated for steady-state, fully-developed flow, to dynamic developing-flow situations for the same apparatus.

This sensitivity analysis was performed for flow conditions leading to both the bubbly and annular flow regimes at the 36 in. axial position. Results for these simulated experiments are reported in turn.

(a) Bubbly Flow Regime

The sensitivity of the response to the distribution parameter, C_o, was investigated by considering the parameter value to differ by fixed percentages from the steady-state value expected to pertain for the local flow condition. Based upon the analysis presented by Zuber and Findlay [17], the range of variation of the distribution parameter for the case of zero wall void fraction should be limited to about -25% to 30% for the bubbly flow regime. Consequently, C_o was assumed to differ by ±(10, 20 and 30)% and the resulting changes in the four variables mentioned above were calculated for a typical experimental condition ($G_g = 0.033$ gm/cm^{2}sec, $G_\ell = 42.53$ gm/cm^{2}sec and $\Delta G_g/G_g = 80\%$). These differences in C_o represent the worst conditions that can be imagined to occur in the bubbly flow regime. In order to test the effect of introducing these differences on the model predictions over the different regions of the flow system, the following two cases were considered:

(i) The differences in C_o were assumed to occur only in the mixing section, that is, up to $z = L_1$ (L_1 = 6 in.); thereafter the expected values of C_o were used.

(ii) The differences in C_o were assumed to occur in both the mixing and developing sections, that is, from the inlet of the mixing section at z=0 to the measuring location at $z = L_1+L_2$ (z = 36 in.)

The results of this analysis are summarized in table (6.1-a) from which the following observations can be made:

(i) For the two cases mentioned above, identical changes are introduced in the starting value of the steady-state void fraction, $\langle\alpha\rangle_1$, as well as in the total change, $\Delta\langle\alpha\rangle$. On the other hand, different changes are observed in the delay time, t_1, as well as in the rise time, Δt. This is expected, however, since the average value of the void fraction is predicted to remain constant in the developing section which acts only to introduce a transport delay to the void response.

(ii) The resulting changes in $\langle\alpha\rangle_1$ and $\Delta\langle\alpha\rangle$ are not large and, as will be shown later, are of the order of the confidence limits of the experimental measurements. Again this is due to the fact that in the flow system under consideration, the changes in the average void fraction only occur in the mixing section which is much shorter than the rest of the flow tube. This observation indi-

Variable	Reference Value	Case No.	% Change in C_o					
			-30	-20	-10	10	20	30
$\langle\alpha\rangle_1$	0.3209	(i)	- 7.74	- 4.64	- 2.11	1.78	3.30	4.61
		(ii)	- 7.74	- 4.64	- 2.11	1.78	3.30	4.61
$\Delta\langle\alpha\rangle$	0.1183	(i)	-10.87	- 6.40	- 2.85	2.33	4.27	5.89
		(ii)	-10.87	- 6.40	- 2.85	2.33	4.27	5.89
t_1 (sec)	0.6528	(i)	- 0.88	- 0.57	- 0.27	0.25	0.47	0.67
		(ii)	38.64	22.90	10.30	- 8.58	-15.82	-22.02
Δt (sec)	0.3127	(i)	42.27	23.65	10.16	- 7.89	-14.18	-19.30
		(ii)	55.42	31.82	13.94	-11.13	-20.18	-27.67

Table (6.1-a): Percentage changes introduced in the variables characterizing the void transient response due to fixed percentage differences in the distribution parameter for a typical case of the bubbly flow regime.

cates that with the measuring instrumentation used here, neither measurements of $\langle\alpha\rangle$ nor $\Delta\langle\alpha\rangle$ can be used to test the validity of the steady-state values of C_o for the transient situations. On the other hand, the large changes which are observed in t_1 and Δt suggest that these variables can be used in performing this test.

(iii) From the comparison of the resulting changes in t_1 for the two cases considered, it is evident that most of these changes occur in the developing section. Again this observation emphasizes the fact that most of the delay occurs in the developing section which is much longer than the mixing section.

It can be concluded from the above observations that the sensitivity of the variables t_1 and Δt to the differences introduced in C_o can be used as a basis to check the applicability of the steady-state values of C_o to transient situations. This will be achieved by comparing the predicted void transient responses of the average void fraction with those measured experimentally. A reasonably good agreement between these responses would indicate that these estimates of C_o can be used under dynamic developing situations for the flow system employed in the present application. Thus, the continuous functional relationship which was used to interpolate between the estimated values of C_o can be used to predict the void transient response

for the particular range of experimental conditions considered herein. Furthermore, it would support the simplifying assumption that the mean drift velocity is relatively unimportant for the case where the final condition at the measuring location is bubbly flow. On the other hand, if a significant deviation results, it can be concluded that the steady-state values of C_o, as determined for fully-developed flow, cannot be used to predict the void transient response. This would mean that further work is required to determine the values of the flow parameters along both the mixing and developing sections under the dynamic developing-flow conditions.

(b) Annular Flow Regime

In this case, the flow regime starts as an annular flow at the inlet of the mixing section and remains unchanged until the measuring location. This means that the flow parameters can be assumed essentially constant if the observation made in Chapter (5) is also valid under dynamic developing-flow conditions; namely, the flow parameters remain unchanged for a specific flow regime. Moreover, the void transient response has been shown in section (6.3) to be independent of the mean drift velocity as long as the flow regime remains the same. Hence, one can assess the sensitivity of the predicted void transient response to the value of the distribution parameter, C_o,

by introducing specified differences in C_o and calculating the resulting changes in the response. This would show whether a comparison between predicted and measured void transient responses can be used to test the applicability of the steady-state single averaged value of C_o, as estimated for fully-developed flow, to dynamic developing-flow situations in the same apparatus.

Table (6.1-b) presents the results of the sensitivity analysis for a typical case of the annular flow regime (G_g = 2.61 gm/cm^{2}sec, G_ℓ = 2.66 gm/cm^{2}sec and $\Delta G_g/G_g$ = 100%). Three cases were considered where differences of -10%, 10% and 20% were introduced in the constant averaged value of C_o, that is, C_o = 1.082. The range of variation of C_o was based on the analysis presented by Zuber and Findlay [17] which showed that for the case of zero wall void fraction, C_o should not differ by more than -10% to 15% in annular flow. The assumed differences were considered to occur throughout the entire flow tube, that is, from the inlet of the mixing section (at z = 0) to the measuring location (at z = 36 in.).

Table (6.1-b) indicates that, similar to the case where the final condition at the measuring location is bubbly flow, the predicted values of $\langle\alpha\rangle_1$ and $\Delta\langle\alpha\rangle$ are insensitive to the distribution parameter. Again this can be attributed to the fact that in the flow system employed herein, the changes in the average void fraction only occur in the mixing section which is relatively short in comparison with the rest of the flow tube. On the other

Variable	Reference Value	% Change in C_o		
		-10	10	20
$\langle\alpha\rangle_1$	0.8935	0.06	-0.05	-0.09
$\Delta\langle\alpha\rangle$	0.0504	-0.77	0.64	1.18
t_1(sec)	0.0158	10.81	-8.89	-16.32
Δt(sec)	0.0032	10.81	-8.88	-16.32

Table (6.1-b): Percentage changes introduced in the variables characterizing the void transient response due to fixed percentage differences in the distribution parameter for a typical case of the annular flow regime.

hand, much larger changes can be observed in the predicted values of t_1 and Δt. With the measuring instrumentation available, one can conclude that the measurement of t_1 can be used to test the applicability of the steady-state averaged value of C_o to transient developing-flow situations in the same apparatus. A reasonably good agreement between the measurements and predictions would indicate that this value of C_o can be used to predict the void transient response without appreciable errors for the flow system employed in the present investigation.

It is noteworthy to point out that the analysis carried out in this section is limited to one type of perturbation where the compressibility effects can be ignored, in a specific apparatus, with air and water (with limited physical properties) and under specific adiabatic flow conditions. However, this analysis presents the basis for a study of more general situations where the effects of fluid properties and apparatus dimensions under different flow conditions and for different types of perturbations are considered.

It is also important to emphasize that in the flow system considered herein, the changes in the average void fraction occur only in the mixing section which is relatively short in comparison with the rest of the flow tube. Consequently, the variables $\langle\alpha\rangle_1$ and $\Delta\langle\alpha\rangle$ are not expected to be as sensitive to the flow parameters as they might be for other flow systems where changes in the average void fraction occur over a greater length of the flow tube. For example, Hancox and Nicoll [24]

studied the effect of using two different expressions for the distribution parameter on the predicted void transient response to sinusoidal input power. They concluded that the solution was significantly affected especially at low pressure; hence, they recommended that caution should be exercised when predicting the void transient response in a system where the distribution parameter might be varying. Similarly, Kroeger and Zuber [201] showed that the value of the distribution parameter had a major effect on their ability to predict accurately the average void fraction in a subcooled boiling system.

In the overall program of two-phase flow which has been outlined in Chapter (1), the sensitivity analysis presented here should be extended to study the effects mentioned above.

(6.5) Experimental Work

(6.5.1) Experimental Facility

To obtain experimental data which can be used to evaluate the assumptions made concerning the flow parameters, transient void fraction experiments were conducted using the adiabatic test facility described in Chapter (3). As mentioned in that chapter, the experimental facility was designed to provide experimental data on both steady-state as well as dynamic behaviour of cocurrent adiabatic air-water flow in a vertical tube.

The experiments were performed by applying essentially a step change (increase) in the gas inlet flowrate while maintaining a constant liquid flowrate. To minimize the oscillations

in the gas flowrate during the application of the flow transient, a large surge tank was installed in the air line upstream of the apparatus. It acted to suppress any pressure overshooting upstream of the sonic orifice. A differential pressure transducer and a recording oscillograph (Visicorder) were employed to measure the actual changes in the upstream pressure. Since this pressure, under sonic orifice conditions, is a direct measure of the gas mass flowrate at a constant temperature, the variation of the upstream pressure can be considered as an indication of the variation of the gas flowrate. Figure (6.4) presents a typical actual time-variation of the auxiliary gas flowrate for an experimental run in the bubbly flow regime. This figure demonstrates that an ideal step change in the gas inlet flowrate was not achieved; however, this particular change was easily accommodated in the model described in section (6.2).

Although it was originally planned to investigate the transient behaviour of both the bubbly and annular flow regimes, the experimental difficulties accompanying annular flow restricted this study to bubbly flow. In annular flow, it was noted that the initiation of the sudden changes in the gas flowrate introduced flow oscillations which were indicated by vigorous pressure drop fluctuations, as measured by the differential manometer, and by flow chugging, as observed through the lucite

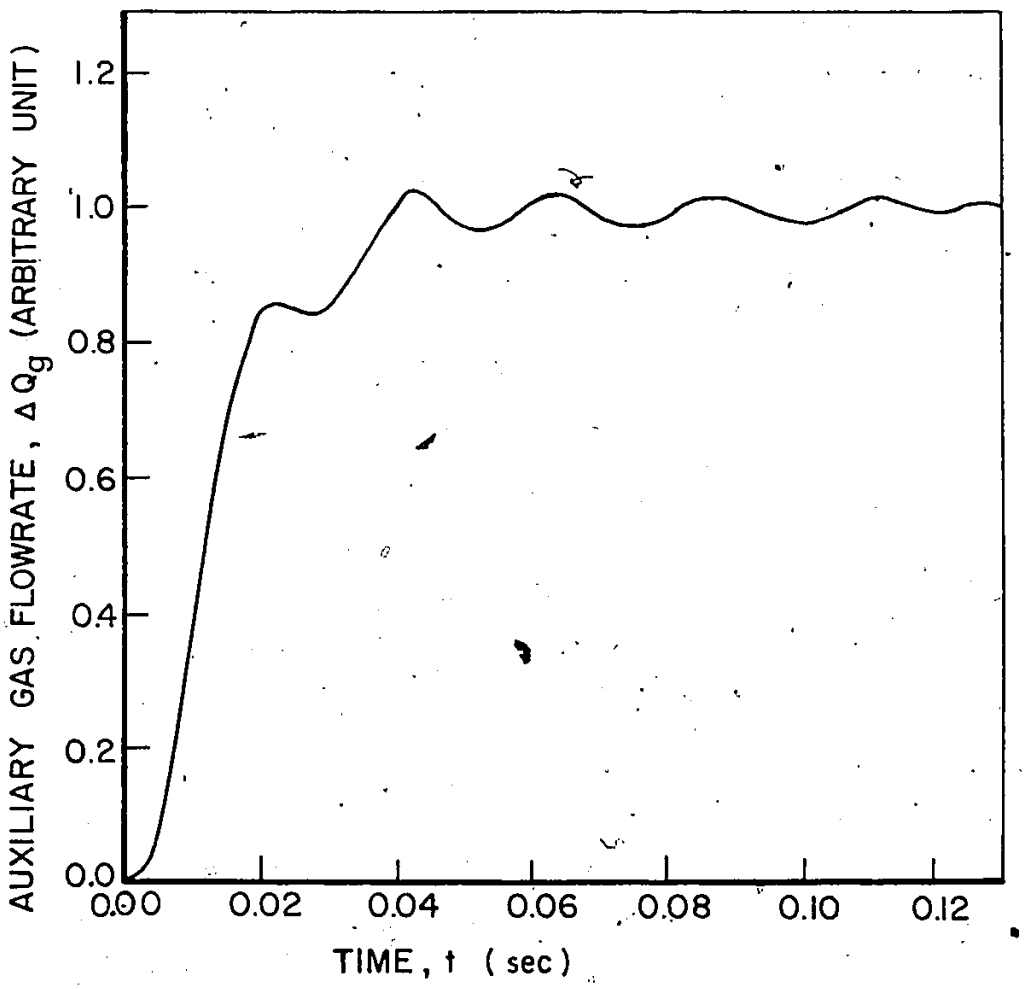

Figure (6.4): Actual time-variation of the auxiliary gas flowrate for a typical experimental run of the bubbly flow regime.

test section. This type of flow oscillation was noted to occur even for small perturbations of gas flow; for large changes of gas flowrate, however, this oscillation was so vigorous as to shake the flow tube. The resulting pressure drop fluctuations were similar to those usually obtained in the slug flow regime. The visual observation of the flow together with these pressure drop fluctuations demonstrated that the simple steady film-core arrangement characterizing annular flow did not persist during the application of the gas flow transient. It was thought that these oscillations might have arisen in the system as a result of the large pressure drop which occurred in the relatively small-diameter and long connecting lines transporting the air and water to the test facility. However, by reducing this pressure resistance, the flow oscillations could not be appreciably reduced and the annular flow could not be stabilized under transient conditions. Alternatively, the severe oscillations in annular flow can be attributed to the multiple effects which were caused by the fluctuations of the inlet gas flowrate and the pressure at the downstream side of the porous tube in the mixing section. Inlet gas flowrate fluctuations would create pressure fluctuations at the downstream side of the porous tube which, in turn, would cause fluctuations in the liquid flowrate through the porous tube. The fluctuations in the liquid flowrate once started would persist and break down the film layer at the tube wall, that is, prevent the formation of the continuous film at the tube wall which characterizes

annular flow. Indeed, the severe variations in liquid flowrate, as characterized by the alternate chugging of large amounts of liquid and gas, made modeling or mathematical description of the liquid addition over the mixing section impossible. Thus, the experiment was abandoned.

Clearly, this problem arises in the liquid-gas mixing section and is attributed to the liquid injection system. In order to reduce the effect of these flow oscillations during the application of gas flow perturbations in the annular flow regime, the following modifications may be helpful:

(i) Use a bigger surge tank in order to further suppress the fluctuations in the inlet gas flowrate.

(ii) Increase the pressure drop across the porous tube in the mixing section in order to reduce the fluctuations in the liquid flowrate. This can be achieved by decreasing the pore size and/or the length of the porous tube. However, extra caution should be exercised in decreasing the pore size since this requires filtering smaller particles from the liquid to prevent or minimize blocking the porous tube.

(iii) Use a different mixing arrangement; for example, try one of the liquid injecting systems suggested by Gill et al. [177] for annular flow, that is, the multijet injector or the annular slot injector. In the first

injecting system, the liquid enters the flow tube through eight radially-placed jets; whereas in the other system, the liquid is introduced to the flow tube through an annular slot after passing through a calming section.

In addition to the experimental difficulties mentioned above, the void transient response in annular flow was found to occur so fast that the present recording system could not handle the experimental data properly. As can be seen from table (6.1-b), the predicted response at the measuring location occurs in about 4 milliseconds which is much faster than the recording system. However, the counting system could be easily modified to transfer the experimental data directly to a minicomputer without the need of an intermediate recording step.

Due to the limited time available for the present program, the modifications suggested above have not been tried. However, in the overall program of two-phase flow outlined in Chapter (1), it is planned to do these modifications. Hence, it will be possible to measure the void transient response in annular flow and to test the applicability of the steady-state value of C_o to transient developing-flow situations in the same apparatus.

In the rest of the present section, a comparison between the measured and predicted transient responses of the average void fraction at an axial location of z=36 in. will be presented. The range of the gas and liquid flowrates used in the experiments together with the corresponding changes in the gas inlet flowrate

are summarized in table (6.2). In all cases, the bubbly flow regime existed at the measuring location before and after the application of the gas flow perturbations; this was readily seen through the transparent lucite test section in the flow tube.

(6.5.2) Experimental Procedure

The void transient response in the bubbly flow regime was measured by means of the neutron attenuation method. As described in Chapter (4), the gating technique, with a sampling period of 10 milliseconds, was used to minimize the measurement bias of void fraction. Under a transient condition, a time-average transmittance measurement cannot be readily obtained by repeating the measurements as in the case of steady-state experiments. To overcome this problem, the entire transient experiment had to be completed and then repeated under the same initial condition for a sufficient number of times. This was found necessary to ensure that a representative average response and an estimate of the measurement variance were obtained.

In order to simplify the experimental procedure and to reduce the number of experiments required, it was decided to measure the transmittance function through the entire flow tube without scanning the transmittance radial distribution. This was thought to be reasonable since the purpose of these measurements was to determine the cross-sectional average void fraction, and not its detailed radial distribution. Hence, the

Experiment No.	G_g (gm/cm^{2}sec)	G_ℓ (gm/cm^{2}sec)	% $\Delta G_g/G_g$
1	0.033	42.53	80
2	0.033	42.53	110
3	0.033	42.53	130
4	0.023	42.53	110
5	0.023	42.53	130
6	0.023	42.53	140

Table (6.2): Summary of the gas and liquid flowrates and the percentage changes in the gas flowrate used in the transient experiments for the bubbly flow regime.

collimated neutron beam of width 3/4 in. and 1/2 in. in height was used in the measurement of the void transient response at the measuring axial location. Furthermore, by performing the transmittance measurements this way, a considerable reduction in the number of the required replicated measurements was achieved. It was found that fifty replicated transmittance measurements reduced the measurement variance to its minimum value; hence all measurements were repeated fifty times.

The time-average transmittance measurements through the tube cross section at an axial location of z = 36 in. are tabulated in Appendix (H) for the six experimental runs performed in the bubbly flow regime.

(6.5.3) Treatment of Data

The transmittance, T, of the neutrom beam of width equal to the tube inside diameter, D_i, and centered at the tube center can be written in the form

$$T = \int_{-D_{i/2}}^{D_{i/2}} K(x)\, dx \ , \qquad (6.17)$$

where the transmittance kernel, K(x), is given in Appendix (C) as

$$K(x) = B(\delta_m)\exp[-(\mu_\omega \delta_\omega + \mu_m \delta_m)] \ . \qquad (6.18)$$

All the terms appearing in equation (6.18) were defined previously and are repeated below for convenience.

$$\delta_\omega = \sqrt{D_o^2 - 4x^2} - \sqrt{D_i^2 - 4x^2} \ , \qquad (6.19\text{-a})$$

$$\delta_m = [1 - \bar{\alpha}(x)]\sqrt{D_i^2 - 4x^2} \ , \qquad (6.19\text{-b})$$

$$\bar{\alpha}(x) = \frac{1}{\delta_t} \int_{-\delta_{t/2}}^{\delta_{t/2}} \alpha(x,y)\, dy \quad , \qquad (6.19\text{-c})$$

$$\delta_t = \sqrt{D_i^2 - 4x^2} \quad , \qquad (6.19\text{-d})$$

and

$$\alpha(x,y) = \alpha_c \left[1 - \left(\frac{2\sqrt{x^2 + y^2}}{D_i}\right)^n\right] \quad . \qquad (6.19\text{-e})$$

From the definition of the cross-sectional average void fraction (equation(4.45-a)), the following relation can be readily derived:

$$\alpha_c = \left(\frac{n+2}{n}\right)\langle\alpha\rangle \quad . \qquad (6.20)$$

It is evident from equations (6.17) to (6.20) that the average void fraction can be determined from the measured transmittance function if an inference is made about the void profile index, n. Since this information cannot be obtained from the measurements of the transmittance function using the 3/4 in. wide neutron beam, an assumption must be made concerning the radial void profile. At the measuring location, it is assumed that the radial void profile, as given by equation (6-19-e), remains unchanged during the flow perturbation. This implies that the void profile index, n, is assumed to be unchanged and equal to the value corresponding to the steady-state condition at the beginning of the transient experiment. The validity of this assumption should be tested in order to ensure that it does not introduce appreciable errors in the average void frac-

tion. This test was performed by introducing fixed changes in the void profile index, n, and calculating the resulting errors in the average void fraction.

According to the analysis presented by Zuber and Findlay [17], the index, n, can vary in the range of 2 to 7 for all practical cases in bubbly flow with zero wall void fraction. Consequently, the effect of varying n, within this range, on the determined average void fraction was investigated for the experimental conditions of the six cases considered in the present study. Table (6.3) summarizes the results of this analysis; it demonstrates that the errors introduced in the average void fraction are relatively small and, as will be shown later, are within the confidence limits of the experimental measurements. It is of interest to note that the resulting error in the average void fraction becomes higher at low values of void fraction. In this region, however, the deviation of the void profile index, n, from the assumed steady-state value is not expected to be large. Furthermore, as will be shown later, the confidence limits on the average void fraction measurements in that region are relatively high. On the other hand, at high values of void fraction, where the deviation of the index, n, from the assumed value is expected to be large, the resulting errors in the average void fraction are relatively small. It can be concluded, then, that although this simplifying assumption reduced the experimental effort considerably,

Transmittance Function, T	Void Profile Index, n	Average Void Fraction, $\langle\alpha\rangle$	Percentage Deviation from $\langle\alpha\rangle_{n=2}$
0.014	2	0.281	0.0
	4	0.275	-2.1
	7	0.260	-7.5
0.020	2	0.409	0.0
	4	0.408	-0.4
	7	0.397	-2.9
0.028	2	0.484	0.0
	4	0.493	1.9
	7	0.490	1.2
0.038	2	0.534	0.0
	4	0.551	3.1
	7	0.554	3.6

Table (6.3): Effect of changing the void profile index on the determined values of the average void fraction for bubbly flow transient experiments.

it did not introduce appreciable error in the average void fraction.

Since the average void fraction measurements were averaged over the counting period t_c, that is, 10 milliseconds, and over the height of the detector collimator h, that is, 1/2 in., the predicted average void fraction should be also averaged in the same way. This is necessary in order to provide a direct comparison with the corresponding measured values. Denoting the two-phase mixture average velocity at the measuring location by $\langle j_m \rangle_{m\ell}$, the time during which the average void fraction was measured can be simply written in the form

$$t_a = t_c + h/\langle j_m \rangle_{m\ell} , \tag{6.21}$$

where $\langle j_m \rangle_{m\ell}$ is given by equation (6.7-b) as

$$\langle j_m \rangle_{m\ell} = Q_\ell' + Q_g' . \tag{6.22}$$

Note that equation (6.21) implicitly assumes that the relative velocity between the phases is negligible. In the bubbly flow regime, this assumption is acceptable since the mean drift velocity is small. Thus, the average value of void fraction which should be compared with the experimental measurements is given by

$$\langle \alpha \rangle_{model} = \frac{1}{t_a} \int_t^{t+t_a} \langle \alpha \rangle \, dt , \tag{6.23}$$

where $\langle\alpha\rangle$ is the predicted average void fraction which is obtained by solving the void propagation equation given in section (6.2).

(6.5.4) Results and Discussions

Figure (6.5) presents the results of the comparison between the measured and predicted transient responses of the average void fraction to gas flow perturbations for two typical experimental runs. These results are representative of all the experimental runs performed for the case where the final condition at the measuring location is bubbly flow with the range of experimental conditions summarized in table (6.2). In general, overall satisfactory agreement between the experiments and analysis is clearly indicated by this figure since most of the predicted values are within (or close to) the confidence limits of the experimental measurements.

It can be seen from figure (6.5-a) that in the region where the average void fraction, $\langle\alpha\rangle$, responds to the flow perturbation and changes from its starting steady-state value, the confidence limits on the measurements vary from ±8.7% to ±4.6% at $\langle\alpha\rangle$ values of .357 and .452, respectively. Similarly, from figure (6.5-b), the corresponding confidence limits vary from ±9.3% to ±3.0% for $\langle\alpha\rangle$ values of .303 and .429, respectively. Thus, it is evident from the comparison with the results summarized in table (6.3) that the errors introduced in the average void fraction due to the assumption made about the void index, n, are

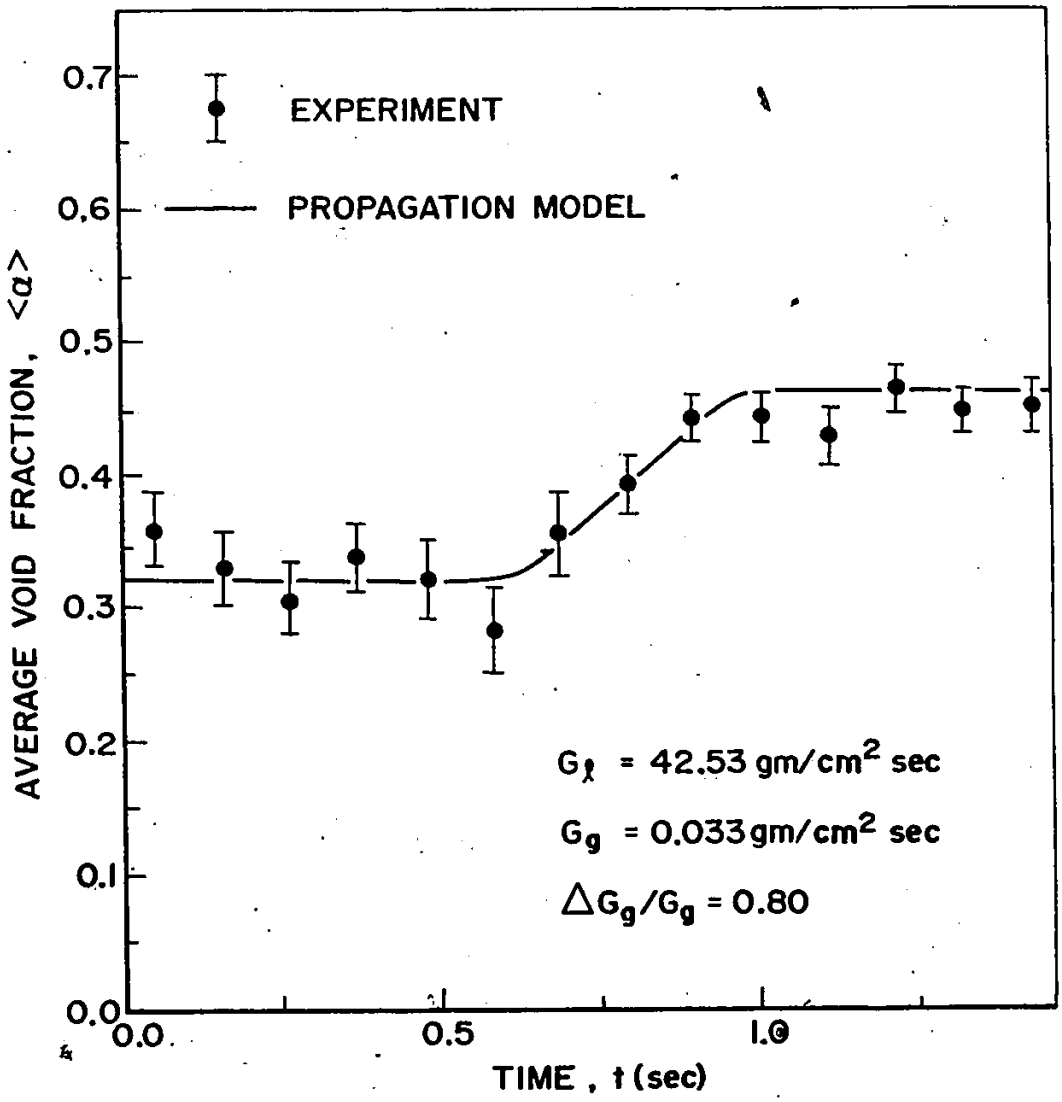

Figure (6.5-a) Comparison between measured and predicted void transient responses to a sudden change in the gas inlet flowrate for a typical experimental run of the bubbly flow regime.

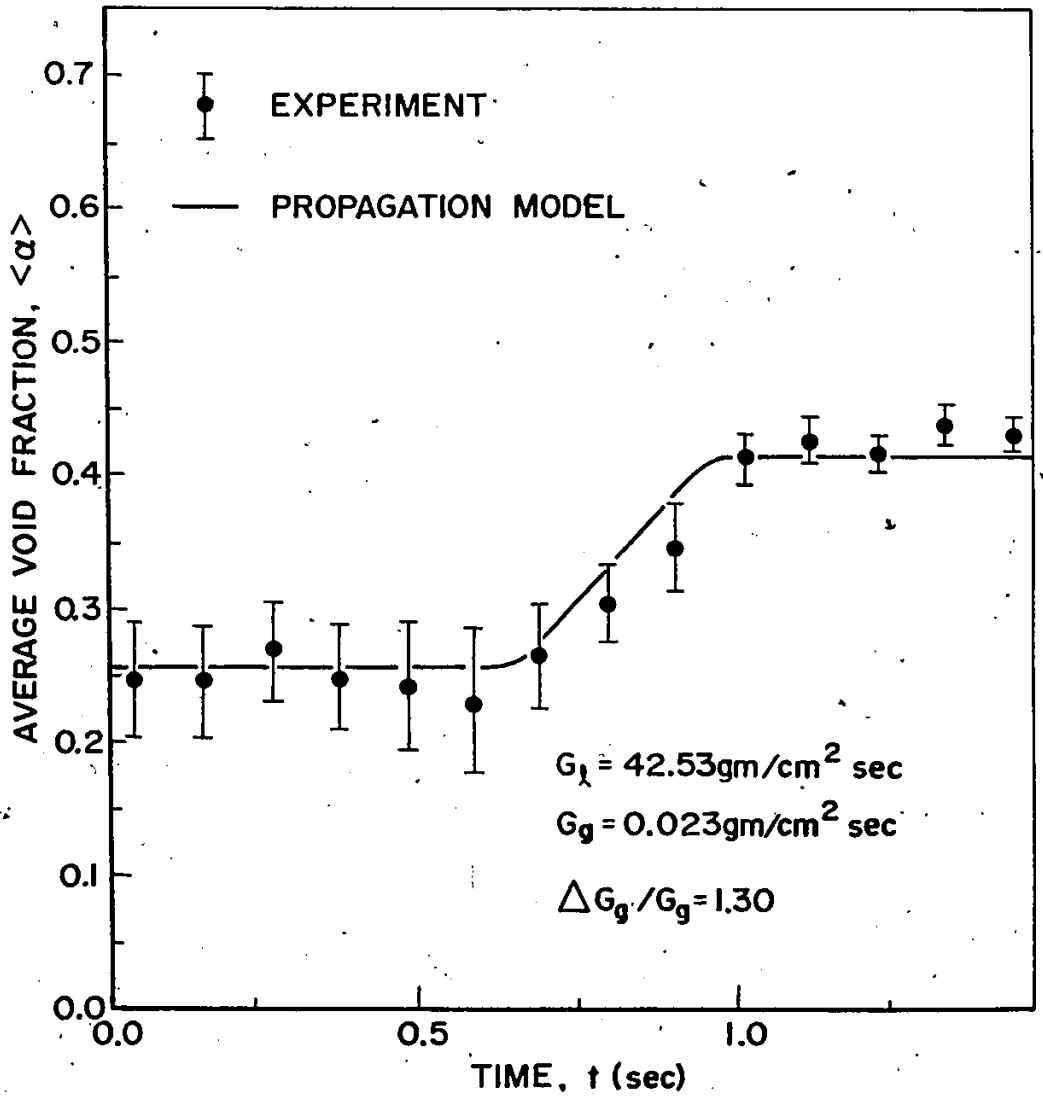

Figure (6.5-b). Comparison between measured and predicted void transient responses to a sudden change in the gas inlet flowrate for a typical experimental run of the bubbly flow regime.

tolerable and lie within these limits.

(6.6) Summary and Conclusions

(i) For annular flow, the steady-state single averaged value of the distribution parameter, C_o, which was estimated for fully-developed flow, has been used for the entire flow tube. On the other hand, for the case where the final condition at the measuring location is bubbly flow, a continuous functional relationship has been assumed to describe the variation of C_o with the average void fraction. This relationship is needed to interpolate between the values of C_o which were estimated for the bubbly and annular flow regimes under steady-state, fully-developed flow conditions in the same apparatus.

(ii) In both cases where the final condition at the measuring location is bubbly or annular flow, the predicted values of the delay time, t_1, and rise time, Δt, are sensitive to C_o. Thus, a comparison between predicted and measured void transient responses can be used to test the applicability of the steady-state values of C_o, as estimated for fully-developed flow, to transient developing-flow situations in the same apparatus.

(iii) The reasonably good agreement between the measured and predicted void transient responses indicates that the assumed functional relationship for C_o can be used to predict these responses at a particular axial location in bubbly flow.

Moreover, it supports the simplifying assumption made in this case; namely, the mean drift velocity is relatively small and, hence, has a negligible effect on the predicted void transient response for the flow system considered.

(iv) The above conclusions are limited to one type of perturbation where the compressibility effects can be ignored, in a specific apparatus, with air and water (with limited physical properties) and under specific adiabatic flow conditions. However, in the overall program of two-phase flow, this study will be extended to investigate more general situations where the effects of fluid properties and apparatus dimensions under different flow conditions and for different types of perturbations are considered.

CHAPTER (7)

SUMMARY AND CONCLUSIONS

(7.1) Introduction

It is evident that although the problem of two-phase flow has been studied for a long time, a satisfactory understanding of two-phase flow and boiling phenomena has yet not been achieved. This is mainly because of the fact that two-phase flow has a complex structure which is generally heterogeneous and usually exhibits large statistical fluctuations. In the study presented herein, an attempt has been made to emphasize the important role played by the distribution effects and the discrete nature of two-phase flow. It is hoped that this investigation will provide a clearer insight into the problem and stimulate more effort to be directed towards a better description of two-phase flow and boiling phenomena. The present chapter reviews the results obtained in the current investigation, summarizes the pertinent conclusions and contributions to knowledge in this field and recommends some areas for useful future work.

(7.2) Contributions to Knowledge

(7.2.1) General

It has been realized that there is a real need to obtain good estimates of the fundamental flow parameters which are re-

quired in the solution of the void propagation equation. Having these parameters allows one to predict quite easily the transient response of the average void fraction in two-phase flow to certain types of perturbations where the compressibility effects are small. The flow parameters are introduced to account for the non-uniformity in the two-phase mixture velocity and void concentration and for the non-equality in the local velocities of the individual phases. To estimate these parameters, two possible methods were presented and evaluated. One of these methods requires fundamental data about the radial distributions of the mixture velocity and void fraction either by experiments or through analysis. These fundamental data can also be used to evaluate existing models and/or correlations which have been developed to describe various aspects of two-phase flow.

(7.2.2) Neutron Diagnostic Technique

Among the different possible methods reviewed, the neutron attenuation method was selected to measure the radial void profiles in two-phase flow since it was found capable of yielding accurate measurements without disturbing the flow.

The neutron beam extracted from McMaster's 2 MW Swimming Pool Nuclear Reactor was conditioned to provide a collimated beam of thermal neutrons which, in turn, provided a successful tool for void fraction measurements. The adequacy of this method was tested by integrating the measured radial void profile and comparing the resulting cross-sectional average void fraction with that obtained directly by a trapping method. This test has indicated that the neutron attenuation method and procedure provide an accurate method to obtain radial void profiles for the bubbly and annular flow regimes in the air-water system which has been employed. The use of this technique required the formulation of a mathematical model for the radial void profile and a simple two-parameter model proved to be adequate.

The time-fluctuations of the transmitted neutron beam through the central part of the flow tube were shown to provide a convenient characteristic "finger print" for each flow regime. Hence, the measurements of these fluctuations were used effectively to recognize the three major flow regimes in the vertical upward adiabatic two-phase flow system, that is, the bubbly, slug and annular flow regimes. This is especially important for non-transparent test sections where direct flow observation is not possible.

Furthermore, the measurements of these fluctuations at two axial locations along the flow tube were also shown to provide a successful way to check the development of the two-phase flow mixture. This information is particularly important for the experimental facility which has been used in the present study since the highest level at which transmittance measurements could be made was limited by the location of the neutron beam, that is, about 40 in. above floor level. These measurements demonstrated that while the bubbly and annular flow regimes became fully developed by the point at which the bulk of the measurements were made, the slug flow regime needed a much longer tube to develop to an invariant condition.

The error introduced in the measurements of void fraction due to the statistical fluctuations of the neutron beam was investigated. For the radiation source employed, it was found that this error became significant only at low values of void fraction, for small counting periods and for low medium thicknesses. This explains the reason why the intensity of radiation sources has usually been measured over considerable counting periods. On the other hand, to reduce the measurement bias due to the inherent fluctuations of two-phase flow, a gating technique has been recommended in which the continuous detector signal is sampled over very short discrete time intervals. However, a compromise was required since very small counting periods

could lead to a high measurement bias due to source fluctuations; consequently, it was suggested to use the gating technique with a counting period of 10 milliseconds. While this counting period provided sufficient counts to yield reasonable counting statistics under all void fraction conditions investigated, it was found that the medium fluctuation error was small and the source fluctuation error was acceptable.

(7.2.3) Steady-State Flow Parameters

Two methods were presented to estimate the flow parameters for both the bubbly and annular flow regimes under steady-state, fully-developed flow conditions. The first method, which was based on the measurements of the radial void profiles and the gas and liquid flowrates, has demonstrated that the flow parameters remain essentially constant for a specific flow regime.

To reduce the experimental effort considerably, an alternative method was suggested which enables the designer to evaluate these parameters by performing a single experiment where the radial void profile is measured. Based on the momentum equation and Prandtl's turbulent mixing length hypothesis, a general form of the shear stress radial distribution was derived and integrated to yield the two-phase mixture radial velocity profile. By combining the predicted mixture radial velocity profile with the measured radial void profile, estimates of the flow parameters were obtained. These results showed systematic variations of the flow parameters with the gas and liquid flowrates which were not consistent with the experimental observations.

In spite of these variations, the suggested method indicated values of the distribution parameter which were close to those obtained using the direct method especially for annular flow. On the other hand, larger deviations were observed between the values of the mean drift velocity, as estimated by the two methods. One may attribute these large deviations to the constitutive relationship for the local drift velocity which was used in bubbly flow. Generally, any small error in the predicted distribution parameter is magnified by a large factor with the result that large uncertainties arise in the predicted mean drift velocity. However, the cross-sectional average void fraction was found relatively less sensitive to the mean drift velocity than to the distribution parameter for both flow regimes. Thus, one can use these estimates of the flow parameters to predict the steady-state average void fraction without appreciable errors in spite of the uncertainties which may arise in the mean drift velocity.

In summary, the mixing length model has been shown adequate to predict the mixture radial velocity profiles in two-phase flow for the purpose of estimating the distribution parameter. Moreover, by performing a sensitivity analysis, it has been shown that the flow parameters are not sensitive to the values of the mixing length. This means that as far as the flow parameters are concerned, it is not necessary to determine the actual values of the mixing length in the two-phase flow system. In other words, this analysis has demonstrated that the values of the mixing length which have been used in single-phase flow can be

applied without appreciable error to determine these parameters in two-phase flow.

It should be mentioned here that the above conclusions are limited to the adiabatic air-water flow system employed and to the range of gas and liquid flowrates considered in the present study.

(7.2.4) Comparison with Existing Models

The results of the present experimental observations and analysis have been used to determine other parameters which have been used to characterize two-phase flow. These parameters have then been compared with selected models and correlations which have been used by many designers to describe two-phase flow behaviour. This has been done to evaluate the validity of the assumptions made in deriving these models and correlations. In general, this comparison has indicated that the present experimental technique and model predictions are consistent with expectations and previous observations and predictions.

However, many of the models and correlations presented in the literature were shown to yield misleading results and conclusions which were attributed to the simplifying assumptions included in their derivation. For example, the deviations between the present results of the mean film thickness and the predictions from the existing correlations can be explained in terms of the wavy nature of the core-film interface which has been neglected in deriving these correlations.

(7.2.5) Void Transient Response

The average void fraction in a two-phase flow has been recognized to be very important since it is required in calculating the pressure drop components as well as the reactivity in nuclear boiling reactors. Hence, an adequate model is needed to predict the transient response of the average void fraction to any perturbation which may occur in the flow system under accident conditions or in normal operation. The void propagation equation suggested by Zuber and Staub [15] was used to study and predict the transient behaviour of the adiabatic gas-liquid flow system under consideration in situations where compressibility effects were small. The solution of this equation has been shown to depend on the flow parameters which emphasizes the need of estimating their values a priori.

In the present investigation, the void propagation equation was solved by means of the method of characteristics to predict the transient response of the average void fraction to perturbations in the gas inlet flowrate. This type of perturbation has been recognized to be of considerable interest in nuclear boiling reactors when one of the circulating pumps and/or connecting pipes fail to provide the reactor with sufficient coolant.

An analysis was performed to assess the sensitivity of the predicted transient response of the average void fraction to errors in the distribution parameter. This analysis has revealed that while the steady-state initial and final values of the average void fraction are not sensitive to these errors, the

delay and rise times of the response are sensitive to them. Consequently, performing a comparison between predicted and measured void transient responses should permit the evaluation of the assumption usually made concerning the distribution parameter. In summary, this assumption states that the parameter values obtained for steady-state, fully-developed flow are valid under transient developing-flow situations. That is to say that the steady-state distribution parameter pertaining to the flow regime and the local average voidage condition applies in the transient system. Since this parameter cannot be obtained from steady-state experiments under all voidage conditions experienced during the transient, a continuous functional relationship was assumed in order to interpolate over those regions where the parameter cannot be obtained.

It was found, however, that the present experimental apparatus was not suitable to study the void transient response in annular flow because serious liquid flow oscillations occurred during the application of the flow perturbations. For the bubbly flow regime, a reasonable agreement between the predicted and measured void transient responses was obtained. This agreement showed that the continuous functional relationship assumed to interpolate between steady-state estimates of the distribution parameter for fully-developed flow can be used under dynamic developing-flow situations in the same apparatus.

It is important to indicate that the above conclusions are limited to one type of perturbation where compressibility effects are small, in a specific apparatus, with air and water (with limited physical properties) and under specific adiabatic flow conditions.

(7.3) Recommendations for Future Work

Although the study presented here has dealt with an adiabatic air-water flow system, it only represents the first part of an overall program to study two-phase flow and boiling phenomena. The flow system was designed with a minimum of complexity in order to test the neutron attenuation technique as a means of obtaining information on radial void distribution and void transient response to perturbations in the system. The main object of this work was to achieve confidence in the experimental technique for void fraction measurement. In future work, then, the complexity of the two-phase flow system under study can be increased in order to investigate the dynamic behaviour of a flow system simulating a boiling channel in a nuclear reactor.

The present study is limited to a particular flow system with certain working fluids in a specific apparatus and for a limited range of experimental conditions. It represents, however, a basis for any future study and can be extended to investigate more general situations where the effects of tube diameter and physical properties of the working fluids are considered over a wider range of flow conditions.

Moreover, the following two shortcomings were recognized in the study presented here:

(i) the study of the fully-developed slug flow regime, and

(ii) the comparison between the measured and predicted transient responses of the average void fraction in the annular flow regime.

To eliminate the first shortcoming, the adiabatic experimental facility should be modified by constructing a much longer horizontal flow tube which would enable slug flow to develop to an invariant condition. On the other hand, the second one can be eliminated by modifying this facility, as recommended in Chapter (6), to reduce the effect of the liquid flow oscillations which occurred in annular flow.

Upon the successful completion of the study of the adiabatic air-water flow system by eliminating the shortcomings mentioned above, it will be possible to proceed with the rest of the overall program. It is recommended to modify the adiabatic experimental facility to simulate a boiling two-phase flow system where the gas phase is added through the channel wall to an air-water flow mixture. The experimental technique and mathematical model developed in the present study should then be applied to estimate the steady-state values of the flow parameters under conditions where the flow is developing. This would require developing a model for each flow parameter as a function of the system operating conditions. It is then recommended to test the applicability of the steady-state values of these

parameters, as determined for a flow developing situation, under dynamic conditions where a perturbation occurs to the injected gas flow. This test requires the solution of the void propagation equation using the models developed for the flow parameters.

Finally, the construction of a boiling two-phase flow system, which accommodates different working fluids, is recommended where the void transient response to perturbations in the inlet flow and/or input power is measured. The previously developed models for the flow parameters should then be tested along with the assumptions concerning thermodynamic equilibrium, the thermal capacity of the heating system, etc.

In summary, it is felt that the consideration of these recommendations will advance the knowledge of two-phase flow and boiling phenomena and help to fill the gaps which exist in the description of the performance of two-phase flow.

APPENDIX (A)

DETAILS OF THE EQUIPMENT

(A.1) Air Filter

5 micron pore size, Model MCC1002-FD10-16, Replacement Cartridge Filtrite, Cat. No. DF10-10N, Scarborough-Grant Co., Downsview, Ontario.

(A.2) Water Filter

5 micron Micro-Klean Cartridge, Model 1B1, Fiber Filtrite, Cat. No. 1B1-G78B3, Peacock Brothers Ltd., Mississauga, Ontario.

(A.3) Control Valves

1/4 in. Trim G and 1/2 in. Trim C, stainless steel Research Control valves, Cat. No. 2315, Stebbins Co., London, Ontario.

(A.4) Pressure Regulator

0-100 p.s.i.g. range, Model PP97A, Honeywell Controls, Minneapolis, Minnesota.

(A.5) Differential Controller

0-100 in. water differential pressure range, Model 292N7, Honeywell Controls, Minneapolis, Minnesota.

(A.6) Water Rotameters

1/2 in. diameter tube, Serial No. 57-05-B-1350/6, Tube No. B4-17-10/77 and 1 1/2 in. diameter tube, Serial No. X25-4045/1,

Tube No. B8-27-10/70-G, Fischer-Porter Co., Downsview, Ontario. The floats were fabricated from aluminum in the department's machine shop.

(A.7) Pressure Gauge

0-500 p.s.i. range, 0.5 p.s.i. graduations and 10 in. diameter, Gauge No. 60363, Heise Bourdon Tube Co., Newtown, Connecticut.

(A.8) Wet Test Meter

0.03-0.40 CFM air flowrate range, 0.1 ft^3 per revolution, 0.001 dial subdivisions and ± 1/2% accuracy of the total volume, Model 63111, Precision Scientific Co., Chicago, Illinois.

(A.9) Calibrated Flow Nozzles

0.516 in. and 1.250 in. diameters, Type Cox-210, Cox Instruments Division, George L. Nankervis Co., Detroit, Michigan.

(A.10) Sintered Tube

3/4 in. I. D. by 1 in O.D. and 40 micron pore size, stainless steel tube, Scarborough-Grant Co., Downsview, Ontario.

(A.11) Vertical Cathetometer

Standard cathetometer telescope No. 236, Griffin-George Ltd., London, England.

(A.12) Dial Gauge

3 in. diameter, 0.001 in. graduations, 0.1 in. per revolution and 2 in. total range, Cat. No. AL13, Ammco Industrial Equipment Ltd., Rexdale, Ontario.

(A.13) Sump Pump

2500 gphr capacity at 10 ft head, Cat. No. 02, Serial No. 73GO25972, Aqua Pump and Equipment Co., Hannon, Ontario.

(A.14) Neutron Detector

1 in. diameter stainless steel cylinder, filled with 96% B^{10}-enriched dry BF_3 gas at a pressure of 40 cm Hg., Model RSN-7S, Reuter-Stokes, Cleveland, Ohio.

(A.15) Pre-Amplifier

0.16 microvolt per ion pair sensitivity, Tennelec Model TC133, Datamex Ltd., Toronto, Ontario.

(A.16) Linear Amplifier

2-640 gain range, Tennelec Model TC211, Datamex Ltd., Toronto, Ontario.

(A.17) Dual Counter/Timer

10^7 count capacity, Tennelec Model TC555P, Datamex Ltd., Toronto, Ontario.

(A.18) Digital Printer

Ten-digit printer, Model 5103, Systron-Donner Co., Concord, California.

(A.19) Digital Ratemeter

10^6 count capacity, Tennelec Model TC592P, Datamex Ltd., Toronto, Ontario.

(A.20) Magnetic Tape Unit

Seven-track digital recorder, 200 bpi packing density, power is supplied from a 12-volt DC power supply, Model PI-1387, Precision Instrument Co., Palo Alto, California.

(A.21) Auto-Recycle Control and Magnetic Tape Interface

Three-digit data field preset, Tennelec Model TC572, Datamex Ltd., Toronto, Ontario.

(A.22) High Voltage Power Supply

0-3000 volt DC range, 15-turn potentiometer and 2 volt graduations, Tennelec Model TC941, Datamex Ltd., Toronto, Ontario.

(A.23) Quick-Closing Valves

0.618 in. I.D., air-activated ball valves, Type AB6, Kamyr of Canada Ltd., Montreal, Quebec.

(A.24) Solenoid Valve

Two-way Asco solenoid valve, 1/2 in. orifice size and 3/4 in. pipe size, 110 volt, Cat. No. 8267A19, Vallance Brown Co., Hamilton, Ontario.

(A.25) Differential Pressure Transducer

0.1-500 p.s.i. differential pressure ranges (depending upon the diaphragm used), Model P7D, operating with Carrier-Demodulator, Model CD10, Dynasciences Corporation, Chatsworth, California.

(A.26) Visicorder Oscillograph

0.4-50 in. per sec paper speed range, Model 906C-169XFOJ, Honeywell, Denver, Colorado.

APPENDIX (B)

BARTLETT'S TEST FOR EQUALITY OF VARIANCE

Bartlett's test [142,143] is commonly used to examine the differences among two or more variances. The homogeneity of the variances is determined by comparing the logarithm of the average variance with the sum of the logarithms of the separate variances. In the test, the following hypothesis is made:

$$H_o : \sigma_1^2 = \sigma_2^2 = \ldots\ldots = \sigma_n^2 = \sigma^2 , \qquad (B.1)$$

where n is the number of independent estimates of variance.

Bartlett showed that

$$\Lambda = \frac{1}{c} np(\ell n\ s^2 - \frac{1}{n} \sum_{i=1}^{n} \ell n\ s_i^2) , \qquad (B.2)$$

has an approximate χ^2 distribution with (n-1) degrees of freedom. In equation (B.2), p is the number of replicates in each sample, s^2 is the pooled sample variance defined as

$$s^2 = \frac{1}{n} \sum_{i=1}^{n} s_i^2 , \qquad (B.3)$$

where s_i^2 is the estimated variance of the ith sample and c is given by

$$c = 1 + \frac{n+1}{3np} \quad . \qquad (B.4)$$

If the value of Λ, as calculated from equation (B.2), exceeds the value of $\chi^2_{0.95}$ for (n-1) degrees of freedom, the test hypothesis, H_o, is rejected. Otherwise, the test hypothesis is accepted and the average variance can be considered as the estimated variance of all samples. It should be also mentioned that, as stated by Hald [143], Bartlett's test is only valid when the observations are normally distributed.

APPENDIX (C)

NEUTRON TRANSMISSION THROUGH A TWO-PHASE MIXTURE FLOWING IN A VERTICAL CIRCULAR CONDUIT

Consider the transmission of a well-collimated neutron beam of thickness δ_b through a vertical tube containing a gas-liquid flow. At steady-state, the neutron transmittance function, T, of the beam centered at a distance L from the tube center is given by

$$T = \int_{L-\delta_b/2}^{L+\delta_b/2} K(x)\, dx \,, \qquad (C.1)$$

where K(x) is the neutron transmittance kernel at the chordal position x. If the neutron attenuation in the gas phase is neglected in comparison with that in the liquid phase, the transmittance kernel can be written as

$$K(x) = B(\delta_m)\exp[-(\mu_w\delta_w + \mu_m\delta_m)] \,. \qquad (C.2)$$

Here μ_w and μ_m are the neutron attenuation parameters for the wall and liquid materials, B is the buildup factor for the liquid and δ_w and δ_m are the wall thickness and the equivalent thickness of liquid intercepting the beam path at the chordal position x, respectively. The attenuation parameters and the buildup factor must be predetermined in

an independent set of experiments.

Let D_i and D_o be the inside and outside diameters of the tube. The wall chordal thickness is, then, given as

$$\delta_w = \sqrt{D_o^2-4x^2} - \sqrt{D_i^2-4x^2} \quad . \tag{C.3}$$

Similarly, the equivalent thickness of the water medium can be written in the form

$$\delta_m = [1-\bar{\alpha}(x)] \sqrt{D_i^2-4x^2} \quad , \tag{C.4}$$

where $\bar{\alpha}(x)$ is the average value of void fraction along the chordal position under consideration and is given by

$$\bar{\alpha}(x) = \frac{1}{\delta_t} \int_{-\delta_t/2}^{\delta_t/2} \alpha(x,y)\, dy \quad , \tag{C.5}$$

where

$$\delta_t = \sqrt{D_i^2-4x^2} \quad . \tag{C.6}$$

In equation (C.5), $\alpha(x,y)$ is the time-averaged local void fraction at the point (x,y). The following mathematical models may be assumed for $\alpha(x,y)$ in the bubbly and annular flow regimes:

(i) Bubbly Flow

$$\alpha(x,y) = \alpha_c \left[1 - \left(\frac{2\sqrt{x^2+y^2}}{D_i}\right)^n\right] \quad . \tag{C.7}$$

(ii) Annular Flow

$$\alpha(x,y) = \alpha_c[1 - (\frac{\sqrt{x^2+y^2}}{a})^n], \quad \text{for } \sqrt{x^2+y^2} \leq a , \qquad (C.8\text{-a})$$

and

$$\alpha(x,y) = 0 \quad , \quad \text{otherwise,} \qquad (C.8\text{-b})$$

where a is the radius of the core region which can be related to the mean film thickness, F, by

$$a = \frac{D_i}{2} - F . \qquad (C.9)$$

From the above, it can be seen that the neutron transmittance for either bubbly or annular flow can be calculated at different strips of the test tube if the void parameters, n and α_c, and the mean film thickness, in case of annular flow, are known. It should be mentioned here that extra caution should be taken in applying equations (C.3) to (C.8). For example, if $x \geq D_i/2$, the second term in equation (C.3) should be cancelled and δ_m should be put equal to zero. Similarly, if $x \geq D_o/2$, both δ_w and δ_m should be set equal to zero. In the annular flow regime, if $x \geq a$, i.e., no part of the core region is lying within the chord x, $\alpha(x,y)$ should be put equal to zero and, hence, δ_m should be set equal to δ_t.

The void fraction models given by equations (C.7) and (C.8) are physically reasonable and both qualitatively and quantitatively in good agreement with the important features of the flow behaviour. For vertical counter-gravity adiabatic systems, it was shown [72], by visual observation

and by high-speed and x-ray photography, that the light phase tends to concentrate in the center of the flow tube whereas the heavy phase concentrates in the region near the wall. Accordingly, in the above models, the wall has been assumed to be wetted by liquid so that the void fraction is considered to be zero at the wall and monotonically increase to the maximum value, α_c, at the tube center. Furthermore, for annular flow, a thin layer comprised entirely of liquid is assumed to flow parallel to the wall.

The symmetry assumed in these models is in agreement with the observations made by Staub and Zuber [145] for bubbly flow and by Gill et al. [162] and Isbin et al. [163] for annular flow. For annular flow, the liquid volume fraction measured by Cravarolo and Hassid [164] showed the general trend given by equation (C.8), except that some gas bubbles were observed in the film region. For bubbly flow, a void fraction model similar to that given by equation (C.7) was assumed by Bankoff [71]. The radial void profiles measured by Neal and Bankoff [79] for bubbly flow can be represented by the assumed model. The parabolic radial void profiles proposed by Brown et al. [111] for bubbly flow had the same features given by equation (C.7). Zuber and Findlay [17] demonstrated that equation (C.7) was in good agreement with Petrick's radial void profile measurements [81]. Finally, Staub and Zuber [145] ascertained the adequacy of equation (C.7) by comparing the chordal average void fraction, as calculated by integrating the proposed radial void profile, with that measured using an x-ray method.

APPENDIX (D)

CONTINUITY AND MOMENTUM EQUATIONS IN TWO-PHASE FLOW

Considering the two-phase flow mixture as a pseudo-continuous medium, the steady-state continuity equation in cylindrical coordinates can be written as [89]

$$\frac{1}{r}\frac{\partial}{\partial r}(r\rho u) + \frac{\partial}{\partial z}(\rho v) = 0 \quad . \tag{D.1}$$

Similarly, the z-component of the momentum equation can be written in the form

$$\frac{1}{r}\frac{\partial}{\partial r}(r\rho uv) + \frac{\partial}{\partial z}(\rho v^2) = -\frac{\partial P}{\partial z} - \rho g + \frac{\mu}{r}\frac{\partial}{\partial r}\left(r\frac{\partial v}{\partial r} + \frac{\partial u}{\partial z}\right)$$

$$+ \frac{2}{3}\mu\frac{\partial}{\partial z}\left[2\frac{\partial v}{\partial z} - \frac{1}{r}\frac{\partial}{\partial r}(ru)\right] . \tag{D.2}$$

In equations (D.1) and (D.2), use has been made of non-swirling and symmetry conditions.

Substituting equations (5.16), (5.20) and (5.21), taking the time-average defined by equations (5.17) and (5.18) and recognizing that such terms as $\overline{\alpha' u' v'}$ are relatively small, the continuity and momentum equations can be put in the form

$$\frac{1}{r}\frac{\partial}{\partial r}(r\bar{\rho}\bar{u} - \Delta\rho r\overline{\alpha' u'}) + \frac{\partial}{\partial z}(\bar{\rho}\bar{v} - \Delta\rho\overline{\alpha' v'}) = 0 \ , \tag{D.3}$$

and

$$\frac{1}{r}\frac{\partial}{\partial r}\left[r\{\bar{\rho}\bar{u}\bar{v} + \overline{\rho u'v'} - \Delta\rho(\overline{v\alpha'u'} + \overline{u\alpha'v'})\}\right] + \frac{\partial}{\partial z}\left(\bar{\rho}\bar{v}^2 + \right.$$

$$\left.\bar{\rho}\overline{v'^2} - 2\Delta\rho\bar{v}\overline{\alpha'v'}\right) = -\frac{\partial\bar{P}}{\partial z} - \bar{\rho}g + \frac{\mu}{r}\frac{\partial}{\partial r}\left(r\frac{\partial\bar{v}}{\partial r} + \frac{\partial\bar{u}}{\partial z}\right) +$$

$$\frac{2}{3}\mu\frac{\partial}{\partial z}\left[2\frac{\partial\bar{v}}{\partial z} - \frac{1}{r}\frac{\partial}{\partial r}(r\bar{v})\right] . \qquad \text{(D.4)}$$

Now consider the following approximations:

(i) $\overline{v'^2} << \bar{v}^2$, which means that the term $\frac{\partial}{\partial z}(\bar{\rho}\overline{v'^2})$ can be neglected; and

(ii) $\overline{\alpha'v'} << \frac{\bar{\rho}\bar{v}}{\Delta\rho}$, which results in the approximations

$$\frac{1}{r}\frac{\partial}{\partial r}(-\bar{v}\Delta\rho\overline{\alpha'v'}) \sim 0 \quad ,$$

and

$$\frac{\partial}{\partial z}(-2\bar{v}\Delta\rho\overline{\alpha'v'}) \sim 0 \quad .$$

Using the above approximations, the momentum equation (D.4) can be reduced to

$$\frac{1}{r}\frac{\partial}{\partial r}\left[r(\bar{\rho}\bar{u}\bar{v} + \overline{\rho u'v'} - \Delta\rho\bar{v}\overline{\alpha'v'})\right] + \frac{\partial}{\partial z}(\bar{\rho}\bar{v}^2) = -\frac{\partial\bar{P}}{\partial z} - \bar{\rho}g$$

$$+ \frac{\mu}{r}\frac{\partial}{\partial r}\left(r\frac{\partial\bar{v}}{\partial r} + \frac{\partial\bar{u}}{\partial z}\right) + \frac{2}{3}\mu\frac{\partial}{\partial z}\left[2\frac{\partial\bar{v}}{\partial z} - \frac{1}{r}\frac{\partial}{\partial r}(r\bar{u})\right]. \qquad \text{(D.5)}$$

For fully-developed flow, one can write

$$\bar{u} = 0 \quad , \qquad \text{(D.6-a)}$$

and

$$\frac{\partial\bar{\rho}}{\partial z} = \frac{\partial\bar{v}}{\partial z} = 0 \quad , \qquad \text{(D.6-b)}$$

which upon substituting into the continuity equation (D.3) yields

$$\frac{1}{r}\frac{\partial}{\partial r}(r\bar{\rho}\bar{u}) + \frac{\partial}{\partial z}(\bar{\rho}\bar{v}) = 0 \quad , \qquad \text{(D.7-a)}$$

and

$$\frac{1}{r}\frac{\partial}{\partial r}(r\overline{\alpha' u'}) + \frac{\partial}{\partial z}(\overline{\alpha' v'}) = 0 \quad . \qquad \text{(D.7-b)}$$

Similarly, the momentum equation (D.5) can be simplified to

$$\frac{1}{r}\frac{\partial}{\partial r}\left[r(\bar{\rho}\overline{u'v'} - \Delta\rho\bar{v}\overline{\alpha' u'})\right] = -\frac{\partial \bar{P}}{\partial z} - \bar{\rho}g + \frac{\mu}{r}\frac{\partial}{\partial r}\left(r\frac{\partial \bar{v}}{\partial r}\right) \quad . \qquad \text{(D.8)}$$

Rearranging equation (D.8), the momentum equation can be finally put in the form

$$\frac{1}{r}\frac{\partial}{\partial r}\left[r(\bar{\rho}\overline{u'v'} - \Delta\rho\bar{v}\overline{\alpha' u'} - \mu\frac{\partial \bar{v}}{\partial r})\right] = -\frac{\partial \bar{P}}{\partial z} - \bar{\rho}g \quad . \qquad \text{(D.9)}$$

APPENDIX (E)

RADIAL SHEAR STRESS DISTRIBUTION IN THE ANNULAR FLOW REGIME

Consider the following two regions:

(a) Film Region ($a < r \leq R$)

Equation (5.36) can be put in the form

$$r\tau = \int r\left[\left(-\frac{\partial \bar{P}}{\partial z}\right) - \rho_\ell g\right]dr + c \quad , \qquad (E.1)$$

which upon integrating from r to R gives

$$R\tau_w - r\tau = \left[\left(-\frac{\partial \bar{P}}{\partial z}\right) - \rho_\ell g\right]\left(\frac{R^2-r^2}{2}\right) \quad , \qquad (E.2)$$

where τ_w is the value of shear stress at the tube wall. Rearrange equation (E.2) to get the radial shear stress distribution in the film region as

$$\tau = \frac{R}{r}\tau_w + \left[\rho_\ell g - \left(-\frac{\partial \bar{P}}{\partial z}\right)\right]\left(\frac{R^2-r^2}{2r}\right) \quad . \qquad (E.3)$$

(b) Core Region ($0 \leq r \leq a$)

Similarly, equation (5.32) can be put in the form

$$r\tau = \int r\left[\left(-\frac{\partial \bar{P}}{\partial z}\right) - \bar{\rho} g\right]dr + c \quad , \qquad (E.4)$$

which upon substituting for $\bar{\rho}$ from equation (5.44) and integrating from r to a yields

$$a\tau_i - r\tau = \left[\left(-\frac{\partial \bar{P}}{\partial z}\right) - \rho_\ell g\right]\left(\frac{a^2-r^2}{2}\right) + \Delta\rho g \alpha_c\left[\left(\frac{a^2-r^2}{2}\right) - \frac{a^{n+2}-r^{n+2}}{a^n(n+2)}\right] \quad . \qquad (E.5)$$

where τ_i is the shear stress value at the core-film interface.

Rearranging equation (E.5) yields the radial shear stress distribution in the core region as

$$\tau = \frac{a}{r}\tau_i - [(-\frac{\partial \bar{P}}{\partial z}) - \rho_c g](\frac{a^2}{r^2} - 1)\frac{r}{2} - \Delta\rho g\alpha_c(\frac{r^n}{a^n} - 1)(\frac{r}{n+2}) \quad , \qquad (E.6)$$

where ρ_c is the density averaged over the core cross-sectional area defined by

$$\rho_c = \frac{1}{\pi a^2}\int_0^a \bar{\rho}\, 2\pi r\, dr \quad . \qquad (E.7)$$

Substituting for $\bar{\rho}$ from equation (5.44) to obtain

$$\rho_c = \rho_\ell - \Delta\rho\alpha_c(\frac{n}{n+2}) \quad . \qquad (E.8)$$

Due to symmetry, set $\tau = 0$ at $r = 0$ in equation (E.6) to get the following expression for the interfacial shear stress:

$$\tau_i = \frac{a}{2}[(-\frac{\partial \bar{P}}{\partial z}) - \rho_c g] \quad . \qquad (E.9)$$

To satisfy the continuity condition of shear stress through the core-film interface, substitute τ_i from equation (E.9) into equation (E.3) at $r = a$ to express the wall shear stress as

$$\tau_w = \frac{R}{2}[(-\frac{\partial \bar{P}}{\partial z}) - \rho_c g\frac{a^2}{R^2} - \rho_\ell g(1 - \frac{a^2}{R^2})] \quad . \qquad (E.10)$$

Now differentiate equation (E.1) to get

$$\frac{d\tau}{dr} = \left[\left(-\frac{\partial \bar{P}}{\partial z}\right) - \rho_\ell g\right] - \frac{\tau}{r} , \qquad (E.11)$$

which upon substituting for τ from equation (E.3) gives the change of shear stress in the film with the radial distance from the tube center as

$$\frac{d\tau}{dr} = \frac{1}{r}\left[\left(-\frac{\partial \bar{P}}{\partial z}\right) - \rho_\ell g\right] - \frac{R}{r^2}\left[\tau_w - \frac{R}{2}\left\{\left(-\frac{\partial \bar{P}}{\partial z}\right) - \rho_\ell g\right\}\right] . \qquad (E.12)$$

Similarly, for the core region, differentiate equation (E.4) and substitute for τ from equation (E.6) to get

$$\frac{d\tau}{dr} = \left[\left(-\frac{\partial \bar{P}}{\partial z}\right) - \bar{\rho} g\right] - \tau_i \frac{a}{r^2} + \frac{1}{2}\left[\left(-\frac{\partial \bar{P}}{\partial z}\right) - \rho_c g\right]\left(\frac{a^2}{r^2} - 1\right)$$

$$+ \frac{\Delta\rho g \alpha_c}{(n+2)}\left(\frac{r^n}{a^n} - 1\right) . \qquad (E.13)$$

Note that according to equations (E.12) and (E.13), possible minimum or maximum values may occur in either the film or the core region.

APPENDIX (F)

AVERAGE VOID FRACTION-QUALITY MODELS AND CORRELATIONS

(F.1) Homogeneous Model

The homogeneous model [180,181] is the simplest model which relates the average void fraction, $\langle\alpha\rangle$, to the quality, x, in a two-phase flow mixture. It assumes uniform mixture velocity and void fraction radial profiles and neglects the relative velocity between the phases. These assumptions yield

$$\langle\alpha\rangle = \frac{1}{1 + \frac{1}{\gamma}\left(\frac{1-x}{x}\right)} \quad , \tag{F.1}$$

where γ is the liquid-to-gas density ratio, i.e., $\gamma = \rho_\ell/\rho_g$. Equation (F.1) is, in fact, equivalent to equation (2.1) if one recognizes that the apparent volumetric concentration, β, is related to the quality by

$$\frac{x}{1-x} = \frac{1}{\gamma}\left(\frac{\beta}{1-\beta}\right) \quad . \tag{F.2}$$

(F.2) Armand's Correlation

As reported by Armand [73], the relation between $\langle\alpha\rangle$ and β for average void fraction values of up to 0.75 can be put in the form

$$\frac{\langle\alpha\rangle}{\beta} = K \quad , \tag{F.3}$$

where K is Bankoff's flow parameter. It is noteworthy that equation (F.3) does not satisfy the condition that $\langle\alpha\rangle$ should tend to unity as x approaches unity; therefore, its application is limited in range. For both air-water and steam-water systems of average void fraction values greater than 0.75, the following correlation was suggested by Armand and reported by Jones [22]:

$$\langle\alpha\rangle = 1 - \frac{4 + \frac{8}{7}\, m}{5 + m\left(\frac{\beta}{1-\beta} + \frac{8}{7}\right)} \quad , \tag{F.4}$$

where

$$\left.\begin{aligned} m &= \frac{4a}{\sqrt{\gamma}} \left(\frac{G_\ell D}{\mu_\ell}\right)^{1/8} \quad , \\ a &= 0.69 + (1-\beta)(4 + \dot{m}_\ell/\dot{m}_{\ell r}) \quad , \\ \dot{m}_\ell &= G_\ell A \quad \text{in} \quad \text{Kg/hr} \quad ; \end{aligned}\right\} \tag{F.5}$$

and

$$\dot{m}_{\ell r} = 4.35 \quad \text{Kg/hr} \quad .$$

(F.3) Kholodovski's Correlation

As indicated by Zuber [72], Kholodovski proposed the following correlation for steam-water mixtures:

$$\frac{\langle\alpha\rangle}{\beta} = K \langle j_m \rangle^{0.019} \quad , \tag{F.6}$$

where $\langle j_m \rangle$ is in m/sec. Kholodovski also stated that equation (F.6) is valid for two-phase flow of air and water as well as of liquid metals. It can be seen from the above

equation that the effect of the mixture velocity, $\langle j_m \rangle$, on the $\langle \alpha \rangle$-β relation is small.

(F.4) Zuber-Findlay's Model

Zuber and Findlay [17] introduced two flow parameters in their model which is given by equation (2.17) as

$$\frac{\langle \alpha \rangle}{\beta} = \frac{1}{C_o + \bar{V}_{gj}/\langle j_m \rangle} \quad . \tag{F.7}$$

(F.5) Hancox' Model

Assuming a negligible local relative velocity between the phases, Hancox [16] simplified the model presented by Zuber and Findlay to

$$\frac{\langle \alpha \rangle}{\beta} = \frac{1}{C_o} \quad , \tag{F.8}$$

which is of the same form as Armand's correlation (equation (F.3)). Hancox concluded that the distribution parameter, C_o, can be adequately represented by the expression

$$C_o' = \left(\frac{1-e^{-C_{o1}\langle \alpha \rangle}}{1-e^{-C_{o1}}}\right)(1 + C_{o2}) - C_{o2}\langle \alpha \rangle \quad . \tag{F.9}$$

The coefficients, C_{o1} and C_{o2}, were estimated by performing a least-squares fit of equation (F.9) to St. Pierre's data [83] to obtain the following values:

$$C_{o1} = 19.0 \quad , \tag{F.10-a}$$

and

$$C_{o2} = 0.2 \quad . \tag{F.10-b}$$

(F.6) Levy's Model

Levy [112] postulated a simplified momentum exchange model which led to a relation between the average void fraction and quality in a two-phase flow mixture. In this model, the momentum is considered to be exchanged between the phases when a change occurs in any of the system parameters in order to maintain the equality of frictional and head losses in the phases. This relation can be expressed as

$$\frac{(1-x)^2}{1-\langle\alpha\rangle} + \frac{\gamma x^2}{\langle\alpha\rangle} - \frac{1}{2}\left[1 + \left(\frac{1-x}{1-\langle\alpha\rangle}\right)^2\right] = 0. \qquad \text{(F.11)}$$

It is important to note that the above equation gives $\langle\alpha\rangle$ equal to unity as x approaches unity and reduces to the accepted relation $x = \langle\alpha\rangle$ at the critical pressure where γ approaches unity.

(F.7) Yagi-Sasaki's Correlation

As reported by Isbin et al. [104], Yagi and Sasaki proposed the following correlation for upward vertical flow of air-water and air-oil mixtures near atmospheric pressure:

$$\frac{1-\langle\alpha\rangle}{\langle\alpha\rangle} = 700\left(\frac{1-\beta}{\beta}\right)^{0.88} G_\ell \mu_\ell^{0.3}, \qquad \text{(F.12)}$$

where G_ℓ is in units of Kg/m^2sec and μ_ℓ is in units of Kg/msec. This correlation was reported by Isbin et al. [104] to yield reasonable predictions of the average foid fraction data at moderate pressures.

(F.8) Nashino-Yamazaki's Correlation

Nishino and Yamazaki [182] correlated the average void fraction data for air-water flow by the following empirical equation:

$$\langle\alpha\rangle = \frac{1}{2}\left[\left(1 + \frac{1}{\beta}\right) - \sqrt{\left(1 + \frac{1}{\beta}\right)^2 - 4}\right] \quad . \qquad (F.13)$$

(F.9) Turner-Wallis' Model

Turner and Wallis [183] derived a simple model for the average void fraction which can be written in the form

$$\langle\alpha\rangle = \frac{1}{1 + \left(\frac{1-x}{x}\right)^{0.72} (\gamma)^{-0.4} \left(\frac{\mu_\ell}{\mu_g}\right)^{0.08}} \quad . \qquad (F.14)$$

Since this model was based on the separate-cylinders approximation, it is expected to be more appropriate for the annular flow regime.

(F.10) Styrikowich et al.'s Correlation

Styrikowich et al. [184] proposed the following average void fraction correlation:

$$\frac{\langle\alpha\rangle}{\beta} = \frac{1 + \langle\alpha\rangle^{1.357}}{1 + \langle\alpha\rangle^{0.357}} \quad . \qquad (F.15)$$

This correlation was reported by Styrikowich et al. [184] to yield average void fraction values which were in satisfactory agreement with the published data.

(F.11) Thom's Correlation

Thom [106] proposed to fit the experimental data of steam-water and air-water average void fraction with a simple empirical correlation of the type

$$\langle\alpha\rangle = \frac{x\varepsilon}{1 + x(\varepsilon-1)} \quad , \qquad (F.16)$$

where the slip factor, ε, was assumed to be a unique function of the system pressure. As indicated by Thom, ε decreases with pressure and approaches unity at a very high pressure where the ratio $\langle\alpha\rangle/x$ approaches unity. For air-water flow systems at atmospheric pressure, ε was assigned a value of 246 [106] Thom's slip factor, ε, was also approximated by Butterworth [185] as

$$\varepsilon = [(\gamma)^{0.555}(\frac{\mu_g}{\mu_\ell})^{0.111}]^{1.6} \quad . \qquad (F.17)$$

Experimental data indicated that ε should be also a function of the system quality and, therefore, the validity of equation (F.17) is expected to be limited [186].

(F.12) Lockhart-Martinelli's Correlation

Lockhart and Martinelli [187] proposed an average void fraction correlation which was approximated by Butterworth [185] as

$$\langle\alpha\rangle = \frac{1}{1 + 0.28(\frac{1-x}{x})^{0.64}(\gamma)^{-0.36}(\frac{\mu_\ell}{\mu_g})^{0.07}} \quad . \qquad (F.18)$$

APPENDIX (G)

VOID PROPAGATION EQUATION

Following Zuber and Staub [15], the void propagation equation can be derived by considering the continuity conditions for the phases. Consider the two-phase flow system which has been described in section (6.2). The two-phase mixture is assumed to move vertically through a tube of uniform cross-section. For a differential length of the flow tube, the mass conservation equations within the gas and liquid phases can be written, respectively, as

$$\frac{\partial(\alpha\rho_g)}{\partial t} + \text{div.}(v_g\ \alpha\ \rho_g) = \Gamma_g\ , \qquad \text{(G.1-a)}$$

and

$$\frac{\partial[(1-\alpha)\rho_\ell]}{\partial t} + \text{div.}[v_\ell(1-\alpha)\rho_\ell] = \Gamma_\ell\ , \qquad \text{(G.1-b)}$$

where Γ_g and Γ_ℓ are the local values of the generation rates, that is, the rates of mass formation per unit mixture volume, of the gas and liquid phases, respectively. In equation (G.1), α, v_g and v_ℓ are the local values of the void fraction and the velocities of the phases, respectively.

As shown by Zuber and Staub [15], it is appropriate to express the void propagation equation in terms of values averaged

over the tube cross-sectional area when analyzing the problem of void transient response in two-phase flow. Consequently, equations (G.1-a) and (G.1-b) are written in terms of cross-sectional averages by integrating each term over the cross-section of the flow tube. Thus,

$$\frac{\partial}{\partial t} \langle \alpha \rho_g \rangle + \frac{\partial}{\partial z} \langle v_g \alpha \rho_g \rangle = \langle \Gamma_g \rangle \ , \qquad \text{(G.2-a)}$$

and

$$\frac{\partial}{\partial t} \langle (1-\alpha) \rho_\ell \rangle + \frac{\partial}{\partial z} \langle v_\ell (1-\alpha) \rho_\ell \rangle = \langle \Gamma_\ell \rangle \ . \qquad \text{(G.2-b)}$$

It is noteworthy that the divergence terms in equation (G.1) have been simplified to one-dimensional differentiations with respect to the length, z, along the tube as a result of this averaging operation.

In most practical problems, the compressibility of the phases can be neglected without appreciable error if the pressure drop along the flow tube is assumed to be small relative to the total pressure. Hence, the densities of the phases can be considered to be constant with time and also across the tube cross-section. Using this simplifying assumption, equation (G.2) can be rearranged to

$$\frac{\partial \langle \alpha \rangle}{\partial t} + \frac{\partial}{\partial z} \langle v_g \alpha \rangle = \frac{\langle \Gamma_g \rangle}{\rho_g} \ , \qquad \text{(G.3-a)}$$

and

$$\frac{\partial \langle \alpha \rangle}{\partial t} - \frac{\partial}{\partial z} \langle v_\ell (1-\alpha) \rangle = - \frac{\langle \Gamma_\ell \rangle}{\rho_\ell} \ . \qquad \text{(G.3-b)}$$

Since the gas phase is added entirely through the bottom end of the mixing section, that is, at z=0 and none is introduced after this level, the gas source term, $\langle \Gamma_g \rangle$, can be considered equal to zero. Thus,

$$\langle \Gamma_g \rangle = 0 \ . \qquad (G.4)$$

Equations (G.3-a) and (G.4) are combined to give

$$\frac{\partial \langle \alpha \rangle}{\partial t} + \frac{\partial}{\partial z} \langle v_g \alpha \rangle = 0 \ . \qquad (G.5)$$

Now equation (G.3-b) can be subtracted from equation (G.5) to yield

$$\frac{\partial}{\partial z} \langle v_g \alpha + v_\ell (1-\alpha) \rangle = \frac{\langle \Gamma_\ell \rangle}{\rho_\ell} \ . \qquad (G.6)$$

From the definition of the mixture volumetric flux density, j_m, given by equations (2.13) and (2.14), one can recognize that the left-hand side of equation (G.6) is, in fact, the derivative of the cross-sectional average mixture volumetric flux density. Thus,

$$\frac{\partial}{\partial z} \langle j_m \rangle = \frac{\langle \Gamma_\ell \rangle}{\rho_\ell} \ . \qquad (G.7)$$

Equation (G.7) demonstrates that the divergence of the mixture average volumetric flux density is equal to the rate of liquid volume formation per unit mixture volume. The above equation may be integrated to obtain the following expression for the axial distribution of the mixture average velocity:

$$\langle j_m \rangle = v_i + \int_0^z \frac{\langle \Gamma_\ell \rangle}{\rho_\ell} \, dz \ , \qquad \text{(G.8)}$$

where v_i is the inlet velocity of the two-phase flow mixture which is equivalent, in the present case, to the volumetric flowrate of the gas phase per unit tube cross-sectional area.

From the definition of the local drift velocity, V_{gj}, (equation (1.6)) and the mixture volumetric flux density (equations (2.13) and (2.14)), it can be easily shown that

$$\langle v_\ell (1-\alpha) \rangle = \langle j_m (1-\alpha) - V_{gj} \alpha \rangle \ , \qquad \text{(G.9)}$$

which upon substituting into equation (G.3-b) gives

$$\frac{\partial \langle \alpha \rangle}{\partial t} - \frac{\partial}{\partial z} \left[\langle j_m \rangle - C_o \langle j_m \rangle \langle \alpha \rangle - \bar{V}_{gj} \langle \alpha \rangle \right] = \frac{-\langle \Gamma_\ell \rangle}{\rho_\ell} \ . \qquad \text{(G.10)}$$

In equation (G.10), use has been made of the definition of the distribution parameter, C_o, and the mean drift velocity, $\bar{V}_{gj}$, as given by equation (1.5). Differentiating the terms between the bracket in equation (G.10) and rearranging yields

$$\frac{\partial \langle \alpha \rangle}{\partial t} + U \frac{\partial \langle \alpha \rangle}{\partial z} = \Omega \ , \qquad \text{(G.11)}$$

where

$$U = C_o \langle j_m \rangle + \langle \alpha \rangle \langle j_m \rangle \frac{\partial C_o}{\partial \langle \alpha \rangle} + \bar{V}_{gj} + \langle \alpha \rangle \frac{\partial \bar{V}_{gj}}{\partial \langle \alpha \rangle}, \qquad \text{(G.12-a)}$$

and

$$\Omega = \frac{\partial \langle j_m \rangle}{\partial z} - \frac{\langle \Gamma_\ell \rangle}{\rho_\ell} - C_o \langle \alpha \rangle \frac{\partial \langle j_m \rangle}{\partial z} \ . \qquad \text{(G.12-b)}$$

Equation (G.11) represents the void propagation equation for the adiabatic gas-liquid flow system under consideration where U and Ω stand for the velocity of the kinematic waves and the characteristic reaction frequency, respectively.

It is important to note that the propagation equation, analogous to the diffusion equation, is an independent one. In general, for any two-phase flow system, it is required along with the conservation equations of mass, momentum and energy of the mixture to properly describe the system behaviour. Furthermore, similar to the diffusion equation, its derivation has been based upon the continuity equations of the phases.

APPENDIX (H)

EXPERIMENTAL DATA OF THE NEUTRON TRANSMITTANCE FUNCTION

This appendix contains the experimental data of the time-average neutron transmittance function which were obtained in the present study under steady-state and transient conditions. The neutron transmittance function is defined as the ratio of the intensity of the transmitted neutron beam to that of the unattenuated beam. Table (H.1) summarizes the steady-state measurements of the chordal transmittance function across the tube radius for the bubbly and annular flow regimes which were performed in the holdup experiments (Section (4.5)). Similarly, table (H.2) summarizes the chordal transmittance measurements across the flow tube for both flow regimes which were obtained to estimate the flow parameters, as described in Chapter (5). In tables (H.1) and (H.2), L/R is used to define the chordal position of the beam center relative to the tube center. Table (H.3) shows the time-variation of the neutron transmittance function through the entire tube cross section for the various experimental runs performed to determine the void transient response to gas flow perturbations in bubbly flow (Chapter (6)). The gas and liquid flowrates used in these experiments are summarized in tables (4.7), (5.1) and (6.2), respectively.

Run No. \ L/R	0.5955	0.4764	0.3573	0.2382	0.1191	0.0000
(1)	0.0236	0.0150	0.0129	0.0114	0.0111	0.0106
(2)	0.0239	0.0137	0.0107	0.0095	0.0088	0.0086
(3)	0.0228	0.0123	0.0095	0.0082	0.0076	0.0072
(4)	0.0300	0.0195	0.0166	0.0147	0.0133	0.0140
(5)	0.0232	0.0132	0.0105	0.0088	0.0086	0.0080
(6)	0.0318	0.0213	0.0182	0.0159	0.0157	0.0153
(7)	0.0270	0.0167	0.0132	0.0113	0.0105	0.0105
(8)	0.0264	0.0153	0.0112	0.0098	0.0088	0.0089

Table (H.1-a): Steady-state measurements of the chordal transmittance function for holdup experiments in bubbly flow.

Run No. \ L/R	0.5955	0.4764	0.3573	0.2382	0.1191	0.0000
(1)	0.3319	0.3563	0.3643	0.3690	0.3715	0.3712
(2)	0.3177	0.3442	0.3521	0.3552	0.3588	0.3584
(3)	0.3104	0.3355	0.3434	0.3470	0.3473	0.3487
(4)	0.2738	0.2888	0.2918	0.2931	0.2937	0.2937

Table (H.1-b): Steady-state measurements of the chordal transmittance function for holdup experiments in annular flow.

Run No. / L/R	(1)	(2)	(3)	(4)	(5)	(6)
-0.6667	0.0196	0.0118	0.0098	0.0105	0.0190	0.0144
-0.5333	0.0151	0.0090	0.0086	0.0068	0.0175	0.0105
-0.4000	0.0140	0.0074	0.0062	0.0048	0.0173	0.0082
-0.2667	0.0129	0.0066	0.0048	0.0042	0.0163	0.0070
-0.1333	0.0128	0.0065	0.0044	0.0041	0.0163	0.0064
0.0000	0.0126	0.0061	0.0044	0.0039	0.0158	0.0064
0.1333	0.0131	0.0063	0.0044	0.0039	0.0157	0.0064
0.2667	0.0132	0.0070	0.0042	0.0041	0.0158	0.0068
0.4000	0.0132	0.0077	0.0047	0.0043	0.0161	0.0078
0.5333	0.0162	0.0099	0.0053	0.0054	0.0169	0.0100
0.6667	0.0199	0.0142	0.0070	0.0088	0.0193	0.0139

Table (H.2-a): Steady-state measurements of the chordal transmittance function for flow parameters experiments in bubbly flow.

Run No. / L/R	(7)	(8)	(9)	(10)	(11)
-0.6667	0.0124	0.0123	0.0182	0.0172	0.0137
-0.5333	0.0082	0.0072	0.0149	0.0119	0.0083
-0.4000	0.0062	0.0050	0.0118	0.0084	0.0056
-0.2667	0.0052	0.0044	0.0102	0.0067	0.0049
-0.1333	0.0048	0.0043	0.0097	0.0062	0.0046
0.0000	0.0047	0.0041	0.0096	0.0059	0.0045
0.1333	0.0049	0.0042	0.0102	0.0060	0.0045
0.2667	0.0053	0.0045	0.0106	0.0065	0.0049
0.4000	0.0061	0.0051	0.0128	0.0076	0.0063
0.5333	0.0076	0.0074	0.0153	0.0108	0.0101
0.6667	0.0120	0.0138	0.0219	0.0152	0.0183

Table (H.2-a) (continued)

Run No. / L/R	(1)	(2)	(3)	(4)	(5)	(6)
-0.6667	0.2953	0.3148	0.3149	0.3255	0.2636	0.3040
-0.5333	0.3181	0.3360	0.3359	0.3435	0.2971	0.3208
-0.4000	0.3337	0.3472	0.3497	0.3557	0.3122	0.3317
-0.2667	0.3413	0.3537	0.3558	0.3617	0.3248	0.3421
-0.1333	0.3453	0.3596	0.3616	0.3630	0.3253	0.3414
0.0000	0.3460	0.3587	0.3633	0.3666	0.3296	0.3421
0.1333	0.3459	0.3573	0.3606	0.3636	0.3295	0.3405
0.2667	0.3395	0.3544	0.3577	0.3597	0.3240	0.3330
0.4000	0.3353	0.3446	0.3509	0.3486	0.3150	0.3244
0.5333	0.3234	0.3312	0.3395	0.3435	0.3036	0.3058
0.6667	0.2966	0.3036	0.3158	0.3255	0.2811	0.2722

Table (H.2-b): Steady-state measurements of the chordal transmittance function for flow parameters experiments in annular flow.

Run No. / L/R	(7)	(8)	(9)	(10)	(11)
-0.6667	0.3071	0.3165	0.2632	0.2796	0.2939
-0.5333	0.3277	0.3333	0.2897	0.3038	0.3166
-0.4000	0.3401	0.3427	0.3087	0.3164	0.3281
-0.2667	0.3446	0.3508	0.3139	0.3219	0.3314
-0.1333	0.3482	0.3538	0.3163	0.3270	0.3369
0.0000	0.3477	0.3530	0.3196	0.3284	0.3353
0.1333	0.3448	0.3483	0.3169	0.3265	0.3374
0.2667	0.3387	0.3433	0.3105	0.3225	0.3294
0.4000	0.3303	0.3331	0.3017	0.3129	0.3236
0.5333	0.3135	0.3200	0.2868	0.2979	0.3073
0.6667	0.2839	0.2886	0.2574	0.2690	0.2761

Table (H.2-b) (continued)

Run No. / L/R	(12)	(13)	(14)	(15)	(16)
-0.6667	0.2996	0.2546	0.2795	0.2921	0.2988
-0.5333	0.3233	0.2797	0.3006	0.3139	0.3169
-0.4000	0.3339	0.2949	0.3148	0.3229	0.3315
-0.2667	0.3383	0.3013	0.3209	0.3267	0.3376
-0.1333	0.3444	0.3118	0.3262	0.3341	0.3394
0.0000	0.3437	0.3087	0.3261	0.3315	0.3394
0.1333	0.3414	0.3059	0.3247	0.3301	0.3363
0.2667	0.3356	0.3033	0.3176	0.3252	0.3328
0.4000	0.3286	0.2970	0.3103	0.3183	0.3208
0.5333	0.3143	0.2826	0.2921	0.2990	0.3050
0.6667	0.2833	0.2562	0.2596	0.2605	0.2735

Table (H.2-b) (continued)

Run No. / Time (sec)	(1)	(2)	(3)	(4)	(5)	(6)
0.055	0.0177	0.0165	0.0162	0.0127	0.0135	0.0130
0.110	0.0160	0.0149	0.0165	0.0140	0.0129	0.0120
0.165	0.0166	0.0169	0.0168	0.0133	0.0134	0.0132
0.220	0.0164	0.0165	0.0159	0.0133	0.0140	0.0134
0.275	0.0155	0.0153	0.0173	0.0133	0.0140	0.0132
0.330	0.0168	0.0170	0.0167	0.0136	0.0129	0.0135
0.385	0.0169	0.0157	0.0177	0.0139	0.0136	0.0129
0.440	0.0161	0.0162	0.0170	0.0135	0.0135	0.0142
0.495	0.0162	0.0161	0.0166	0.0133	0.0132	0.0139
0.550	0.0166	0.0163	0.0156	0.0137	0.0138	0.0130
0.605	0.0148	0.0170	0.0174	0.0133	0.0131	0.0134
0.660	0.0160	0.0165	0.0183	0.0134	0.0133	0.0142
0.715	0.0178	0.0182	0.0208	0.0136	0.0139	0.0134
0.770	0.0177	0.0217	0.0217	0.0146	0.0146	0.0140
0.825	0.0195	0.0220	0.0234	0.0158	0.0151	0.0169

Table (H.3) : Time-variation of the transmittance function through the entire tube cross section for flow transient experiments in bubbly flow.

Run No. / Time (sec)	(1)	(2)	(3)	(4)	(5)	(6)
0.880	0.0219	0.0236	0.0266	0.0163	0.0174	0.0178
0.935	0.0229	0.0239	0.0274	0.0175	0.0167	0.0182
0.990	0.0210	0.0252	0.0272	0.0176	0.0179	0.0198
1.045	0.0231	0.0271	0.0284	0.0175	0.0208	0.0201
1.100	0.0247	0.0279	0.0290	0.0179	0.0192	0.0215
1.155	0.0220	0.0247	0.0331	0.0189	0.0219	0.0223
1.210	0.0239	0.0269	0.0352	0.0191	0.0213	0.0216
1.265	0.0249	0.0308	0.0284	0.0197	0.0211	0.0242
1.320	0.0260	0.0278	0.0308	0.0184	0.0232	0.0238
1.375	0.0231	0.0271	0.0331	0.0200	0.0231	0.0242
1.430	0.0232	0.0329	0.0327	0.0217	0.0226	0.0234
1.485	0.0239	0.0324	0.0362	0.0214	0.0223	0.0234
1.540	0.0253	0.0309	0.0279	0.0214	0.0224	0.0240
1.595	0.0235	0.0373	0.0366	0.0214	0.0231	0.0233
1.650	0.0243	0.0347	0.0356	0.0217	0.0229	0.0252

Table (H.3) (continued)

NOMENCLATURE

(i) Symbols

a	Core radius, cm (equation (C.9)).
$\underline{a}$	Water buildup factor coefficients (equations (4.5) and (4.11)).
A	Tube cross-sectional area, cm^2.
A_0	Cross-sectional area of orifice throat, cm^2.
A_1, A_2	Areas under the peaks of void probability density function in slug flow (equation (4.35)).
B	Water buildup factor (equation (4.5)).
c	Constant of integration (equations (5.26), (5.32) and (5.36)).
c'	Distribution parameter (equation (2.9)).
C	Calibration constant for sonic orifice, $gm°K^{1/2}/cm^2$ sec p.s.i.a. (equation (3.1)).
C'	Flow parameter (equation (2.29)).
C_o	Distribution parameter (equation (1.5-a)).
C_{o1}, C_{o2}	Distribution parameter coefficients (equation (F.9)).
d	Degree of freedom.
D	Diameter, cm or in.
D_e	Equivalent hydraulic diameter, f_t.
e	Correction factor for pressure drop acceleration component (equation (5.11)).

f	Friction factor of two-phase flow mixture (equation (5.6)).
f_o	Single-phase friction factor evaluated at mixture Reynolds number (equation (5.8)).
F	Mean film thickness, cm (equation (C.9)).
F_r	Froude number.
F'	Interfacial friction function (equation (5.55)).
$F_{0.05}$	95% F-distribution function.
g	Gravitational acceleration, cm/sec^2.
G	Mass flowrate per unit tube cross-sectional area, gm/cm^2sec or lb/ft^2hr.
ΔG	Change in mass flowrate per unit tube cross-sectional area, gm/cm^2 sec.
h	Height of detector collimator, cm or in.
H_o	Hypothesis made in Bartlett's test (equation (B.1)).
i	Number of finite steps along z-axis.
I	Intensity of transmitted neutron beam, C/sec.
I_o	Intensity of unattenuated neutron beam, C/sec.
j	Number of finite steps along t-axis.
j	Local volumetric flux density, cm/sec.
k	Transmittance transformation index (equation (4.7)).
k_s	Equivalent grain size of "sand roughness", cm (equation (5.53)).
K	Transmittance kernel (equations (4.2), (6.18) and (C.2)).
K	Bankoff's flow parameter (equation (2.6)).
K'	Distribution parameter (equation (2.42)).

K_1, K_2	Void fraction and velocity profile parameters (equation (2.40)).
ℓ	Total medium thickness, cm.
ℓ	Turbulent mixing length, cm.
L	Distance from tube center, cm.
L_1, L_2	Lengths of mixing and developing sections, cm.
m	Distribution parameter coefficient (equation (6.14)).
$\dot{m}$	Mass flowrate, gm/sec.
MS	Mean-square.
n	Number of independent estimates of variance.
n	Void fraction profile index (equations (4.41) and (4.42)).
p	Probability density function (PDF).
P	System pressure, dyne/cm^2 or p.s.i.a.
P_r	Probability function (equations (4.18) and (4.35)).
$(-\frac{\partial P}{\partial z})$	Pressure drop per unit tube length, dyne/cm^3.
q,q'	Constants of proportionality (equations (2.25) and (2.27)).
Q	Volumetric flowrate, cm^3/sec, CFM or Imp. gpm.
ΔQ	Auxiliary volumetric flowrate, cm^3/sec.
Q'	Volumetric flowrate per unit tube cross-sectional area, cm/sec.
r	Number of coefficients in water buildup factor expression (equation (4.5)).
r	Radial position, cm.

R	Tube radius, cm.
R'	Homogeneity correction factor.
R_e	Reynolds number.
s^2	Pooled sample variance (equation (B.3)).
s_i^2	Estimated variance of the ith sample (equation (B.3)).
s'^2	Estimated variance on transformed transmittance function.
S	Velocity slip ratio (equation (2.19)).
SS	Weighted sum of squares of residuals (equation (4.4)).
S_1, S_2	Velocity slip ratio components (equations (2.32) and (2.33)).
t	Time, sec.
Δt	Increment size along t-axis, sec.
Δt	Rise time, sec (figure (6.3)).
t_a	Time over which void transient response is averaged, sec (equation (6.21)).
t_1	Time at which average void fraction starts to respond to flow perturbations at measuring location, sec (figure (6.3)).
T	Absolute temperature, °K.
T	Chordal transmittance function (equations (4.1) and (4.36)).
T'	Transformed transmittance function (equation (4.7)).
u	Radial component of local velocity, cm/sec.
u^*	Wall shear stress velocity, cm/sec (equation (5.60)).

U	Velocity of kinematic waves, cm/sec (equations (1.2), (6.2) and (G.12-a)).
v	Axial component of local velocity, cm/sec.
v_∞	Terminal rise velocity of a single bubble in an infinite medium, cm/sec (equation (2.4)).
$\bar{v}$	Weighted mean velocity, cm/sec (equqtion (2.20)).
V	Volume, cm^3.
V_b	Velocity of slug bubbles with respect to liquid ahead of them, cm/sec (equation (2.35)).
V_{gj}	Local drift velocity, cm/sec (equation (1.6)).
$\bar{V}_{gj}$	Mean drift velocity, cm/sec (equation (1.5-b)).
$\underline{V}$	Variance-covariance matrix for transmittance measurements (equation (4.4)).
w	Azimuthal component of local velocity, cm/sec.
x	Mass quality of two-phase flow mixture (equation (2.23)).
x	Thickness, cm.
x	Chordal position, cm.
y	Distance along a chordal line, cm.
y	Distance from tube wall, cm.
z	Axial position, cm.
Δz	Increment size along z-axis, cm.
$\bar{z}$	Weighted transmittance function (equation (4.8)).
α	Local void fraction.
$\Delta\alpha$	Void fraction bias (equation (4.24)).
α_0	Actual void fraction (equation (4.19)).

$\bar{\alpha}(x)$	Average void fraction along a chordal line x (equations (4.39) and (C.5)).
$<\alpha>_1$	Starting value of steady-state average void fraction (figure (6.3)).
$\Delta<\alpha>$	Total change in average void fraction (figure (6.3)).
β	Apparent volumetric flow concentration (equation (2.2)).
γ	Liquid-to-gas density ratio ($\gamma = \rho_\ell/\rho_g$).
δ	Chordal thickness, cm.
δ_b	Neutron beam width, cm or in.
ε	Slip factor (equations (2.45) and (F.17)).
λ	Medium thickness in units of mean free path ($\lambda = \mu_m x_m$).
λ	Dimensionless group (equation (5.5)).
ρ	Density, gm/sm^3.
$\Delta\rho$	Difference between liquid and gas densities ($\Delta\rho = \rho_\ell - \rho_g$), gm/cm^3.
σ	Surface tension, dyne/cm.
σ^2	Estimated variance (equation (B.1)).
θ	Azimuthal angle, degree.
τ	Local shear stress, $dyne/cm^2$.
Γ	Mass flowrate per unit wetted perimeter, gm/cm sec (equation (5.66)).
Γ	Local rate of mass formation per unit mixture volume, $gm/cm^3 sec$.

Ω Characteristic reaction frequency, sec^{-1} (equations (1.3), (6.3) and (G.12-b)).

ψ Arbitrary variable (equation (1.4)).

π Mathematical constant ($\pi = 3.14159$).

μ Viscosity coefficient, gm/cm sec or lb/ft hr.

μ Neutron attenuation parameter, cm^{-1}.

ξ Ratio of gas-to-liquid volumetric flowrates (equation (2.50)).

(2) Subscripts

a Average.

al Aluminum.

c Core region, tube center, counting or calculated.

e Entrained liquid or empty tube.

expect. Expected value.

f Film or frictional component.

g gas (or vapour) phase.

i Inlet condition, tube inside or core-film interface.

I Characteristic curves.

ℓ Liquid phase.

L Lack of fit term.

m Medium, mixture or measured.

meas. Measured value.

mℓ Measuring location.

n Neutron attenuation method.

ns No-slip condition.

o	Orifice or tube outside.
PE	Pure error residual term.
r	Rod or relative.
t	Tube or trapping method.
TP	Two-phase flow mixture.
w	Wall.
1	Upstream.
2	Downstream.

(3) Superscripts

(ℓ)	Laminar component.
(t)	Turbulent component.
+	Dimensionless.
^	Expected value.
———	Time-averaged component.
'	Fluctuating component.

(4) Special Notations

exp	Exponential.
ℓn	Natural logarithm.
%	Percentage.
| |	Absolute value.
< >	Quantities averaged over tube cross-sectional area (equation (1.4)).

REFERENCES

1. Vohr, J., MTI-70-TR-15 (1970).
2. Pan, C., and J. Vohr, MTI-70-TR-16 (1970).
3. Miropolskii, Z., AEC-TR-6431, From Teploenergetika, 9, 79 (1962).
4. Moeck, E., AECL-3656 (1970).
5. Polomik, E., APED-4625 (1964).
6. Verheugen, A., et al., European Two-Phase Flow Heat Transfer Meeting, Bournemouth (1967).
7. Janssen, E., GEAP-5480 (1967).
8. Jahnberg, S., RFR-197 (1962).
9. Bestenbreur, T., WW-30-M-75 (1967).
10. Baker, O., Oil Gas Journal, 53, 185 (1954).
11. Hughmark, G., and B. Pressburg, A.I.Ch.E. Journal, 7, 677 (1961).
12. Palmer, R., et al., Proc. New Developments in Reactor Physics and Shielding, AEC Conference-720901, New York (1972).
13. Moody, F., APED-4827 (1965).
14. Fauske, H., D. Quinn and W. Jeans, Trans. Amer. Nucl. Soc., 12, 354 (1969).
15. Zuber, N., and F. Staub, Nucl. Sci. Eng., 30, 268 (1967).
16. Hancox, W., Ph.D. Thesis, University of Waterloo (1971).
17. Zuber, N., and J. Findlay, Journal Heat Transfer, 87, 453 (1965).

18. Shiralkar, B., L. Schnebly and R. Lahey, Jr., Nucl. Eng. Design, 25, 350 (1973).

19. Garland, W., Ph.D. Thesis, McMaster University (1975).

20. Beattie, D., Nucl. Eng. Design, 21, 46 (1972).

21. Levy, S., Journal Heat Transfer, 85, 137 (1963).

22. Jones, O., Jr., Ph.D. Thesis, Rensselaer Polytechnic Institute (1973).

23. Younis, M., T. Hoffman and A. Harms, Submitted for publication in Nucl. Technology.

24. Hancox, W., and W. Nicoll, Inst. Journal Heat Mass Transfer, 14, 1377 (1971).

25. Jones, O., Jr., and J. Delhaye, Int. Journal Multiphase Flow, 3, 89 (1976).

26. Solomon, V., M.Sc. Thesis, MIT (1962).

27. Neal, L., and S. Bankoff, A.I.Ch.E. Journal, 9, 490 (1963).

28. Nassos, G., and S. Bankoff, Canad. Journal Chem. Eng., 45, 271 (1967).

29. Malnes, D., KR-110 (1966).

30. Herringe, R., and M. Davis, Journal Physics Scientific Instruments, 7, 807 (1974).

31. Lecroart, A., and R. Porte, Proc. International Symposium on Two-Phase Systems, Paper No. 3-11, Haifa (1971).

32. Burgess, J., and P. Calderbank, Chem. Eng. Sci., 30, 743 (1975).

33. Hsu, Y., F. Simon and R. Graham, Winter Annual ASME Meeting, Philadelphia (1963).

34. Miller, N., and R. Mitchie, British Nucl. Energy Soc. Journal, 9, 94 (1970).

35. Galaup, J., D. Eng. Thesis, Grenoble National Polytechnique Institute (1975).

36. Schraub, F., R. Simpson and E. Jannsen, GEAP-5739 (1969).

37. Quandt, E., A.I.Ch.E. Journal, 11, 311 (1965).

38. Agostini, G., et al., CISE-R-291 (1969).

39. Schrock, V., National Heat Transfer Conference, Minneapolis (1969).

40. Jones, O., Jr., KAPL-3859 (1970).

41. Pike, R., B. Wilkins, Jr., and H. Ward, A.I.Ch.E. Journal, 11, 794 (1965).

42. Smith, A., British Nucl. Energy Soc. Journal, 10, 99 (1971).

43. Gustafsson, B., and B. Kjellen, European Two-Phase Flow Group Meeting, Paper No. A-5, Riso (1971).

44. Perkins, H., Jr., M. Yusuf and G. Leppert, Nucl. Sci. Eng., 11, 304 (1961).

45. Cook, W., ANL-5621 (1956).

46. Hooker, H., and G. Pooper, ANL-5766 (1958).

47. Petrick, M., and S. Swanson, Rev. Sci. Inst., 29, 1079 (1958).

48. Richardson, R., ANL-5949 (1958).

49. Gardner, R., R. Bean and J. Ferrell, Nucl. Applications Technology, 8, 88 (1970).

50. LeVert, F., and E. Helminski, Nucl. Technology, 19, 58 (1973).

51. Heidrick, T.,J. Saltvold and S. Banerjee, AIChE Symposium Series, 73, 248 (1977).

52. Kennett,T., W. Prestwich and A. Robertson, Int. Journal Applied Radiation Isotopes, 27, 529 (1976).

53. Untermyer, S., Second Geneva Conference, 9, 455 (1958).

54. Thie, J., J. Beidelman and B. Hoglund, Nucl. Sci. Eng., 11, 1 (1961).

55. Untermyer, S., Nucleonics, 20, 52 (1962).

56 Sha, W., and C. Bonilla, Nucl. Applications, 1, 69 (1965).

57. Moss, R., and A. Kelly, Int. Journal Heat Mass Transfer, 13, 491 (1970).

58. Harms, A., S. Lo and W. Hancox, Journal Applied Physics, 42, 4080, (1971).

59. Harms, A., and C. Forrest, Nucl. Sci. Eng., 46, 408 (1971).

60. Hancox, W., C. Forrest and A. Harms, AIChE-ASME National Heat Transfer Conference, Paper No. 72-HT-2, Denver (1972).

61. Younis, M., A. Harms and T. Hoffman, Nucl. Eng. Design, 24, 145 (1973).

62. Rousseau, J., J. Czerny and B. Riegel, Invited paper at OECD-NEA Specialists Meeting on Transient Two-Phase Flow, Toronto (1976).

63. Banerjee, S., et al., Sixth International Heat Transfer Conference,Paper No. FB-14, Toronto (1978).

64. Arnold, C., and G. Hewitt, AERE-R-5318 (1967).

65. Feldberg, L., et al., Fifth All-Union Heat and Mass Transfer Conference, Paper No. 3-75, Minsk (1976).

66. Dengler, D., Ph.D. Thesis, MIT (1952).

67. Rouhani, S., Nucl. Sci. Eng., 14, 414 (1962).

68. Nassos, G., ANL-7053 (1965).

69. Wallis, G., One-Dimensional Two-Phase Flow, McGraw-Hill, New York (1969).

70. Behringer, H., Zeit. Ges. Kälte-Ind., 43, 55 (1936), Also AEC-Translation No. 1777, O.T.S. Department of Commerce, Washington, D.C.

71. Bankoff, S., Journal Heat Transfer, 82, 265 (1960).

72. Zuber, N., Journal Heat Transfer, 82, 255 (1960).

73. Armand, A., AERE-Trans-828 (1959).

74. Griffith, P., and G. Wallis, Journal Heat Transfer, 83, 307 (1961).

75. Bartolomei, G., and R. Georgescu, AERE-Trans-1076 (1967).

76. Nicklin, D., J. Wilkes and J. Davidson, Trans. Instn Chem. Engrs, 40, 61 (1962).

77. Neal, L., A.I.Ch.E. Journal, 11, 747 (1965).

78. Nobel, L., EUR-4811-E (1972).

79. Neal, L., and S. Bankoff, A.I.Ch.E. Journal, 11, 624 (1965).

80. Staub, F., N. Zuber and G. Bijwaard, Nucl. Sci. Eng., 30, 279 (1967).

81. Petrick, M., ANL-6581 (1962).

82. Bailey, R., et al., AIChE Meeting, New Orleans (1956).

83. St. Pierre, C., ANL-7041 (1965).

84. Zuber, N., Int. Journal Heat Mass Transfer, 10, 1638 (1967).

85. Birkhoff, G., Journal Math. Analysis Applications, 8, 66 (1964).

86. Meyer, J., and R. Rose, Journal Heat Transfer, 85, 1 (1963).

87. Zuber, N., and F. Staub, Int. Journal Heat Mass Transfer, 9, 871 (1966).

88. Ahmad, S., Journal Heat Transfer, 92, 595 (1970).

89. Bird, R.; W. Stewart and E. Lightfoot, Transport Phenomena, John Wiley, New York (1960).

90. Van Der Walle, F., and H. Lamein, NWD-16-R-50 (1963).

91. Spinks, N., Int. Journal Heat Mass Transfer, 10, 1637 (1967).

92. Hudson, J., K. Atit and S. Bankoff, Chem. Eng. Sci., 19, 387 (1964).

93. Christensen, H., ANL-6385 (1961).

94. Staub, F., and N. Zuber, Nucl. Sci. Eng., 30, 296 (1967).

95. Zuber, N., et al., GEAP-5417 (1967).

96. Zuber, N., Proc. All-Union Heat and Mass Transfer Conference, Minsk (1964).

97. Lighthill, M., and G. Whitham, Proc. Roy. Soc. A, 229, 281 (1955).

98. Lighthill, M., and G. Whitham, Proc. Roy. Soc. A, 229, 317 (1955).

99. Staub, F., and N. Zuber, GEAP-4631 (1964).

100. Hancox, W., and W. Nicoll, International Symposium on Two-Phase Systems, Haifa (1971).

101. Larsen, P., and L. Tong, Journal Heat Transfer, 91, 471 (1969).

102. Gonzalez-Santalo, J., and R. Lahey, Jr., Journal Heat Transfer, 95, 470 (1973).

103. Hopkinson, A., AEEW-M-1123 (1972).

104. Isbin, H., et al., A.I.Ch.E. Journal, 5, 427 (1959).

105. Govier, G., B. Radford and J. Dunn, Canad. Journal Chem. Eng., 35, 58 (1957).

106. Thom, J., Int. Journal Heat Mass Transfer, 7, 709 (1964).

107. Meyer, J., WAPD-BT-20 (1960).

108. Neal, L., KR-62 (1963).

109. Griffith, P., Journal Heat Transfer, 86, 327 (1964).

110. Zuber, N., and J. Findlay, GEAP-4592 (1964).

111. Brown, R., A. Gomezplata and J. Price, Chem. Eng. Sci., 24, 1483 (1969).

112. Levy, S., Journal Heat Transfer, 82, 113 (1960).

113. Untermeyer, S., ASME Paper No. 57-NESC-80 (1957).

114. Martinelli, R., and D. Nelson, Trans. Amer. Soc. Mech. Engrs, 70, 695 (1948).

115. Zivi, S., Journal Heat Transfer, 86, 247 (1964).

116. Haywood, R., et al. Proc. Instn Mech. Engrs, 175, 669 (1961).

117. Thom, J., Ph.D. Thesis, Cambridge University (1959).

118. Petrick, M., ANL-5787 (1958).

119. Hewitt, G., and R. Semeria, International Seminar on Recent Development in Heat Exchangers, Lecture H, Yugoslavia (1972).

120. Fohrman, M., ANL-6256 (1960).

121. Mills, A., and D. Chung, Int. Journal Heat Mass Transfer, 16, 694 (1973).

122. Levy, S., Int. Journal Heat Mass Transfer, 9, 171 (1966).

123. Tippets, F., Journal Heat Transfer, 86, 23 (1964).

124. Calvert, S., and B. Williams, A.I.Ch.E. Journal, 1, 78 (1955).

125. Seban, R., and A. Faghri, Journal Heat Transfer, 98, 315 (1976).

126. Anderson, G., and B. Mantzouranis, Chem. Eng. Sci., 12, 109 (1960).

127. Van Driest, E., Journal Aero. Sci., 23, 1007 (1956).

128. Pai, S., Journal Applied Mechanics, 22, 41 (1955).

129. Dukler, A., Chem. Eng. Progr. Symposium Series, 56, 1 (1960).

130. Hewitt, G., AERE-R-3680 (1961).

131. Fluid Meters - Their Theory and Application, Report of ASME Research Committee on Fluid Meters, Fifth Edition, New York (1959).

132. Dye, D., Journal Basic Eng., 87, 1025 (1965).

133. Butterworth, D., Chem. Eng. Sci., 22, 911 (1967).

134. Brockhouse, B., Rev. Sci. Inst., 30, 136 (1959).

135. Neutron-Gamma Shielding, Reactor Experiments, Inc., General Catalog No. 10-F, San Carlos, California (1970).

136. Glower, D., Experimental Reactor Analysis and Radiation Measurements, McGraw-Hill, New York (1965).

137. Glasstone, S., and A. Sesonske, Nuclear Reactor Engineering, Van Nostrand, New York (1963).

138. Lamarsh, J., Introduction to Nuclear Reactor Theory, Addison-Wesley Canada Ltd., Don Mills (1966).

139. Lo, S., M.Eng. Thesis, McMaster University (1972).

140. Seiveright, G., Atomic Power Division, Westinghouse Canada Ltd., Private Communication (1975).

141. Marquardt, D., Journal Soc. Ind. Applied Math., 11, 431 (1963).

142. Himmelblau, D., Process Analysis by Statistical Methods, John Wiley, New York (1970).

143. Hald, A., Statistical Theory with Engineering Applications, John Wiley, New York (1952).

144. Myers, B., and N. Enrick, Statistical Functions, Kent State University Press, Kent (1970).

145. Staub, F., and N. Zuber, GEAP-4733 (1964).

146. Baker, J., ANL-7093 (1965).

147. Hsu, Y., and R. Graham, NASA-TN-D-1564 (1963).

148. Gouse, S., Jr., and C. Hwang, MIT-8973-1 (1963).

149. Hewitt, G., R. King and P. Lovegrove, AERE-R-3921 (1962).

150. Scott, D., Advances in Chemical Engineering, Academic Press, New York (1963).

151. Moisses, R., Journal Heat Transfer, 85, 366 (1963).

152. Bennett, A., et al., Proc. Instn Mech. Engrs, 180, 260 (1965).

153. Golan, L., and A. Stenning, Proc. Instn Mech. Engrs, 184, 108 (1969).

154. Hewitt, G., and D. Roberts, AERE-M-2159 (1969).

155. Hoogendoorn, C., Chem. Eng. Sci., 9, 205 (1959).

156. Newson, I., Ph.D. Thesis, Imperial College of London (1964).

157. Hewitt, G., and N. Hall-Taylor, Annular Two-Phase Flow, Pergamon Press, New York (1970).

158. Hewitt, G., British Nucl. Energy Soc. Journal, 12, 213 (1973).

159. Webb, D., AERE-R-6426 (1970).

160. Jones, O., Jr., and N. Zuber, Proc. Fifth International Heat Transfer Conference, Paper No. B-5-4, Japan (1974).

161. Merilo, M., R. Dechene and W. Cichowlas, Journal Heat Transfer, 99, 330 (1977).

162. Gill, L., G. Hewitt and P. Lacey, Chem. Eng. Sci., 19, 665 (1964).

163. Isbin, H., N. Sher and K. Eddy, A.I.Ch.E. Journal, 3, 136 (1957).

164. Cravarolo, L., and A. Hassid, CISE-R-98 (1963).

165. Adorni, N., et al., CISE-R-35 (1961).

166. Gill, L., et al., Chem. Eng. Sci., 18, 525 (1963).

167. Adorni, N., et al., CISE-R-53 (1963).

168. Dukler, A., M. Wicks and R. Cleveland, A.I.Ch.E. Journal, 10, 44 (1964).

169. Schlichting, H., Boundary Layer Theory, McGraw-Hill, New York (1955).

170. Hsu, Y., and J. Smith, Journal Heat Transfer, 83, 176 (1961).

171. Hunsaker, J., and B. Rightmire, Engineering Applications of Fluid Mechanics, McGraw-Hill, New York (1947).

172. Lapidus, L., Digital Computation for Chemical Engineers, McGraw-Hill, New York (1962).

173. Wallis, G., Journal Basic Eng., 92, 73 (1970).

174. Kunz, H., and S. Yerazunis, Journal Heat Transfer, 91, 413 (1969).

175. Henstock, W., and T. Hanratty, A.I.Ch.E. Journal, 22, 990 (1976).

176. Francis, J., Proc. Roy. Soc. A, 206, 1086 (1951).

177. Gill, L., G. Hewitt and P. Lacey, Chem. Eng. Sci., 20, 71 (1965).

178. Nicklin, D., and C. Koch, International Symposium on Research in Cocurrent Gas-Liquid Flow, Paper No. C-2, Waterloo (1968).

179. Bergles, A., and J. Roos, International Symposium on Research in Cocurrent Gas-Liquid Flow, Paper No. E-6, Waterloo (1968).

180. Andeen, G., and P. Griffith, Journal Heat Transfer, 90, 211 (1968).

181. Isbin, H., R. Moen and D. Mosher, AECU-2994 (1954).

182. Yamazaki, Y., and M. Shiba, International Symposium on Research in Cocurrent Gas-Liquid Flow, Paper No. D-3, Waterloo (1968).

183. Turner, J., and G. Wallis, NYO-3114-6 (1965).

184. Styrikowich, M., E. Nevstrueva and G. Dvorina, International Symposium on Research in Cocurrent Gas-Liquid Flow, Paper No. D-2, Waterloo (1968).

185. Butterworth, D., Int. Journal Multiphase Flow, 1, 845 (1975).

186. Madsen, N., Proc. Fifth International Heat Transfer Conference, Paper No. B-5-1, Japan (1974).

187. Lockhart, R., and R. Martinelli, Chem. Eng. Progr., 45, 39 (1949).

188. Wallis, G., Journal Basic Eng., 92, 59 (1970).

189. Moody, L., Trans. Amer. Soc. Mech. Engrs, 66, 671 (1944).

190. Moeck, E., and J. Stachiewicz, Int. Journal Heat Mass Transfer, 15, 637 (1972).

191. Kutateladze, S., Fundamentals of Heat Transfer, Academic Press, New York (1963).

192. Kosky, P., Int. Journal Heat Mass Transfer, 14, 1220 (1971).

193. Collier, J., and G. Hewitt, AERE-R-3455 (1960).

194. Chien, S., Ph.D. Thesis, University of Minnesota (1961).

195. Charvonia, D., Purdue University Report, I-59-1 (1959).

196. Belkin, H., Ph.D. Thesis, Carnegie Institute of Technology (1953).

197. McLeod, A., Ph.D. Thesis, Carnegie Institute of Technology (1951).

198. McManus, H., Jr., Ph.D. Thesis, University of Minnesota (1956).

199. Zuber, N., Chem. Eng. Sci., 19, 897 (1964).

200. Lance, G., Numerical Methods for High-Speed Computers, Iliffe and Sons Ltd., London (1960).

201. Kroeger, P., and N. Zuber, Int. Journal Heat Mass Transfer, 11, 211 (1968).